UNIVERSITY OF CALGARY

# Genotype-phenotype correlations in mouse musculoskeletal development and disease

by

Alice Fiona Ford-Hutchinson

A THESIS

SUBMITTED TO THE FACULTY OF GRADUATE STUDIES

IN PARTIAL FULFILMENT OF THE REQUIREMENTS FOR THE

DEGREE OF DOCTOR OF PHILOSOPHY

DEPARTMENT OF BIOCHEMISTRY AND MOLECULAR BIOLOGY

CALGARY, ALBERTA

NOVEMBER, 2006

## Abstract

The mouse is an excellent model to investigate gene function and musculoskeletal disease. In this thesis we examine three different mouse models: *progressive ankylosis* (*ank*), murine *brachymorphism* (*bm*), and *Pten*$^{flox/flox}$*:Col2a1Cre*. Using diverse technologies, such as micro-computed tomography (micro-ct) and histology, we characterized these models of musculoskeletal disease. The *ank/ank* and *bm/bm* mice were examined in the context of developing these techniques, especially micro-ct, a powerful tool for identifying and monitoring the progression of developmental or acquired skeletal abnormalities in rodent models. The bulk of the thesis examines the role of phosphatidylinositol 3'-kinase (PI3K), via inactivation of *Pten*, in the context of cartilage and bone.

Skeletogenesis is a complex process that depends on a variety of extracellular stimuli that activate diverse intracellular signalling pathways. Although many such stimuli activate PI3K, the exact role of this pathway in cartilage development and bone formation remains unclear. The 3' phosphoinositide phosphatase tumour suppressor, Pten, is described as a pivotal downstream negative regulator of the PI3K signalling. To gain insight into this pathway's role in skeletogenesis, mice with floxed *Pten* alleles were crossed with a type II collagen gene promoter Cre recombinase-expressing line to yield *Pten*$^{flox/flox}$*:Col2a1Cre* mice. *Col2a1Cre*-mediated gene alterations are observed in mature chondrocytes, as well as in osteo-chondroprogenitors. As revealed by micro-ct, *Pten*$^{flox/flox}$*:Col2a1Cre* mice exhibited not only increased skeletal growth post-natally, particularly of vertebrae, but also massive trabeculation and increased cortical thickness of long bones. Primary spongiosa development and perichondrial bone collar formation were also augmented in *Pten*$^{flox/flox}$*:Col2a1Cre* mice. Growth plates of *Pten*$^{flox/flox}$*:Col2a1Cre*

mice appeared disorganized, with evidence of accelerated hypertrophic differentiation. Consistent with cartilage germinal zone exhaustion, tibial growth plate fusion was observed at 6 months of age. At 9 and 10 months two of these animals manifested exactly the same type of cancer, osteogenic sarcoma (osteosarcoma), with pulmonary and hepatic metastases, this is consistent with the role of *Pten* as a tumour supressor. Our results are in keeping with the PI3K pathway functioning as a key integrator of extracellular signals responsible for determine skeletal size and structure.

**Acknowledgements**

I would first and foremost like to acknowledge my supervisor, Dr. Frank Jirik, for his support and guidance throughout my thesis. I would next like to thank my supervisory committee members Drs Jay Cross, Doug Demetrick, Benedikt Hallgrimsson, and John Matyas for all their help and guidance. I would also like to extend my thanks to Dr. Zenobia Ali for her tremendous technical mentorship and guidance. I would further like to thank all past and present members of Dr. Frank Jirik's lab for help with all aspects of laboratory life.

I would further like to thank the Alberta Heritage Foundation for Medical Research and Dr. Frank Jirik for their financial support throughout my studies.

## Dedication

I dedicate this thesis to my ever supportive husband, Dave, to my parents, for believing that I could achieve any goal I set, to my two brothers, for teaching me strength, and to my friends, who have cheered me along the way.

**Table of Contents**

## List of Tables

## List of Figures and Illustrations

## List of Symbols, Abbreviations and Nomenclature

| Symbol | Definition |
|---|---|
| 3D | 3-dimensional |
| ADAM 12 | A disintegrin and metalloproteinase domain 12 |
| Ank | Progressive ankylosis |
| ASPN | Asporin |
| ALP | alkaline phosphatase |
| AR | androgen receptor |
| BCP | basic calcium phosphate |
| bHLH | basic helix-loop-helix factor |
| BMP | bone morphogenic protein |
| Bm | Brachymorphism |
| CPPD | calcium pyrophosphate dehydrate |
| COX2 | cyclooxygenase-2 |
| EGF | endothelial growth factor |
| ECM | extracellular matrix |
| ePPi | extracellular PPi |
| ER | estrogen receptor |
| ERM | ezrin-radixin-moesin |
| FGR3 | fibroblast growth factor receptor-3 |
| FOXO | Forhead box transcription factors |
| GPCRs | G-protein-coupled receptors |
| GSK3 | glycogen synthase kinase-3 |
| GAG | glycosaminoglycan |
| GDF | growth and differentiation factor |
| HGF | hepatocyte growth factor |
| HIF-1$\alpha$ | Hypoxia-inducible factor 1$\alpha$ |
| Ihh | indian hedgehog |
| iNOS | inducible nitric oxide synthase |
| IGFs | insulin-like growth factor 1 |
| IL-1 | interleukin-1 |
| IL-1ra | IL-1 receptor antagonist |
| IL-8R | interleukin-8 receptor |
| ID | inhibitor of bHLH |
| TIMPS | inhibitors of MMPs |
| LCM | laser capture microdissection |
| MMP | matrix metalloproteinases |
| Micro-ct | micro-computed tomography |
| NPP | nucleotide pyrophosphatase phosphodieasterase |
| OA | osteoarthritis |
| OPG | osteoprotegerin |

| | |
|---|---|
| PTH/PTHrP receptor | parathyroid hormone/parathyroid hormone related peptide receptor |
| PTC | Patched |
| Pten | phosphatase and tensin homolog deleted on chromosome 10 |
| PI(4,5)P2 | phosphatidylinositol (4,5)-bisphosphate |
| PAPS | phosphoadenosine-phosphosulfate |
| Papss2 | phosphoadenosine-phosphosulfate syntethase 2 |
| PDK1 | phosphoinositide-dependent kinase 1 |
| PH | pleckstrin homology |
| PKA | protein kinase A |
| PKB | protein kinase B |
| PPi | Pyrophosphate |
| R6K | P90 ribosomal S6 kinase |
| RTKs | receptor tyrosine kinases |
| RB | retinoblastoma |
| S6K | P70 ribosomal S6 kinase |
| S6K1 | S6 kinase 1 |
| SGK | serum and glucocorticoid-induced kinase |
| SHH | sonic hedgehog |
| SEMD | spondyloepimetaphyseal dysplasia |
| SH2 | Src homology-2 |
| SMI | structural model index |
| TRAP | tartrate resistant acid phosphatase |
| Ttp | tiptoe walking |
| TGF | transforming growth factor |
| TSC | tuberous sclerosis |
| Col2a1 | type II collagen |
| VEGF | vascular endothelial growth factor |
| VHL | von Hippel-Lindau |

# Chapter One: Introduction

## 1.1 The Skeletal System

The skeletal system has numerous roles including: providing a rigid framework and support to give shape to the body, protecting internal organs, allowing for movement of the body, acting as a primary storage site for mineral salts, and playing a role in hematopoiesis. The skeleton is subdivided into two components, the axial (skull, spine sternum, and ribs) and appendicular skeleton (bones of the extremities). The skull is further divided into the chondrocranium (where the elements are first derived from cartilage), and the dermatocranium, consisting of the cranial vault and most of the upper facial skeleton (which are derived from direct conversion of undifferentiated mesenchymal cells to bone) [1]. Skeletogenic cells of the limb are derived from the lateral plate mesoderm, whereas cells from the head skeleton are derived from cephalic mesoderm and the neural crest [2]. Bone formation that arises from an initial cartilaginous template is termed to as endochondral bone formation, whereas bone formation that occurs in the absence of a cartilage template is named intramembranous ossification. The following sections will focus on mesenchymal condensations, and intramembranous and endochondral bone formation.

## 1.2 Mesenchymal Cells

### *1.2.1 Mesenchymal Stem Cells*

Postnatal tissue of mammals contains multipotent stem cells. These stem cells are characterized by their ability to self-renew and capacity for multilineage differentiation. Adult stem cells are found in numerous tissue types such as bone marrow, skeletal muscle, brain, and intestine [reviewed in [3]]. Mesenchymal stem cells arise from bone

marrow and can differentiate into a variety of tissues types including: bone, cartilage, muscle, fat, and tendon. Transforming growth factor β (TGFβ) is known to play a critical role in mesenchymal stem cell differentiation [reviewed in [3]].

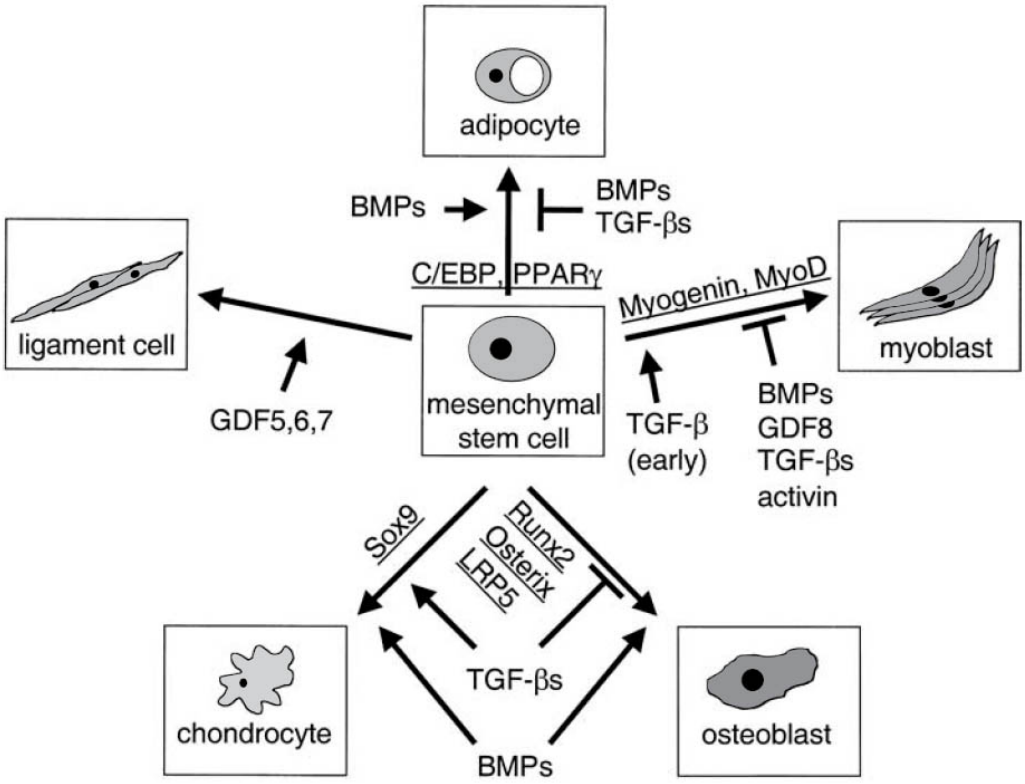


**Figure 1-1. Potential differentiation routes of mesenchymal stem cells highlighting the role of TGFβ family members in differentiation to multiple cell lineages. The key factors involved in determining a cell lineage are underlined [3].**

Bone morphogenic proteins (BMPs) are able to induce mesenchymal cells into chondroblasts or osteoblast lineages. TGFβ acts on a number of factors important for mesenchymal stem cell differentiation, such as Runx2, homeobox genes (MSX1, MSX2), and on factors in the Wnt signalling pathway [reviewed in [3]]. While TGFβ plays a pivotal role in mesenchymal stem cell differentiation, many factors are involved in the

process of mesenchymal differentiation to chondroblasts or osteoblasts. The next section reviews current knowledge on this process.

### *1.2.2 Mesenchymal Condensations*

Mesenchymal condensations are the result of epithelial-mesenchymal interactions, and form in areas where cartilage will appear, or bone due to intramembranous ossification. Condensations occur when dispersed mesenchymal cells form aggregates. Sonic hedgehog (Shh), BMP (-2, -3, -4, -5, -7), FGF, and Hox genes determine the timing, position, and shape that the condensations will form. The formation of mesenchymal condensations is a multistep process: starting with initiation, setting boundaries, proliferation, adherence, growth, and ending with differentiation [reviewed in [1]]. In the case of intramembranous ossification, cells differentiate directly into osteoblasts, while in endochondral bone formation, the cells differentiate into chondrocytes [reviewed in [1]] (Figure 1-2).

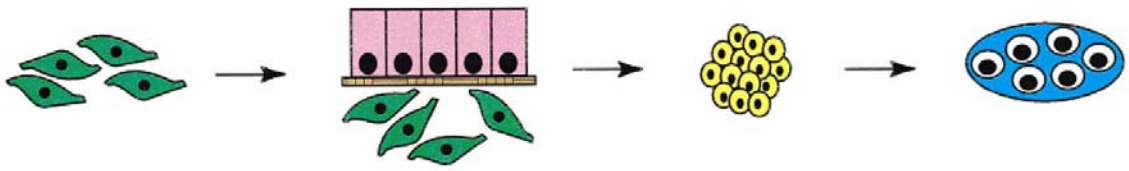

**Figure 1-2. Illustration of the four steps in the development of a skeletal element. First, migration of pre-skeletal cells (green) to a site of future skeletogenesis. Second, epithelial (purple) and epithelial basement membrane (brown) interactions with mesenchymal cells. Third, initiation of condensations (yellow), fourth, overt-differentiation of chondroblasts or osteoblasts (blue) [4].**

Arising from epithelial-mesenchymal interactions, the initiation step causes an upregulation of numerous molecules involved in prechondrogenic or preosteogenic condensations (see Figure 1-3); they include tenascin (leads to condensation and

transition from condensation to overt differentiation), fibronectin (when bound by syndecam, indirectly allows for differentiation), N-CAM (regulates condensation formation), and N-Cadherin (role in adhesion of cells during condensation) [reviewed in [5]].

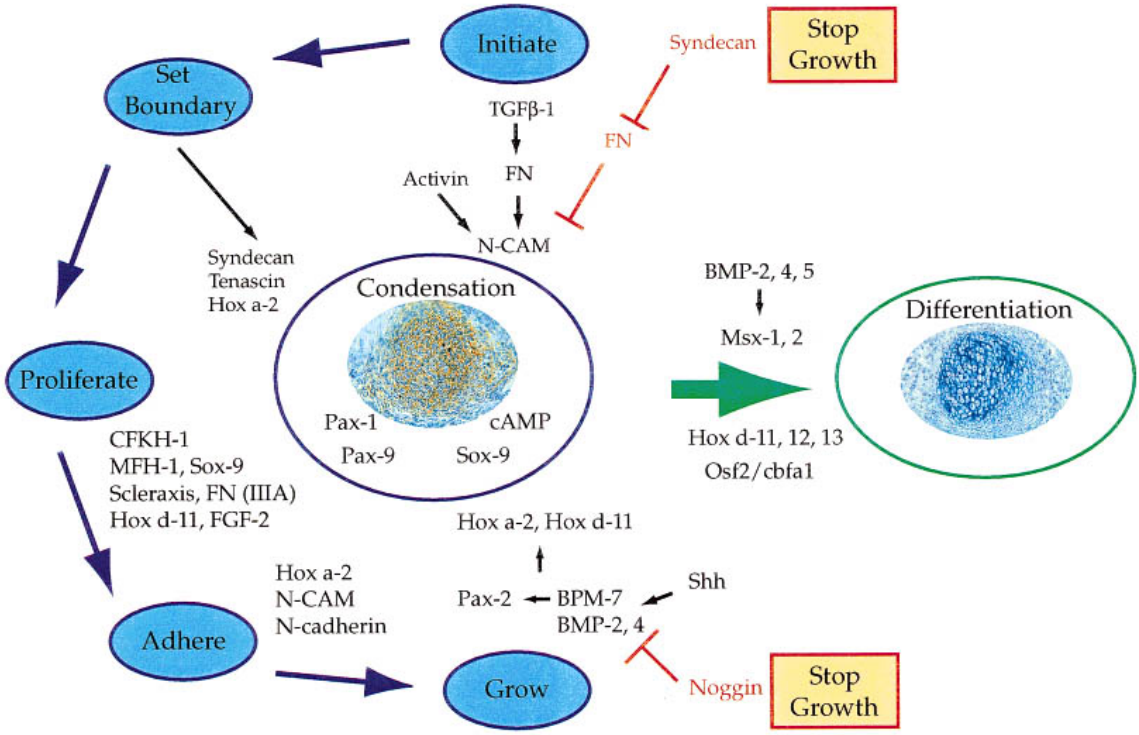


**Figure 1-3. Summary of the major players involved in mesenchymal condensations (blue), and the transition from condensation to overt-differentiation (green). Condensations can be visualized by peanut agglutin lectin. Shown are the elevated levels of cAMP, and major expressed genes at the condensation stage (*Pax-1, -9, Sox-9*). Also shown are the major genes involved in the five steps of condensation (Initiate, Set Boundary, Proliferate, Adhere, and Grow). Two pathways that are able to stop condensation growth (Stop Growth) are in yellow and red. Stopping of condensation leads to differentiation (green arrow), which requires an upregulation of genes to initiate differentiation and downregulation of genes to terminate condensation. FN = fibronectin. [4]**

By regulating various aspects of growth and differentiation, the TGFβ superfamily (including several TGFβ isoforms, BMPs, growth and differentiation factor (GDF), and the activin and inhibins) enable condensations by aiding in the establishment of cell-cell and cell-extracellular matrix (ECM) interactions [1, 2]. More specifically, BMPs aid in the recruitment of cells into condensations, and is antagonized by Noggin. The BMP-Noggin feedback loop is important for the regulation of condensation location, size, and duration during limb development (Figure 1-3). Condensation formation is further aided by cell surface receptors and ECM proteins that play a role in cell attachment, growth, differentiation, and survival. The integrin family also play an important role by regulating cell-matrix interactions, enabling a connection between ECM and intracellular signalling, and altering gene expression. Examples of integrins expressed early during the condensation include: fibronectin (α5β1), types II and VI collagen (α1β1, α2β1, α10β1), laminin (α6β1), and vitronectin and osteopontin (α5β3) [reviewed in [6]].

During prechondrogenic condensations, levels of intracellular cAMP increases along with cell-cell interactions believed to be involved in upregulating chondrogenic genes. One of the major transcription factors involved in this process is Sox9, part of the Y-type high mobility group box (Sox) family. It functions as a potent inducer of genes vital to cartilage formation such as type II collagen (Col2a1) and aggrecan. Sox9 transcriptional activity is increased by phosphorylation with protein kinase A (PKA) [7]. Sox5 and Sox6 are also important transcription factors, and have been shown to cooperate with Sox9 in the activation of the type II collagen enhancer [8]. Sox9 expression begins in the mesenchymal chondroprogenitor cells and reaches its highest

expression in differentiated chondrocytes. It is believed that Sox9 controls the expression of cell surface proteins required for mesenchymal condensations, suggesting that it is the first transcription factor required for chondrocyte differentiation and cartilage formation [1].

Pax genes are important for regulating epithelial-mesenchymal interactions. Pax-1, -9 encode nuclear transcription factors, and their strongest expression is at the condensation stage, consistent with their role in condensation. Pax-2, regulated by BMP-7, is important for regulating the size of condensations [reviewed in [4]].

Once the condensations have stopped growing, differentiation occurs. Progression from condensation to overt differentiation to chondroblasts or osteoblasts requires a decrease in N-CAM and other genes controlling proliferation, in addition to an increase in genes associated with differentiation. In turn, this requires signals that cease condensation growth and favour differentiation. This can occur indirectly, syndecan binding to fibronectin to downregulate N-CAM, or directly, through such pathways as BMP-2, -4, -5, and activation of homeobox genes MSX1, MSX2 [2] (Figure 1-3).

Overt differentiation is hallmarked by the transient expression of Runx2 in both prechondrogenic and preosteogenic condensations. Expression ceases in the prechondrogenic cells once differentiation is complete. Loss of Runx2 leads to the absence of both intramembranous and endochondral bone, indicating its essential role in bone formation [9-11]. Condensed mesenchymal cells that differentiate into chondroblasts are characterised by production of type II collagen matrix and glycosaminoglycans (GAGs). Condensed mesenchymal cells that differentiate into

osteogenic cells make type I collagen along with numerous noncollagenous ECM proteins to produce osteoid. Onto the later mineral phase, hydroxyapatite is deposited.

## 1.3 Intramembranous Ossification

### *1.3.1 Intramembranous ossification of cranial sutures*

Intramembranous ossification occurs when mesenchymal cell condensations arise due to epithelial-mesenchymal interactions and form into bone without a cartilage intermediate. This occurs in the flat skull bones of the cranial vault, including the cranial suture lines, some facial bones, and parts of the mandible and clavicle [1]. Bone collar formation is also associated with intramembranous ossification, however current studies are indicating that they in fact differ developmentally (see section 1.4.3). In intramembranous ossification of cranial sutures, for example, mesenchymal cells condense and ossification occurs in the centres. The centres expand, and where the two bones come together, a joint called a *suture* is formed. A suture consists of interdigitating membranous bones and the interposed mesenchymal tissue. Later in development, the sutures become the primary site of osteoblast differentiation and bone formation for the skull. Important signalling mechanisms are FGFs, TGFβ, MSXs, and Runx2 [reviewed in [12]]. Unlike endochondral bone ossification, which has an intrinsic growth potential, intramembranous ossification produces new bone at the sutural edges of the bone fronts in response to external stimuli, such as signals from the underlying brain transmitted via pressure from the underlying dura matter. This allows for growth of the cranial vault to be coordinated with growth of the brain. [reviewed in [13]].

Intramembranous ossification of the sutures is a complex event, with numerous factors involved that may either work independently or within the same pathway. MSX2

expression has been shown to be regulated by BMP-4, and together they regulate FGF-2 mediated reactions, such as Twist expression and TGFβ production [reviewed in [13]]. TWIST is able to inhibit terminal differentiation of osteoprogenitors into osteoblasts, and is also believed to work upstream of FGFs. ID, stimulated by BMP-2, is able to inhibit TWIST, thereby promoting osteoblast differentiation (Figure 1-4).

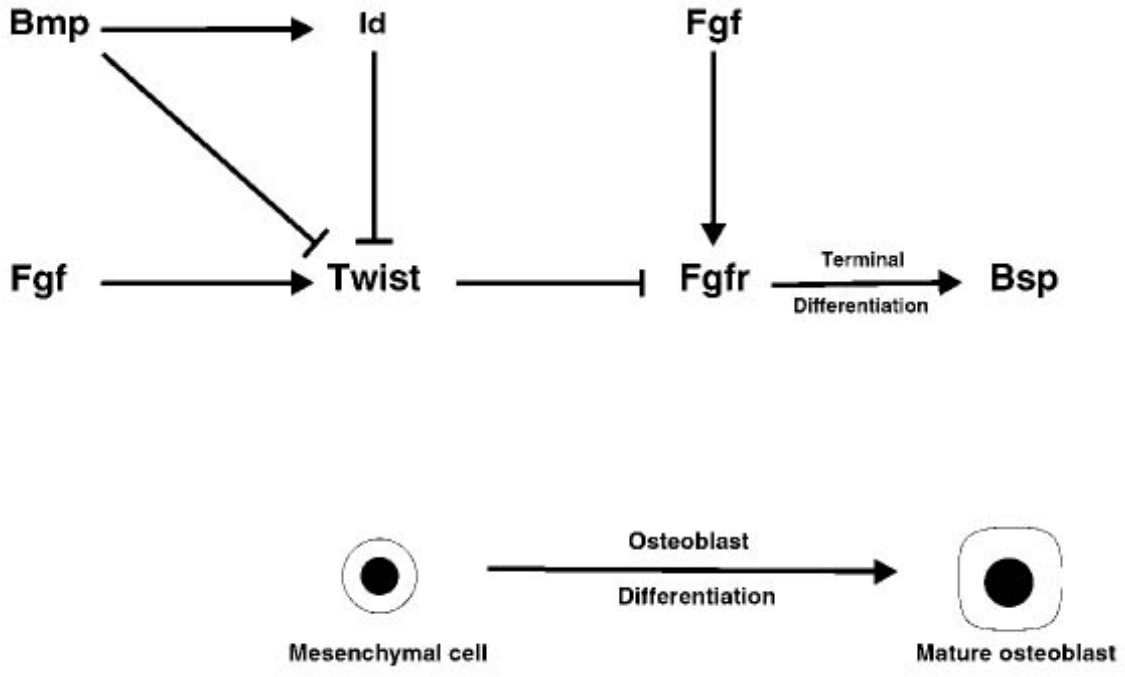


**Figure 1-4. Schematic model of how TWIST and ID interact with FGF signalling during osteoblast differentiation. BMP-2 and ID inhibit TWIST and FGFR, promoting cell differentiation. BMP-2 is also able to inhibit TWIST directly. In upregulating TWIST, FGF antagonizes BMP-2, stopping the inhibition by FGFR. FGF can directly bind to FGFR promoting terminal differentiation, which then allows osteoblasts to produce bone sialoprotein [12].**

## 1.4 Endochondral Ossification

### *1.4.1 Endochondral bone formation in the limb*

Endochondral bone formation is a two-step mechanism, in which chondrocytes form a matrix template, named the growth plate, and osteoblasts differentiate to initiate the ossification process [14]. As mentioned above, the majority of the vertebrate skeleton is derived from cartilage templates via endochondral bone ossification [1]. In endochondral bone formation of the limb, mesenchymal cells from the lateral plate mesoderm condense and differentiate into a cartilage anlagen surrounded by a layer of fibroblast-like cells that make up the perichondrium [reviewed in [15]]. The chondrocytes of the anlagen form a growth plate where rounds of controlled proliferation, maturation, and apoptosis occurs [reviewed in [14]]. Round proliferating chondrocytes arrange in columnar layers, and produce type II collagen. They will eventually stop proliferating and become pre-hypertophic chondrocytes that will exit the cell cycle, differentiate, and hypertrophy. This hypertrophy results in a down regulation in the expression of type II collagen and an increase in the expression of type X collagen. During differentiation, the hypertrophic chondrocytes express Runx2. At this time the hypertrophic chondrocytes are able to stimulate calcification of the cartilage matrix by taking on some of the features of osteoblasts by expressing alkaline phosphatase (ALP), Runx2, osteopontin, and osteocalcin [16-18]. These cells are also able to release critical paracrine and autocrine factors, including: Indian hedgehog (Ihh), vascular endothelial growth factor (VEGF), autocrine insulin-like growth factor 1 (IGF-1), matrix metalloproteinases (eg. MMP-13), as well as BMP-2, and -6 [16, 19-21]. It is believed that the hypertrophic chondrocyte

undergo apoptosis and die, however, it has also been suggested that these cells are able to trans-differentiate into osteoblasts [reviewed in [22]].

Coincident with chondrocyte hypertrophy, release of Ihh stimulates the perichondrium to produce a number of BMPs and osteoblasts begin to appear [15, 23] in areas adjacent to the hypertrophic region. The perichondrium is the entry point for blood vessel influx from surrounding tissues, and the invasion begins the removal of the hypertrophic zone [15, 24]. The latter process is aided by MMP-13 and MMP-9 released by late hypertrophic cells [20, 25]. The resulting vasculature also leads to the importation of osteoblasts and osteoclasts. The perichondrium is essential not only for normal endochondral ossification which leads to the trabecular bone of the primary spongiosa, [14, 15, 24], but also for forming the bone collar, which serves as the template for cortex formation by appositional growth.

The primary centre will eventually split into two opposite growth plates, whereby chondrocyte hypertrophy and bone remodelling continues as long as new chondrocytes are generated in the growth plate. This chondrocyte proliferation is the driving force of longitudinal bone growth during post-natal life. Hypertrophic chondrocytes provide scaffolds for new trabecular bone formation, and, via the perichondrium, help modulate the formation of the bone collar, which will later become cortical bone [reviewed in [14]] (Figure 1-5).

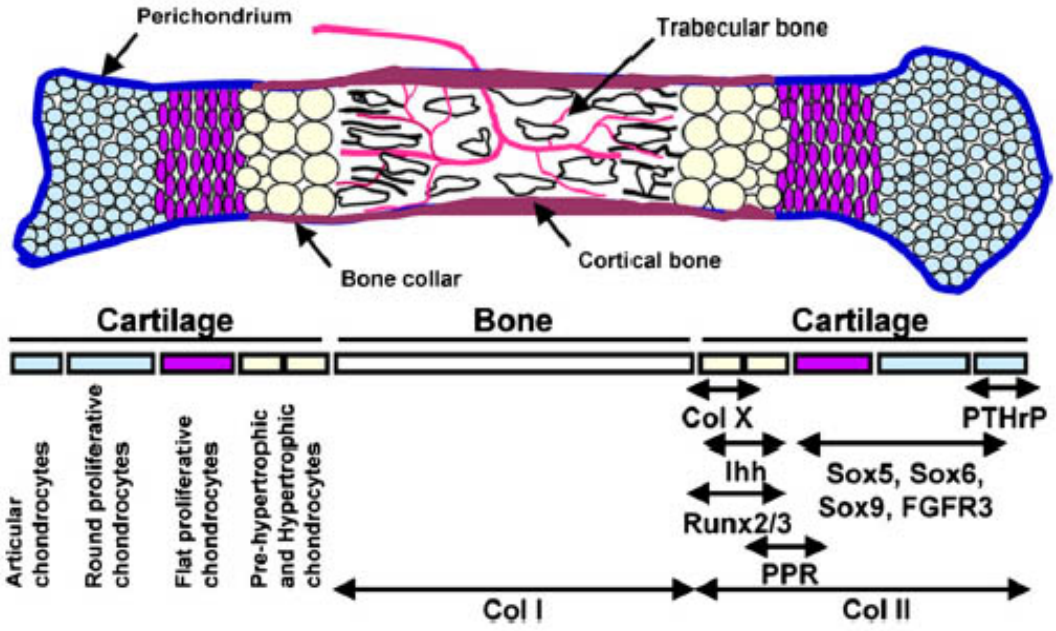


**Figure 1-5. Schematic representation of endochondral bone formation in a mouse tibia during the late stage of fetal development. Illustrated are the normal markers for bone, periarticular, flat, pre-hypertrophic, and hypertrophic chondrocytes [14].**

The regulation of the growth plate is a complex event, that requires many factors such as: Sox5, 6 (important for chondrogenesis), and 9 (required for chondrocyte differentiation and positively regulates proliferation), fibroblast growth factor receptor-3 (FGFR3) (shown to modulate chondrocyte hypertrophy *in vitro*, and gain of function mutations lead to achondroplasia), BMPs (important in formation of both mesenchymal condensations and joints), parathyroid hormone/parathyroid hormone related peptide receptor (PTH/PTHrP receptor: PPR) (a central regulator in mineralization homeostasis and bone development), PTHrP (keeps chondrocytes in proliferative state), Ihh (inhibits hypertrophic chondrocyte differentiation, and therefore mineralization via the up-regulation of PTHrP, works in a negative feedback loop with PTHrP), Runx2 (essential for osteoblast differentiation, is an initiator of chondrocyte hypertrophy, and can promote

VEGF), hypoxia-inducible factor 1α (HIF-1α) (is important for chondrocyte survival, negatively regulates chondrocyte proliferation, and can activate VEGF), and VEGF (also important for chondrocyte survival and angiogenesis) [reviewed in [14]] (see Figure 1-6 and Figure 1-7).

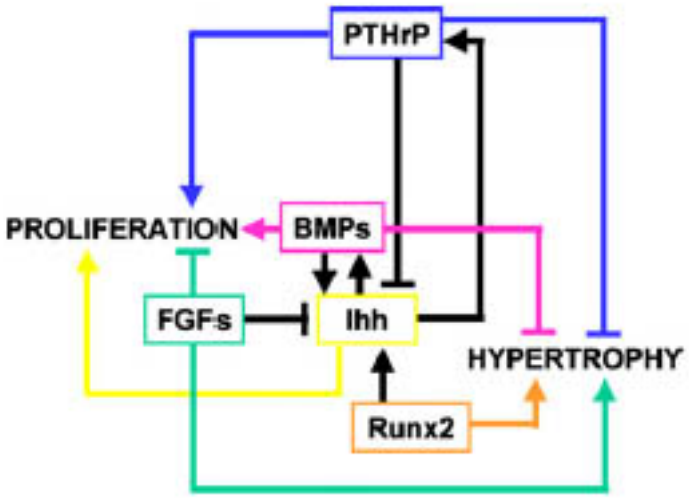


**Figure 1-6. Representation of the feedback loop and biological activities of PTHrP, Ihh, BMPs, and FGFs in the fetal growth plate. Ihh and PTHrP work in a negative feedback loop where Ihh promotes PTHrP expression at the articular region, which turn represses Ihh. A positive feedback loop involves Ihh promoting BMPs, who are then able to promote Ihh expression. FGFs, in turn, negatively regulate Ihh. PTHrP, Ihh, and BMPs all positively promote proliferation and negatively affect maturation. Ihh's effect on maturation is PTHrP dependent, while it's affect on proliferation is PTHrP independent. BMPs' effects on proliferation and maturation are able to occur independently of PTHrP/Ihh axis. FGFs negatively regulate proliferation and positively affect terminal differentiation, and this effect occurs independently of PTHrP/Ihh. Runx2 is a positive modulator of chondrocyte hypertrophy, and is also able to upregulate Ihh expression [14].**

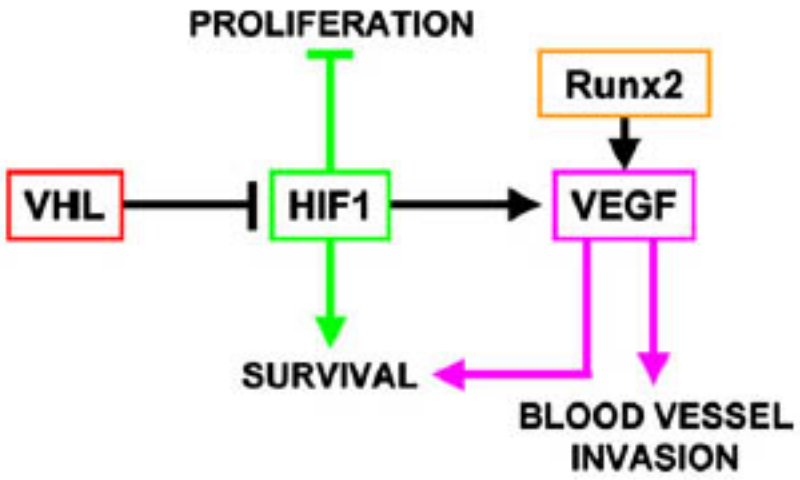


**Figure 1-7. Representation of the regulation of expression and biological activities of von Hippel-Lindau (VHL), HIF-1α, VEGF, and RUNX2 in the fetal growth plate. Transcription factors Hif-1α and Runx2 are able to induce VEGF expression. VHL negatively regulates HIF-1α by ubiquination under normoxic conditions, under hypoxic conditions, VHL is unable to recognize Hif-1α. Runx2 promotes angiogenesis through the induction of VEGF expression. Hif-1α and VEGF are both required for chondrocyte survival in the growth plate, but HIF-1α as a survival factor in the growth plate only partially depends on VEGF. Lack of VHL in the growth plate leads to negative regulation of chondrocyte proliferation, the effect of VHL in the growth plate is mostly due to upregulation of HIF-1 activity [14].**

### *1.4.2 Perichondrium: a source of osteoblasts and vascular invasion*

Cartilage, the adjacent perichondrium, and the invading vasculature, are the three tissues required for proper endochondral bone formation. Cells that are at the centre of the mesenchymal condensations can form into chondrocytes; however the cells that surround the condensations become the perichondrium. Cartilage differentiation influences the perichondrium maturation, and vice versa. As chondrocytes hypertrophy there is a close link to the conversion of the perichondrium to the periosteum. Furthermore, the factors involved in chondrocyte maturation are also involved in the conversion of the perichondrium to the periosteum. Signals from the perichondrium, such as Ihh and TGFβ,

are able to control the rate of chondrocyte differentiation [reviewed in [15]]. The factors that interplay between cartilage and the perichondrium include BMPs, FGFs, and Wnt families [reviewed in [15]]. Being so similarly regulated has made it difficult to distinguish the signalling between the perichondrium and hypertrophic chondrocytes.

The perichondrium is also required to promote the initiation of cartilage angiogenesis; this is done by connecting with surrounding vasculature networks [24]. This vascular invasion into the perichondrium, and subsequently, into the cartilage template, enables for ossification and the formation of the bone marrow cavity [reviewed in [15]]. The perichondrium is also the source of osteoblasts in the cortex and trabecular bone during development [24]. Thus, the perichondrium plays two roles in the process of endochondral ossification, the first is providing osteoblast precursors, and the second is regulating vascular invasion [24].

### *1.4.3 Bone Collar Formation: appositional growth distinct from intramembranous ossification.*

Appositional growth of the bone collar, formed in the perichondrium, is another process associated with intramembranous ossification. Current studies are now showing that it is actually a developmentally distinct process [26, 27]. While the molecular factors that influence perichondral osteogenesis are largely unknown, hypertrophic chondrocytes are thought to have a regulatory role in the coordination of growth plate chondrogenesis and periosteal osteogenesis. This was first indicated when *Ihh* null mice were discovered not to form a bone collar [26], while overexpression of Ihh leads to the induction of bone collar formation [27]. It has been further shown that Ihh expression in the

prehypertrophic chondrocytes is responsible for determining the site of bone collar formation and the induction of mature osteoblasts in the adjacent perichondrium [28].

### 1.5 Articular Cartilage

Articular cartilage is found at the epiphyseal tip of long bones. Articular cartilage chondrocytes are able to resist becoming fully differentiated and produce ECM in order to maintain normal joint function. Articular cartilage is a resilient load bearing tissue that forms the articulating surface of diarthrodial joints. It is supported by bone and protects it by transferring load across the subchondral bone due to its viscoelastic properties. Cartilage is highly hydrated (80%) and mostly composed of ECM. The ECM is composed of a network of collagen (type II fibers), proteoglycans (aggrecan), and macromolecules [29]. Cartilage can be divided into four zones: the superficial zone, the middle (transitional) zone, the deep zone, and the calcified zone (Figure 1-8) [29].

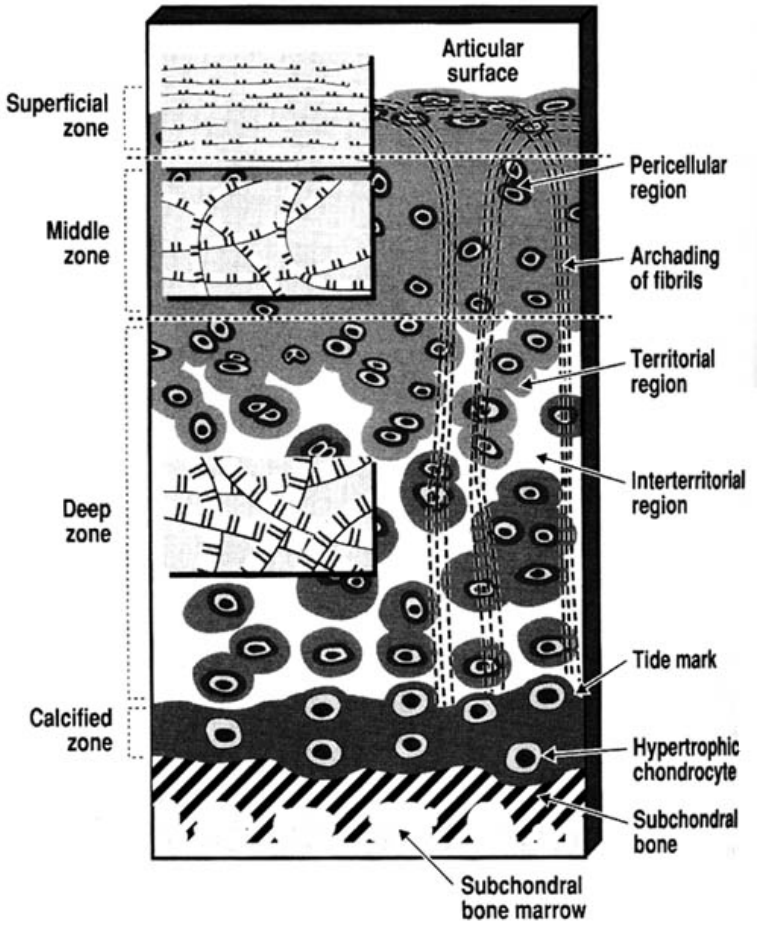


**Figure 1-8. Organization of articular cartilage matrix. It is composed of pericellular, territorial, and interterritorial regions. Surrounding the chondrocyte is the pericellular region, it contains a high concentration of aggrecan, the proteoglycan decorin, and type VI collagen. The pericellular matrix is surrounded by the territorial matrix, which is composed of collagen fibrils that appear to form a fibrillar network distinct from the surrounding interterritorial matrix. The interterritorial matrix is the largest area and is composed mostly of the material properties of articular cartilage. The articular cartilage is divided into four zones: the superficial zone (10-20%), the middle (superficial) zone (40-60%), the deep zone (30%), and finally the calcified zone. The collagen fibrils within these zones form structural frameworks that provide the articular cartilage with support for the chondrocyte and proteoglycan aggregates. The arcading of collagen fibrils is also shown by the broken lines [30].**

The properties of these zones are determined by the orientation of the collagen fibers and shape of the chondrocytes. The ECM is further divided into the pericellular, territorial, or

interterritorial regions, which vary depending on their proximity to the chondrocyte (Figure 1-8). The chondrocyte is responsible for the formation and maintenance of the articular cartilage. Being metabolically active, chondrocytes are able to respond to a number of environmental stimuli such as soluble mediators, growth factors, interleukins (IL), matrix molecules, mechanical loads, and hydrostatic pressure [29]. For instance, TGFβ is believed to maintain cartilage homeostasis [31]. Chondrocytes are responsible for maintaining a stable matrix, but some factors, such as IL-1, can lead to the degradation of the matrix by stimulating catabolic factors. Cartilage is both aneural and avascular and as such is not regulated by messages commonly used to regulate other body processes [29].

## 1.6 Chondro- and osteosarcomas

### *1.6.1 Etiology and General Features*

Osteosarcomas and chondrosarcomas are a tumour type that arises from mesenchymal cells. Osteosarcomas are primary malignancies of bone. They are the cause of 5% of childhood cancers, but are the most common malignancy in children and adolescents and the fifth most common malignancy in young adults aged 15-19 years [reviewed in [32]]. Most osteosarcomas are sporadic, however a small number are due to genetic predispositions [32]. Patients with no metastatic disease have a 70% long-term survival rate, however the remaining patients relapse within the first 5 years, with pulmonary metastasis or reoccurrence in the bone [reviewed in [33]]. Chondrosarcomas are primary tumours characterized by the production of hyaline cartilage [34]. They represent the third most common skeletal malignancy and occur primarily in adults between the ages of 35 and 60 years [35]. Most chondrosarcomas (75%) are located centrally within the

medullary cavity of bone (central chondrosarcoma), while a minority (15%) are able to develop from the surface of bone (peripheral chondrosarcoma) [35].

Classifications of sarcomas heavily depended on the tumour's resemblance to mature tissue [36]. Immunohistochemically defined antigens are used to further define the proper diagnosis of sarcoma lesions which are difficult to identify. The use of immunohistochemical and genetic markers has been further used to define growth deregulation pathways in sarcomas [36].

Molecularly, sarcomas can be divided into two major classes: those with specific aberrancies in known cell cycle regulatory pathways [such as retinoblastoma (RB) and p53], and those with simple (chromosomal translocation) or complex (aneuploidy) karyotypes [36]. Disruptions in cell cycle control are known to play a large role in sarcomas and are depicted in Figure 1-9.

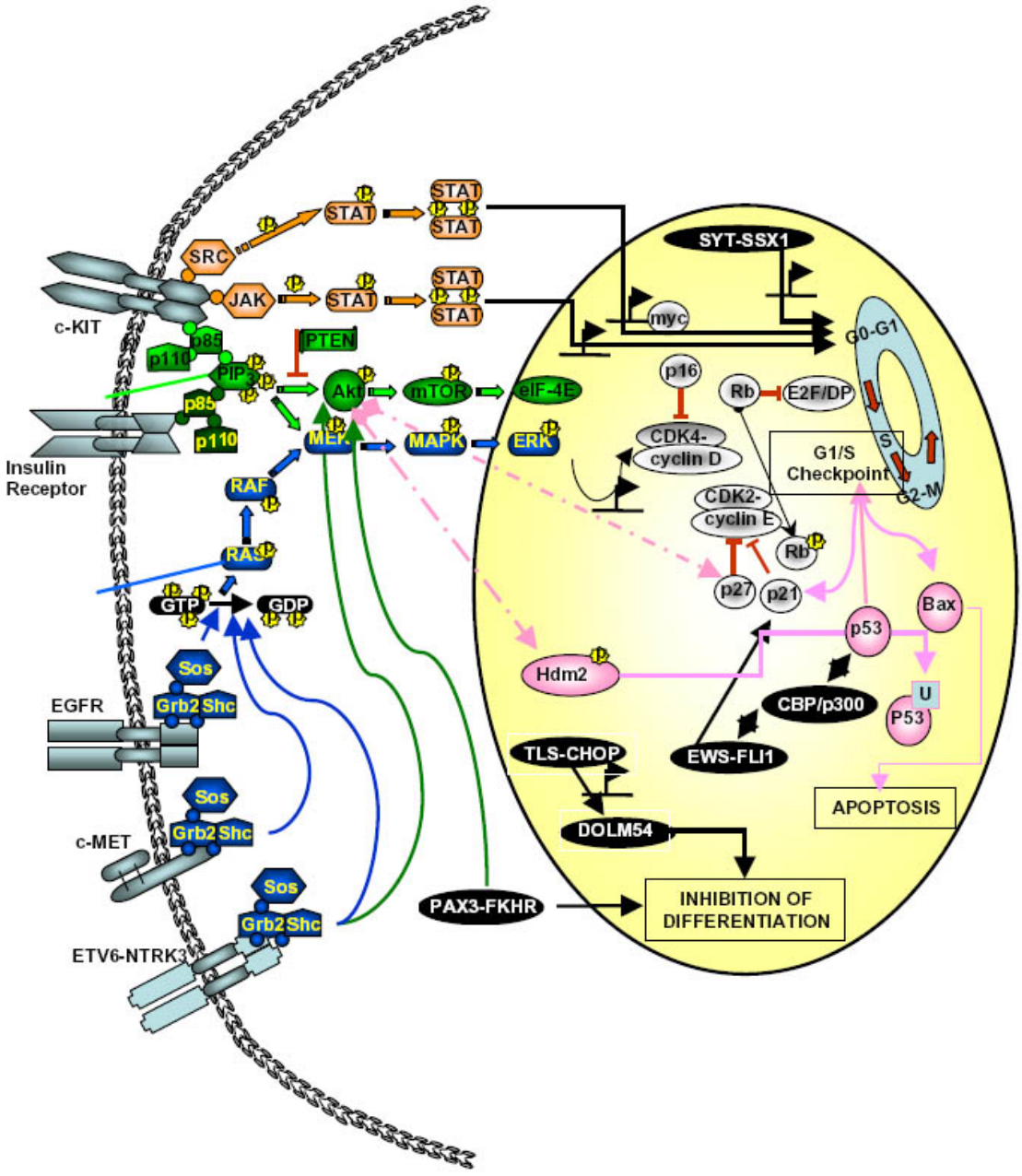


**Figure 1-9. Schematic representation of the major pathways thought to be involved in the development of sarcomagenesis [36].**

While the exact mechanism leading to cell cycle deregulation is unknown, the PI3K/AKT pathway is a prime candidate as it is the common point of convergence of many of the

signal transduction pathways known to be affected by sarcomas (see section 1.11 for a full description of PI3K signalling). The signalling understood in chondro- and osteosarcomas is discussed below.

### *1.6.2 Chondrosarcomas*

Chondrosarcomas are malignant bone tumours characterized by the synthesis of pure hyaline cartilage. Chondrosarcomas are categorized by their location in bone, and most are located centrally in the medullary cavity [34, 37]. The molecular pathogenesis is not well-characterized for these tumours. There is evidence that VEGF is crucial for chondrosarcoma progression and that the JNK/ERK MAPK's downstream effectors c-jun and c-Fos, with interactions with Runx2, play a role in the pathobiology [34]. Other molecular changes implicated are p16 inactivation, p53 alterations, and increases in the IHH signalling pathways [34, 37, 38]. *Pten* mutations in chondrosarcomas are rare [39]. Further studies are required to better understand the molecular changes that occur in chondrosarcomas, and how they relate to the different subgroups and affect disease severity.

### *1.6.3 Osteosarcomas*

Osteosarcomas are the most common primary tumour of bone, and account for the majority of cancer-related deaths in the paediatric group. Osteosarcomas most commonly affect children and adolescents, with a peak incidence occurring during the period of rapid skeletal growth. A small number of older patients develop osteosarcomas, which are generally related to pre-existing conditions such as Paget's disease or radiation exposure. Many osteosarcomas arise in what appears as normal bone. Over 30% of patients with osteosarcomas develop lung metastasis [40, 41]. An osteosarcoma is

defined as a malignant tumour of bone that produces either osteoid or bony matrix [40]. While most osteosarcomas are sporadic, there are genetic conditions that predispose individuals to osteosarcomas; these include hereditary Retinoblastoma, Li-Fraunmeni syndrome, Rothmund-Thomson, and Werner Syndrome. These syndromes are all characterized by mutations in genes that either regulate cell cycle or DNA metabolism, and have provided some clues about sporadic osteosarcomas [32]. It is now known that there are some factors involved in osteosarcomas such inactivation of tumour suppressor such as p53 and Rb, or overactivity of oncogenes such as myc and Her-2. However, their exact roles have yet to be defined. Also implicated are p16, CDK4, Cyclin D1, and MDM2, all of which play a role in cell cycle control. RECQ helicase, which has a role in DNA replication, transcription, and repair, is also associated with osteosarcoma development (reviewed in [32]). Metastases of osteosarcomas are frequent and is a strong predictor of poor patient outcome. Proposed factors that can act as predictors for metastasis in osteosarcomas are ezrin, annexin 2, CXCR4/SDF-1, and resistance to Fas signalling pathway (reviewed in [32]). Two murine osteosarcoma cell lines have also revealed a role for PI3K-AKT signalling in MMP secretion, *in vitro* invasiveness, cell locomotion, and *in vivo* pulmonary metastasis, implicating AKT in pulmonary metastasis of osteosarcomas [42], while an analysis of 6 human cell lines (and 2 sub-clones) did not show losses of Pten [43]. In canine osteosarcomas and osteosarcoma cell lines, frequent evidence of Pten loss (associated with increased Akt phosphorylation) was described [44]. Although the status of Pten in primary osteosaromas remains to be thoroughly studied, as very few publications on the topic exist, it is interesting that chromosome 10 and 10q losses are cytogenetic abnormalities seen in osteosarcomas [45]. Future research

lies in discerning how the different factors interact functionally and how they intersect one another in timing during tumour formation and progression [32].

Little is known about the aetiology of human osteosarcomas, and less is known about the interactions occurring between host and tumour cells that regulate growth and progression *in vivo*. A mouse model would provide insight into the governing factors that regulate development and pathogenesis of osteosarcomas [41]. A desired mouse model of osteosarcoma should develop a tumour reliably in the life span of a mouse, express osteoblastic markers (ALP, type I collagen, osteopontin, matrix Gla protein, osteocalcin), produce osteoid matrix, and develop spontaneous lung metastasis [41]. Animal models of osteosarcomas have been reported, including a spontaneously occurring osteosarcoma in dogs [46], in mice [47, 48], radiation-induced osteosarcoma in Sprague-Dawley rats [49], and subcutaneous [50] and orthotopic [51] implantation of osteosarcoma cells in mice. There has been a move towards the use of either immunocompromised or immunodeficient hosts to study the *in vivo* allotransplanted or xenotransplanted tumour cells [41]. These models have lead to many discoveries, such as the up-regulation of tumour determinants integrin β4, ezrin, clusterin, decorin, and ceruloplasmin, which are all involved in cell motility, adhesion, and angiogenesis, and could potentially be used as markers for tumour aggression. Ezrin, a member of the ezrin-radixin-moesin (ERM) family, has been shown to be necessary for metastatic behaviour in murine osteosarcoma and rhabdomyosarcoma, as suppression of ezrin significantly reduced the metastatic behaviour in both models [52-54]. Also elucidated was the mechanism by which the epiphyseal growth plate is able to function as a barrier for the progression of osteosarcomas, it was determined to be from two anti-angiogenic factors: pigment

epithelium-derived factor and chondromodulin [41]. A third cell line revealed that its higher metatastic potential is due to increased expression of MMP-2, -9, and VEGF facilitating neovascularization at the site of metastasis, providing the tumour with a higher metastatic potency [reviewed in [41]]. Further understanding of the molecular mechanisms that underlie the pathogenesis of osteosarcomas and discovering the critical factors required for metastasis will aid greatly by providing greater clinical predictors of outcome and provide rationals for targeted therapies [32].

## 1.7 Osteoarthritis

### *1.7.1 Etiology and General Features*

Osteoarthritis (OA), also known as degenerative joint disease, degenerative arthritis, osteoarthrosis, or hypertrophic arthritis, is one of the most frequent and symptomatic diseases in both middle aged and elderly populations [55-57]. It is present in both men and women of all ethnic groups and geographic locations. It is the most common cause of long-term disability in people aged 65 years and over [55, 57]. OA is characterized by the progressive loss of articular cartilage, accompanied by its attempted repair, remodelling and sclerosis of subchondral bone, and in many instances the formation of subchondral bone cysts and marginal osteophytes [57]. In severe cases OA can result in crippling deformity and joint instability. OA can lead to a decrease in proteoglycan concentration, alterations in the size and aggregation of PGs, alterations in collagen fibril size and weave, as well as an increase in synthesis and degradation of matrix macromolecules [58]. OA occurs most frequently in the hand, foot, knee, hip, and spine joints, with degenerative changes increasing with age [56, 58]. OA can be classified as idiopathic (primary), which results either from an unknown cause or genetic predisposition (one

example being mutations causing matrix abnormalities, such as type II collagen gene mutations), or classified as secondary, whereby an underlying disease leads to the progression of OA (injury, infection, or hereditary, developmental, metabolic, or neurologic disorders) [29].

OA was once thought to be a degenerative disease due to "wear and tear" and the natural result of aging [58]. It is now believed that OA results from a metabolically-active, dynamic and evolving process that can be triggered by a wide variety of biochemical or mechanical insults [58]. OA is further defined as a group of overlapping diseases which have similar biologic, morphologic, and clinical outcomes, but diverse etiologies. Furthermore, it not only affects articular cartilage, but involves changes in the entire joint which includes the subchondral bone, ligaments, capsule, synovial membrane, and periarticular muscles. The end result is articular cartilage degeneration, with fibrillations, fissures, ulcerations, and full thickness loss of the articular cartilage [59].

### *1.7.2 OA and Genetics*

Genetic studies looking for genes that cause susceptibility to OA are being performed. It is estimated that 50% or more of cases of OA are heritabile [60]. Surprisingly, there is little evidence that common forms of OA are due to mutations in collagen [60]. Linkage studies have pointed to susceptibility genes being located on chromosomes 2q, 9q, 11q, and 16p [60-65]. This has lead to a number of candidate genes being explored which include fibronectin, alpha-2 chain of type V collagen, the interleukin-8 receptor (IL-8R), and the MMP cluster on 11p [60]. A different approach looked for single nucleotide polymorphisms (SNPs) in 24 candidate genes, and found significant associations with such genes as ADAM 12 (a disintegrin and metalloproteinase domain 12), BMP2,

cyclooxygenase-2 (COX2), osteoprotegerin (OPG) and others [66]. A third study found a significant association with a polymorphism in the aspartic acid (D) repeat of the gene encoding asporin (ASPN) and OA [67]. These studies show the number of genes that can potentially play a role in the pathogenesis of OA, and illustrate the complexity of the disease.

Currently, no disease modifying treatments exist for OA. Treatments consist primarily of prevention (promoting joint stability through range-of-motion and muscle exercise, avoidance of certain activities or occupations, and weight loss), symptomatic management (analgesics, anti-inflammatory drugs, and intra-articular steroid injection), and finally joint replacement, performed at the end stage of the disease.

### *1.7.3 Molecules involved in OA and animal models*

OA is a complex disease and numerous molecules are implicated in its progression. Examples include MMPs, ADAMTs, tissue inhibitors of MMPs (TIMPS), aggrecanases, TGF-β, inducible nitric oxide synthase (iNOS), interleukin-1 (IL-1), IL-1 receptor antagonist (IL-1Ra), FGFs, IGFs, and PPARgamma [30, 68, 69]. The players of OA are often classified as being either anabolic or catabolic (Figure 1-10 and Figure 1-11).

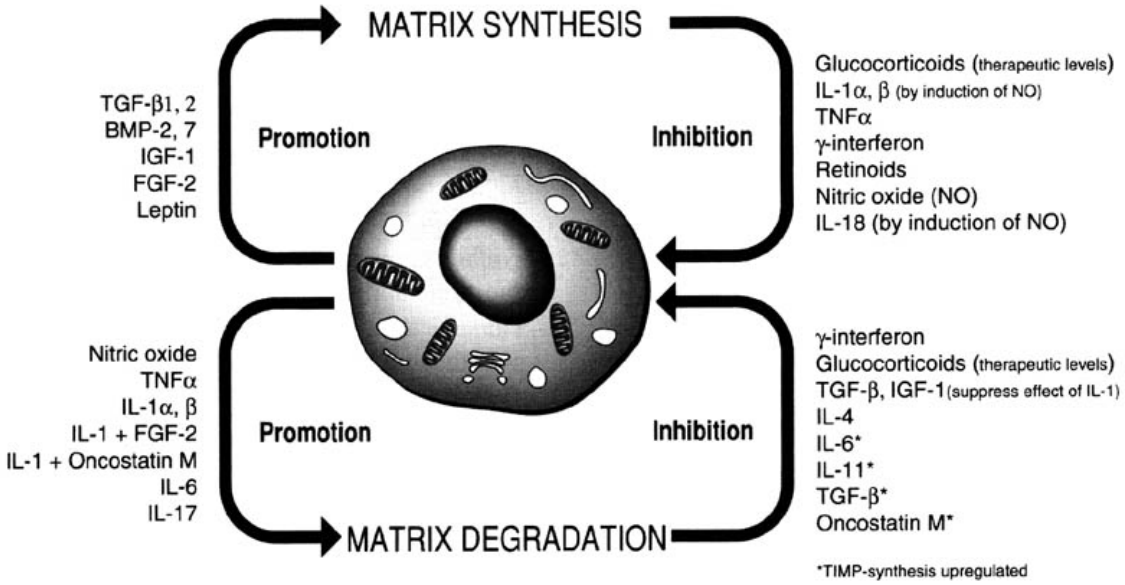


**Figure 1-10. Anabolic and catabolic effects of cytokines, growth factors, and other molecules on the cartilage matrix [30].**

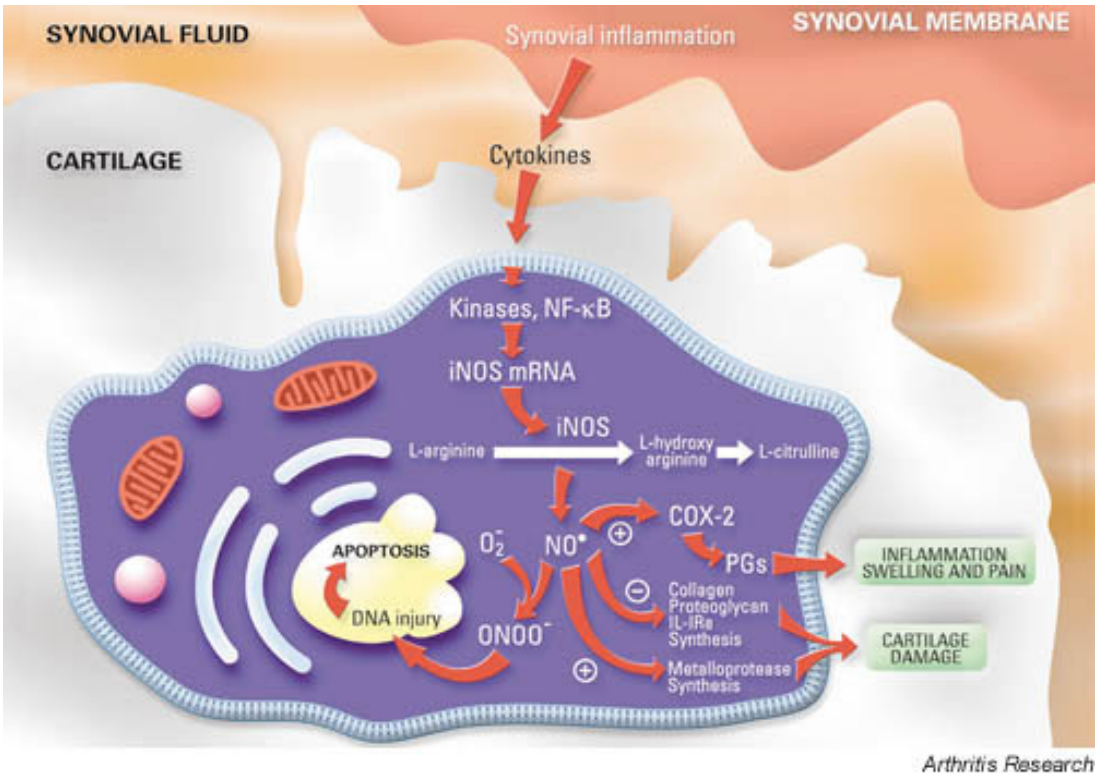


**Figure 1-11. Inhibitory (-) and stimulatory (+) effects of the nitric oxide pathway on articular cartilage. NF = nuclear factor, PGs = prostaglandins, (-) = inhibitory, (+) = stimulatory [68].**

Many studies have been performed in large animal models and *in vitro* characterizing the responses of mammalian cartilage cells to various stimuli [70-72]. Mouse models of OA have also been examined; they can be spontaneous (C57BL/6) [73], chemically induced (by injection with papain, iodoacetate, collagenase) [74], mechanically or surgically-induced (transection of medial collateral ligament, partial medial meniscectomy), or genetically engineered (TGF-β dominant negative, type IX collagen knockout, biglycan knockout, fibromodulin knockout, cho mice, α1β1 integrin knockout, membrane type I MMP knockout, stort, and Cre-*Gdf5/BmpR1a*$^{floxP}$ ) [31, 75-85]. Animal models are crucial for studying the mechanism and pathogenesis of OA, as they could lead to new therapeutic targets that may potentially stop progression of the disease, reverse the damage that has already occurred, or, more ideally, prevent the disease from occurring.

## 1.8 Micro-Computed Tomography

### *1.8.1 An overview of the technique and analysis*

Micro-ct is a powerful tool that provides non-invasive and non-destructive 3-dimensional (3D) analysis of bone. The use of micro-ct has expanded since its inception as a tool for analyzing trabecular bone architecture in 1989 [86]. This first application was for *in vitro* quantification of osteoporotic changes in bone architecture by looking at changes in trabecular bone. More recently these analyses have been extended to cortical bone (Table 1) [87, 88].

**Table 1 Trabecular and Cortical bone quantitative analysis [88]**

TABLE 1. Analogous morphological parameters for trabecular and cortical bone*

| Trabecular bone | Cortical bone |
|---|---|
| Tissue Volume (TV) | Tissue Volume (TV) |
| Bone Volume (BV) | Canal Volume (Ca.V) |
| Bone Surface (BS) | Canal Surface (Ca.S) |
| Bone Volume Fraction (BV/TV) | Cortical Porosity (Ca.V/TV) |
| Bone Surface to Tissue Volume (BS/TV) | Canal Surface to Tissue Volume (Ca.S/TV) |
| Trabecular Thickness (Tb.Th) | Canal Diameter (Ca.Dm) |
| Trabecular Separation (Tb.Sp) | Canal Separation (Ca.Sp) |

*All abbreviations are based upon standard nomenclature (Parfitt et al., 1987).

Analysis of trabecular bone can be divided into two types. The first are those that look at the individual trabeculae (calculate the amount of trabecular bone and individual characteristic of each trabeculae). The second are those that examine the trabeculae as a collective (describe the complex architecture as a whole) [87, 88]. While some analytical techniques translate well from trabecular bone analysis to cortical bone analysis, there remain techniques which are uniquely applicable. For example, while the structural model index (SMI) is useful for examining changes in plate-like versus rod-like trabeculae, it is of greater use to study changes in connectivity of the canal network found in cortical bone [88].

The increase in number of quantification methods has been greatly aided by improvements in imaging technology. While Feldcamp's micro-ct device originally allowed for a spatial resolution of ~60 μm [86], new devices allow for resolutions down to 5 μm. Higher resolutions have been achieved by combining micro-ct with such technologies as synchrotron radiation sources [89] and x-ray microscopy [90], which

yielded resolutions of 1.6μm and 0.6 μm, respectively. While this high resolution can yield excellent detail, this level is not always necessary for quantification of either trabecular or cortical bone. When selecting a desired resolution, one must also consider the trade-off between spatial resolution, sample size, signal to noise ratio, radiation exposure and acquisition time [91].

### *1.8.2 In vivo micro-ct*

One of the newest advances in micro-ct application is the ability to image *in vivo*. This has opened a number of new avenues for researchers in that one can now perform longitudinal studies, which reduces both the variability between samples, and the total number of animals required per study. One of the major concerns is the effects of x-ray dosage when performing weekly scans on the animals. While the dosage is not lethal, there may be effects upon the rate of bone metabolism which could potentially alter experimental results. This is an area that is being actively investigated and additional validation studies into the effect of multiple exposures *in vivo* are needed [92-94]. In theory, *in vivo* scanning will enable one to track bone architecture changes at the level of a single trabeculas. While a delightfully simple concept, the actual approach can be non-trivial. For instance, it would be very difficult to position a leg the same for every scan, partly because one must account for animal growth. To overcome this obstacle, registration algorithms have been created [95]. The algorithm permits a longitudinal study to follow changes in bone architecture while tracking new bone growth in animals. Ultimately, *in vivo* imaging will yield additional insight into the bone remodelling process and disease processes.

### *1.8.3 Micro-ct and soft tissue analysis*

Recently, the use of contrast agents has enabled researchers to study quantitatively the vasculature of soft tissues such as the heart, lung, liver, tumours, and even demonstrate ischemia with high resolution [96-99]. This technique allows further investigation into conditions such as vascular injury, tumorigenesis, coronary artery disease, aneurysm formation, skeletal development, and fracture healing [96]. One main advantage is the ability to look at intact organs at high resolution with preserved structural continuity of the vasculature and, in the case of lungs, bronchial trees [99]. Being non-destructive, micro-ct analysis could be performed and the tissue used later for histologic analysis to provide cellular/molecular information [99]. Micro-ct imaging coupled with an appropriate contrast agent can render high resolution, volumetric, objective, and highly quantitative analysis of vasculature networks [99].

### *1.8.4 Qualitative analysis and examining morphological changes*

Qualitative analysis permits researchers to investigate gross morphological changes. Given the high level of resolution of micro-ct, it is possible to obtain very detailed images of different musculoskeletal areas (Figure 1-12).

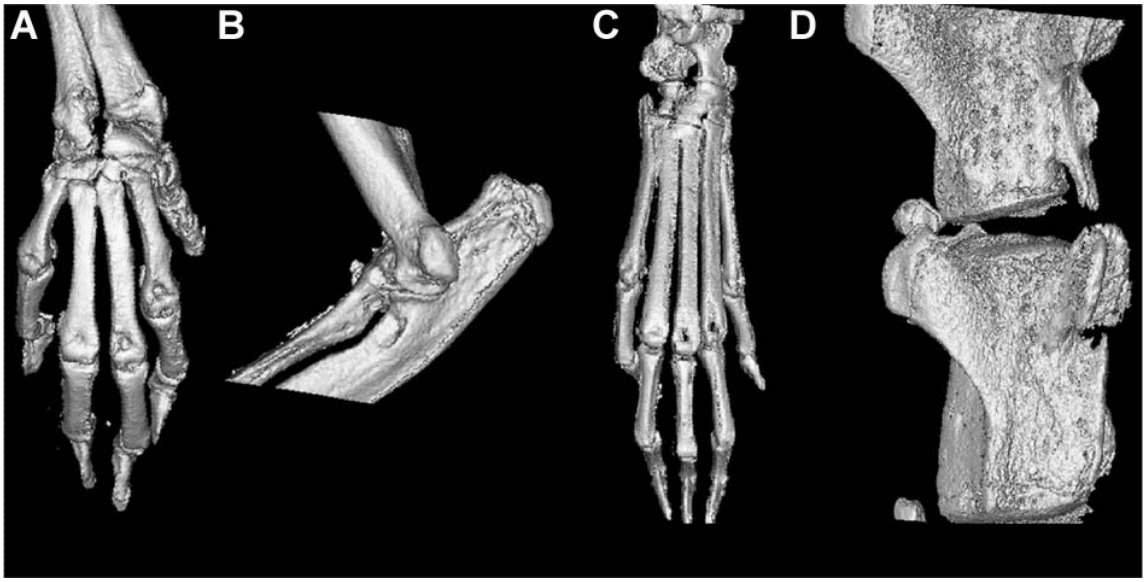


**Figure 1-12. Micro-ct views of mouse skeleton (from left to right): [a] front paw; [b] elbow; [c] hind paw (15μm); [d] 3rd and 4th caudal vertebrae (4.95μm).**

Micro-ct scanning has now become a way to rapidly obtain detailed information about musculoskeletal pathology in 3D, while obviating the need for laborious reconstructions based on the examination of multiple histological sections [100, 101]. To demonstrate this, we examined mice with *progressive ankylosis* (*ank*), a disease characterized by ectopic calcification and joint fusion (see section 1.9). While micro-ct provides exquisite detail of the skeleton, histological analysis is needed to look at soft tissue changes. These two techniques provide complimentary information and we illustrated this by examining murine *bm/bm*, which has a mutation in the gene encoding phosphoadenosine-phosphosulfate syntethase 2 (*Papss2*) [102-106], an enzyme required for sulfation reactions on a variety of different substrates, such as proteoglycans (see section 1.10). Together, the *ank/ank* and the *bm/bm* murine models demonstrate the utility of micro-ct as a sole method of analysis, or in combination with conventional histology.

## 1.9 Progressive ankylosis; a model examined by micro-ct

### *1.9.1 The ank mutation, a phenotypic description*

The *ank* mutation spontaneously appeared in 1973 as a severe autosomal recessive musculoskeletal disorder of mice characterized by spontaneous fusion of multiple joints secondary to new bone formation and ectopic calcification (hydroxyapatite), both within and around the articulations of the limbs and axial skeleton [107, 108]. As a result of this pathology, *ank/ank* mice demonstrate a flat-footed gait due to ankle and foot joint fusion, and over time the ankylosis spreads to involve multiple joints in the extremities as well as the vertebral column. The disease is first apparent at 4 weeks of age at the forefeet and eventually affects all the joints, limbs, and vertebral column. The disease will involve distal joints before proximal, and moves from the forelimb to the hindlimbs [108]. The *ank* mice have an increase in calcified cartilage and joint soft tissue. The disease is also associated with hyperplasia of the cells and tissues of the joints, degeneration within and around the tissues, tendons, and ligaments of the joints [108]. Most recently, joint disease in the *ank/ank* mice was shown to have an inflammatory component (proliferative synovitis) that precedes the calcification [109, 110].

### *1.9.2 ANK signaling and its role in mineralization*

The *ank* mutation has been identified as a nonsense G to T substitution [107] in a gene that encodes a multipass transmembrane protein, ANK, with a putative role in the transport of pyrophosphate (PPi) [107]. PPi has been shown to function as an inhibitor of mineralization within connective tissue matrices. PPi is produced as a by-product of many biosynthetic reactions and via hydrolysis of ATP and other nucleoside triphosphates by nucleotide pyrophosphatase phosphodiesterase (NPP ectoenzymes)

[111-113]. The NPP ectoenzyme of most interest to the *ank* mutant is PC-1, which is required for 30-50% of the extracellular PPi (ePPi) levels in skeletal cells [112, 114, 115]. PPi, made intracellularly by PC-1, is channeled by ANK to the exterior of the cells, leading to the inhibition of mineralization [107, 116, 117]. ALP is thought to play a role in controlling the feedback on this process [118]. *ALP* -/- mice have hypomineralization, which is not too surprising since ALP had been shown to hydrolyze inorganic phosphatases, leading to the formation of basic calcium phosphate (BCP, which includes hydroxyapatite, octacalcium phosphate, and tricalcium phosphate) crystals [118, 119]. In addition to this, crossing *ank* mice with ALP deficient mice lead to a partial rescue of the phenotype [120]. A feedback mechanism for PPi transport is very important since too much ePPi will cause excess calcium pyrophosphate dehydrate (CPPD) and too little leads to deposition of BCP [121]. One suggested mechanism is through osteopontin, a secreted glycoprotein which can limit hydoxyapatite formation and deposition [120, 122, 123]. It is suggested that osteopontin is regulated by PPi, causing inhibition of hydroxyapatite formation [120, 124]. When expression patterns of ANK were investigated, it was found to be high at sites of endochondral ossification and intramembranous bone development, indicating that ANK has a role in inhibiting and regulating mineralization during development of both mineralized and non-mineralized skeletal tissues [125] (Figure 1-13).

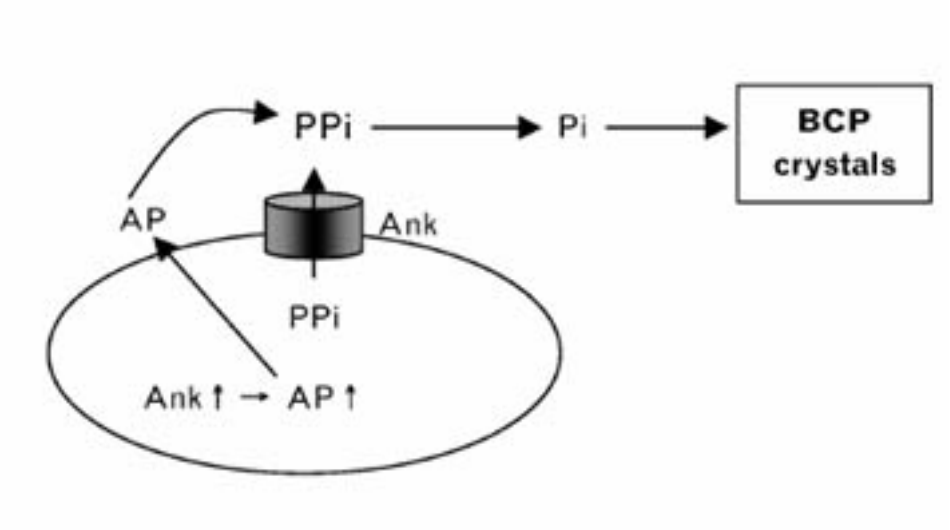


**Figure 1-13. Depiction of ANK's role during physiological mineralization of the growth plate. Chondrocytes from the terminally differentiated growth plate are able to upregulate ANK expression. This in turn is able to increase the efflux of PPi into the extracellular space, whereupon is can be hydrolysed by ALP (which is also upregulated by Ank expression) to form inorganic Pi. Pi is able to further stimulate ALP activity and this will result in the deposition of BCP crystals [119].**

Furthermore it has been shown that TGFβ can regulate ANK translation and PC-1, and could potentially have a role in regulating normal mineralization [125-127].

The *Tiptoe walking* (*ttp*) mutation results from a nonsense mutation in the NPP ectrozyme, PC-1. It is also characterized by excess calcification of ligaments of the axial skeleton, myelopathy, and an abnormal gait [128]. The mechanism of action is different from that of ANK since a double knockout of both *ank* and *pc-1* leads to an increase in soft tissue calcification and further decrease in ePPi levels [120].

### *1.9.3 The ANKH gene*

The human homologue (ANKH) is found on chromosome 5p and two mutations are known to be associated with human disease; craniometaphysal dysplasia [129] and familial calcium pyrophosphate deposition disease (CPPD), both of which result in pathological

calcification of skeletal tissues [117, 130]. ANKH has also been shown to have a role in human OA. Greater than 60% of OA patients have evidence of calcium Pi crystals, hydroxyapatite crystals, or both in synovial fluid. Whether or not the crystals are the primary cause of OA or a secondary phenomenon is still debated [107, 131, 132]. More recently, ANK expression was shown to be upregulated in human OA cartilage. This upregulation is associated with increased calcification, increased expression of MMP-13, and accelerated matrix loss with suppressed collagen and proteoglycan synthesis [112]. Further work is still required to decipher fully the role of ANKH in the balance of the components require for both physiological and pathological crystal deposition in cartilage [119].

### *1.9.4 Thesis goal, approach, and hypothesis*

Traditionally, analysis of the rodent skeleton has been carried out using conventional radiological and histological techniques. With the introduction of micro-ct it has become possible to visualize all aspects of the rodent skeleton as 3D images in exquisite detail. The aim of this study was to illustrate the power of micro-ct scanning as a way to rapidly obtain detailed information about musculoskeletal pathology by examining various skeletal sites of the *ank/ank* mouse. We hypothesized that the *ank* model would show severe ectopic calcification of the joints, which could be easily visualized by micro-ct.

## 1.10 Murine brachymorphism; employing micro-ct and histological analysis methods

### *1.10.1 bm mice; a defect in the sulfation pathway*

Murine *bm/bm* results from an autosomal recessive mutation of *Papss2*, which encodes phosphoadenosine-phosphosulfate syntethase 2 [102-106], an enzyme required for

sulfation reactions on a variety of different substrates. Papss2 is a bi-functional enzyme, with both ATP-sulfurylase and adenosine-phosphosulfate (APS)-kinase activities. After sulfate import into the cell this molecule is converted (by reaction with ATP) into the 'high energy' species, phosphoadenosine-phosphosulfate (PAPS) (Figure 1-14).

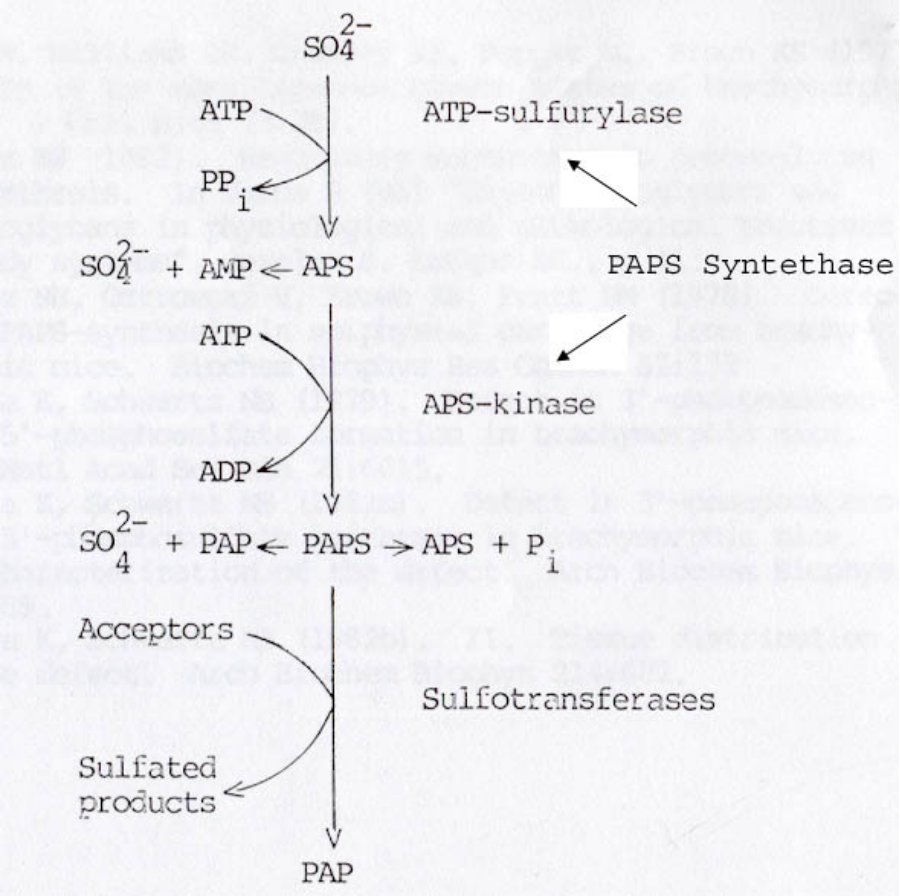


**Figure 1-14. Sulfate activation pathway.**

PAPS is subsequently translocated into the golgi where the sulfate groups are transferred, by a sulfotransferase, onto a variety of different recipient molecules. Sulfate group addition is important in many contexts, including the deactivation or activation of xenobiotics, hormone (e.g. catecholamine) inactivation, elimination of specific end-

products of catabolism, and in maintaining both the structure and function of ECM macromolecules [133]. With respect to the latter, one of the key substrates of sulfation reactions are the GAGs [102, 134], disaccharide units that are covalently linked to the core proteins of proteoglycans.

The *Papss2* defect in brachymorphic mice results from a point mutation causing a Gly to Arg substitution within a highly-conserved region of the adenosine-5'-phosphosulfate kinase domain that greatly impairs enzymatic activity [106]. Although *bm/bm* cartilage contains normal levels of GAGs, these are hypo-sulfated [102, 103, 134], and as a result, less negatively-charged than the GAGs of control cartilage [103]. Although *bm/bm* mouse cartilage matrix contained normal collagen fibrils, proteoglycan aggregate granules were smaller and reduced in number as compared to control mice, particularly in the columnar and hypertrophic zones of the growth plate [134]. It has also been suggested that premature mineralization may occur in the *bm/bm* mice given that hyposulfated proteoglycans are less effective at inhibiting hydroxyapatite deposition [135, 136].

### *1.10.2 Phenotype of bm mice*

The *bm/bm* mouse phenotype is characterized by foreshortened limbs, a short stout tail, and a complex craniofacial phenotype (with a characteristic dome-shaped cranium). Despite these abnormalities, *bm/bm* mice are fertile, and have normal life-spans [137]. Consistent with the role of the Papss2 in sulfate donation, *bm/bm* mice exhibit abnormal hepatic detoxification of specific chemicals, increased bleeding times (attributed to platelet dysfunction), and diminished postnatal growth (due to epiphyseal growth plate

disruption). The latter results in *bm/bm* limbs being ~50% shorter than controls by 4 weeks of age, and axial skeleton length being reduced by ~25%.

### *1.10.3 Spondyloepimetaphyseal dysplasia and PAPSS2*

Recently, a novel form of spondyloepimetaphyseal dysplasia (SEMD) was reported in a Pakistani kindred, that was associated with a truncation mutation of the human *PAPSS2* gene [138, 139]. Affected individuals exhibited various skeletal malformations, including short stature (already evident at birth), short bowed lower limbs (*genu varum*), mild brachydactyly, and kyphoscoliosis [138]. They also exhibited early onset of an OA-like degenerative disease in various joints, including knees, hands, and spine.

### *1.10.4 Thesis goal, approach, and hypothesis*

Degenerative joint disease has not been previously reported in *bm/bm* mice. We hypothesized that, with age, *bm/bm* mice would show cartilage pathology due to the absence of *Papss2*. Our intent was to characterize the changes in the skeletal system of *bm/bm* mice using micro-ct and complement this analysis by histological methods.

## 1.11 PI3K signalling pathway and its regulation

### *1.11.1 The PI3K signalling pathway and downstream effectors*

The *in vivo* role of PI3K signalling in bone and cartilage is poorly understood. We therefore set out to study the role of PI3K, via deletion of *Pten*, in chondrocyte growth, differentiation, and endochondral bone formation.

Members of the PI3K family of lipid kinases have key roles in regulating a variety cellular functions: proliferation, differentiation, cell size control, regulating the translation of proteins, cell migration, control of metabolism, glucose homeostasis, and susceptibility to apoptosis and anoikis **(**Figure 1-15**)** [140-142].

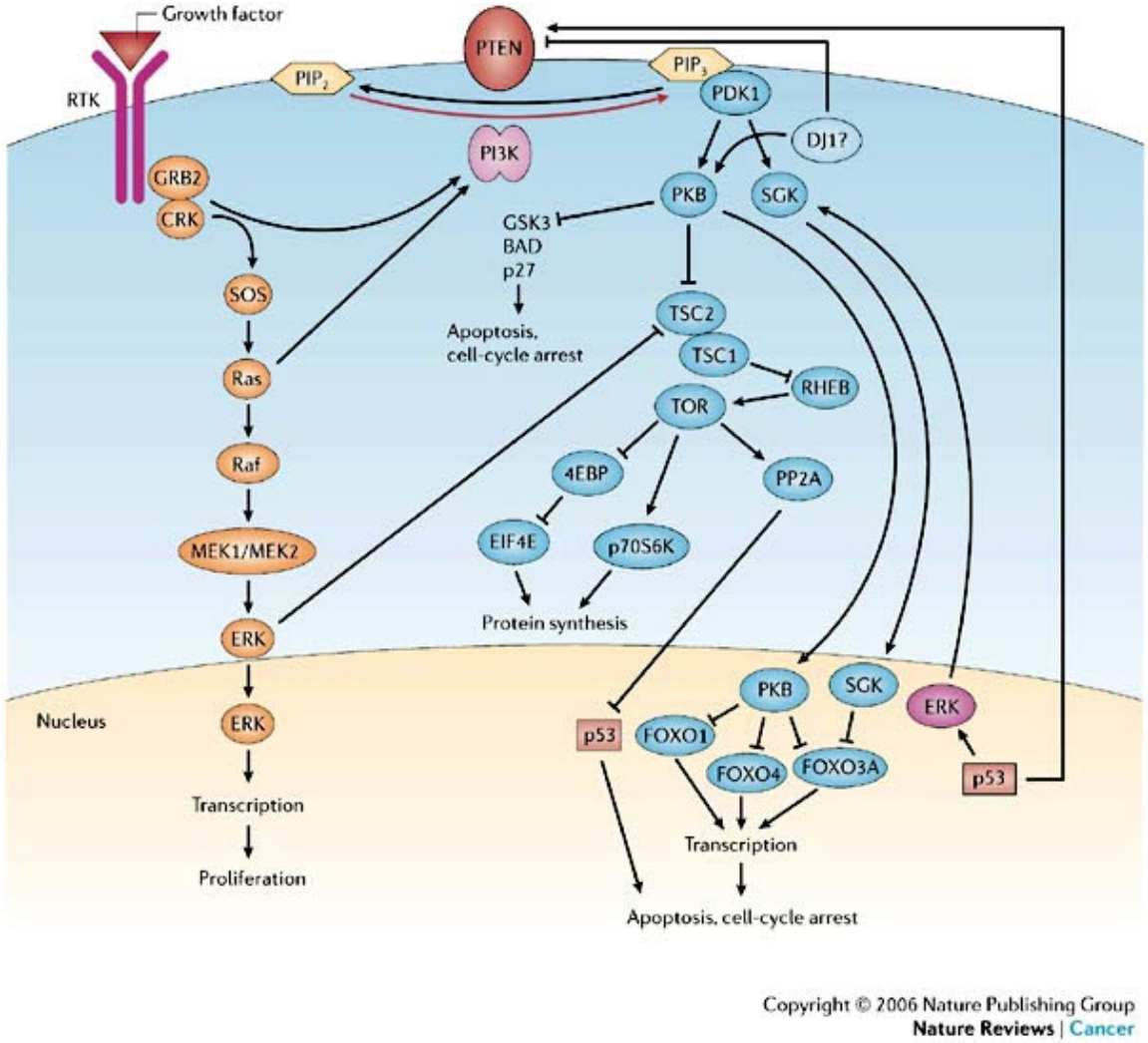


**Figure 1-15. Signaling pathways downstream of PI3K that are regulated via Pten's ability to dephosphorylate PIP3, the product of PI3K activity [143].**

The PI3K pathway comprises of eight members divided into three different classes (class IA and IB, class II, and class III) based on their sequence homology, substrate specificity, and mode of regulation. Class I PI3Ks are divided into two subfamilies. Group IA is activated by growth factors receptor tyrosine kinases (RTKs), while group IB PI3Ks are activated by G-protein-coupled receptors (GPCRs). Members of class Ia form heterodimeric complexes composed of a catalytic (p110) and regulatory (p85, p55, or

p60) subunits. The regulatory subunits contain Src homology-2 (SH2) domains which interact with phosphotyrosines on activated RTKs, triggering the phosphorylation of membrane phosphoinositides. Class IB PI3Ks are composed of a p110γ subunit and a Gβγ subunit of the trimeric G proteins.

Recruitment of PI3K to the membrane by receptors brings it into proximity with its lipid substrate, phosphatidylinositol (4,5)-bisphosphate, PI(4,5)P2, to generate the second messenger via phosphorylation of the D-3 position of the inositol ring, PI(3,4,5)P3. The phosphatidylinositol 3'-phosphatase, Pten (phosphatase and tensin homolog deleted on chromosome 10) [144, 145], an important tumor suppressor in humans, reverses the effects of PI3K by dephosphorylating PI(3,4,5)P3 at the D-3 position, to yield PI(4,5)P2 (Figure 1-16).

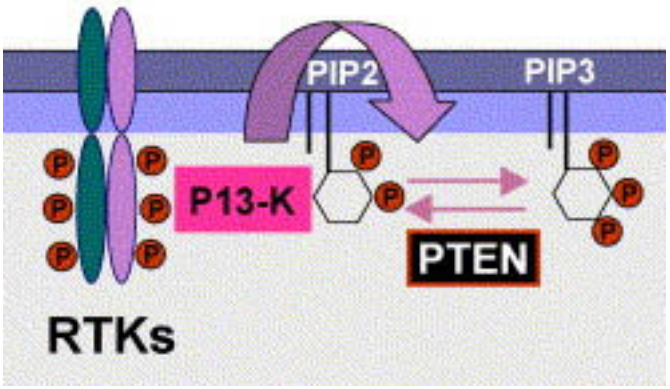


**Figure 1-16. Depiction of how Pten regulates PI3K. Pten is able to inhibit PI3K signalling by dephosphorylating PI(3,4,5) at the D-3 position to yield PI(4,5)P2 [adapted from [146]].**

Thus in cells lacking Pten, levels of PI(3,4,5)P3 remain elevated, leading to sustained activation of PI3K pathways. Of these, the PDK1/PDK2 → Akt/protein kinase B (PKB) axis appears to be the most important, being responsible for many of PI3K's effects [142]

(Figure 1-15). By virtue of its pleckstrin homology (PH) domain, phosphoinositide-dependent kinase 1 (PDK1) initially binds to PI(3,4,5)P3 species in the inner leaflet of the cell membrane, and there it phosphorylates any one of the three PKB/Akt isoforms (Thr308 on Akt-1), which is also recruited to the membrane via its PH domain. For full activation PKB/Akt must also be phosphorylated on Ser473 by PDK2, recently identified as mTOR, a rapamycin-insensitive complex of mTOR/rictor/GβL [147].

PDK1, considered a prime regulator of the PI3K pathway [142], also phosphorylates and activates several other kinases in an indirect, although P(3,4,5)P3-dependent manner [148], including: p70 ribosomal S6 kinase (S6K), serum and glucocorticoid-induced kinase (SGK), possibly p90 ribosomal S6 kinase (RSK) (after ERK-mediated activation), as well as atypical isoforms of PKC (activated by diacylglycerol), thereby increasing their stability [148] (Figure 1-15). The dominant physiological role of the PDK1, however, appears to lie in its ability to regulate the PDK1→PKB/Akt axis [142]. As the knockout of PDK1 is embryonic-lethal, mice with 'floxed' (i.e. part or all of the gene flanked by *loxP* sequences allowing Cre recombinase excisions) PDK1 alleles have been made, and viable Cre-mediated knockouts of PDK1 in liver and heart, with their respective disease phenotypes, have been generated [148-151]. There is also a hypomorphic allele of PDK1, which, when homozygous, leads to a 90% reduction in PDK1, and runty mice [152]. Consistent with its important role upstream of the PKB/Akt →>>>mTOR pathway (see below), loss of PDK1 in these models led (along with other phenotypes) to normal cell number, but reduced cell size [148].

Activated AKT mainly inactivates proteins via phosphorylating proteins on their serine and threonine residues. These include, cell–cycle inhibitor p27, forkhead box

transcription factors (FOXO) [142], glycogen synthase kinase-3 (GSK3) [153], Bcl-cL/Bcl-2 associated death promoter (BAD) [140] and the tuberous sclerosis-2 (TSC2) [154] (Figure 1-15). Phosphorylation of p27 by AKT results in its inactivation and promotes cell cycle entry [143]. When in the nucleus, FOXO is an important effector of cell-cycle progression and apoptosis. It works by acting as a transcription factor for p27, the cell cycle-inhibitor cyclin G2, the pro-apoptotic BIM-1, and FasL [143, 155]. Once phosphorylated by AKT, FOXO is unable to translocate to the nucleus, resulting in increased cell survival and proliferation. GSK3 is able to phosphorylate proteins such as glycogen synthase, c-Myc, and cyclin D rendering them inactive and promoting their degradation [156]. Phosphorylation of GSK-3 by AKT leads to its inactivation, thereby promoting cell cycle, transcription, and translation. In its unphosphorylated state, BAD progresses to the mitochondria, interacting and inhibits the pro-apoptotic factors Bcl-2 and $BCL_{xl}$. Upon phosphorylation by AKT, BAD is restricted to the cytoplasm via its interaction with 14-3-3 proteins [157, 158]. TSC2 is an obligate partner of the TSC1/TSC2 heterodimer, a GTPase activating protein that negatively regulates the small GTPase, Rheb [141, 159, 160] (Figure 1-17).

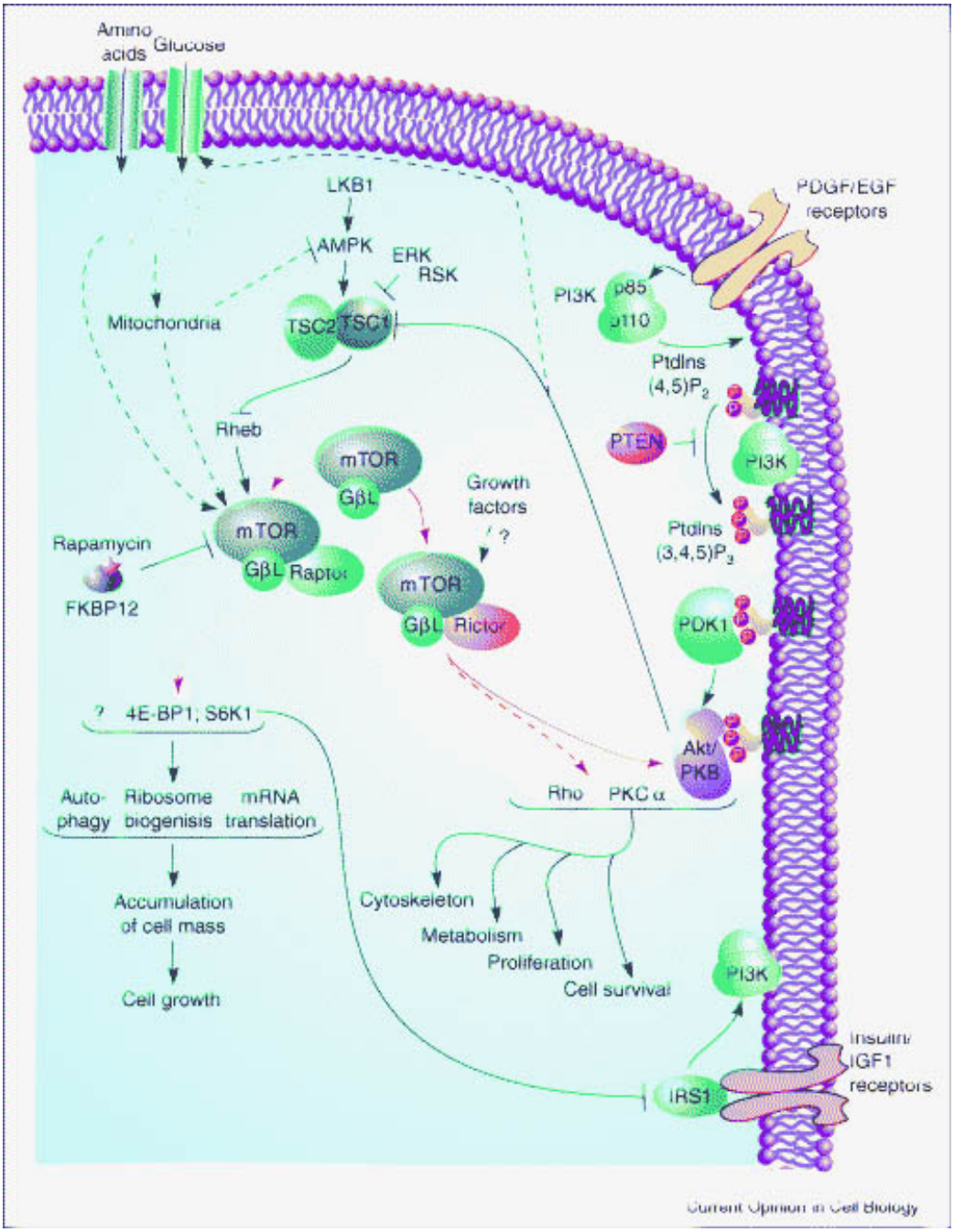


**Figure 1-17. Schematic illustrating the interconnections between the mTOR and PI3K/AKT signalling pathways. mTOR is able to interact with either rictor or raptor, enabling for two branches of signalling of the mTOR pathway. The raptor-mTOR pathway regulates cell growth via S6K and 4E-BP1 as well as other unidentified effectors. The rictor-mTOR pathway regulates AKT/PKB, PKCα, Rho/Rac to control cell survival, proliferation, metabolism and the cytoskeleton [36].**

Rheb, in its active GTP-bound form, stimulates mammalian target of rapamycin, mTOR [154, 159, 160]. When mTOR is in the rapamycin-sensitive complex with raptor and GβL [147], it phosphorylates various substrates most notably activating S6 kinase 1 (S6K1) and inhibiting initiation factor 4E-binding protein 1 (4E-BP1), an important negative regulator of translation [161] (Figure 1-15). These and other mTOR-mediated phosphorylation events stimulate the activity of ribosomal protein translation machinery.

The mTOR- and S61-mediated phosphorylations can lead to increased cell size (hypertrophy), increased production of ribosomal components, increased translation of mRNAs (and increased protein production) and activation of factors promoting translation of mRNAs having highly structured 5'-UTRs [141, 161, 162]. Increased mTOR activity also increases VEGF production, an effect that is enhanced by increased levels of the PI3K and HIF-1α [163-165]; it is therefore unsurprising that deletion of Pten or PI3K activation promotes angiogenesis [166, 167]. This effect is also seen with disruption of TSC1 and TSC2 [168, 169], whose actions negatively-regulate mTOR (within TORCH1) activity.

### *1.11.2 PI3K signalling and the skeletal system*

The PI3K signalling pathway is implicated in skeletal development. Of most interest to our study, *Akt-1/Akt-2* double knockout mice were dwarfed, weighed approximately 50% less, and had delayed ossification of their bones causing severe growth deficiency [170]. This phenotype is similar to that found in the IGF-1 receptor deficient mouse, and it has been proposed that the IGF receptor function during development is heavily dependent on AKT signalling [170]. Also of interest, it was shown that AKT-1 and AKT-2 do not play a role in developmental apoptosis, and that AKT may have a more active role in

maintaining tissue homeostasis and in response to environmental cues [170]. One would hypothesize that over-activation of AKT, via inhibiting Pten, would lead to increased bone formation causing mice to be larger.

The effect of mTOR and HIF-1α on VEGF would be relevant to loss of Pten in hypertrophic chondrocytes as they may be over-producing VEGF [171] owing to: (*a*) the avascular, hypoxic (HIF-1α-inducing) matrix; together with (*b*) increased mTOR activity (lack of Pten leading to increased PKB/Akt-mediated inhibition of TSC1/2 the negative regulator of the Rheb→mTOR pathway) [168, 169] (Figure 1-15). As mentioned above, VEGF, as well as HIF-1α, stimulate chondrocyte survival, angiogenesis and cell influx [172] during endochondral ossification [21, 173-176], and matrix biosynthesis [177]. Interestingly, chondrocyte cultures revealed a role for IGF-1 in promoting proteoglycan synthesis via the PI3K/AKT/mTOR pathway [178].

Research investigating the direct role of PI3K in osteoblasts and chondrocytes has mostly been performed *in vitro*. Different pathways of cell survival were shown to be regulated by PI3K signalling, such as by IGF-1 expression in chick limb bud mesenchymal cells and murine mesenchymal cells [179, 180], FGF-2 in cultured osteoblasts [181], and BMP-2 in prehypertrophic chondrocytes [182]).

PI3K has also been postulated to have a role in osteoblast and chondrocyte differentiation. IGF-1 could inhibit NO-induced dedifferentiation in articular chondrocytes and stimulate chondrogenesis via the activation of PI3K [179]. Runx2 is able induce both osteoblast and chondrocyte differentiation and enhances their migration and coupling via PI3K-Akt signalling [183]. Cell migration is thought to be important for

precursors of either osteoblasts or chondrocytes to migrate to their appropriate sites during skeletal development, and during bone remodelling by inducing osteoblast migration to bone surfaces undergoing osteoysis by osteoclasts [183]. Runx2 enhances PI3K-Akt signalling through upregulation of PI3K subunits and Akt, PI3K signalling in turn is able to enhance DNA binding of Runx2 and Runx2 dependent transcription, forming a positive feed back loop [183]. It has been further shown that in osteoblasts, Akt phosphorylation of GSK-3 and subsequent activation of β-catenin can lead to the expression of both ALP and Runx2 [184, 185], two important markers of bone mineralization.

### *1.11.3 Pten, a negative regulator of the PI3K signalling pathway*

As previously mentioned, Pten is a negative regulator of the PI3K signalling pathway. First discovered in 1997, this tumour suppressor was mapped to cytoband 10q23 [186-188], an area associated with somatic mutations in malignant tumours which results in either the total or partial loss of Pten mRNA or protein, or total inactivation of its phosphatase activity [144]. Genetic mutations causing *PTEN* germline heterogozity can lead to Cowden's disease, Lehrmitte-Duclos disease, Bannayan-Zonana syndrome, and Proteus syndrome, all of which are characterized by the development of harmartomas, and other benign tumours. Pten is a protein and lipid phosphatase capable of dephosphorylating any serine-, threonine-, or tyrosine- phosphorylated peptide [189]. Structurally, Pten has a catalytic domain that is critical for its tumour suppression activity [190], a C2 domain for binding to lipids and perhaps mediating the binding of Pten to the cell membrane [190], and a C-terminal tail containing a PDZ domain which facilitates the interaction of Pten with other PDZ containing proteins. Phosphorylation of three residues

(S380, T383, and T383) within the tail are necessary for maintenance of protein stability and alterations within this region can cause inhibition of PTENs function [191-194]. A negative regulator of Pten has yet to be identified and is a active area of research. Very recently a study has identified the histone acetyltransferase, PCAF (p300/CBP-associated factor), as a potential regulator of Pten. PCAF is thought to acetylate Pten in the nucleus, causing inhibition of Pten-regulated cell cycle arrest [195]. Validation studies will be needed to further investigate this mechanism *in vivo*.

### *1.11.4 Examining the role of PI3K signalling in vivo*

Global deletion of Pten in mice leads to embryonic lethality. Therefore, early work examining the PI3K signalling pathway was performed on Pten heterozygotes. With the ability to specifically knockout a gene of interest in a tissue specific manner, there has been much work on generating tissue specific knockouts using the Cre/*lox*P system (see section 1.11.5). This system has been utilized to remove Pten from many cell types such as T and B cells, brain cells, cardiomyocytes, mammary gland cells, and keratinocytes leading to resistance in apoptosis, increased proliferation, tumourigenesis, increased cell size, and migration [196-202].

### *1.11.5 Conditional knock out mice*

The Cre/*lox*P system is a widely used technique for the generation of conditional knock-out mice. This technique is important since it permits for the generation of null alleles at a later stage in development, thereby bypassing any embryonic lethality and more closely represents a model of human disease where a gene loses its function due to a somatic mutation. The Cre-lox system can be utilized for gene activation [203], gene inactivation [204], and deletion of large chromosomal regions [205]. This system works by having a

site specific recombinase catalyze the recombination between two consensus DNA sequences. This can result in either a new function or loss of function of a locus [206]. Cre recombinase is a P1 phage-derived site-specific DNA recombinase. This DNA recombinase recognizes and mediates the recombination between 34 base pair sequences, called *loxP* sites. Cre does not require any accessory proteins or cofactors to mediate *loxP*-specific recombination and its optimal activity is at 37$^{o}$C [207]. A *loxP* site contains two 13 base pair repeats with an 8 base pair asymmetric space that determines the orientation of the *loxP* site (Figure 1-18a).

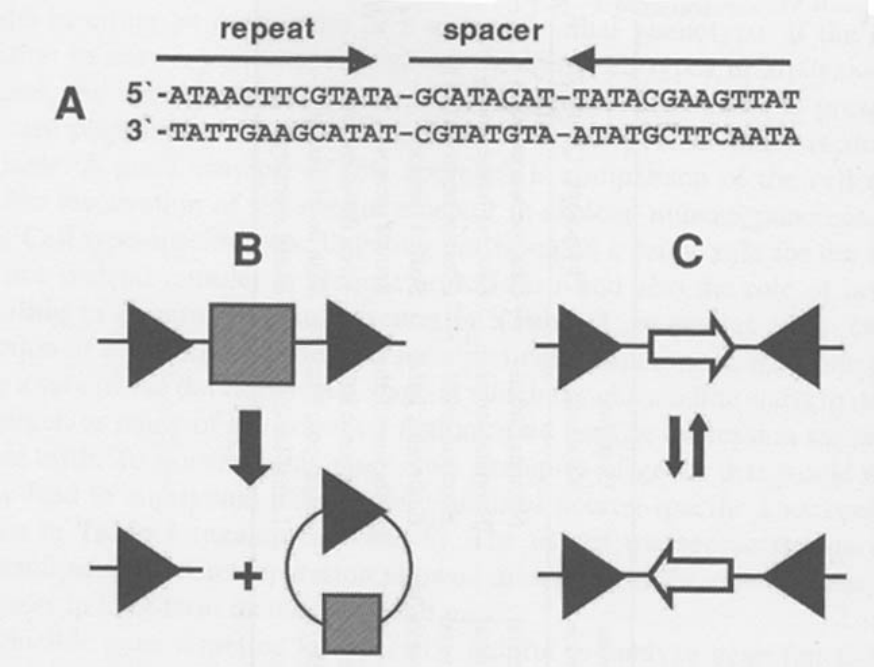


**Figure 1-18. The Cre/lox system. (A) The sequence of the *loxP* site. It is composed of two 13 base pair repeats separated by a 8 base pair asymmetric spacer sequence, this sequence determines the orientation of the *loxP* sites. (B) If the *loxP* (triangles) sites are facing in the same direction, the Cre recombinase will delete the DNA segment (square) flanked by the lox P site. (C) If the *loxP* sites are in opposite directions, a Cre-mediated inversion will occur [208].**

When the two *loxP* sites are facing in the same direction, Cre mediated recombination excises the DNA between them. If the two *loxP* sites are facing in opposite directions, a Cre-mediated inversion of the DNA flanked by the two *loxP* sites takes place (Figure 1-18b and c). If the *loxP* sites are located on different strands of DNA, Cre can mediate intermolecular translocations [208]. The Cre-lox system can be further regulated by controlling the expression pattern on the Cre recombinase. Using tissue specific promoters, expression of the Cre recombinase can be directed to the tissue of choice. One would then cross the tissue-specific Cre with a mouse containing a gene flanked by two *loxP* sites to generate a tissue specific knockout (Figure 1-19).

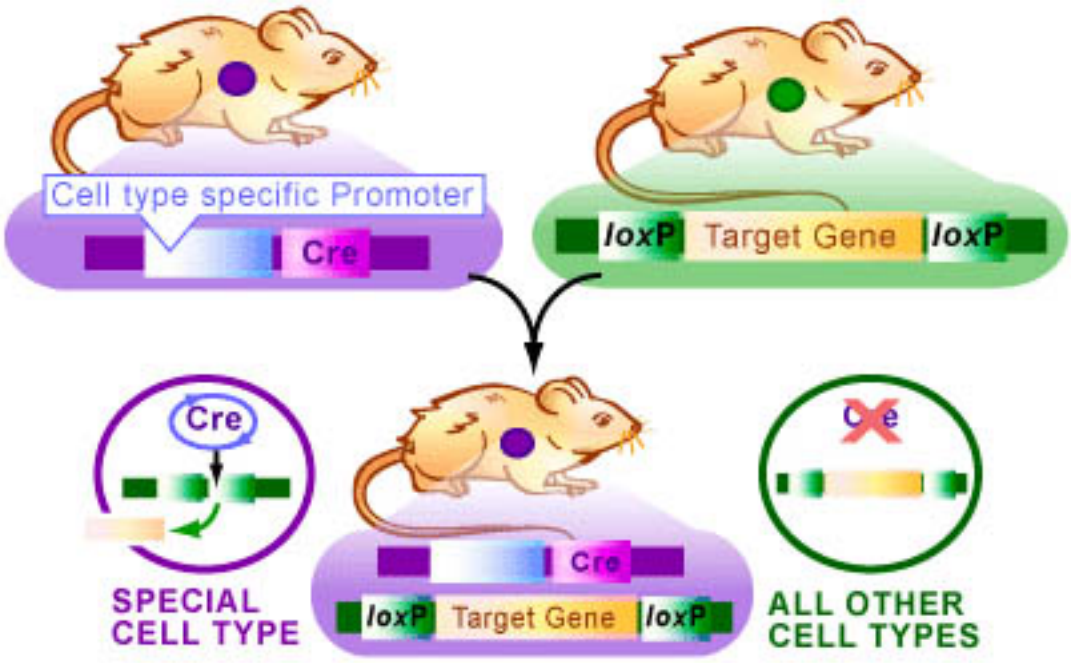


**Figure 1-19. Schematic illustrating spatial control of the Cre-lox system. A mouse containing the Cre recombinase is driven by a tissue specific promoter is bred with a mouse containing the gene of interested flanked by two loxP sites. Some of the resulting progeny will then have the gene excised in the tissue of interest (taken from www.bioteach.ubc.ca/MolecularBiology/TargetingYourDNAWithTheCreloxSystem)**

### 1.12 Thesis goals, approach, and hypothesis

In view of the demonstrated importance of PI3K signaling pathways to maintenance of normal tissue homeostasis and in disease pathogenesis [196-202], this study was carried out to examine the role of this pathway in the regulation of skeletogenesis. To achieve this goal, Cre/*lox*P technology was used to effect the disruption of a key negative-regulator of the PI3K pathway, Pten [144], in chondrocytes. To generate a chondrocyte-specific knockout, we chose the type II Collagen (*Col2a1)Cre*-recombinase. Col2a1 is the major structural component of cartilage. Originally, *Col2a1*Cre activity was reported to lead to gene activation in sclerotomal cells of the developing spinal column and in chondrocytes. During development, the *Col2a1* promoter is also known to direct expression of the Cre transgene in notochordal cells and a subset of neuroprogenitors [209]. However, *Col2a1Cre*-recombinase was very recently found to be active in osteo-chondroprogenitors, meaning that both osteoblasts and chondroblasts could potentially exhibit Cre-mediated genetic changes [210], [211].

We hypothesized that loss of the *Pten* gene in chondrocytes would increase responses of these cells to extracellular stimuli that activate the PI3K pathway. More specifically, we hypothesized that the tissue specific knockout of Pten in cartilage would produce the following effects: (1) increased growth of bone that depended on cartilage growth, (2) an enlarged hypertrophic zone in growth plate and a decreased proliferative zone, stemming from cells moving faster through the different parts growth plate and not undergoing apoptosis, (3) increased expression of Type X Collagen and VEGF in the hypertrophic zone due to the increased number of hypertrophic cells, (4) increase in cell size in the

proliferative zone as this has been observed in other tissues in Pten deleted phenotypes, (5) presence of chondrosarcomas stemming from loss of this tumor surpressor.

# Chapter Two: Material and Methods

*Author's contribution note*: Histology sections and staining (with hematoxylin, fast green, and safranin-O) of joints was performed by a research technician, Ms. R. Seerattan (University of Calgary). Soft tissue histology was processed by the Calgary Laboratory Services. Sectioning and staining (with hematoxylin and eosin) was performed by the Centre for Mouse Genomics (University of Calgary).

## 2.1 Ank Study

### *2.1.1 Animals:*

Mice homozygous for the *ank/ank* mutation on a C57BL/6J background were obtained from The Jackson Laboratories (Bar Harbor, ME). Controls consisted of two 4 month old female C57BL/6J mice, as well as 4 additional female mice 7-13 months of age. All *ank/ank* mice examined were female, 4 months of age. Mice were maintained in a barrier facility in accordance with University of Calgary and Canadian Council on Animal Care guidelines, and euthanized by $CO_2$ inhalation. In preparation for scanning, limbs were removed at the level of the hip and shoulder joint. The proximal portion of the tail was isolated for intervertebral joint examination. As we showed that cryopreservation did not significantly alter the micro-ct morphology of bone and joint samples, all skeletal samples were stored at $-20^{o}C$ prior to analysis [101].

### *2.1.2 Micro-ct analysis:*

Samples from *ank/ank* mice, and controls were scanned using a SkyScan 1072 (Aartselaar, Belgium) x-ray microtomograph, using a cone-beam configuration with standardized x-ray tube settings of 100 kV and 100 μA. All appendicular joints were scanned at an isotropic voxel resolution of $15.19\mu m^3$ with an exposure time of 1.3 seconds and a rotation step of

0.90°. To obtain higher spatial resolution, the tail segments were scanned at a voxel resolution of 6.84μm$^3$ and exposure time of 2.1 seconds with a rotation step of 0.45°. These protocols produced serial cross-sectional 1024 x 1024 pixel images. These image files were cropped in Scion Image, beta 4.0.2 (Scion Image Corporation) and then exported to ANALYZE 4.0 (Mayo Clinic, Rochester, MN, U.S.A.) for volume rendering. Median filtration was used to reduce image noise and improve 3D visualization of joint structures.

## 2.2 Brachymorph Study

### *2.2.1 Animals*

Mice homozygous for the *Papps2* gene mutation, *bm/bm*, on a C57BL/6J background were obtained from Jackson Laboratories (Bar Harbor, ME, USA). Six C57BL/6J control mice (3 males and 3 females) were examined at 12-14 months of age, and four (1 male and 3 females*)* at 6-9 months. Six *bm/bm* mice (3 males and 3 females) were examined at 12 months, and three at 6-7 months of age (2 males and 1 female). Mice were maintained in a barrier facility in accordance to University of Calgary Animal Care Committee and Canadian Council on Animal Care guidelines, and euthanized by $CO_2$ inhalation. Limbs to be scanned were removed at the level of the hip and shoulder. Following dissection, limbs to be examined by histology were immediately placed in 10% neutral buffered formalin for fixation and then processed for histological examination. Skeletal samples to be examined by micro-ct were stored at -20$^o$C. We have established that cryopreservation does not alter the morphology of skeletal samples for micro-ct [101].

### *2.2.2 Micro-ct analysis*

*Author's contribution statement:* 3D thickness of tibial plateau was measured and analyzed by Dr. B. Hallgrìmsson (University of Calgary) and Dr. D.M.L. Cooper (University of Calgary).

Intact limbs were scanned using a Skyscan 107 (Aartselaar, Belgium) as described in section 2.1.2. Two isotropic scan resolutions, 15, and 5 microns, were used for the visualization of gross limb morphology, and morphometric analysis of proximal tibial subchondral plates, respectively. 3D volumetric renderings were produced using Analyze 5.0 (AnalyzeDirect, Lenexa, KS). Software provided with the scanner was used to measure the 3D thickness distributions of the tibial plateaus, using a model-independent method [214]. The proximal articular surfaces of the tibia were segmented manually prior to morphometric analysis using the same software.

### *2.2.3 Histology*

*Author's contribution statement:* OA scoring was performed by Dr. P. Salo and Ms. R. Seeratten (University of Calgary).

Hind-limbs were transected 1 cm above and below the knee joint line, fixed in 10% neutral buffered formalin (Fisher Scientific) for 7 days and then decalcified in either Cal Ex, or Cal Ex II (Fisher Scientific), for 10-14 days at room temperature, with daily changes of the solution. Following decalcification, joints were thoroughly rinsed with water, dehydrated, cleared and then infiltrated using an automatic processor (Autotechnicon Mono 2A). Paraffin wax-embedded tissue blocks were cut (8 μm serial sagittal sections) and mounted on glass slides, with every other slide being sequentially

stained with hematoxylin, fast green, and safranin-O (VWR), and mounted with Permount (Fisher). The complete set of serial alternate sections of each knee joint were examined on a Leitz DMRB microscope (Leica). Joints were individually assessed by the grading system of Maier and Wilhelmi [215, 216], with scoring is based on a scale of 0 to 4, with 4 being the most severe (Figure 2-1). Statistical analysis of OA scoring was performed using a Mann-Whitney (Wilcoxon) test.

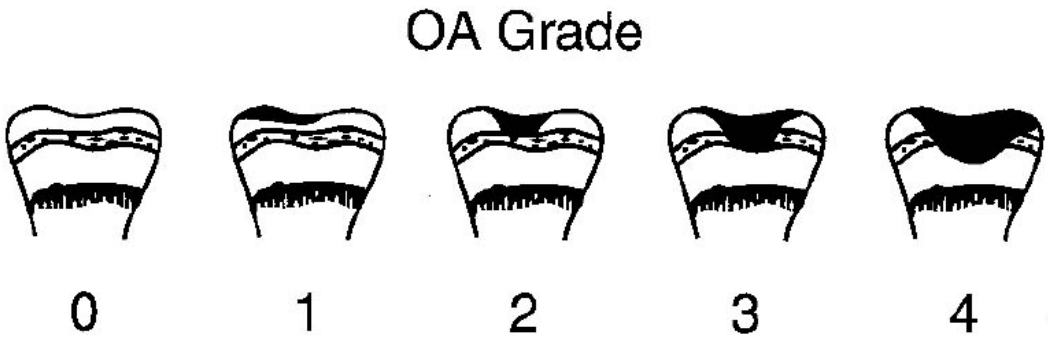


Grade 0: joint surface intact.
Grade 1: superficial fissuring and fibrillation.
Grade 2: small "punched out" defects, no deeper than the tidemark.
Grade 3: shallow defects extending into calcified cartilage, subchondral sclerosis.
Grade 4: deep defects extending into bone, eburnation, prominent osteophytes.

**Figure 2-1. OA grading adapted from Maier and Wilhelmi 1987 [215, 217].**

## 2.3 Pten Study

### *2.3.1 Animals and PCR genotyping procedures*

Mice were maintained in a barrier facility in accordance with University of Calgary and Canadian Council on Animal Care guidelines, and euthanized by $CO_2$ inhalation. *Pten*$^{flox/flox}$ mice, on a mixed C57BL/6J x 129 genetic background [198], were kindly provided by Dr. T.W. Mak, Ontario Cancer Institute. After 3 backcrosses to C57BL/6J these mice were mated with the mixed background (SJL/J x C57BL/6J) *Col2a1Cre* transgenic line [218] (Jackson Laboratory) to generate mice hemizygous for both the floxed *Pten* and the *Col2a1Cre* transgene loci: these animals (of mixed genetic background) were then interbred to yield not only the experimental group, *Pten*$^{flox/flox}$*:Col2a1Cre*, but also the littermate controls for the experiments, which consisted of either *Pten*$^{flox/flox}$ and *Pten*$^{flox/wt}$ mice. Weights of control and *Pten*$^{flox/flox}$*:Col2a1Cre* mice where recorded from 3 to 15 weeks of age.

For genotyping, genomic DNA was isolated from tail tips or soft tissue, incubated overnight at 55˚C in lysis buffer (50 mM Tris pH7.5, 50 mM EDTA, pH 8.0, 5% SDS) and 1 mg/mL proteinase K (Sigma). The solution was then vortex with 2.4 M ammonium acetate, and spun at 14 000 rpm for 5 minutes. The supernatant was collected, and then DNA was then precipitated with 100% ethanol, followed by a wash in 70% ethanol, and reconstituted in 10mM Tris for PCR analysis. PCR to detect the Cre transgene employed the following primers: Cre5' (ATT TGC CTG CAT TAC CGG TC) and Cre3' (ATC AAC GTT TTC TTT TCG G). DNA was amplified for 32 cycles of denaturation at 94 $^{o}$C for 45s, annealing at 52 $^{o}$C for 45s and elongation at 72 $^{o}$C for 45s. To detect Cre recombinase-mediated loss of floxed *Pten* alleles, a PCR, previously designed in the lab,

was performed using the following primers: Ptenflox1F (AAA AGA GTA AAG GTC TGG CTT ACA A), Ptenflox2F (TGT CAT AAT GTC TCT CAG CAC ATC), and Ptenflox3R (TCT GAC ACA GCC TAC TTT AAT TGG). DNA was amplified for 35 cycles of denaturation at 95 $^{o}$C for 1 min followed by annealing and elongation for 1 min each at 55 $^{o}$C and 72 $^{0}$C respectively. These primers generated 3 PCR products: 600 bp wild-type *Pten*, 800 bp floxed *Pten* post-excision, and 1.5 kb floxed (un-excised) *Pten* fragments.

### *2.3.2 Chondrocyte Isolation*

Chondrocytes were isolated from the ventral parts of the rib cages of 1 to 3 day old mice from control and *Pten$^{flox/flox}$:Col2a1Cre* mice as previously described [219, 220]. In summary, rib cages were rinsed with PBS, incubated in Pronase (2 mg/ml in PBS, Roche) for 30 minutes at 37˚C, rinsed again with PBS, and then incubated in bacterial collagenase (3mg/ml collagenase D, Roche) in high glucose Dulbecco's modified Eagle's medium supplemented (DMEM, Gibco-BRL) supplemented with 10% heat inactivated fetal bovine serum (FBS), penicillin (25 units/ml), and streptomycin (25 μg/ml), for 1 hour and 30 minutes at 37˚C under 5% $CO_2$. Cartilage was washed twice with PBS and digested again in 3.5 mg/ml Collagenase D in high glucose DMEM (as described above) for an additional 3 hours and 30 minutes at 37˚C under 5% $CO_2$. For immunohistochemistry, isolated chondrocytes were cultured onto 6 well dishes in suspension over 1.5% agarose in PBS to maintain their chondrogenic phenotype. After 3 days the chondrocyte clusters were digested with collagenase D (3 mg/ml), washed 1x media, then 1x PBS, and finally cells were cytospun onto Superfrost slides (Ficher) for

immunohistochemistry (see section 2.3.3). For excision PCR, isolated cells were washed 1 x in media, and 2 xs in PBS, collected and processed as described in section 2.3.1.

### *2.3.3 Histology and immunohistochemistry*

*Author's contribution statement*: Collagen type X and osteopontin immunohistochemistry was performed by Dr. Z. Ali (University of Calgary).

Knee joints from 1 week-old mice were fixed in 4% paraformaldehyde (PFA) for 1 week and decalcified in 14% EDTA for 1 week; knees obtained from 6 and 15 week old mice were fixed for 2 weeks and decalcified for 3 weeks; knees obtained from animals of 6 months and older were fixed for 2 weeks and decalcified for 4 weeks. Joints were then rinsed in water, dehydrated, cleared and infiltrated using an automatic processor (Autotechnicon Mono 2A) before embedding in paraffin wax. For histology, 8 μm serial sagittal sections were cut and mounted on glass slides, with every other section stained with hematoxylin, fast green, and safranin-O (VWR). For soft tissue, samples were fixed in 10% formalin (Fisher) for a minimum of 24 hours, and processed by Calgary Laboratory services. Blocks were sectioned at 4-5μm thickness and stained with hematoxylin and eosin. For immunohistochemistry, rabbit polyclonal anti-rat collagen type X (Calbiochem, cat #234196) was employed; paraffin sections were digested with hyaluronidase prior to incubation at 1 in 60 dilution of the antibody overnight at 4 $^{o}$C. An anti-rabbit antibody detection kit (Vector labs ABC kit) was then used where the secondary antibody was added for 45 minutes at room temperature. A rat monoclonal anti-mouse CD31 (BD Pharmingen, cat #550274) was used on frozen sections that had been first heated for 2 hours at 37 $^{o}$C, with the primary antibody used at a 1 in 50 dilution and left overnight at 4 $^{o}$C. An anti-rat secondary (Vector labs ABC kit) was then left on

for 3 hours and detected with an anti-rat detection kit (Vector labs). Rabbit polyclonal anti-mouse collagen type I (Chemicon, cat # AB756P) was used on paraffin sections. Rehydrated slides were placed in 1% Triton X-100 for 30 minutes; the primary antibody was used at a 1 in 40 dilution overnight at 4$^{o}$C. An anti-rabbit antibody detection kit (Vector Labs ABC kit) was then used where the secondary antibody was added for 1 hour at room temperature. Rabbit anti-mouse osteopontin (IBL, cat #18621) was used on paraffin sections at a 1 in 200 dilution overnight at 4 $^{o}$C. An anti-rabbit antibody detection kit (Vector ABC kit) was then used where the secondary antibody was added for 1 hour at room temperature. For isolated chondrocytes, cells were fixed in 1:1 acetone:methanol for 10 minutes prior to overnight incubation with 1:100 rabbit anti-rabbit Pten (Cell Signalling, cat # 9559), or 1:50 mouse anti-mouse phospho-Akt (Cell Signaling, cat # 4051). An anti-rabbit, for Pten signal, or anti-mouse, for phospho-Akt signal, detection kit (Vector Labs ABC kit) was used then used, where the secondary antibodies were added for 1 hour at room temperature

### *2.3.4 Stereological Analysis*

*Author's contribution statement*: Sterological analysis technique was taught by Dr. J Matyas (University of Calgary).

To determine growth plate volumes, total cell number, area fraction (cells versus ECM), and cell size within the growth plates, a Zeiss Axioplan2 (Bernried, Germany) light microscope was used in conjunction with the StereoInvestigator software package (MicroBrightField, Colchester, Version 7.0). Manually drawn contours around the proliferative and hypertrophic region was performed on eight sections per control (n=3) and *Pten$^{flox/flox}$:Col2a1Cre* (n=3) mouse, this allowed for the computation of an estimated

volume ($\mu m^3$) for each region. All quantification was done at a magnification of 630x using a 25μm counting frame on a 200μM grid placed on a random orientation. The number of cells within both the proliferative zone and hypertrophic zone were quantified by use of the optical fractionator probe, permitting for unbiased estimates. The nucleator probe was used in conjunction with the later probe to measure cell size of both proliferative and hypertrophic cells. Lastly, the area fractionator probe was used to discern the ratio of cells to ECM within both regions of the growth plate. Statistical analysis was performed using a 2-tailed Student t-test.

### *2.3.5 Embryo Clearing*

Embryos were euthanized at 18.5 dpc by Euthanyl injection, then scalded in 60˚C water, and skin and muscle was removed. All embryos were placed in 95% ethanol for 3 to 5 days, placed for 24 hours in Alcian blue (1.5mg/ml in 80% ethanol (95%) and 20% glacial acetic acid) stain, washed two times with 95% ethanol, then placed in two changes of 95% ethanol for 24 hours. Embryos were cleared for 24 hours 1% KOH , then stained with in Alizarin Red (50μg/ml in 2% KOH) for one hour. Clearing continued in 2% KOH for 3 to 5 days at 4˚C. Once cleared, embryos were passed through graded 2% KOH:glycerol (80:20, 60:40, 40:60, 20:80). Images where then taken using the Zeiss Stemi SVII (Bernried, Germany) light microscope.

### *2.3.6 β-galactosidase, ALP, and TRAP staining procedures*

*Author's contribution statement*: β-galactosidase and ALP staining was performed by Dr. Z. Ali (University of Calgary).

Mice were euthanized and the knees were harvested and cut in half. Tissues were fixed in 4% paraformaldehyde for one hour at 4 $^{o}$C. Tissues were then rinsed three times 15

minutes in rinse buffer containing 5 mM EGTA , 0.01% deoxycholate, 0.02% NP40, 2 mM $MgCl_2$ in PBS. Tissues were stained at 37 $^oC$ for 2 hours in 5 mM $K_3Fe(CN)_6$, 5 mM $K_4Fe(CN)_6$, 5 mM EGTA, 0.01% deoxycholate, 0.02% NP40, 2 mM $MgC1_2$, and 1 mg/ml 5-bromo-4-chloro-3-indolyl-β-galactosidase (X-gal) in PBS. The knees were re-fixed in 4% paraformaldehyde overnight and then decalcified in 14% EDTA for 3 days prior to paraffin embedding; 8 μm serial sagittal sections were mounted onto glass slides and counterstained with eosin. ALP staining was performed on frozen sections warmed for 2 hours at 37 $^oC$ and rehydrated in TBST. Sections were incubated in ALP-developing solution (100 mM Tris-HCL, 100 mM NaCl, 5 mM $MgCl_2$, 0.05% Tween-20%), containing 0.45 mg/ml 4-nitro blue tetrazolium chloride (NBT) (Roche) and 0.175 mg/ml 5-bromo-4-chloro-3-indolyl-phosphate (BCIP) 4-toluidine salt (Roche) for 2 hours, rinsed in water, and then mounted on slides. Tartrate resistant acid phosphatase (TRAP) staining was performed on paraffin sections using the acid phosphatase kit (Sigma 387A) with the following changes: slides were incubated at 37 $^oC$ for 28 minutes in the incubation buffer (containing acetate buffer, tartrate buffer, napthol AS-BI, and $dH_20$, in amounts outlined in kit), diazotized fast garnet GBC solution was added following the incubation and left for 5 minutes at RT. Slides were washed with water and counterstained with hematoxylin (Zymed).

### *2.3.7 X-Ray and micro-ct*

Animals were sacrificed by $CO_2$ inhalation and x-rays obtained (Phillips Film Diagnostics, 40Kv, 4mAS, SID 130). Lateral x-ray views were used for measuring lengths of spine (from C2 to tip of tail) and anterior-posterior x-ray views were used for measuring femoral length of 15 week control (n=6) and $Pten^{flox/flox}$*:Col2a1Cre* mice

(n=6). For micro-ct analysis, intact limbs were harvested and placed at -20$^{o}$C, as cryopreservation was shown not to change the samples [101]. Micro-ct scanning was performed (VivaCT 40, Scanco Medical, Bassersdorf, Switzerland) on a single tibia at the midshaft and proximal metaphyseal region (55 kV, 145 μA, 400 ms integration time, 2000 projections on 360º, 2048 CCD detector array, cone-beam reconstruction). Nominal isotropic resolution was 10.5 μm, and the analysis region was represented by 212 micro-tomographic slices (2.23 mm) at the midshaft, and 100 slices (1.05 mm) at the proximal tibia. The trabecular and cortical regions were separated by semi-automatically drawn contours, and the complete secondary spongiosa of the proximal tibia was evaluated. The resulting gray-scale images were Gaussian filtered ($\sigma$ = 1.2, support = 1) and globally thresholded (19.5% of maximum gray value) to form binarized images for morphological analyses. Three-dimensional analysis techniques were utilized to assess bone volume ratio (BV/TV), bone surface ratio (BS/BV), trabecular thickness (Tb.Th), trabecular separation (Tb.Sp), trabecular number (Tb.N), connectivity density (Conn.D), SMI and cortical thickness (Ct.Th). The knee, rib cage, and vertebrae were scanned (50kV, 145uA, 200 ms integration time, 2000 projections on 360º, 2048 CCD detector array, cone-beam reconstruction) with an isotropic resolution of 21 μm for the knee and 38.5 μm for the ribcage and vertebrae. The gray-scale images were globally thresholded (15.2% of maximum gray value) to form binarized images. Micro-ct scanning was performed on the bone tumour of the arm in addition to the neoplastic osteoids collected from the peritoneal cavity and lung (55 kV, 145 μA, 400 ms integration time, 2000 projections on 360º, 2048 CCD detector array, cone-beam reconstruction). Nominal isotropic resolution

was 10.5 μm, the grey-scale images were all optimally thresholded to form binarized images.

# Chapter Three: Results

## 3.1 *Progressive ankylosis*: a model system for examination by micro-ct

The limbs and proximal tails of four *ank/ank* female mice, 4 months of age, were subjected to micro-ct to obtain the representative images depicted below. Control images shown were derived from two age- and sex-matched mice. In addition, the joints of 4 additional female controls, aged 7-13 months, were examined (data not shown). In no instance did any of the control mice examined exhibit any of the musculoskeletal abnormalities evident in the *ank/ank* mutant.

### *3.1.1 Distal extremities:*

As seen in Figure 3-1, 3D micro-ct imaging revealed advanced bony ankylosis of all the joints of the carpus and paw of the *ank/ank* mice, with the digits fixed in a hyperextended position.

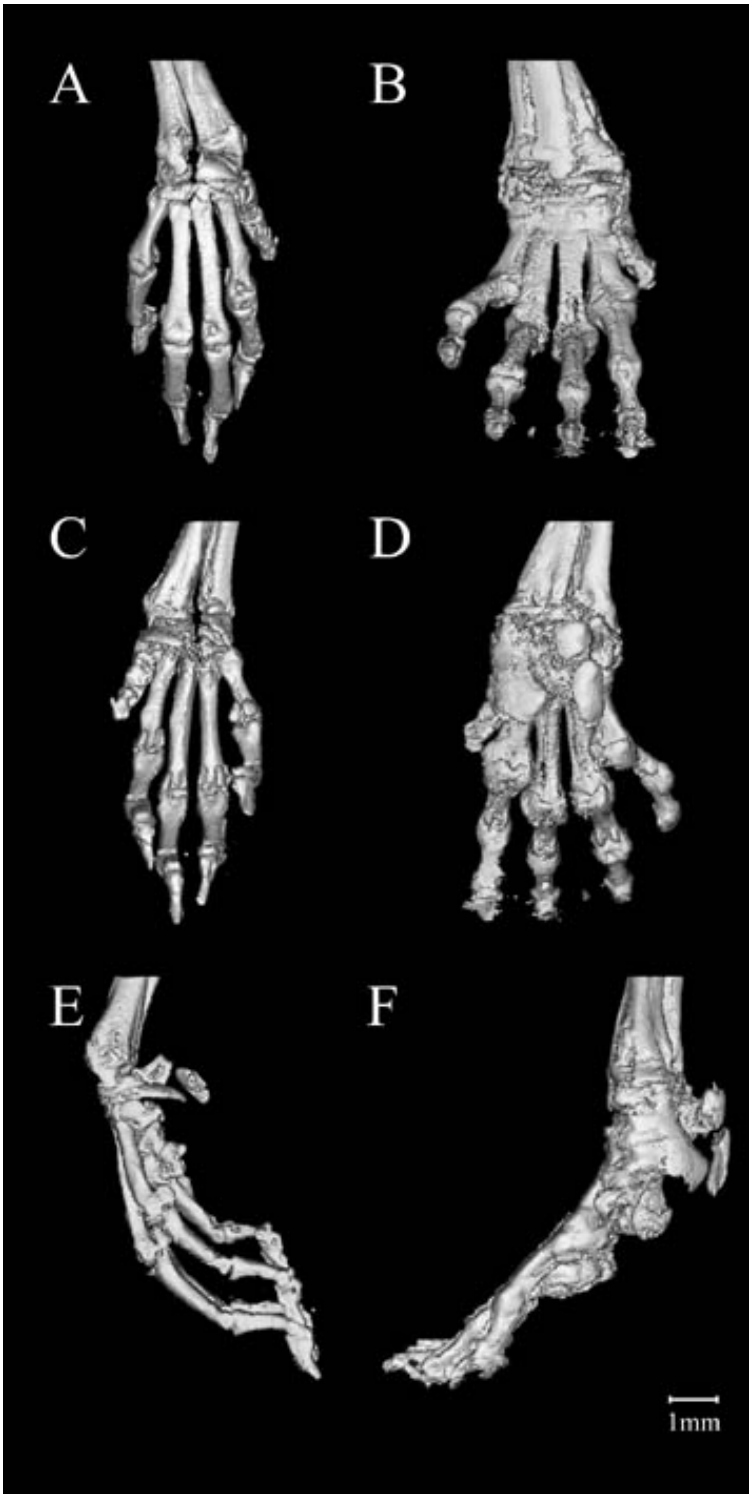


**Figure 3-1. Representative micro-ct reconstruction of the right distal fore-limb from 4-month old female control (left) and *ank/ank* mutant (right) mice at 18x magnification. Shown are dorsal (A,B), palmar (C,D), and medial (E,F) views. Note that the digits are fixed into a hyperextended postion, while control digits are loose.**

Both the distal and proximal interphalangeal joints were obliterated, being largely encased by calcified soft tissue. The metacarpophalangeal joints were fused, and the distal condyles of the metacarpals were enlarged and fused with their associated sesamoid bones. Although the latter had been largely assimilated into the calcified mass surrounding the metacarpophalangeal joints, they also appeared to be grossly enlarged (compare C and D, Figure 3-1). The metacarpal bone shafts were thickened, likely due to periosteal new bone formation and or soft tissue calcification, a process which is also strikingly evident in the distal radius and ulna of the *ank/ank* mouse. Indeed, the space between these two bones has been obliterated by soft tissue calcification. The carpus of the *ank/ank* was an amorphous calcified mass fused to the ends of the radius and ulna, associated with a flexion deformity of the paw. Changes in the hind-limb (Figure 3-2), while possibly somewhat less severe, mirrored those of the fore-limb, including the presence of bony ankylosis of the digits and tarsus in a hyperextended position.

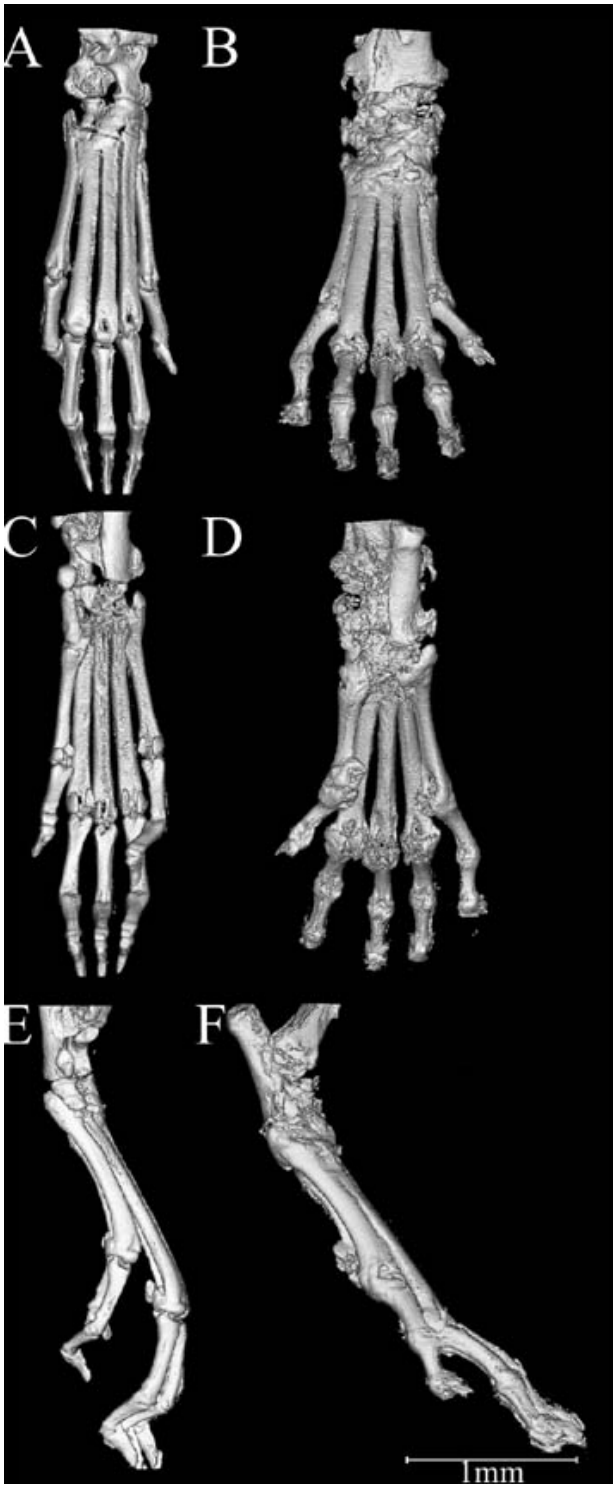


**Figure 3-2. Representative micro-ct reconstruction of the right distal hind-limb from 4-month old control (left) and *ank/ank* mutant (right) female mice at 18x magnification. Dorsal (A,B), plantar (C,D), and medial (E,F) views are shown. Note that the digits are fixed into a hyperextended postion, while control digits are loose.**

### *3.1.2 Elbows:*

The radius and ulna of the *ank/ank* mouse were fused to the humerus in a position of flexion (Figure 3-3).

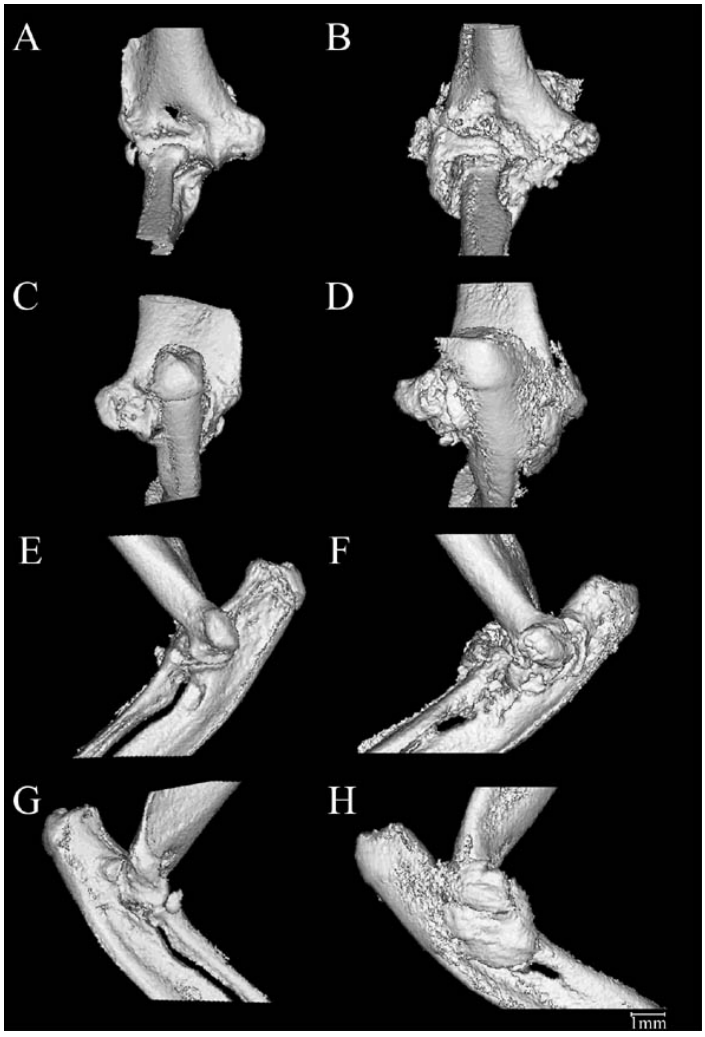


**Figure 3-3. Representative micro-ct reconstruction of the right elbow joint from 4-month old normal (left) and *ank* mutant (right) female mice at 18x magnification. Depicted are the anterior (A,B), posterior (C,D), medial (E,F), and lateral (G,H) views. Note that the elbow joint is fused into a flexed position, and the entire joint capsule is calcified as are other soft tissue structures.**

Calcification was found to extend around the joint capsule both anteriorly and posteriorly, with the olecranon process being apparently encased posteriorly by the calcified joint

capsule and other soft tissue structures. The humero-radial joint was extensively involved, as a result of a plaque of bone which incorporated the lateral sesamoid bone as well as the annular ligament (B and H, Figure 3-3). There was also a reduction in the size of the lateral supracondylar ridge of the humerus in an *ank/ank* animal as compared to a control mouse, best seen in the anterior (A,B) and posterior (C,D) views of the elbow in Figure 3-3. The medial epicondyle was less involved, but appeared enlarged by the addition of irregular nodular masses of new bone. The humeral trochlea and semi-lunar notch of the ulna were extensively involved by proliferation of new bone at the margins of the joint surface. In one *ank/ank* specimen, the bony enlargement of the ulnar coronoid process had produced notching of the humerus (data not shown). The radius and ulna were fused proximally in the region of the radial neck, and also more distally, along the interosseous membrane as seen in Figure 3-3 (E,F).

### *3.1.3 Knees:*

Changes in the knee of *ank/ank* mice were most pronounced in the menisci and the patella (Figure 3-4).

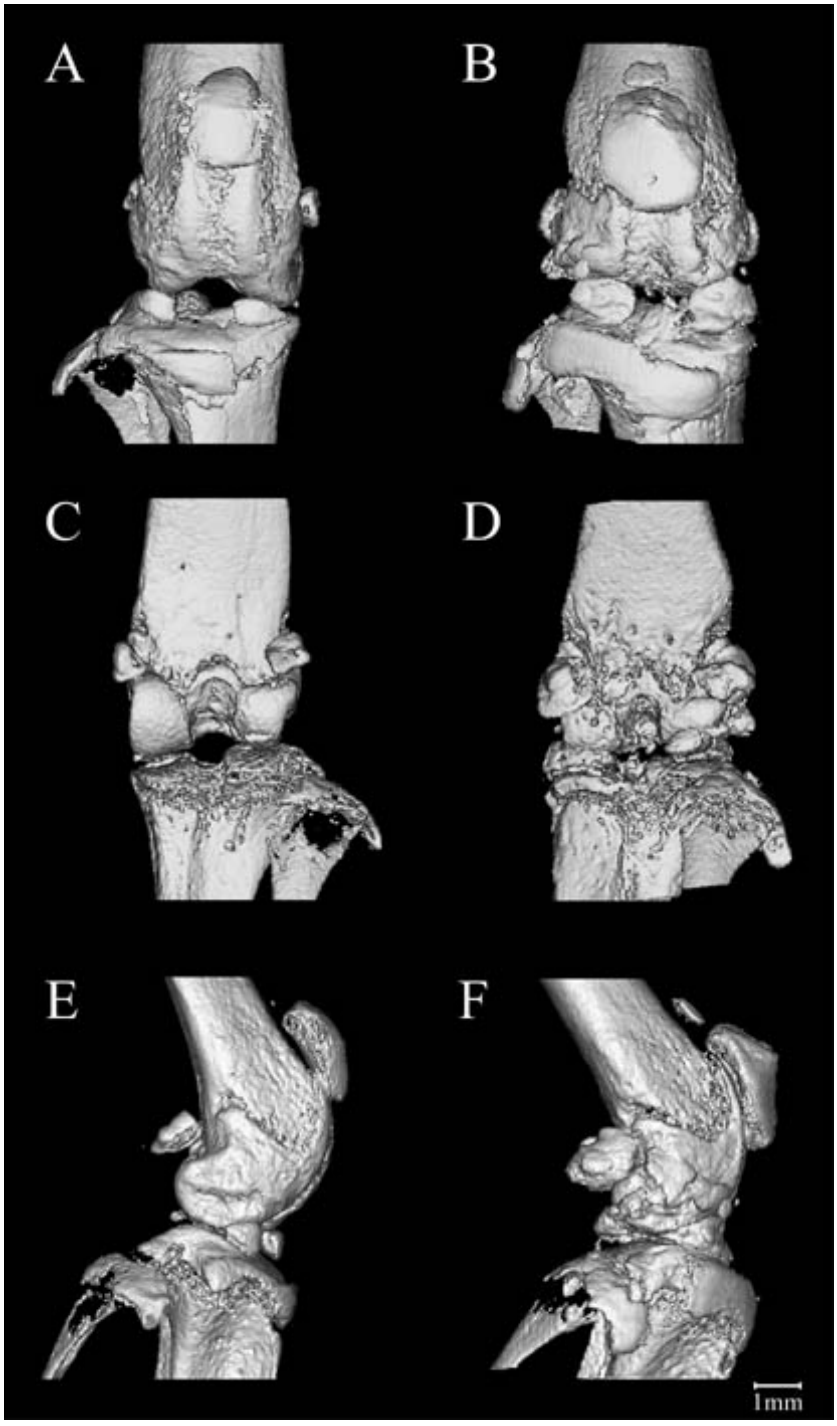


**Figure 3-4. Representative micro-ct reconstruction of the right knee from 4-month old normal (left) and *ank* mutant (right) female mice at 18x magnification. Shown are anterior (A,B), posterior (C,D), and lateral (E,F) views. The menisci and patella are enlarged in the *ank* mice. In some cases the patella became fused to the femur.**

Both menisci appeared enlarged as a result of extensive calcification (best seen in the anterior views, Figure 3-4A and B) and in some cases these were fused together. This, perhaps in combination with chondrocalcinosis resulted in an apparent narrowing of the joint space, however, fusion between the femur and tibia was not observed. The posterior views (Figure 3-4C and D) nicely demonstrate the proliferation of subchondral bone and/or chondrocalcinosis that has resulted in the loss of femoral condyle surface integrity. The size of the patella was increased due to calcification, a process that was also visible within the quadriceps tendon of some mice (Figure 3-4B and F). In several cases the patella became fused to the patellar groove of the femur. As seen in the distal extremity sesamoid bones, the two posterior sesamoids underwent irregular enlargement due to new bone formation. Additional changes in the knee included the enlargement of the proximal tibia and the formation of calcified nodules, possibly osteophytes, on the lateral epicondyle of the femur, and within the intercondylar groove of the femur (Figure 3-4).

### *3.1.4 Proximal tail vertebrae:*

Changes observed in the proximal tail involved the fusion of vertebral elements (Figure 3-5).

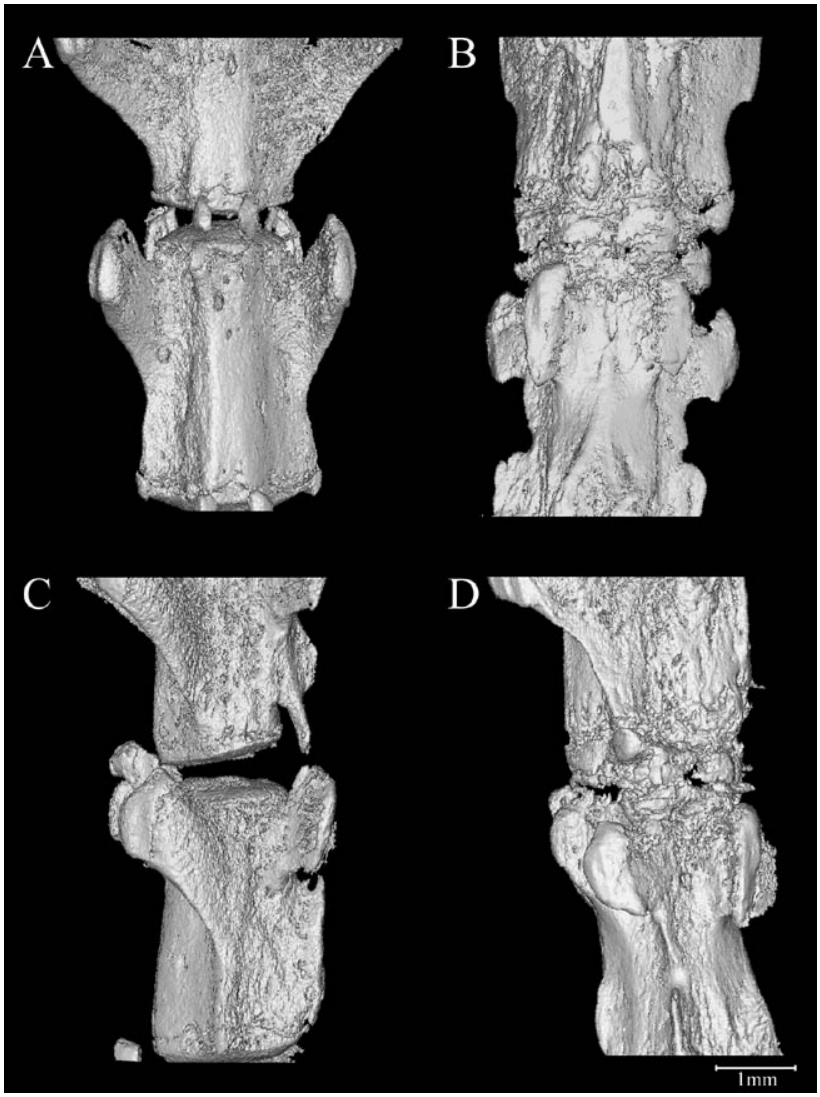


**Figure 3-5. Reconstruction of the intervertebral space between 3rd and 4th caudal vertebrae of a representative 4-month old female normal (left) and *ank/ank* mutant (right) mice at 40x magnification. Inferior (A,B) and lateral (C,D) views are shown. The *ank* vertebrae has major calification of the ligamentous structure around the annulus fibrosis.**

These included primarily the calcification of ligamentous structures concentrated around the annulus fibrosis. Thus the intervertebral space appeared highly irregular due to the formation of calcified nodules around joint capsule, however, at least at this stage in the disease, the intervertebral disks were free of detectable calcification (Figure 3-6).


**Figure 3-6. Mid-sagittal section of a representative micro-ct reconstruction of the intervertebral space of the 3rd caudal vertebra, shown at 40x magnification. The cross-section reveals that the intervertebral disk are free of calcification.**

While the articular processes (pre- and post-zygapophyses) were enlarged, the transverse processes were reduced in size relative to the control group. On the inferior surfaces, the hemal processes were considerably enlarged as were the adjacent sesamoid bones.

## 3.2 Brachymorphic mice: investigating the pathology with micro-ct and histology

### *3.2.1 Micro-ct analysis of bm/bm limbs*

Volumetric 3D renderings, based upon the micro-ct data, revealed striking morphological differences between wild-type and *bm/bm* limbs. In general, the bones of the *bm/bm* mice appeared more robust due to their reduced diaphyseal lengths and relatively enlarged epiphyses. This is illustrated in the humeri shown in Figure 3-7 A.

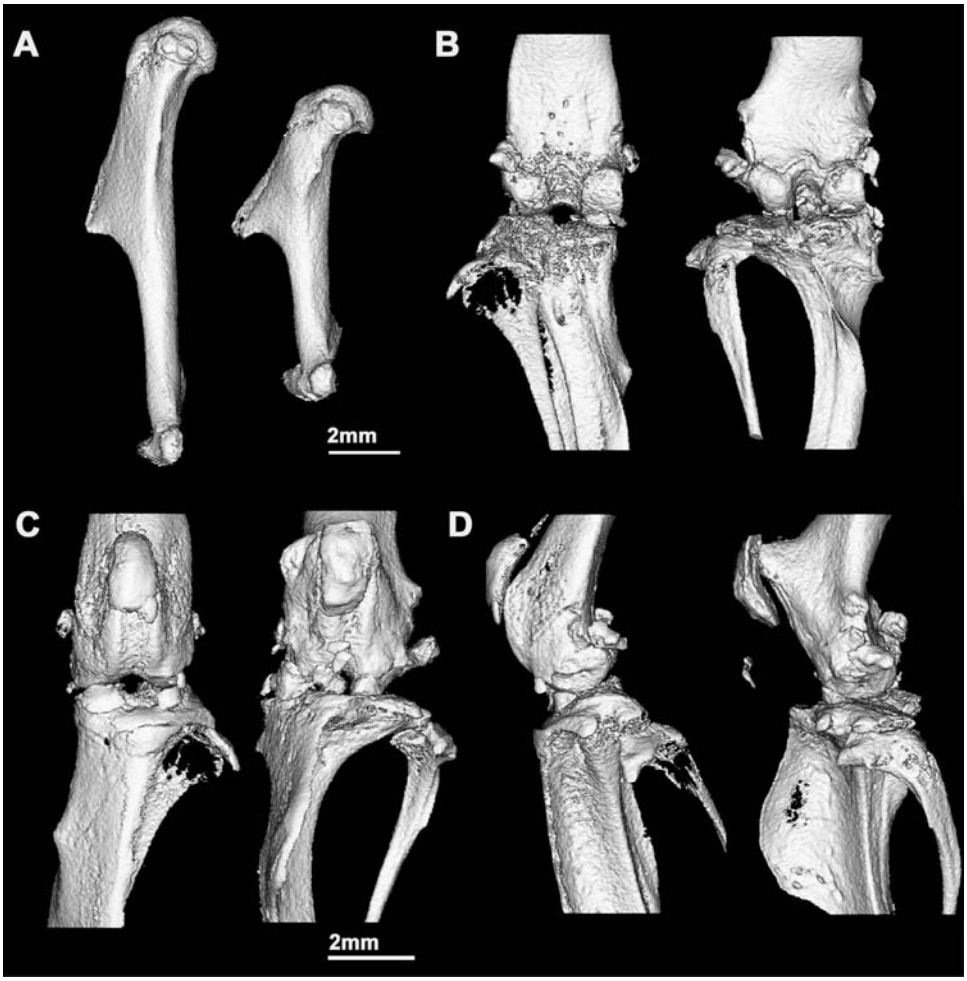


**Figure 3-7. 3D reconstruction of left humeri and knees from representative 12-month-old normal (left) and *bm/bm* (right) mice. The image of the humeri (A) illustrates the distinctive limb morphology of the *bm/bm* mutant. Also shown are posterior (B), anterior (C), and lateral (D) views of the knees: bowing of the tibia is seen in the *bm/bm* mice (B,C) compared to controls; and the enlarged, anteriorly-displaced patellar groove (with overlying patella), as well as the excessive growth of the tibial tuberosity resulting in a fin-like structure in the *bm/bm* sample, are best seen in panel D.**

Along with this diaphyseal shortening, metaphyseal flaring was a distinctive characteristic of *bm/bm* long bones. In the femur, for example, this flaring was associated with a pronounced change in the shape of the distal epiphysis, associated with an extensive alteration in the configuration of the patello-femoral groove that resulted in

the distal femurs having a hammer head-like shape (Figure 3-7 D). This alteration was also clearly evident in histological cross-sections of the distal *bm/bm* femur, as seen in Figure 3-8 D.

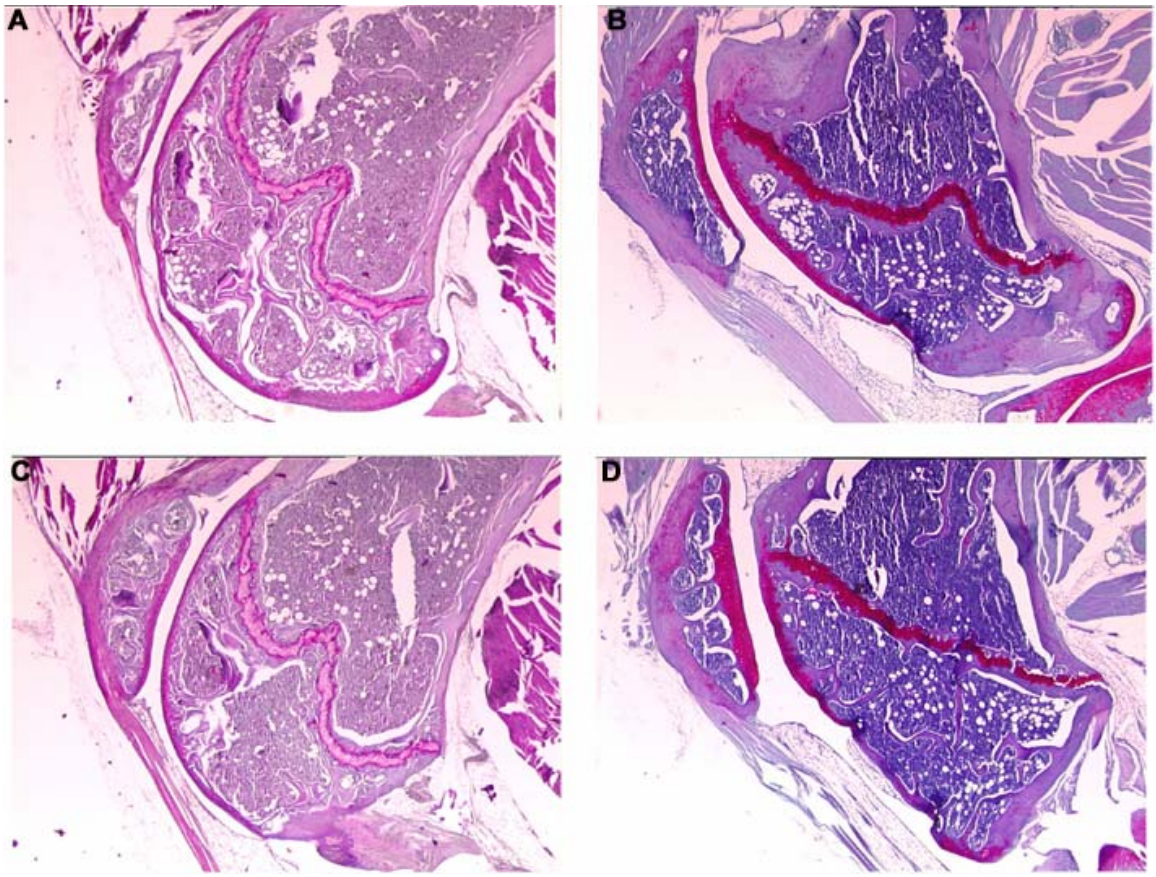


**Figure 3-8. Matched pairs of sagittal sections taken through the distal femoral heads of representative 12 month-old control (A,C) and *bm/bm* (B, D) mice. A and B illustrate the medial compartments, C and D the patello-femoral compartments of the knees. Note the altered, hammer head-like (inverted in this image) shape of the distal femur in the *bm/bm* mouse (D) which correlates with the changes seen in the micro-ct scan (Figure 3-7D).**

Additional changes in *bm/bm* limbs included enlarged muscle and tendon insertion points, as seen in the deltoid (Figure 3-7 A) and tibial (Figure 3-7 D) tuberosities. Bowing of the tibia and fibula (Figure 3-7 B,C,D) was also present, as was evidence of

abnormal calcification about the knee and irregularities of menisci in *bm/bm* samples. The abnormal morphology of the distal femur was also evident histologically (Figure 3-8 B,D). We compared proximal tibial subchondral plate thicknesses between wild-type and *bm/bm* tibiae to search for the possibility of an abnormality in subchondral bone structure, but found no significant difference (*bm* = 122 μm, wild-type = 119, t-test, two tailed, p=0.7)

### *3.2.2 Histological analysis of bm/bm knee joints*

While the synovial lining of control 6-7 month C57BL/6 mice was approximately 1-2 cells thick (Figure 3-9 A), the lining of brachymorph knees appeared thickened and hypercellular (Figure 3-9 B).

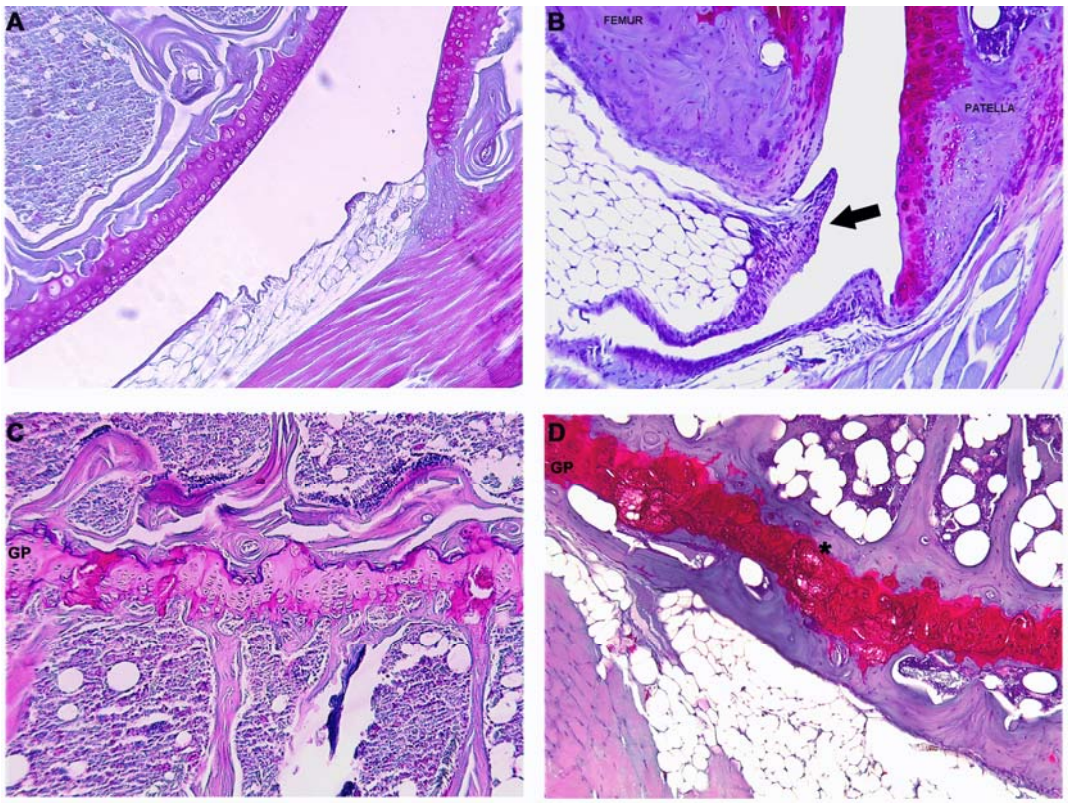


**Figure 3-9. Synovial lining of control (A) and *bm/bm* (B) mice at 6-9 months of age. Note the thickened synovium in B as indicated by arrows compared to the control (A). Representative growth plates of control (C) and *bm/bm* (D) mice at 6-9 months of age. The growth plate of the *ank* mice (D) were irregular and lacking the regular columnar organization, as seen in the controls (c)**

The same was observed for our 12-14 month knees (data not shown). The significance of this synovial hypertrophy is unclear, but suggests the presence of a chronic low-grade inflammation. In control mice, the narrow yet well-organized epiphyseal growth plates were consistent with slowed growth of long bones. These plates showed a columnar organization of cells and an organized progression from proliferating to hypertrophic cells (Figure 3-9 C). As previously reported, the growth plates of *bm/bm* mice were abnormal, lacking the regular columnar organization of proliferating and hypertrophying chondrocytes of C57BL/6 mice (Figure 3-9 D). Indeed, in the *bm/bm* samples there was

no clear distinction between the different zones of the growth plate, with these tending to collapse into disorganized, often round, clumps of cells. The epiphyseal growth plates of the 12 month-old *bm/bm* mice also appeared less cellular than those of controls and showed evidence of impaired endochondral ossification, with accumulation of mineralized cartilage matrix.

Knee joints of 6-9 month-old C57BL/6 mice exhibited histologically normal articular cartilage with regularly-distributed and densely packed chondrocytes on all joint surfaces (Figure 3-10A).

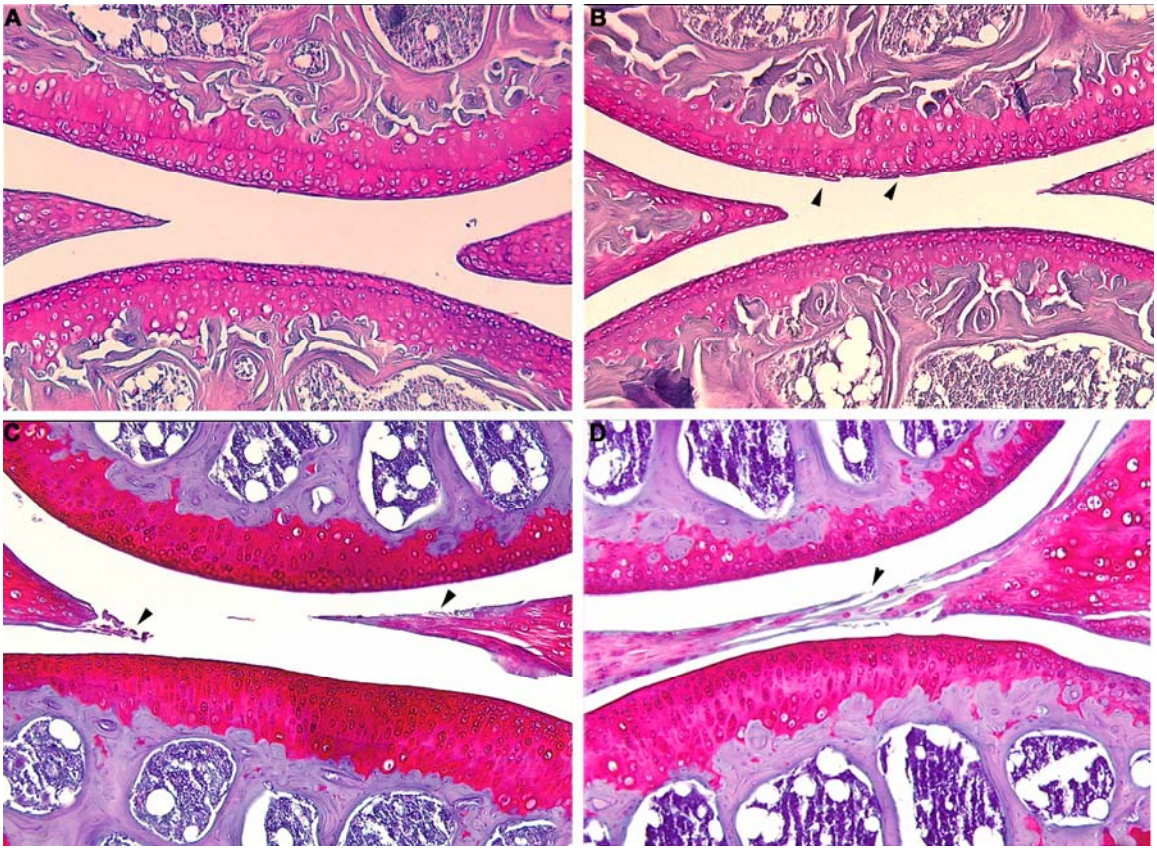


**Figure 3-10. Sagittal section of representative C57BL/6 control and *bm/bm* mice. Six month (A) and 12 month-old (B) control mice. Minor fibrillation of condylar cartilage is seen in (B) (see arrows). Meniscal fraying can be seen in the 6 month-old *bm/bm* knee (C) and, more pronounced, in a representative 12 month-old (D) *bm/bm* knee (see arrows).**

At 12-14 months all knee joints isolated from C57BL/6 mice showed some areas of superficial fibrillation in the medial joint compartment, and occasional fraying, typically on the tibiae but also on femoral condyles (Figure 3-10 B). This was consistent with the age-related cartilage degeneration (grade 1) seen in this inbred strain.

At 6-7 months of age *bm/bm* knee joints showed normal appearing articular cartilage in all joint compartments, although all samples exhibited some degree of fraying or shredding of the thin central portions of the menisci (Figure 3-10 C). Simple or complex tears of the medial meniscus were seen in all brachymorph joints obtained from 12 month-old animals (Figure 3-10 D). At 12 months of age, degenerative changes were evident in the medial and/or patello-femoral compartments of all mutant mouse samples (Figure 3-11).

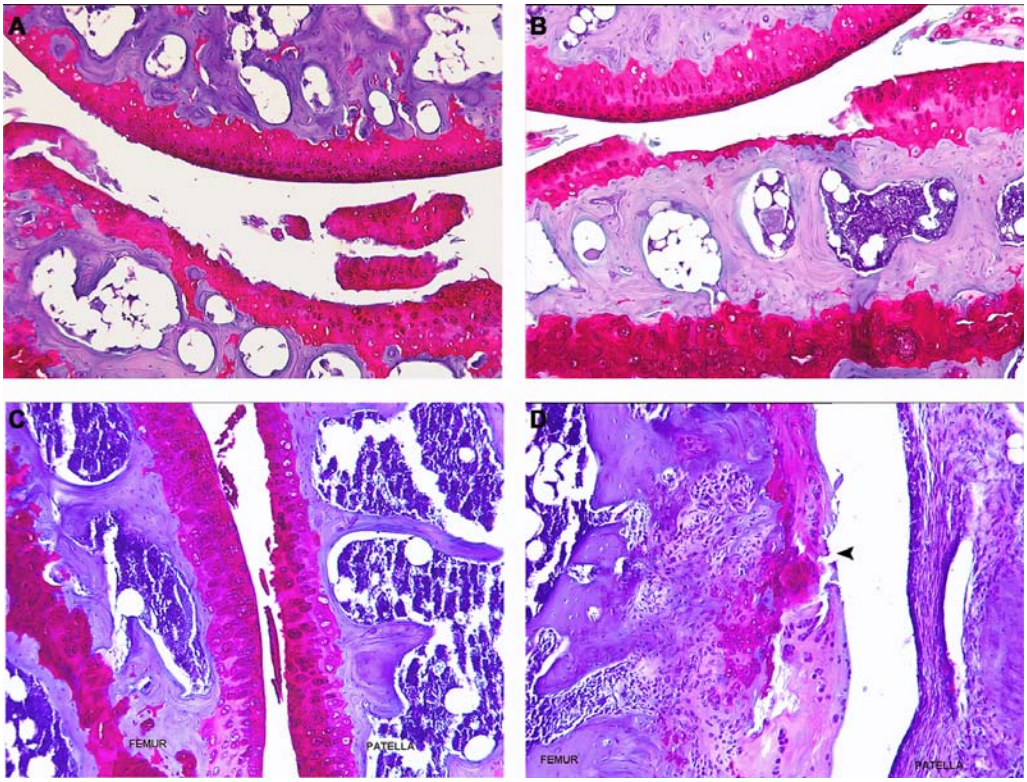


**Figure 3-11. Sagittal sections of representative 12 month-old *bm/bm* knees. Lateral compartment shows grade 2 and 3 changes in the articular cartilage (A,B). The grade 3 changes in (A) reveals a loss of a large area of articular cartilage right down to the tide-mark, grade 2 changes are depicted in (B). Patello-femoral compartments showing surface damage of the articular cartilage (C) and deep fissuring of the cartilage (D) on the femoral side of this joint as illustrated by arrow.**

All *bm/bm* mice exhibited degradation of the articular cartilage on medial tibial plateaus (Figure 3-11 A,B), although the opposing femoral cartilage remained intact in most cases. Fragmentation and loss of tissue down to the level of the tidemark was seen in half the *bm/bm* animals (Figure 3-11 A,B); with the remainder showing either horizontal ruptures along the tidemark, considered a precursor to cartilage loss (data not shown), or deep fibrillations (data not shown). The patello-femoral compartment was irregular in all brachymorph mice and half the joints had erosions on the patella and/or femur (Figure 3-11 C,D). Interestingly, despite the advanced degenerative changes in the patello-

femoral and medial joint compartments, the lateral compartments consistently presented a normal appearance (data not shown). Applying the grading system of Maier and Wilhelmi, 1987 [216], the 12 month-old C57BL/6 knees had a mean score of 1.2, while the score for *bm/bm* mice was 2.5 (

Table 2).

**Table 2. Comparison of control and *bm/bm* OA grades.**

| Control | | *bm/bm* | |
|---|---|---|---|
| Mouse | Score | Mouse | Score |
| 1 | 1 | 7 | 2 |
| 2 | 1 | 8 | 2 |
| 3 | 1 | 9 | 2 |
| 4 | 1 | 10 | 3 |
| 5 | 1 | 11 | 3 |
| 6 | 2 | 12 | 3 |
| mean: | 1.2 | | 2.5 |

Control mice include 3 male and 3 female 12-14 month C57BL/6 mice. *bm/bm* mice consisted of 3 male and 3 female 12 month old mice. 6-9 month C57Bl/6 and bm were also examined (data not shown) and found to have a score of 0. A Mann- Whitney (Wilcoxon) test was performed where U= 3.45, $p<0.001$.

A Mann-Whitney (Wilcoxon) test was performed where U= 3.45, $p<0.001$. It was thus concluded that the *bm/bm* mutation on a C57BL/6 background was associated with premature degenerative joint disease.

## 3.3 Inactivation of *Pten* in osteo-chondroprogenitor cells leads to epiphyseal growth plate abnormalities and skeletal overgrowth

### *3.3.1 Deletion of Pten in chondrocytes*

To generate mice with *Pten* gene deletions in chondrocytes, *Pten* $^{flox/flox}$ mice [198] were crossed with a transgenic line expressing the Cre recombinase under the control of the *Col2a1* (type II collagen) gene promoter [218]. In this line, Cre activity was reported to lead to gene activation in sclerotomal cells of the developing spinal column and in chondrocytes. During development, the *Col2a1* promoter is also known to direct expression of the Cre transgene in notochordal cells and a subset of neuroprogenitors [209]. The initial characterization of *Col2a1* promoter-Cre mouse [218] did not demonstrate significant ROSA26 (R26) *lacZ* reporter expression in osteoblasts of the primary spongiosa or perichondrium, however, as shown below, we found that the *Col2a1Cre* transgene leads to R26R reporter gene activation more generally, involving the osteo-chondrogenic lineage (see below). To confirm the presence of chondrocyte-specific excisions of the floxed *Pten* gene, chondrocyte DNA was obtained from the ventral ribs of 2-3 day old mice. PCR analysis of these DNA samples revealed the presence of a floxed *Pten* gene-derived excision band in *Pten*$^{flox/flox}$ *Col2a1Cre* mice, but not control mice (Figure 3-12).

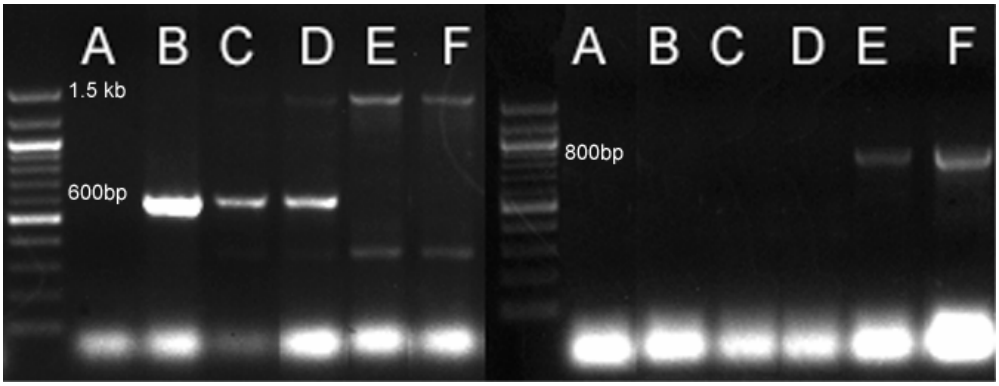


**Figure 3-12. Cre Excision PCR performed on DNA isolated from ventral ribs of pups. [A] negative control, [B, C] wild type, [D] *Pten* flox/wt, [E,F] experimental *Pten*$^{flox/flox}$*:Col2a1Cre*. Right side, *Pten* PCR where: 1.5 KB band = *Pten* flox 600 bp band = wild type band. Left side, *Pten* excision PCR where: 800 bp band = *Pten* post-excision.**

Thus, Cre-mediated *Pten* gene deletions were occurring in the chondrocytes of *Pten*$^{flox/flox}$ *Col2a1Cre* mice. We also looked for Pten and P-Akt expression in chondrocytes isolated from the ventral ribs, however we were not able to see a difference between control and *Pten*$^{flox/flox}$*:Col2a1Cre* chondrocytes, and very little expression was detected in either the control or *Pten*$^{flox/flox}$*:Col2a1Cre* cells.

### *3.3.2 Growth and general features of Pten*$^{flox/flox}$ *Col2a1Cre mice*

Examination of spinal column lengths (from C1 to the tail tip) on lateral view x-ray images, revealed that *Pten*$^{flox/flox}$*:Col2a1Cre* mice were longer than controls (Figure 3-13).

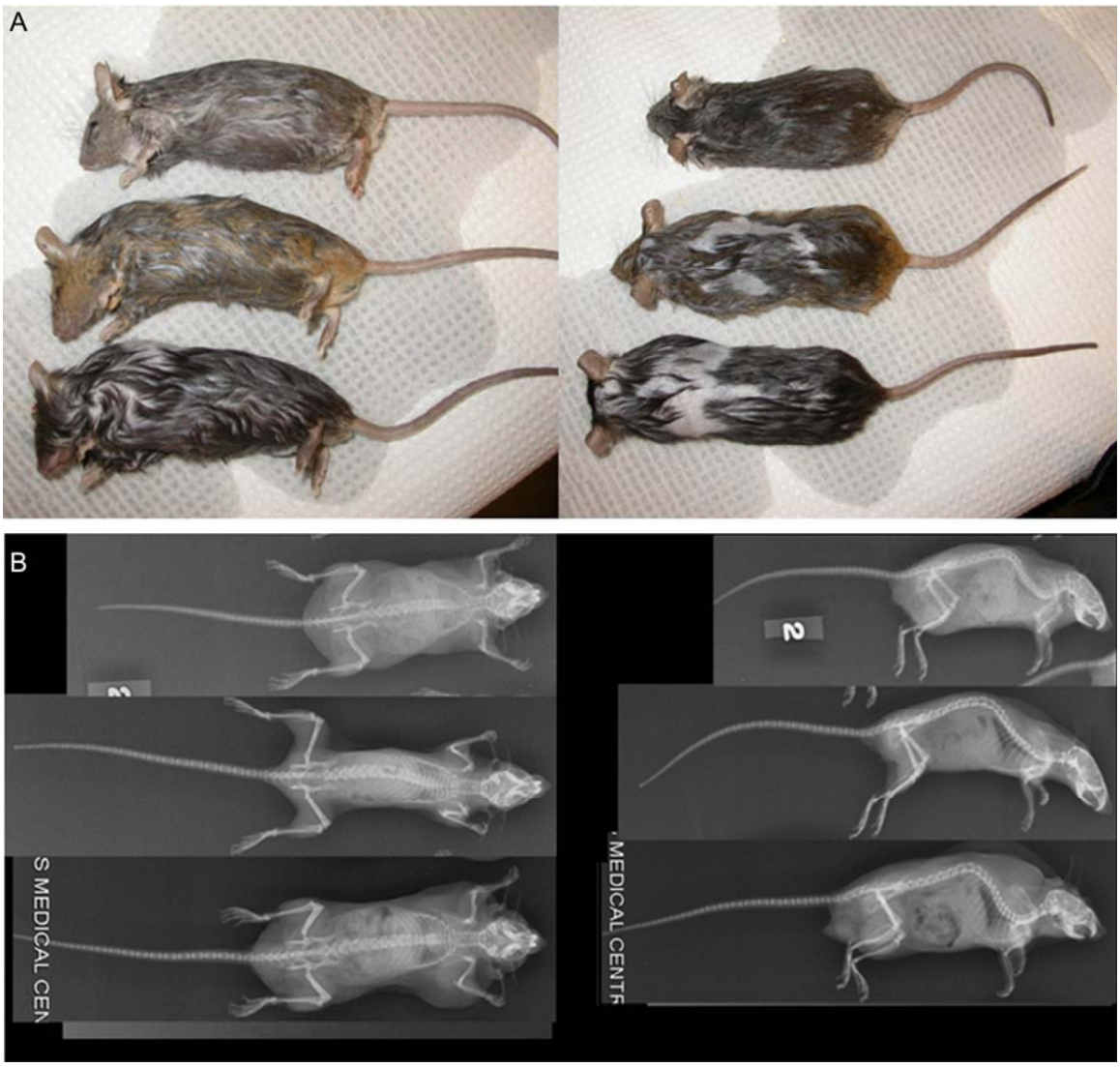


**Figure 3-13 [A]: Lateral and dorsal views of representative 15 week-old mice (top control male; bottom two *Pten*$^{flox/flox}$*:Col2a1Cre* males. [B]: Frontal and lateral view digital x-rays of representative 15 week-old mice (top control female; middle *Pten*$^{flox/flox}$*:Col2a1Cre* female; bottom *Pten*$^{flox/flox}$*:Col2a1Cre* male). Note the upper thoracic and cervical soft tissue swelling in the *Pten*$^{flox/flox}$*:Col2a1Cre* males [A, middle and bottom mice; B, bottom mouse], and both the increased size and x-ray density of the vertebral columns and hind limbs of both male and female *Pten*$^{flox/flox}$*:Col2a1Cre* mice [B, middle and bottom mice].**

Thus, by 15 weeks of age *Pten*$^{flox/flox}$*:Col2a1Cre* were an average of 1.15 times ($p<0.0002$) longer than control mice (Figure 3-14).

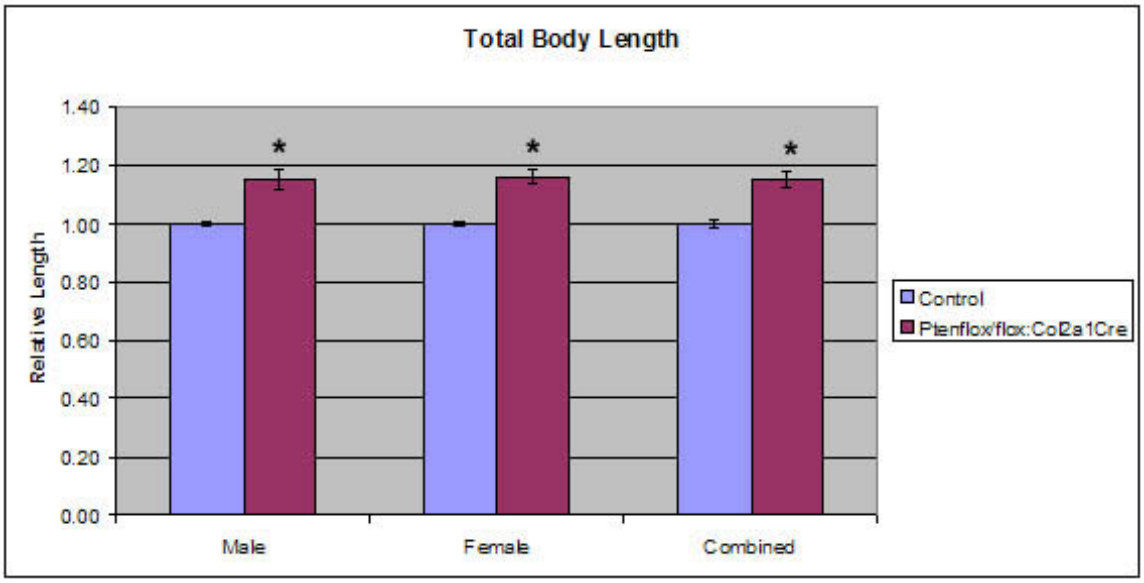


**Figure 3-14. Graph depicting total body length (measured from C2 to the end of the tail) of control male (n=3), female (n=3), and combined mice versus *Pten*$^{flox/flox}$*:Col2a1Cre* male (n=3), female (n=3), and combined mice (* = p<0.0002). *Pten*$^{flox/flox}$*:Col2a1Cre* mice were consistently longer than controls.**

Lateral x-rays were used to assess the 'true' spine lengths by obviating the effects of varying degrees of kyphosis (the latter affects nose-to-tail measurements). Examination of femoral length measured on anterior-posterior x-ray images revealed that *Pten*$^{flox/flox}$*:Col2a1Cre* femurs were 1.07 times longer than those of control mice (p=0.004) (Figure 3-13).

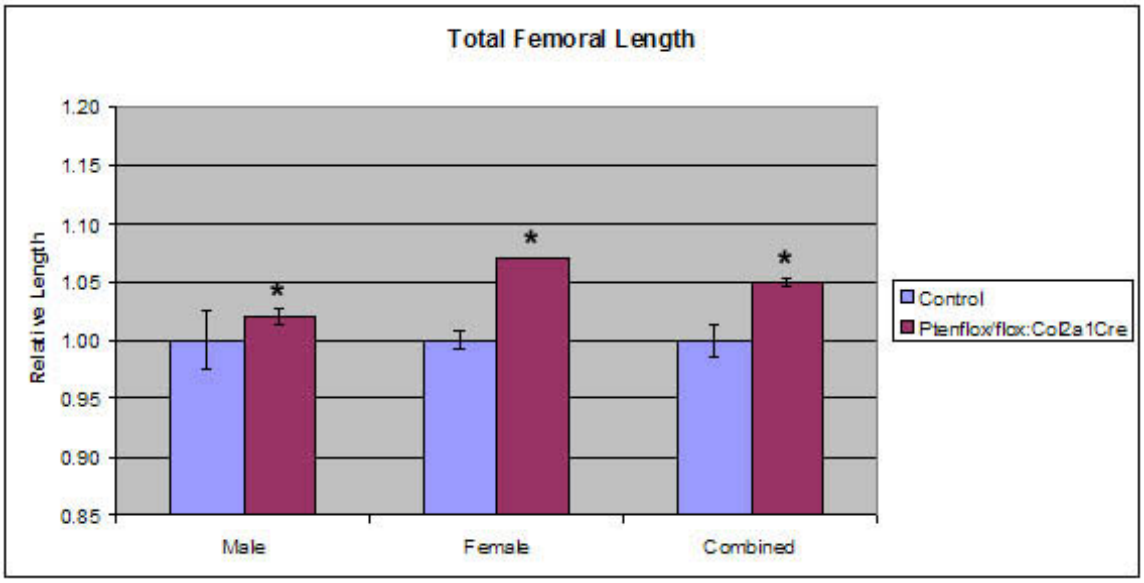


**Figure 3-15. Graph depicting total femur length of control male (n=3), female (n=3), and combined mice versus *Pten*$^{flox/flox}$*:Col2a1Cre* male (n=3), female (n=3), and combined mice (* = p<0.004). *Pten*$^{flox/flox}$*:Col2a1Cre* femurs were longer than the control femurs.**

Mice followed over 15 weeks clearly showed that the *Pten*$^{flox/flox}$*:Col2a1Cre* mice weighed more than controls (Figure 3-16).

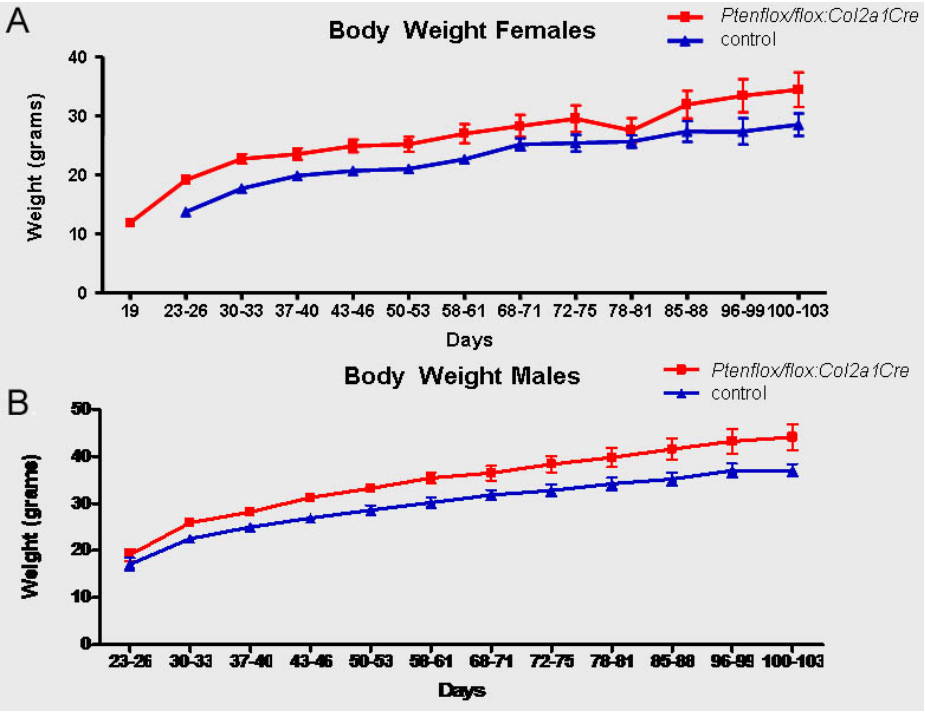


**Figure 3-16. Body weights taken weekly from 3 to 15 weeks of [A] female (control n=4 *Pten*$^{flox/flox}$*:Col2a1Cre* n=7 ) (p<0.001) and [B] male mice (control n=7, *Pten*$^{flox/flox}$*:Col2a1Cre* n=5) (p<0.001). *Pten*$^{flox/flox}$*:Col2a1Cre* male and female mice weighted more than control mice.**

Adult females *Pten*$^{flox/flox}$*:Col2a1Cre* mice lacked the progressive adiposity typically seen in control female mice, and remained lean for up to 9 months. Adult *Pten*$^{flox/flox}$*:Col2a1Cre* males, in contrast, almost invariably developed prominent upper body, cervical, and cranial soft-tissue swelling (Figure 3-13A, B). Histological evidence of excess fluid was seen in the dermal layers (subcutaneous and deep) of these mice, with separation of collagen bundles and dermal appendages (Figure 3-17B), compared to control mice (Figure 3-17A).

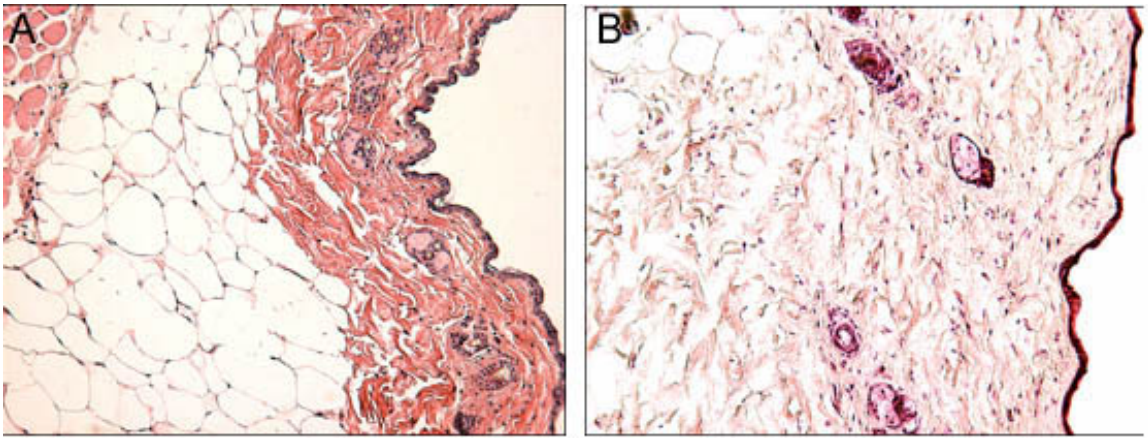


**Figure 3-17. Representative images of the dermal layer of [A] control and [B] *Pten*$^{flox/flox}$*:Col2a1Cre* mice. Note the excess fluid present in the *Pten*$^{flox/flox}$*:Col2a1Cre* mice.**

The lack of inflammatory cell infiltrates, or abnormal matrix deposition observed (Figure 3-17) indicated the swelling was likely edema or lymphedema. Since veins and lymphatics draining the upper body converge at the thoracic outlet, we hypothesized that the upper body fluid accumulation was secondary to interference with fluid return, stemming from a 'thoracic outlet syndrome' due to skeletal overgrowth in *Pten*$^{flox/flox}$*:Col2a1Cre* males. As seen in Figure 3-18, the thoracic outlet is comprised of the manubrium anteriorly, the body of T1 posteriorly and is bounded laterally by the 1$^{st}$ ribs.

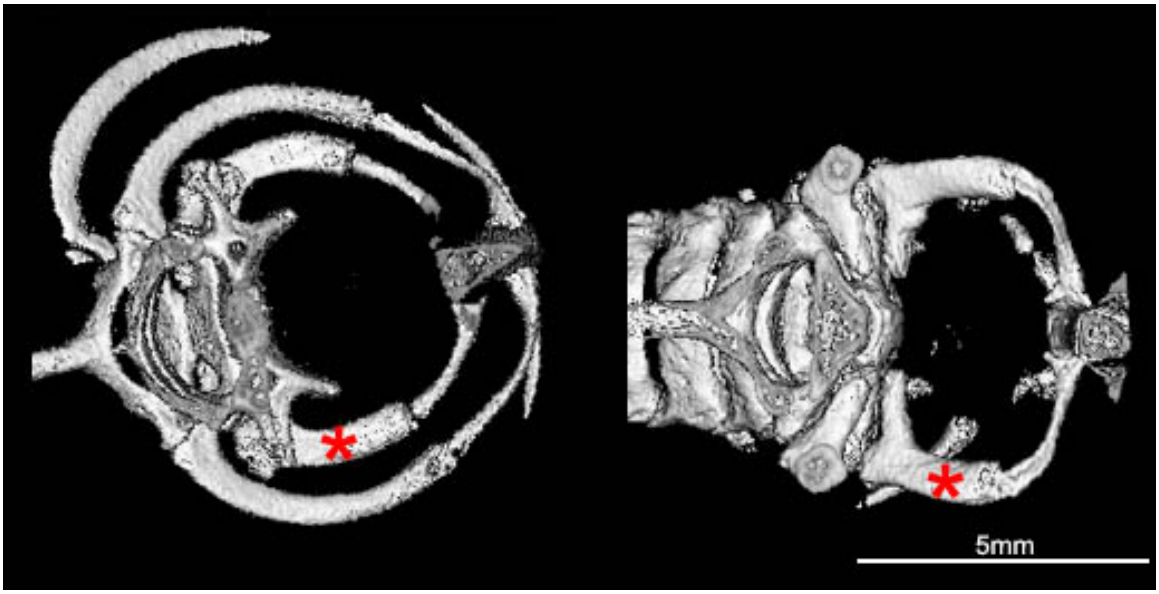


**Figure 3-18. Images show coronal views of the thoracic outlet at level of the first rib (the latter is indicated by an asterisk). Controls are on the left, and *Pten*$^{flox/flox}$*:Col2a1Cre* mice are on the right. The thoracic outlet in all *Pten*$^{flox/flox}$*:Col2a1Cre* mice examined was more squared than controls.**

Antero-medially, the heads of the clavicles (missing from Figure 3-18) would also encroach on this space. Micro-ct images of the thoracic outlet of *Pten*$^{flox/flox}$*:Col2a1Cre* mice revealed this space to have an abnormal squared shape (Figure 3-18) that could be responsible for the edema we observed.

### *3.3.3 Vertebral abnormalities and bone overgrowth in Pten*$^{flox/flox}$*:Col2a1Cre mice*

Conventional radiographs of *Pten*$^{flox/flox}$*:Col2a1Cre* mice provided the first evidence of a skeletal abnormality. Compared to controls, *Pten*$^{flox/flox}$*:Col2a1Cre* skeletons (of either sex) revealed increased radiographic density, vertebral enlargement, and lengthening of the vertebral columns and tails (Figure 3-13B). No changes were observed in the numbers of cervical, thoracic, lumbar, or caudal vertebrae between control and *Pten*$^{flox/flox}$*:Col2a1Cre* mice. *Pten*$^{flox/flox}$*:Col2a1Cre* mice almost invariably exhibited a

thoracic kyphosis (Figure 3-13B lateral views), that tended to be more pronounced than the variable kyphosis occasionally seen in the controls. Furthermore, the thoracic cages of the mutants, instead of having the normal bell-like shape of the controls, were elongated and narrowed (Figure 3-19), consistent with the increased length of the thoracic portion of the *Pten*$^{flox/flox}$*:Col2a1Cre* spinal columns.

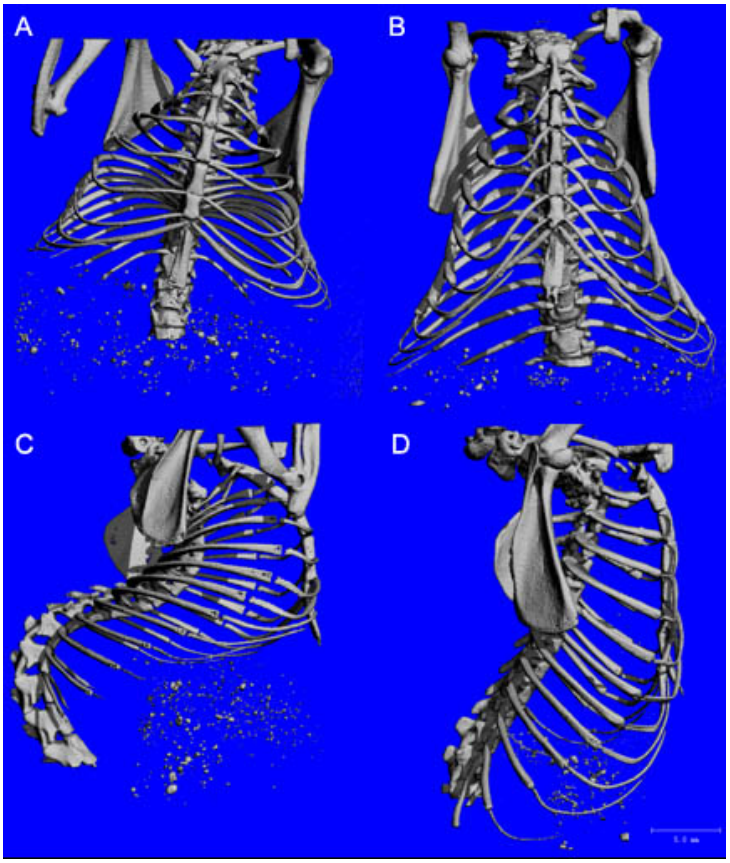


**Figure 3-19. Micro-ct reconstructions (38 μM resolution) of the thoracic cages of representative control [A, C] and *Pten*$^{flox/flox}$*:Col2a1Cre* [B, D] mice. A and B shows frontal views, C and D shows lateral views. The speckled radio-opaque debris seen below the thoracic cages of the mice was derived from the mouse chow. Control rib cages were bell-shaped, while *Pten*$^{flox/flox}$*:Col2a1Cre* ribcages looked more elongated.**

The radiographic abnormalities were more evident with micro-ct imaging of the mutant mouse skeletons. There was an increase in the size of all vertebrae as seen by digital radiograph (Figure 3-13B), and micro-ct (Figure 3-20), and histology (Figure 3-21).

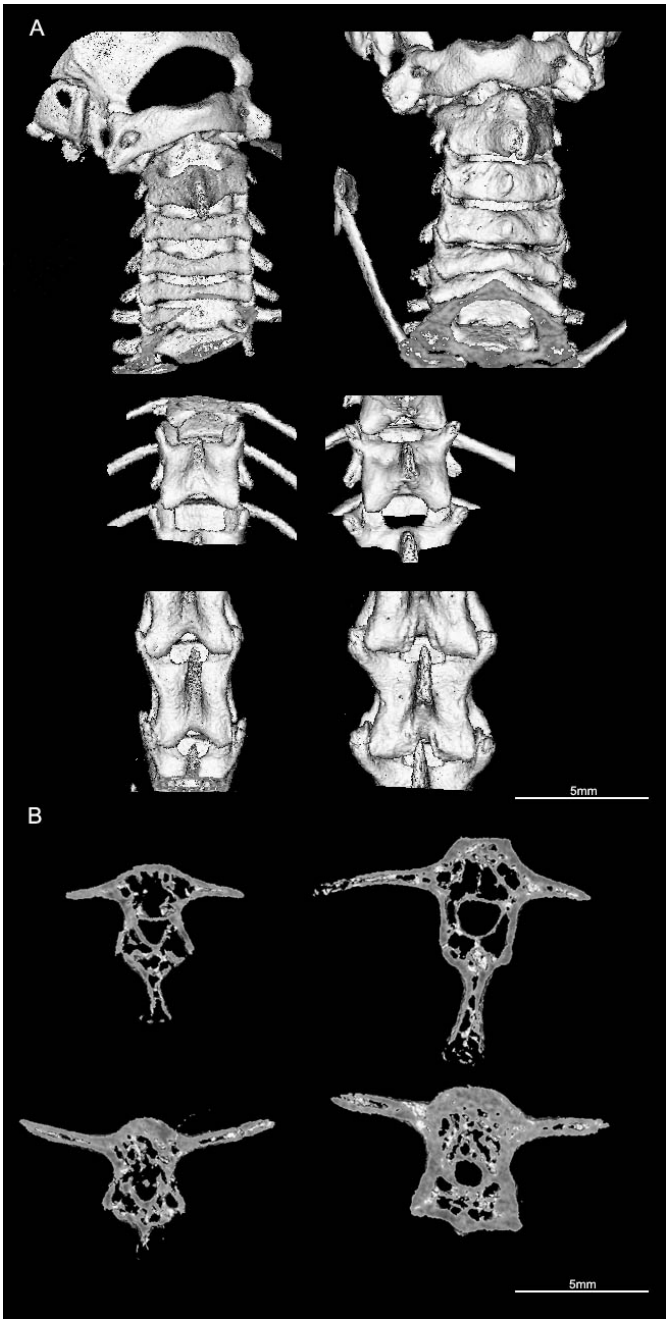


**Figure 3-20. Panel [A] depicts micro-ct reconstructions (38 μM resolution) of representative regions of the spinal columns (posterior views) of control and *Pten*$^{flox/flox}$*:Col2a1Cre* mice: [top pair] entire cervical spine segment; [middle pair] thoracic vertebrae, centered on T11; [bottom pair] lumbar vertebrae, centered on L3. Panel [B] transverse cross section through vertebrae illustrating the increase in vertebral body size. In each set of images [A, and B], controls are on the left, and *Pten*$^{flox/flox}$*:Col2a1Cre* mice are on the right. All *Pten*$^{flox/flox}$*:Col2a1Cre* vertebrae are bigger than in control mice.**

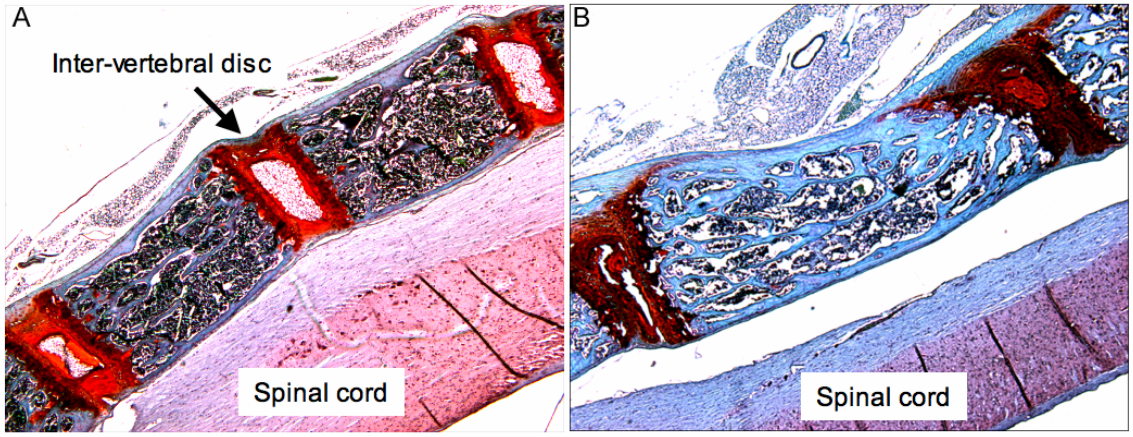


**Figure 3-21. Mid-thoracic vertebral bodies from 15 week control and *Pten*$^{flox/flox}$*:Col2a1Cre* mice. As shown by micro-ct (Figure 3-20), the vertebral bodies of the *Pten*$^{flox/flox}$*:Col2a1Cre* mice are larger than controls. The intervertebral disks also appeared larger in the *Pten*$^{flox/flox}$*:Col2a1Cre* mice.**

The femora was significantly longer in *Pten*$^{flox/flox}$*:Col2a1Cre* mice, being more noticeable in females than males (Figure 3-15). The most striking feature of the long bones was the increased diameter, cortical thickness, and dramatic extent of trabeculation (Figure 3-22). Trabeculation was even present at the level of the femoral mid-shaft, a site where trabeculae tended to be relatively sparse in littermate controls (Figure 3-22). However, the bone marrow microenvironment was not sufficiently depleted to lead to extra-cellular hematopoiesis.

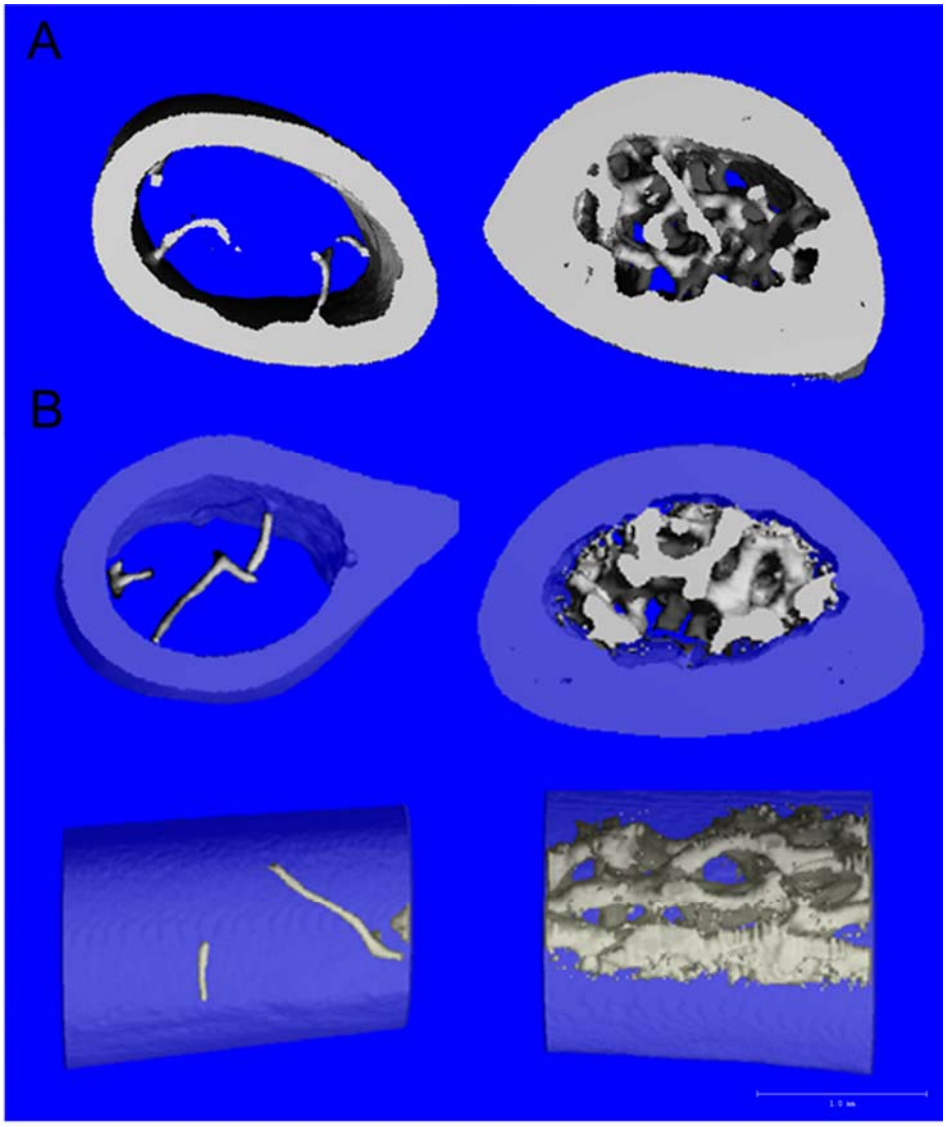


**Figure 3-22. Micro-ct images in [A] are cross-sections through mid-shaft of femurs of representative control (left) and *Pten*$^{flox/flox}$*:Col2a1Cre* (right) mice. Note the extensive trabeculation and increased cortical thickness in the *Pten*$^{flox/flox}$*:Col2a1Cre* sample. [B] Representative volumetric presentations of the femoral mid-shaft trabeculae of control (left) and *Pten*$^{flox/flox}$*:Col2a1Cre* (right) mice are also depicted. Excess trabecualtion has entered into the mid-shaft of the *Pten*$^{flox/flox}$*:Col2a1Cre* femur. In addition, the *Pten*$^{flox/flox}$*:Col2a1Cre* cortical bone is much thicker compared to controls.**

The 3D micro-ct data also revealed that *Pten*$^{flox/flox}$*:Col2a1Cre* males tended to have more robust long bones than the females (Figure 3-23).

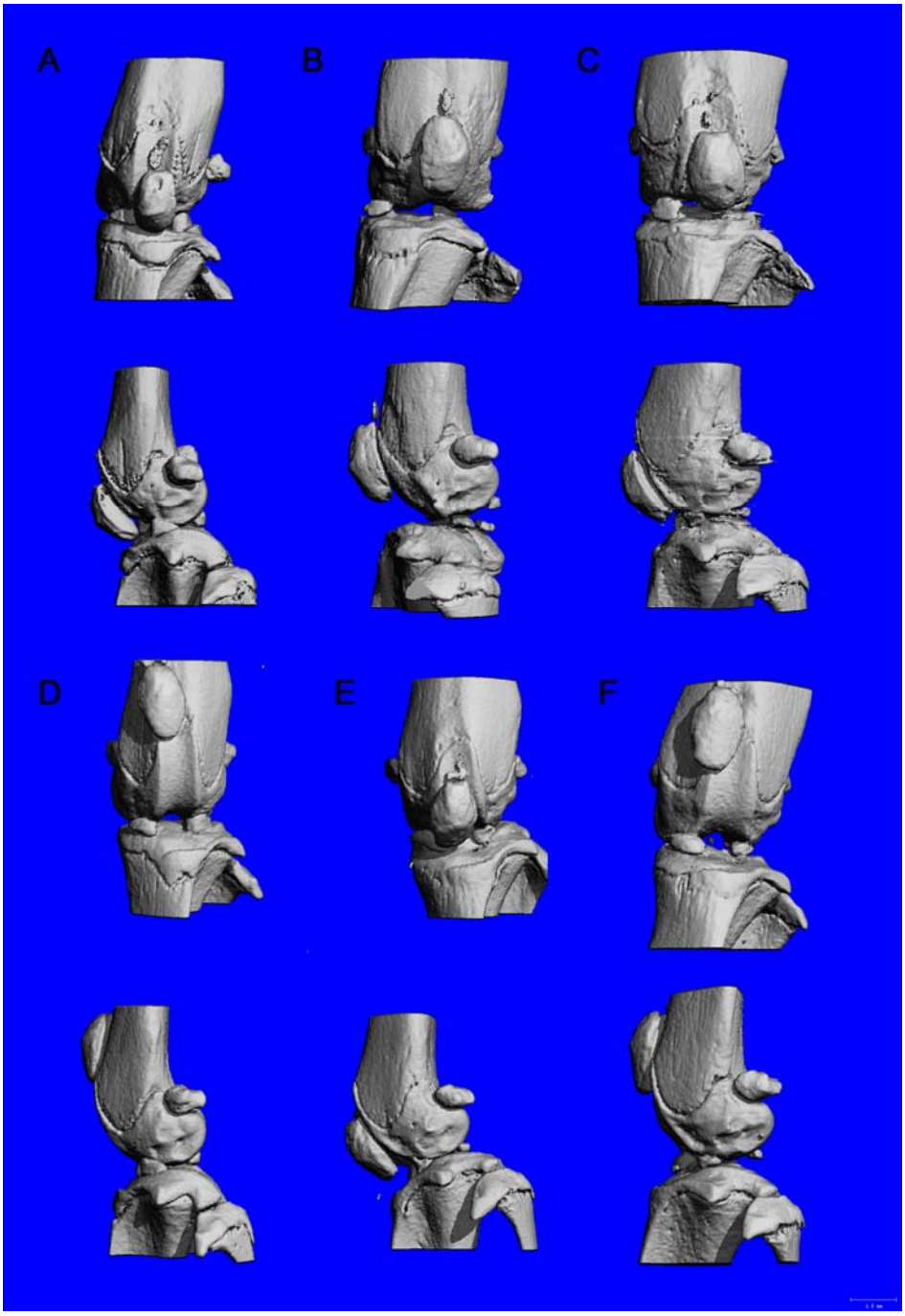


**Figure 3-23. Micro-ct reconstructions (21 μM resolution) of knees from 15 week control [A, D] and *Pten*$^{flox/flox}$*:Col2a1Cre* [B,C,E,F] mice: [top row] anterior view; [bottom row] lateral view; [top group] male; [bottom group] female. Two *Pten*$^{flox/flox}$*:Col2a1Cre* mice were selected for each of the male and female group to represent the variation seen with the phenotype. Note how *Pten*$^{flox/flox}$*:Col2a1Cre* mice have larger bones, such as a wider femur and tibia, enlarged patella, and in some cases enlarged menisci compared to control mice.**

Quantification (Figure 3-24) of the structure of cortical and trabecular bone of mid-femur segments was carried out by micro-ct (n=10 to 12 mice per group; student t-tests).

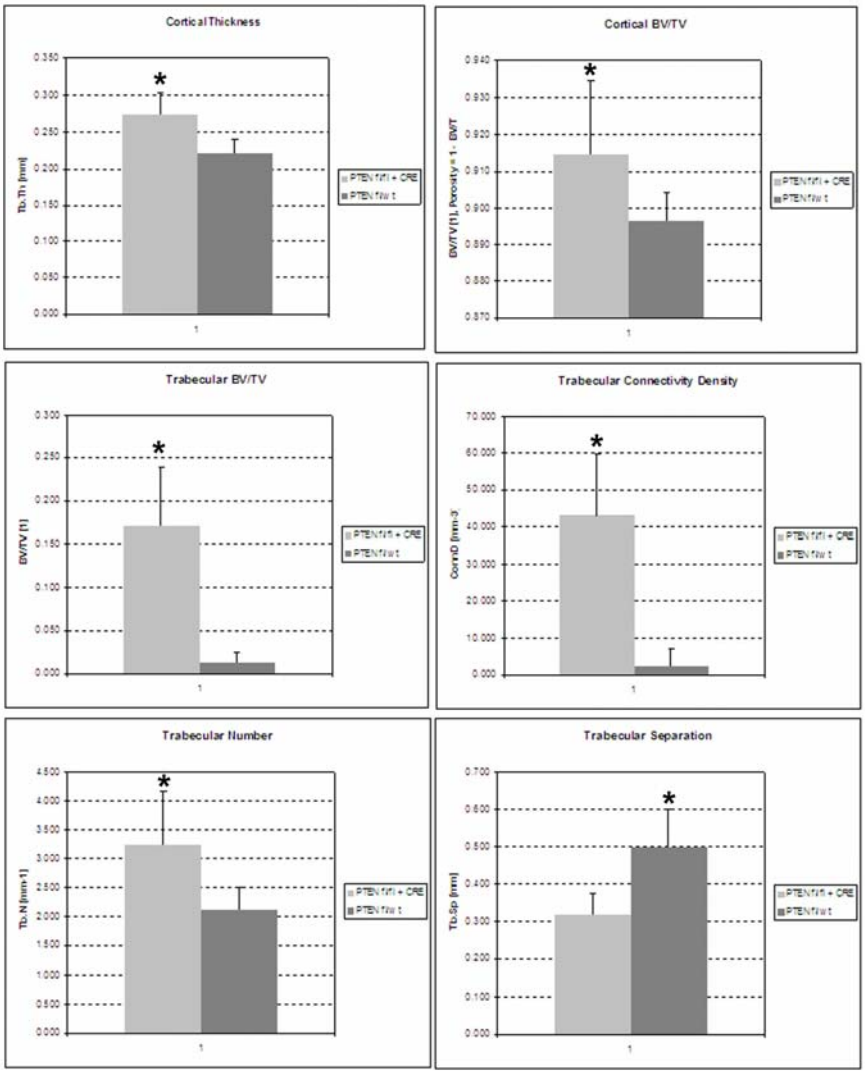


**Figure 3-24. Micro-ct quantitative analysis of cortical and trabecular bone structure of control (n=10, equal numbers of both genders) and experimental (n=12, 7 female and 5 male) mice (one femur per mouse) as indicated. BV = bone volume, TV = tissue volume (* = p<0.001). *Pten*$^{flox/flox}$*:Col2a1Cre* cortical bone had lower 1-BV/TV, but greater thickness. *Pten*$^{flox/flox}$*:Col2a1Cre* trabecular bone had significantly larger BV/TV, TB.N, ConnD, but less Tb.Sp. See text for legends.**

For cortical bone, porosity (1-BV/TV) was lower ($p<0.0092$) in the *Pten$^{flox/flox}$:Col2a1Cre* mice, and thickness was greater ($p<0.00001$). Tissue density differences were not observed. For the trabecular bone, there was an increased bone volume ratio in the *Pten$^{flox/flox}$:Col2a1Cre* group (BV/TV; $p<0.0001$), and more trabeculae (Tb.N; $p<0.0014$) with less separation between trabeculae (Tb.Sp; $p<0.0002$). The number of connections was also higher in the *Pten$^{flox/flox}$:Col2aCre* group (ConnD; $p<0.00001$). Quantitative results showed an increased extent of trabeculation and cortical bone thickening in *Pten$^{flox/flox}$:Col2a1Cre* mouse femora and was in agreement with qualitative assessment of the micro-ct images (Figure 3-22).

To determine whether the enlargement of the vertebrae might be evident pre-natally, we examined the developing skeletons of 18.5 dpc cleared and alcian blue/alizarin red-stained embryos (Figure 3-25).

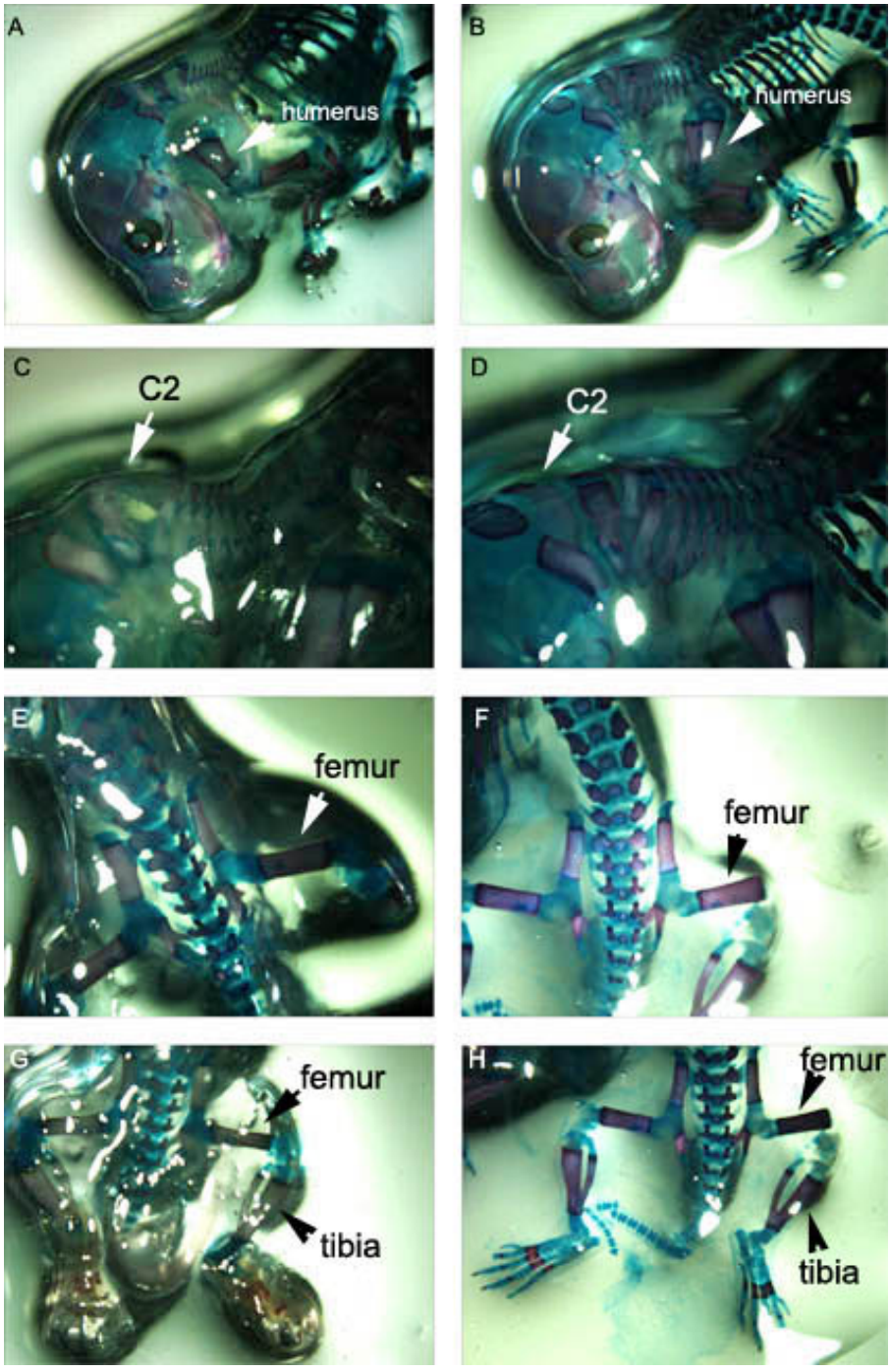


**Figure 3-25. Representative images of 18.5 dpc embryo [A, B] skull (x6), [C,D] cervical spine (x12), [E,F] humeri and femora (x8), [G,H] pelvis (x10). [A,C,D, E] Control embryos and [B, D, F, H] *Pten*$^{flox/flox}$*:Col2a1Cre* embryos. No difference in size of the humerus, pelvis, femur, or C2 width was noted.**

No significant differences (all values p>0.1) were observed in the length of the humeri, femora, pelvis, or size of the C2 vertebrae in the experimental (n=4) or control (n=5) embryos (Figure 3-26), suggesting that the effects of *Pten* deletion on the skeleton occur largely after birth, into adulthood.

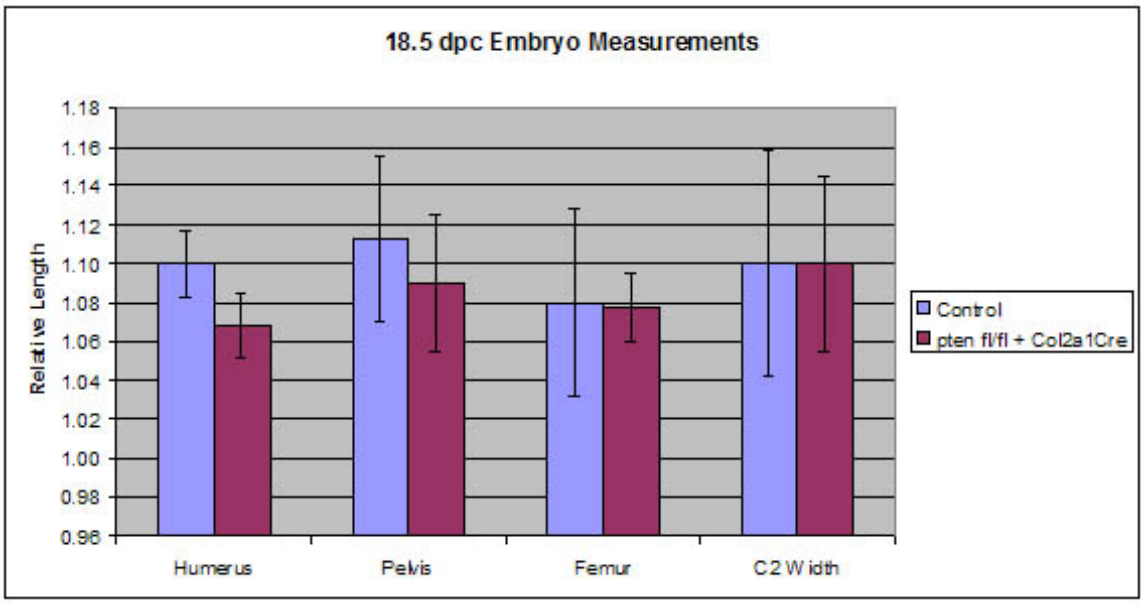


**Figure 3-26. Relative lengths of humeri, femora, pelvis, and C2 vertebrae of 18.5dpc embryos (all values P>0.01). No difference between control and *Pten*$^{flox/flox}$*:Col2a1Cre* embryos was noted at all measured locations.**

### *3.3.4 Epiphyseal growth plate abnormalities in Pten$^{flox/flox}$:Col2a1Cre mice*

A stereological analysis from one week-old growth plates (A-D) from multiple mice revealed no significant changes in the widths of the proliferative (p=0.27), or hypertrophic zones (p=0.22) (Figure 3-27B, Figure 3-28).

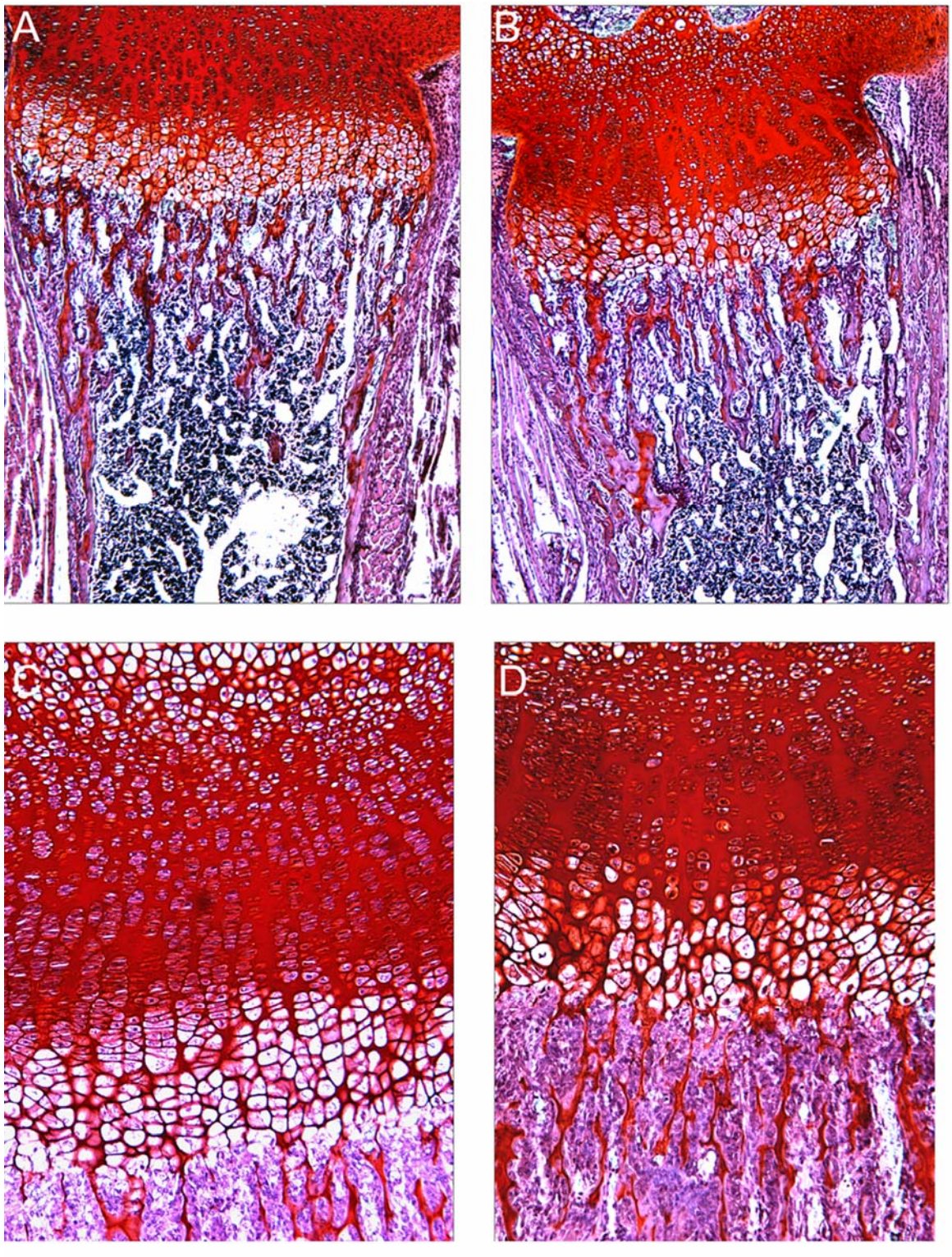
A
B
C
D

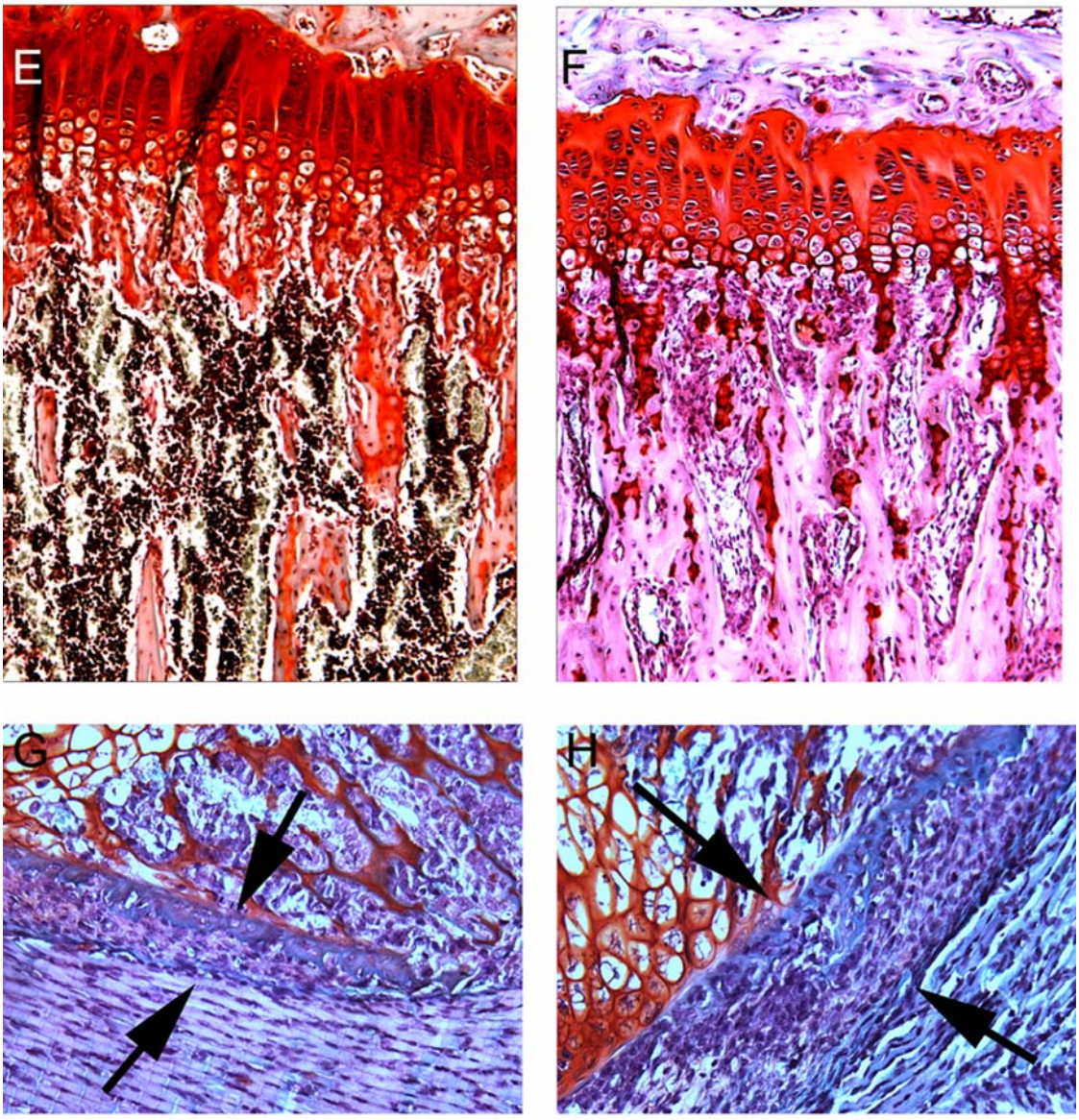


**Figure 3-27. Sections through representative proximal tibial growth plates of control [A, C, E, G] and *Pten*$^{fl/fl}$*:Col2a1Cre* [B, D, F, H] of one week-old (x50) [A, B] and (x100) [C, D], and six week-old (x100) [E, F] mice. Note the disorganization of the growth plate in both one and six week-old mice. In [D], note that the proliferating zone cells look more rounded compared to the control mice [C]. Note the excess mineralization under the growth plate at 6 week old of the *Pten*$^{flox/flox}$*:Col2a1Cre* mouse [F] compared to the control [E]. [G,H] Representative images of perichondrium and nascent bone collar formation adjacent to proximal tibial growth plates of one week-old control [G] and *Pten*$^{fl/fl}$*:Col2a1Cre* [H] mice. Arrows indicate the lateral boundaries of the perichondrium at the level of the sub-hypertrophic chondrocyte region. No male/female difference was noted in the growth plates.**

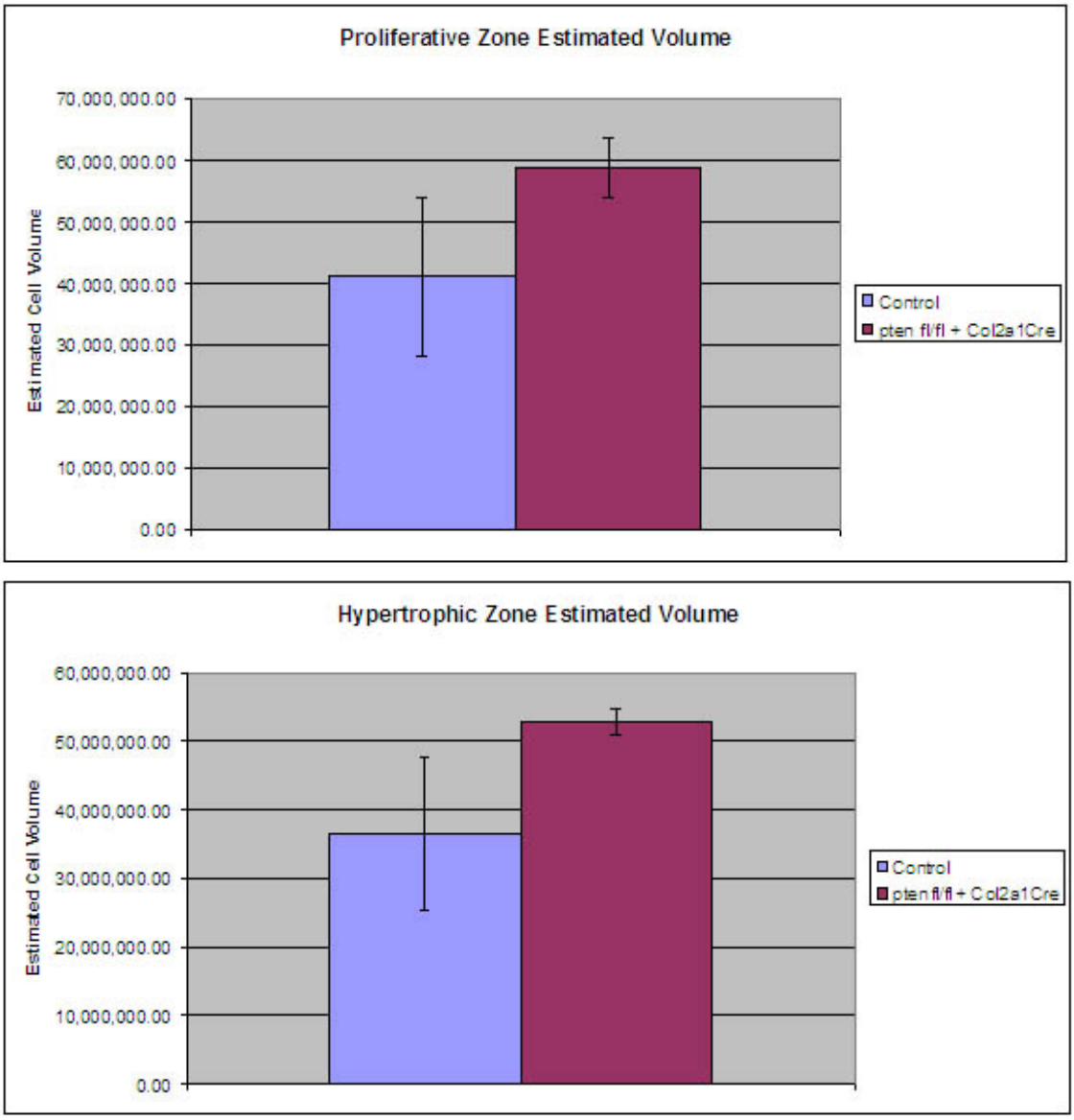


**Figure 3-28. Growth plate volume ($\mu m^3$) of the proliferative and hypertrophic zone in one week old control and *Pten$^{flox/flox}$:Col2a1Cre* mice, p=0.27, and p=0.22, respectively. No difference was seen between between control and *Pten$^{flox/flox}$:Col2a1Cre* mice. An outlier control mouse makes there a appear to be a trend for the *Pten$^{flox/flox}$:Col2a1Cre* to have larger growth plate volumes.**

In both the one (Figure 3-27A-D) and six (Figure 3-27E,F) week-old mice, chondrocytes in the *Pten$^{flox/flox}$:Col2a1Cre* growth plates appeared more disorganized relative to those

of controls (Figure 3-27A, B), with a less well-defined demarcation between the proliferative zone and the start of the hypertrophic zone, and less of a smooth progression in cell size when moving from the proliferative to the hypertrophic zone (Figure 3-27C, D). Cells of the proliferative zone of the *Pten*$^{flox/flox}$*:Col2a1Cre* growth plates also tended to be less discoid, and more rounded in shape, hinting that premature hypertrophic differentiation might be present (Figure 3-27E, F). However, there was no change in cell size, cell size distribution (Figure 3-29), or cell number (Figure 3-30) in either the proliferative or hypertrophic zone.

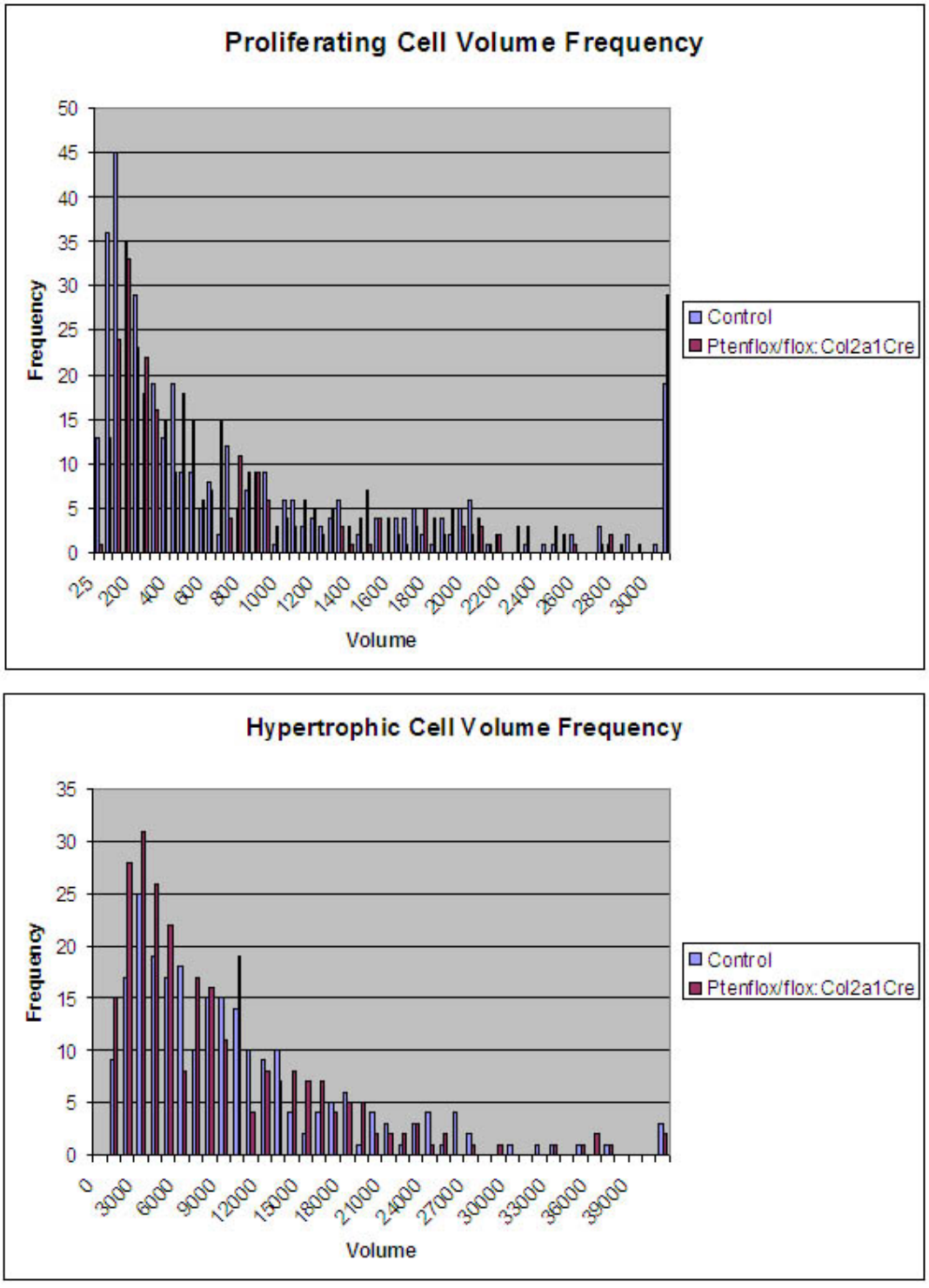


**Figure 3-29. Cell volume distribution in the proliferative [A] and hypertrophic [B] zones of one week old control and *Pten*$^{flox/flox}$*:Col2a1Cre* mice. No change was observed in average cell size or cell size distribution between control and *Pten*$^{flox/flox}$*:Col2a1Cre* mice despite the application of multiple statistical tests.**

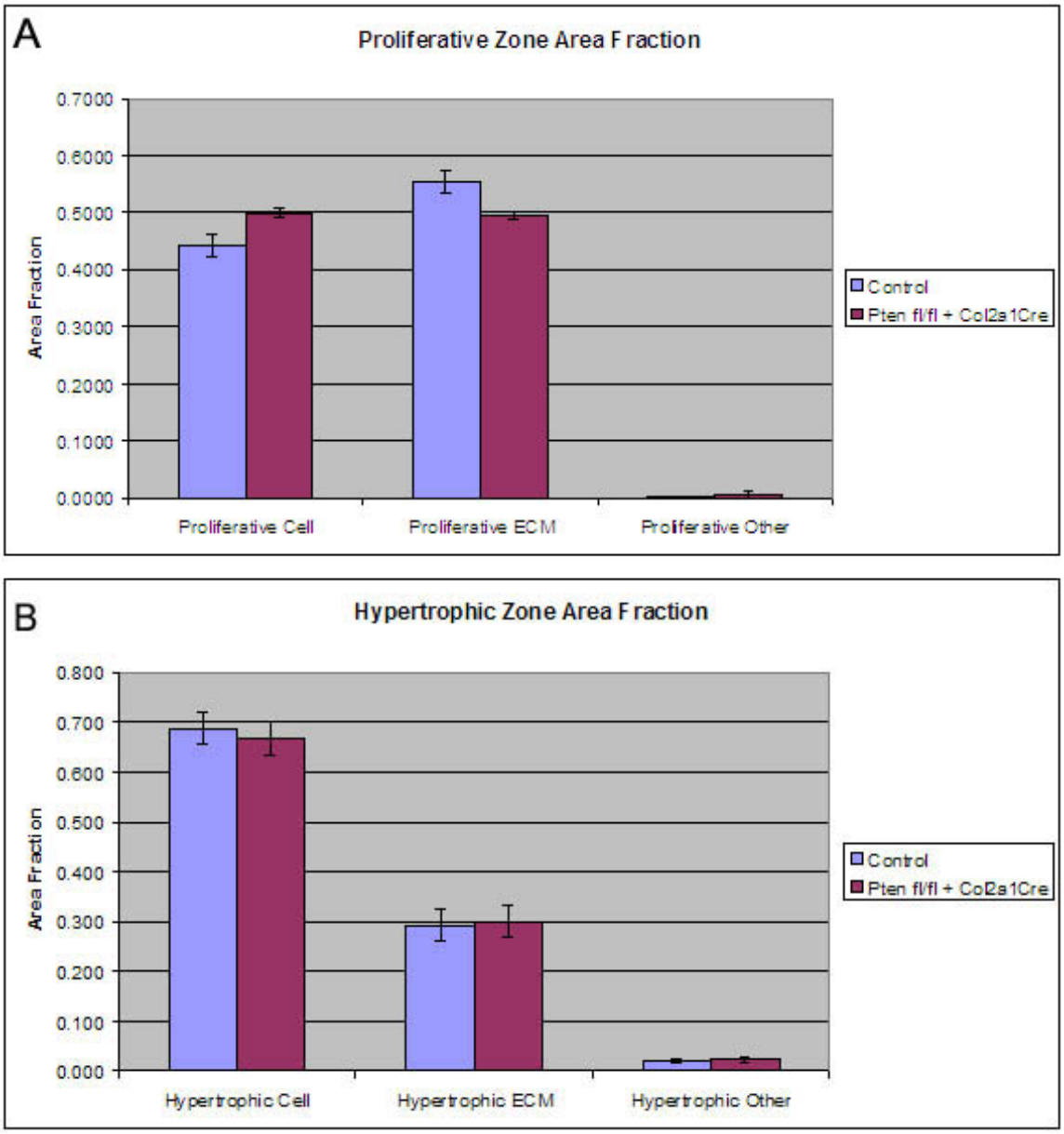


**Figure 3-30. Total cell number in proliferative [A] and hypertrophic [B] regions, as measured by the optical dissection probe, in control and *Pten*$^{flox/flox}$*:Col2a1Cre* mice. No difference is cell number in either the proliferative (p=0.25) or hypertrophic (p=0.48) zones was observed.**

In keeping with the micro-ct results (Figure 3-22) there was a qualitative increase the number, size, and disorganization of the trabeculae within the primary spongiosa (Figure

3-27E, F), and perichondrial bone collar formation was also more exuberant in *Pten$^{flox/flox}$:Col2a1Cre* mice (Figure 3-27G, H). The thickness of the nascent bone collars being formed by osteoblasts beneath the perichondria was also increased in the *Pten$^{flox/flox}$:Col2a1Cre* tibiae (Figure 3-27H).

Within the proximal tibial epiphyses of *Pten$^{flox/flox}$:Col2a1Cre* mice, we invariably observed a bony 'bridge' that developed across in the mid-region of the growth plate (Figure 3-31A).

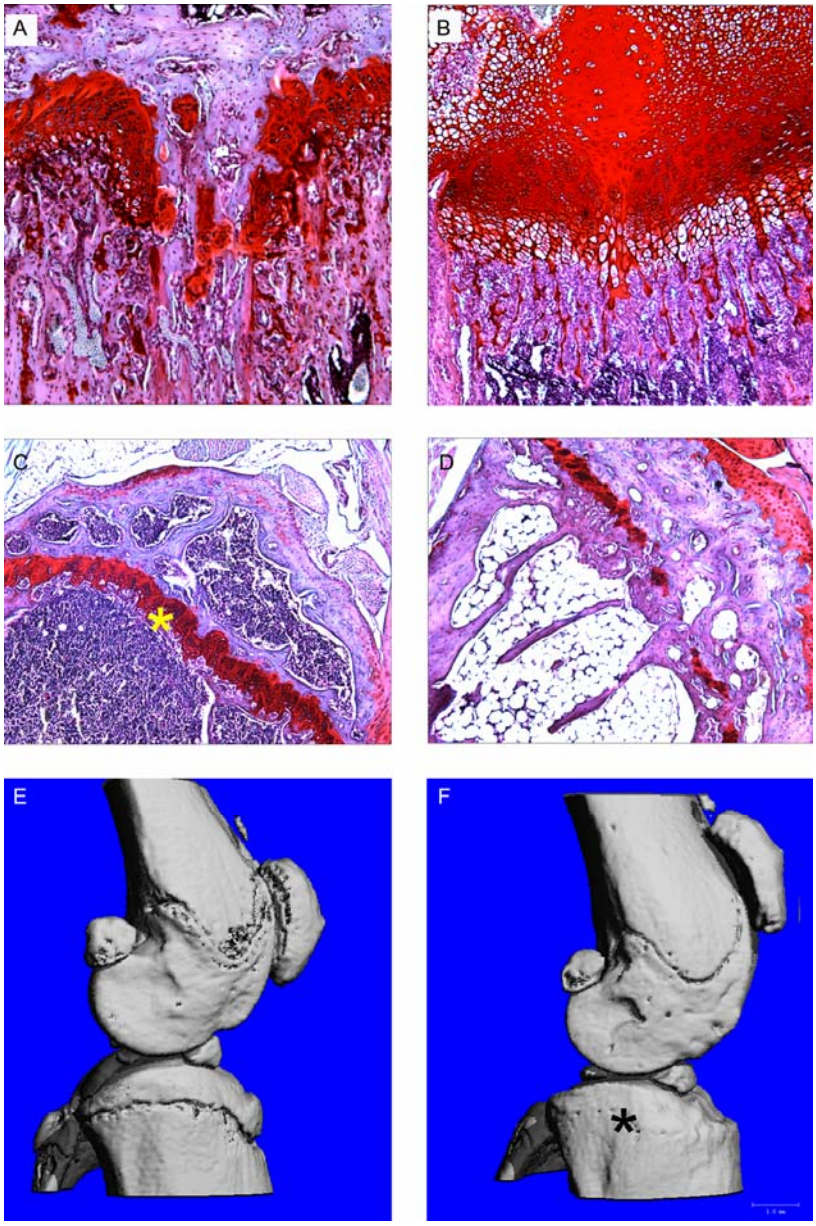


**Figure 3-31. [A] Representative *Pten*$^{flox/flox}$*:Col2a1Cre* proximal tibia at six weeks of age showing the characteristic bony 'bridge' that develops across the mid-region of the growth plate. [B] Distal femoral head of a representative one week-old mouse showing characteristic GAG-rich matrix 'lake' seen in *Pten*$^{flox/flox}$*:Col2a1Cre* mice. [C, D] Representative proximal tibial epiphysial growth plates of six month old control (marked by asterisk) [C], and *Pten*$^{flox/flox}$*:Col2a1Cre* [D] mice. Note fusion of the growth plate in *Pten*$^{flox/flox}$*:Col2a1Cre* mice. There are was an increased marrow fat in the *Pten*$^{flox/flox}$*:Col2a1Cre* mice [E, F] Representative micro-ct reconstructions (21 μM) of the medial aspect of the knees of six month male control [E] and *Pten*$^{flox/flox}$*:Col2a1Cre* [F] mice. Asterisk in [F] indicates site of proximal tibial growth plate fusion. No male/female difference was noted.**

We also observed ‘lakes’ of strongly GAG-staining matrix in the distal femoral heads of all 1 week-old *Pten*$^{flox/flox}$*:Col2a1Cre* mice examined (Figure 3-31B). Perhaps consistent with this latter feature, there were larger amounts of matrix between clusters of hypertrophic and proliferative chondrocytes in *Pten*$^{flox/flox}$*:Col2a1Cre* mice (Figure 3-27D, Figure 3-31B). However, when we examined the areal fraction of cells to ECM, we found that there was a higher ratio of cells to ECM in the proliferative zone of *Pten*$^{flox/flox}$*:Col2a1Cre* mice to control mice; no difference in areal fraction was seen in the hypertrophic region (Figure 3-32).

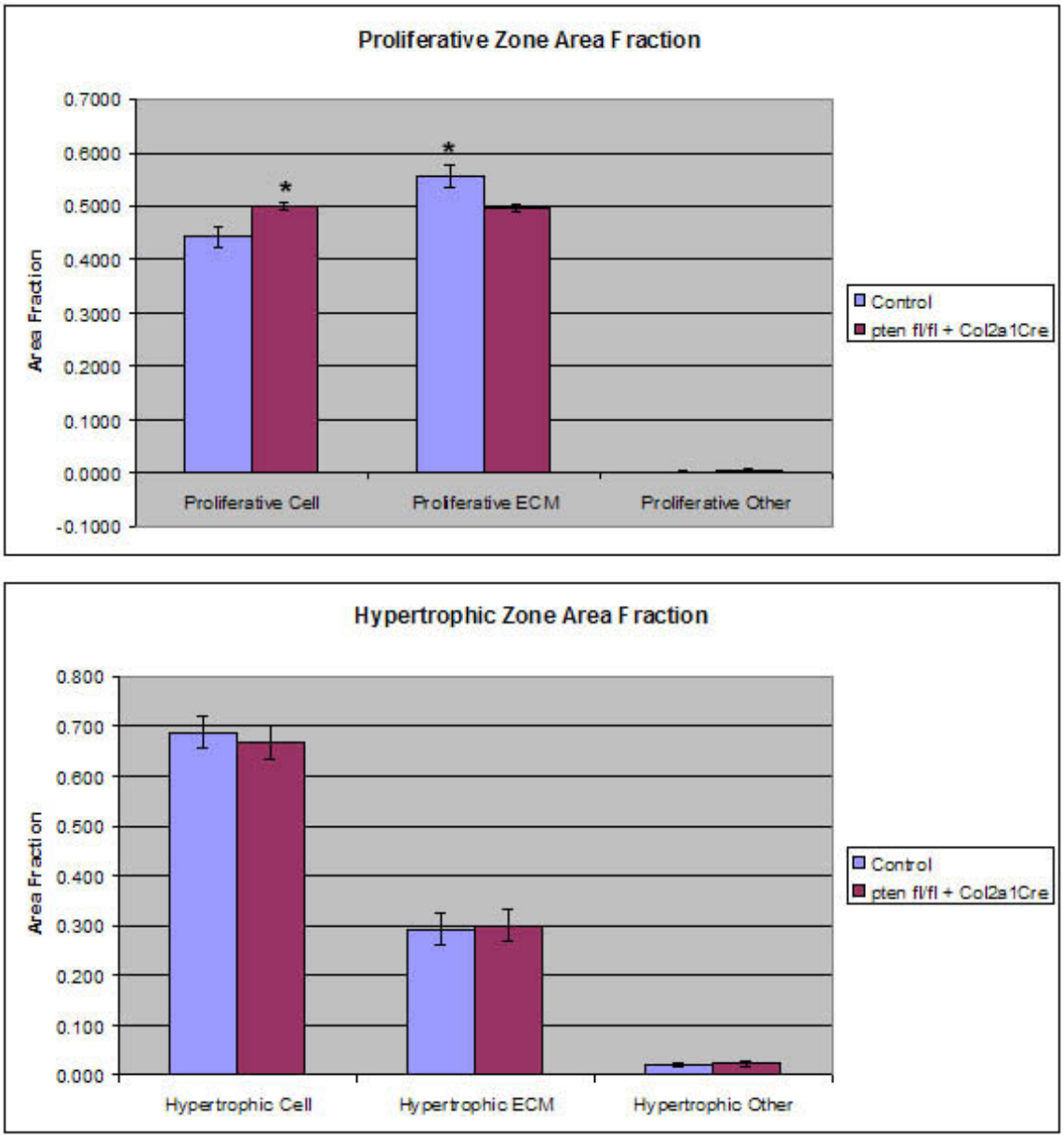


**Figure 3-32. Total area fraction of cells, ECM, and other (bone) in the proliferative and hypertrophic regions of one week old control [A] and *Pten*$^{flox/flox}$*:Col2a1Cre* [B] mice. A significant difference in total ratio of cells and ECM between control and *Pten*$^{flox/flox}$*:Col2a1Cre* mice (* = p<0.05) in the proliferative zone was observed, but not in the hypertrophic zone (p>0.05).**

Lastly, and in contrast to wild-type mice whose proximal tibial epiphyseal growth plates do not fuse with age, the tibial growth plates of *Pten*$^{flox/flox}$*:Col2a1Cre* mice were fused by

6 months of age (Figure 3-31 C, F), suggesting there may be a defect in the germinal zone of the growth plate. Also with age, there was increased marrow fat compared to control mice (Figure 3-31 C, D)

Lack of Pten activity has been associated with increased cellular resistance to apoptosis [146], however, TUNEL assay of *Pten$^{flox/flox}$:Col2a1Cre* growth plates revealed no change in the normally low levels of apoptotic cells observed in the lower hypertrophic zone (Figure 3-33).

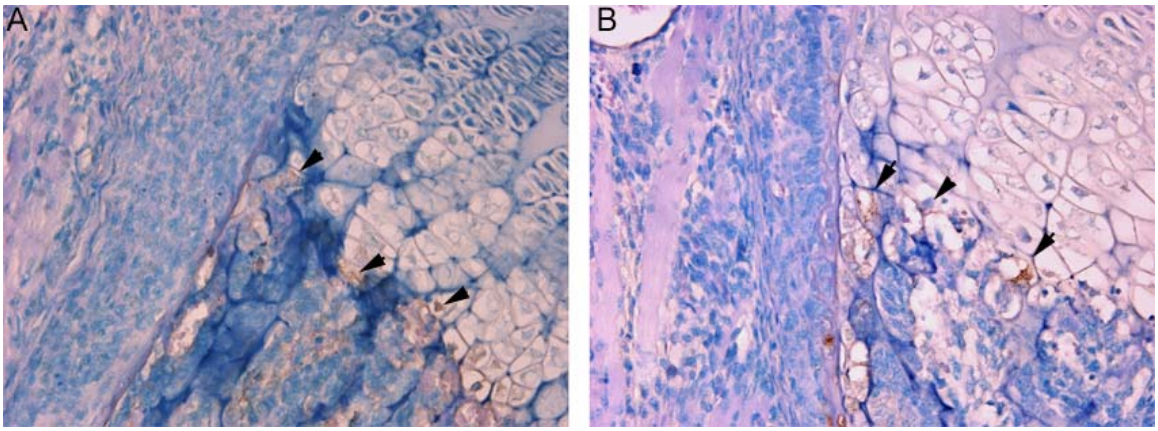


**Figure 3-33. Representative TUNEL staining in one week control [A] and *Pten$^{flox/flox}$:Col2a1Cre* [B] mice. No difference was apparent between the two groups (arrows mark some positive cells).**

Although Pten deficiency has also been associated with increased cell proliferation [146], BrdU incorporation by proliferative zone chondrocytes of one week-old *Pten$^{flox/flox}$:Col2a1Cre* pups was not significantly different from that of controls (p=0.2) (Figure 3-34).

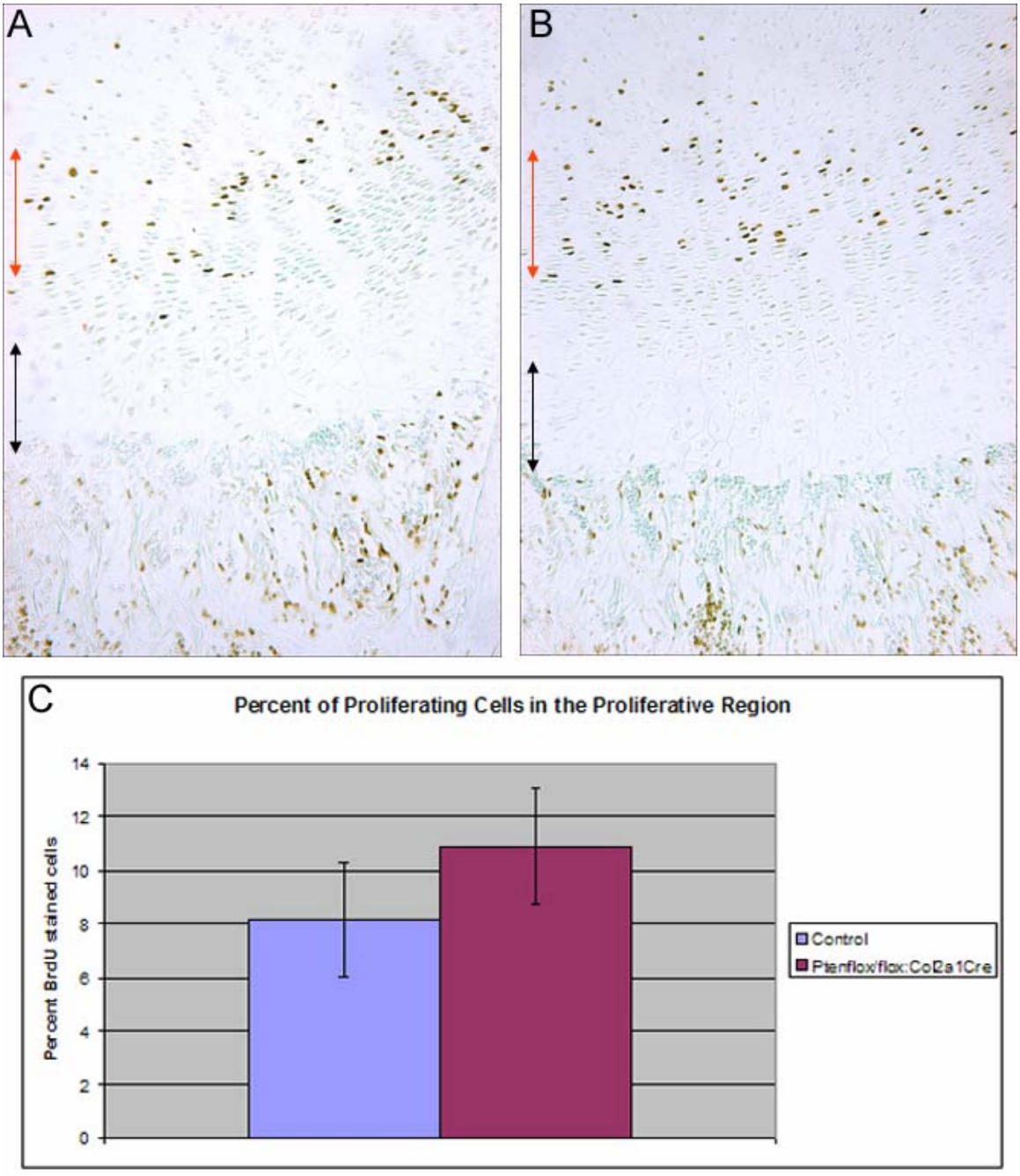


**Figure 3-34. [A,B] BrdU incorporation (following 2-hr *in vivo* exposure) shows S-phase cells in proliferative zone (red arrow) of one week old tibial growth plates of [A] control and [B] *Pten*$^{flox/flox}$*:Col2a1Cre* mice; hypertrophic zone is marked by black arrows. [C] Percent of BrdU positive cells in the proliferative zone of one week old growth plates control (n=5) and *Pten*$^{flox/flox}$*:Col2a1Cre* (n=6) mice. No significant difference was seen (p=0.2).**

Since Pten loss could lead to altered differentiation, we next determined whether the transit of chondrocytes into the hypertrophic stage might be altered in the growth plates of *Pten$^{flox/flox}$:Col2a1Cre mice.* Immunohistochemistry for type X collagen, a marker of hypertrophic differentiation was evaluated. Compared to controls, expression of type X collagen protein in one week-old *Pten$^{flox/flox}$:Col2a1Cre* mouse growth plates was not only increased, but also appeared to be accelerated, with expression of this protein encroaching well into the proliferative zone (Figure 3-35 A, B).

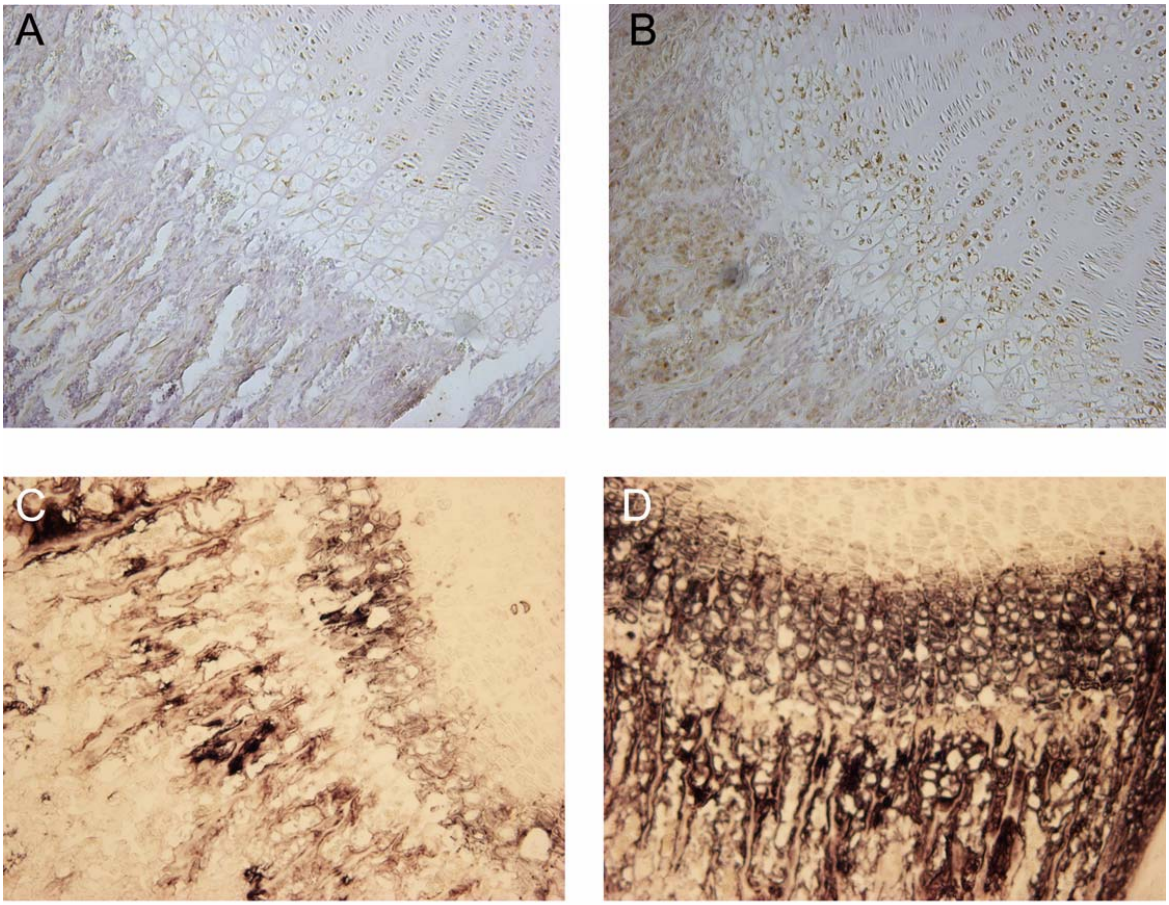


**Figure 3-35. [A, B] Representative proximal tibial growth plates of one week-old control [A] and *Pten*$^{flox/flox}$*:Col2a1Cre* [B] mice stained for type X collagen protein expression. Note that staining develops higher in the growth plate than in control mice. [C, D] ALP activity in the growth plates of representative one week-old control [C] and *Pten*$^{flox/flox}$*:Col2a1Cre* [D] mice. Staining was more intense in both the osteoblasts and the hypertrophic chondrocyte layer, and also wider, extending up into the proliferative layer of *Pten*$^{flox/flox}$*:Col2a1Cre* growth plates [D].**

The growth plates of *Pten*$^{flox/flox}$*:Col2a1Cre* mice were also stained for ALP activity, another marker of hypertrophic differentiation as well as product of differentiating osteoblasts. Interestingly, compared to controls, a dramatic increase in ALP staining was evident in not only in hypertrophic zone chondrocytes, but also in osteoblasts of the primary spongiosa of *Pten*$^{flox/flox}$*:Col2a1Cre* tibiae (Figure 3-35 C, D). Furthermore, the

width of the ALP-positive hypertrophic zone was considerably wider than that of the controls, again suggestive of accelerated differentiation of growth plate chondrocytes. As the width of the growth plates, and the hypertrophic zones did not vary significantly between *Pten*$^{flox/flox}$*:Col2a1Cre* and control mice, we attribute these findings to accelerated chondrocyte differentiation rather than to an accumulation (for example, due to reduced apoptosis) of differentiated hypertrophic cells or hyperproliferation.

To determine whether the increased trabecular bone seen in *Pten*$^{flox/flox}$:*Col2a1Cre* mice might be related to augmented hypertrophic chondrocyte-derived VEGF production, and hence increased vascularization of the primary spongiosa, immunostaining for CD31 (PECAM) was performed (Figure 3-36).

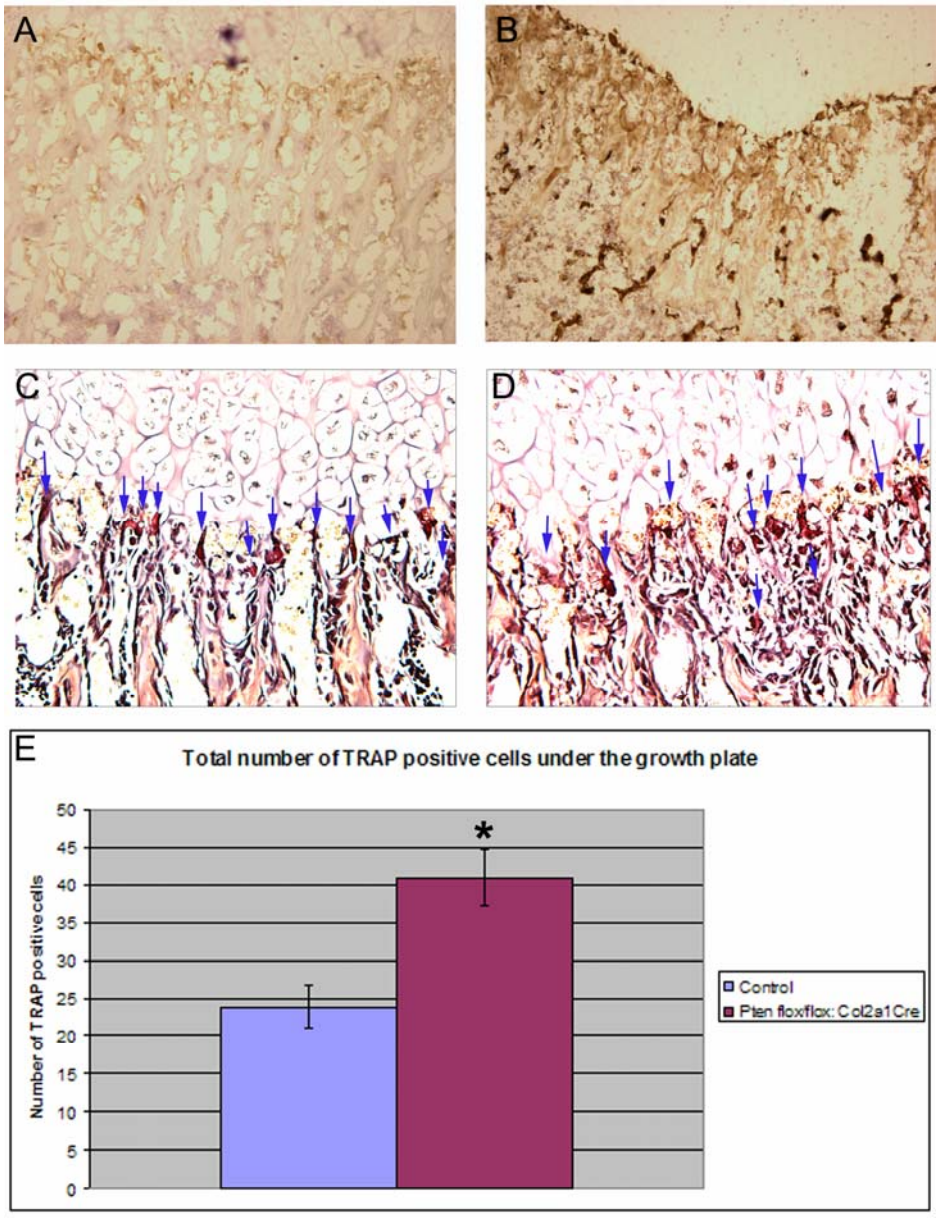


**Figure 3-36. [A, B] Representative proximal tibial growth plates of one week-old control [A] and *Pten*$^{flox/flox}$*:Col2a1Cre* [B] mice stained CD31 (PECAM) expression, as a measure of vascularity, in representative one week-old control [A] and *Pten*$^{flox/flox}$*:Col2a1Cre* [B] mice. Expression of CD31 was more prominent in the *Pten*$^{flox/flox}$*:Col2a1Cre* mice. [C,D] TRAP staining, as a measure of osteoclast number, in representative 1 week-old control [C] and *Pten*$^{flox/flox}$*:Col2a1Cre* [D] mice. [E] Table showing the number of TRAP staining cells immediately beneath the proximal tibial growth plates (5-6 sections per animal) of control (n=6) versus *Pten*$^{foxl/flox}$ *:Col2a1Cre* (n=6) 1 week-old mice. There were 1.7 times more osteoclasts present below *Pten*$^{flox/flox}$ *:Col2a1Cre* growth plates (* p= 0.0023).**

The increased prominence of CD31 (PECAM) stained vessels in *Pten$^{flox/flox}$:Col2a1Cre* mice would be in keeping with an alteration in the differentiated state of the hypertrophic zone. Perhaps in keeping with the increased vascularity and VEGF production, there was evidence of increased osteoclast influx into the primary spongiosa: when TRAP (tartrate-resistant acid phosphatase) staining was used to enumerate osteoclasts beneath the sub-hypertrophic zone, a significant (1.7-fold) increase in their numbers was found in *Pten$^{flox/flox}$:Col2a1Cre* mice (Figure 3-36 C to E).

With the increased trabeculae within the primary spongiosa and perichondrial bone collar formation we wished to investigate if there was an increase in osteoblast activity markers. We looked at both type I collagen, the chief organic component of bone, and osteopontin, a molecule produced by osteoblasts and is involved in cell adhesion (involved in osteoclast binding) [221]. We found no difference in the expression pattern or staining intensity of either type I collagen (Figure 3-37A, B) or osteopontin (Figure 3-37C, D).

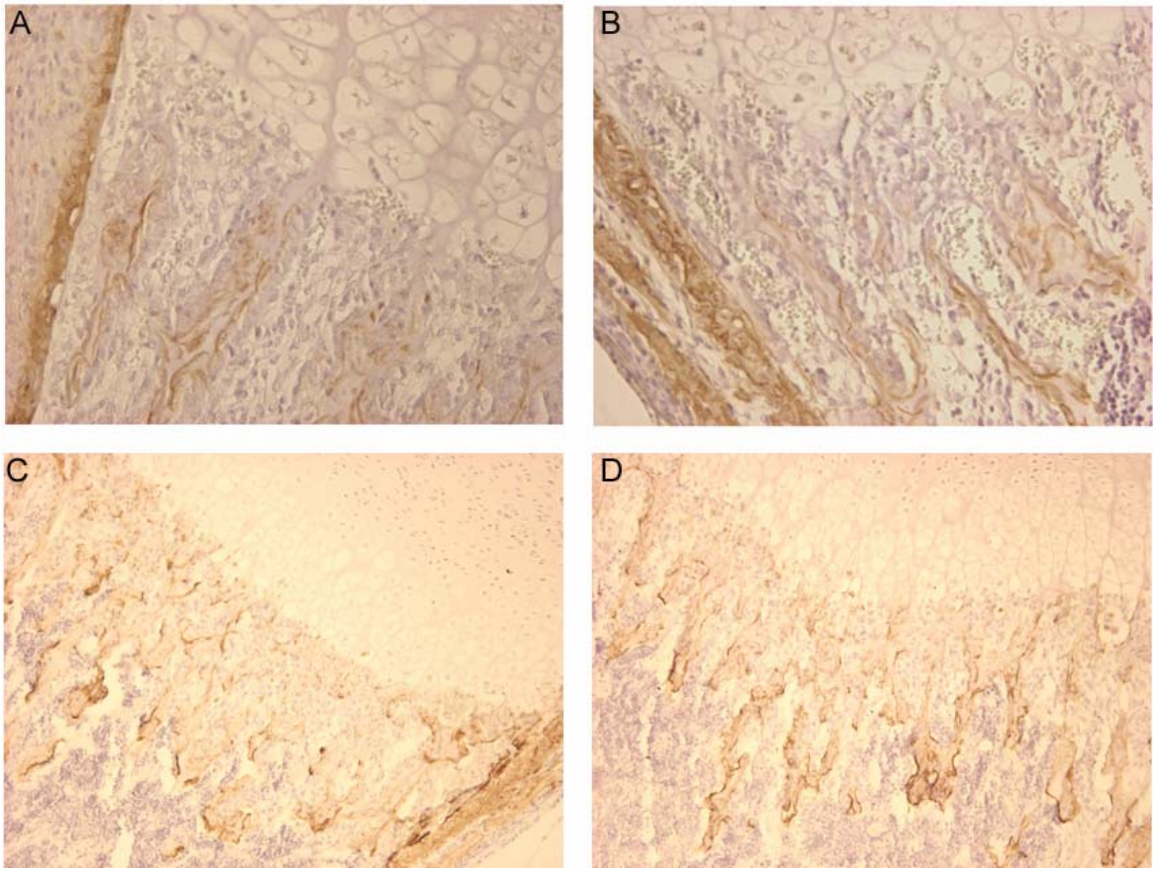


**Figure 3-37. [A, B] Representative proximal tibial growth plates of one week-old control [A] and *Pten*$^{flox/flox}$*:Col2a1Cre* [B] mice stained for type I collagen protein expression. No differences in staining was observed between the control and *Pten*$^{flox/flox}$*:Col2a1Cre* mice. [C, D] Osteopontin staining in the growth plates of representative one week-old control [C] and *Pten*$^{flox/flox}$*:Col2a1Cre* [D] mice. There was no change in expression patterns between the control and *Pten*$^{flox/flox}$*:Col2a1Cre* mice.**

### *3.3.5 Cell types undergoing Col2a1Cre-mediated gene excisions*

The *Col2a1Cre* line [218] has been widely employed to trigger genetic alteration in chondrocytes, however, given the prominent skeletal phenotype (involving both trabecular and cortical bone) of the *Pten*$^{flox/flox}$:*Col2a1Cre* mice we investigated the nature of the cells undergoing gene excisions in more detail. To accomplish this *Col2a1Cre* mice were crossed with the ROSA26 *lacZ* reporter (R26R) strain [222]. In one week-old

mice, whole mount staining for *lacZ* was followed by paraffin embedding and histological sectioning. We found *lacZ* expression not only in all chondrocytes and perichondrium (Figure 3-38), but also in osteoblastic cells within the primary spongiosa and the nascent sub-perichondrial bone collar (Figure 3-38).

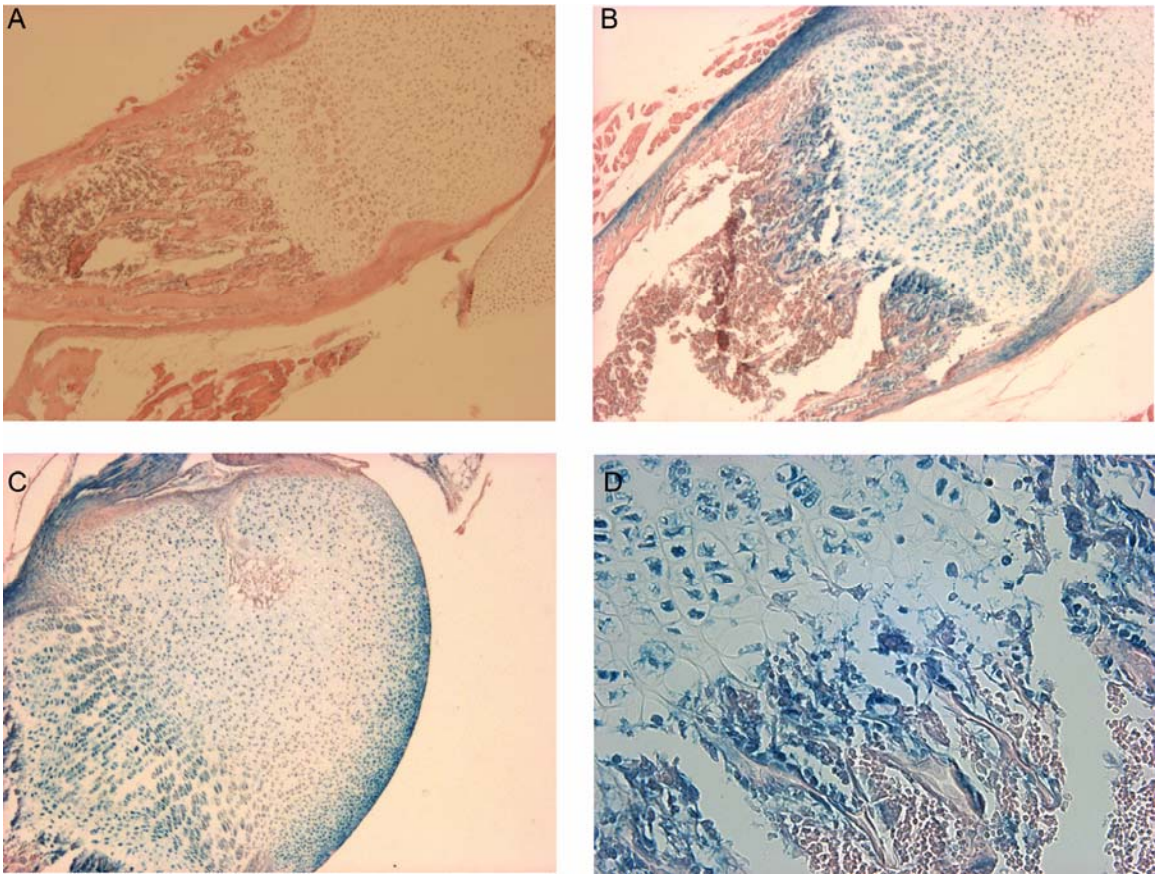


**Figure 3-38. Representative β-galactosidase expression patterns in knee joint sections from 1 week-old control [A] and *R26R:Col2a1Cre* [B, C, D] mice. While no staining was evident in control mice [A], β-galactosidase expression was present in articular [C] and epiphyseal growth plate chondrocytes [B], the perichondrium [B], as well as osteoblasts within the primary spongiosa adjacent to the hypertrophic chondrocyte zone [D].**

Furthermore, we observed *lacZ*-positive staining of osteocytes in the skull bones derived from both the chondrocranium (e.g. occipital bone) (Figure 3-39A) and dermatocranium (e.g. frontal bone) (Figure 3-39B).

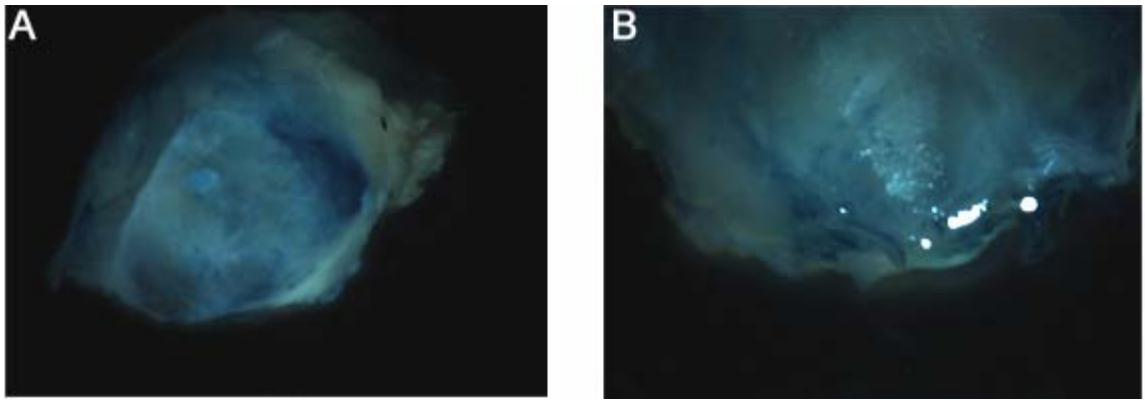


**Figure 3-39. Representative β-galactosidase expression patterns in the chondrocranium [A] and dermatocranium [B] of *R26R:Col2a1Cre* mice.**

These results indicate that *Col2a1Cre*-mediated excisions of the *lacZ* reporter transgene, and likely the floxed *Pten* gene, are not confined to chondrocytes, but occurr more widely in the osteo-chondral lineage.

### 3.4 Aging Study

#### *3.4.1 Changes in articular cartilage and the joint structure at 6 months of age:*

Wild type littermate controls, like many other normal six month old mice we have analyzed in the past, show no histological evidence of knee joint pathology. *Pten*$^{flox/flox}$*:Col2a1Cre* mice, in contrast, exhibit a novel form of spontaneous knee joint pathology. The medial compartments had some minor articular damage (Figure 3-40A, B), while the lateral tibio-femoral compartment was spared. Most of the changes resulted in meniscal degeneration (Figure 3-40C), and articular fibrillations in the patellofemoral compartment (Figure 3-40D).

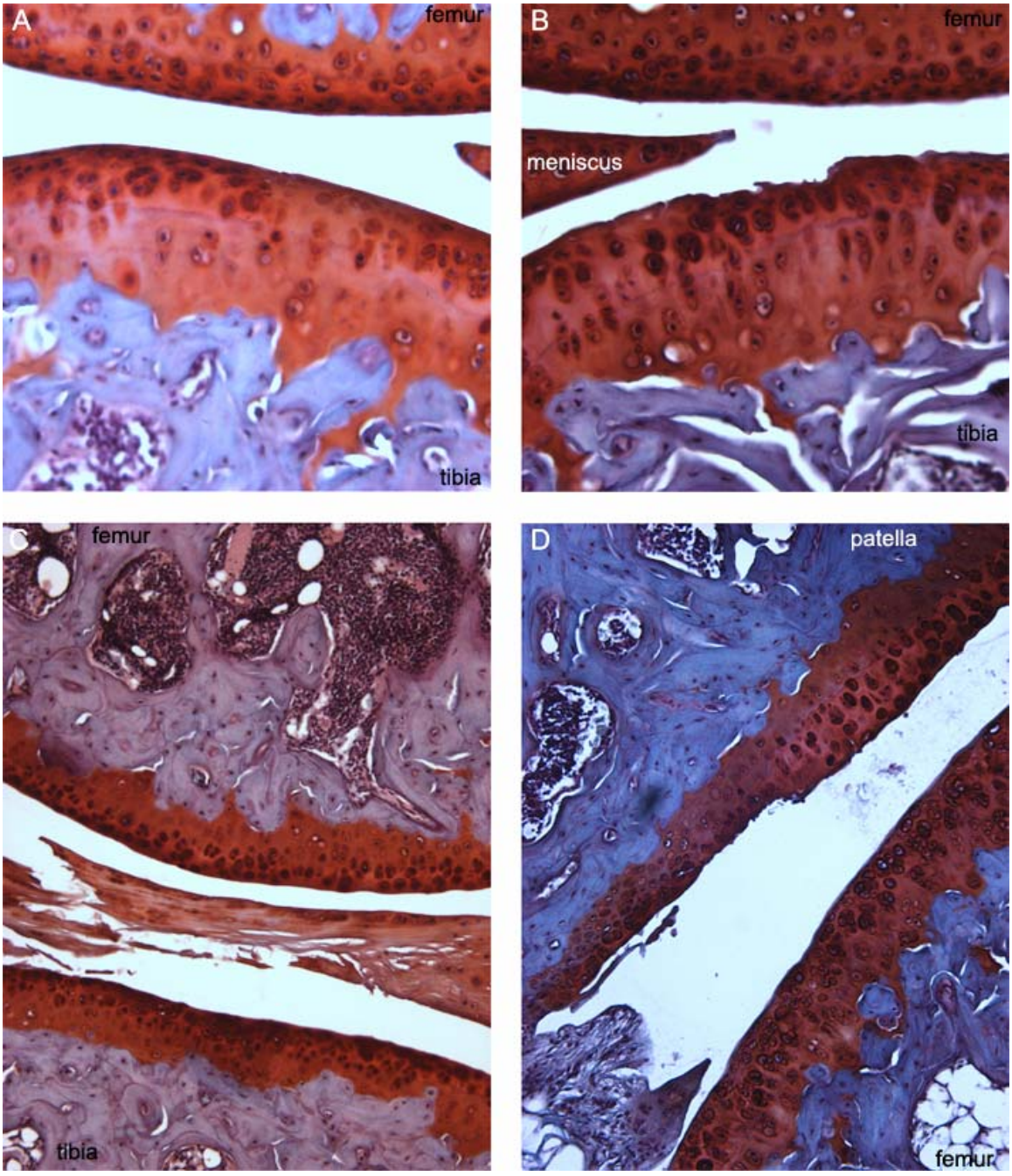


**Figure 3-40. Representative sections of six month old knees from control [A] and *Pten*$^{flox/flox}$*:Col2a1Cre* mice [B to D]. [A, B] Representative image from cartilage in the lateral tibio-femoral compartment, control mice [A] are unaffected while *Pten*$^{flox/flox}$*:Col2a1Cre* mice [B] have some minor fraying and roughness to the articular surface. [C] Damage to meniscus, with fraying, and fragmentation in *Pten*$^{flox/flox}$*:Col2a1Cre* mice. [D] Cartilage degeneration of the patella in *Pten*$^{flox/flox}$*:Col2a1Cre* mice. Very little meniscal tearing was present in the controls, while no damage to the patellar-femoral compartment was present in controls.**

GAG depletion was also present in all *Pten*$^{flox/flox}$*:Col2a1Cre* mice examined (Figure 3-41).

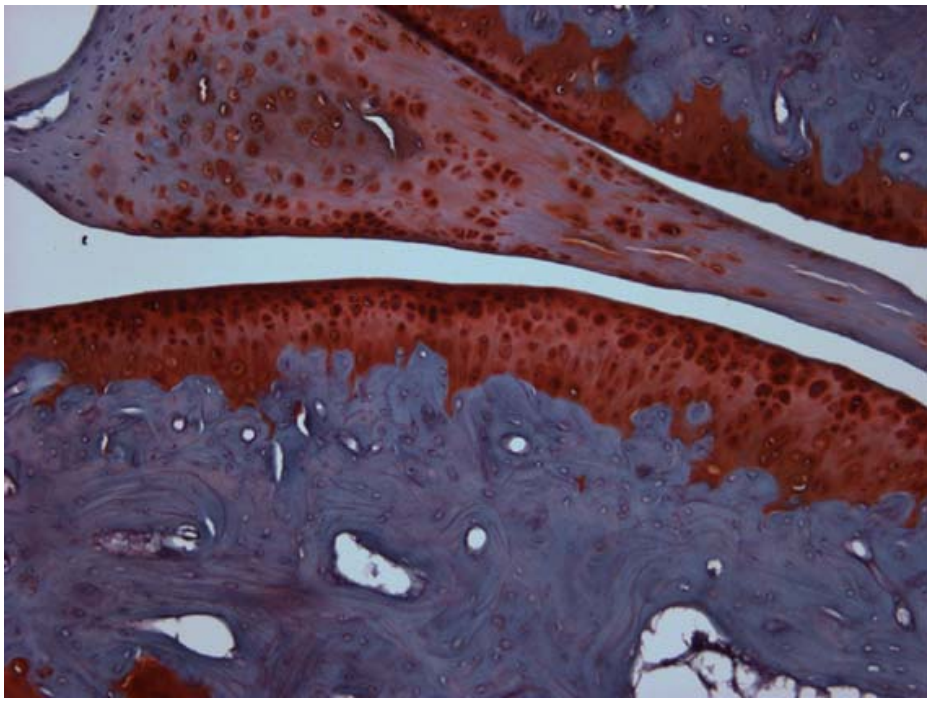

**Figure 3-41. GAG depletion observed in *Pten*$^{flox/flox}$*:Col2a1Cre* articular cartilage.**

The *Pten*$^{flox/flox}$*:Col2a1Cre* mice also show a synovial reaction to joint damage, most evident in sagittal sections taken at the level of the cruciate ligaments. This was characterized by: (a) chronic inflammatory infiltrates within the synovium and around vessels (Figure 3-42); (*b*) mild synovial hyperplasia and activation (manifested by increased membrane processes) (Figure 3-42); and (*c*) increased synovial fibrous tissue content and striking capsular fibrous thickening (Figure 3-43 and Figure 3-44).

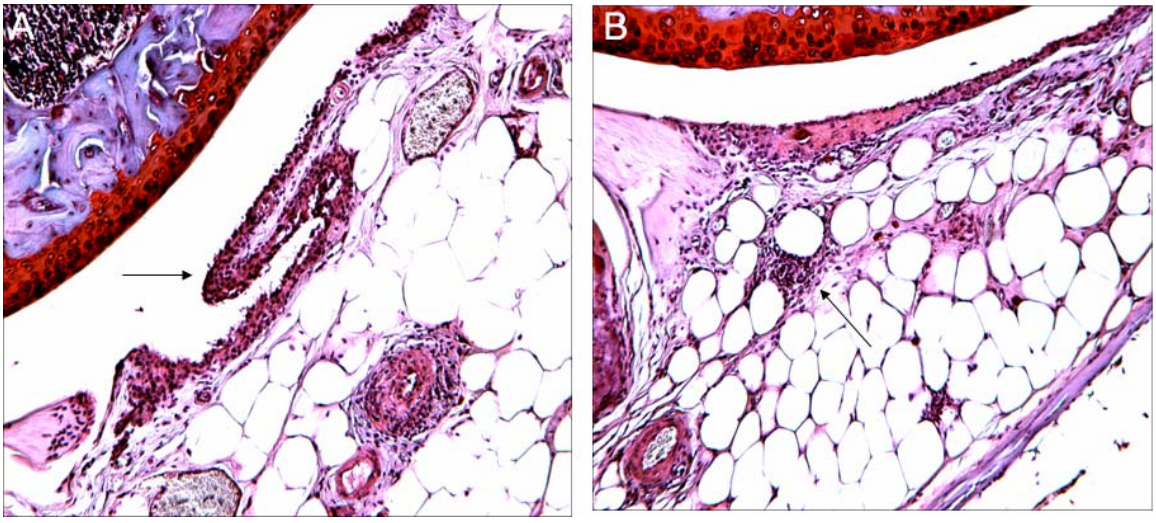


**Figure 3-42. [A, B] Synovium of six month *Pten*$^{flox/flox}$*:Col2a1Cre* knees. [A] Synovial hyperplasia is observed in the *Pten*$^{flox/flox}$*:Col2a1Cre* mice, but is not present in the controls (arrow indicates synovial hyperplasia). [B] Arrow indicates an area with a chronic inflammatory cell infiltrate, again not seen in controls.**

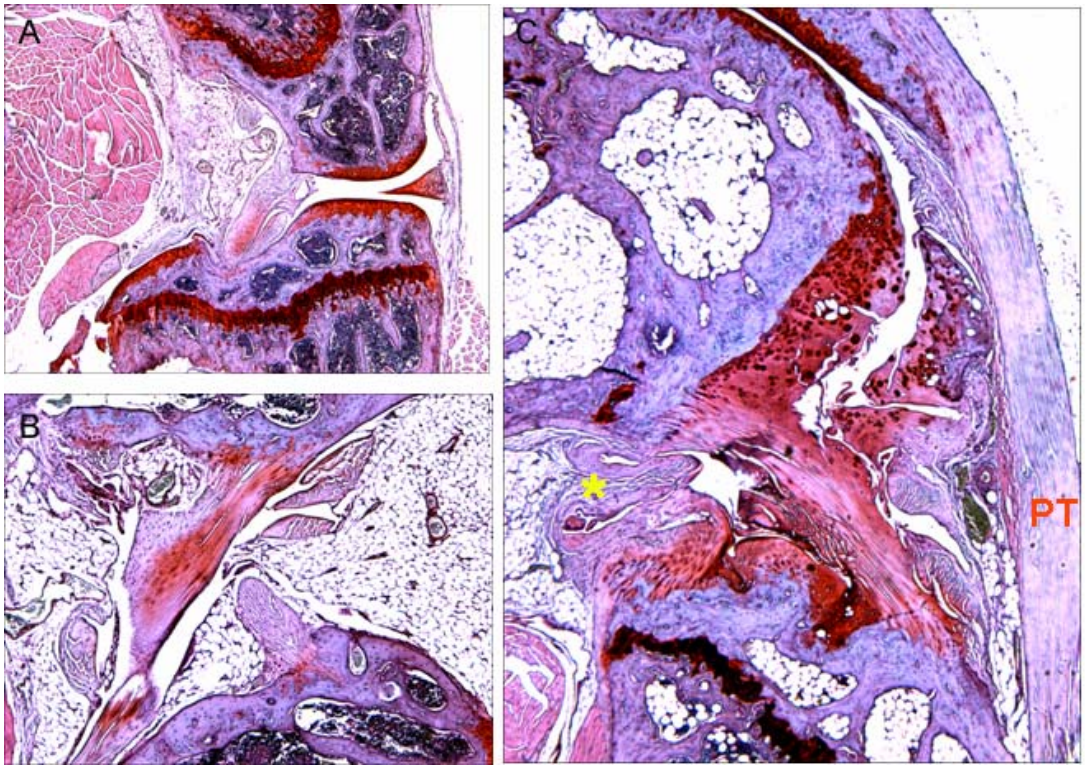


**Figure 3-43. Knee sections from mid-region of joint (at level of cruciate ligaments) of six month old control [A, B] and *Pten*$^{flox/flox}$*:Col2a1Cre* [C] mice. Note large loose body in retro-patellar tendon [11] position in *Pten*$^{flox/flox}$*:Col2a1Cre* mouse [C], loss of fat pads, capsular fibrosis (*).**

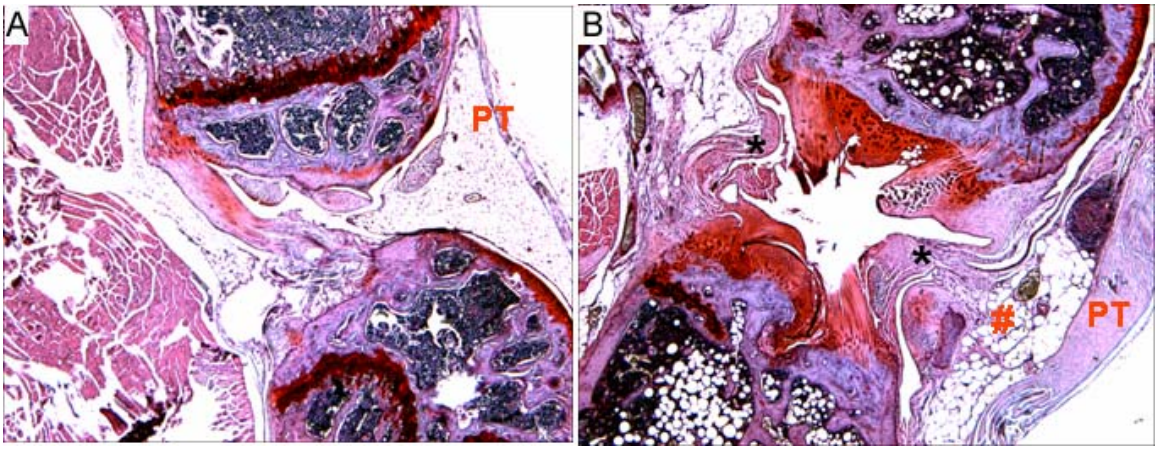


**Figure 3-44. Knee sections from mid-region of joint (at level of cruciate ligaments) in control [A] and *Pten*$^{flox/flox}$*:Col2a1Cre* [B] mice. In [B], note the capsular fibrosis (*) and reaction to joint damage in the synovium (#) in the as seen in Figure 3-42. Again, the patellar tendon is enlarged compared to the control.**

In the mutants there may be damage to the cruciate ligaments, and there are aberrantly positioned structures that either represent damaged portions of menisci (which in the mouse are composed of cartilage and bone), and/or osteophytes (Figure 3-43A).

Micro-ct revealed a spectrum of damage, from mild changes (Figure 3-45B, E, H) to severe, with large osteophytes, loose bodies, and damage to menisci (Figure 3-45C, F, I).

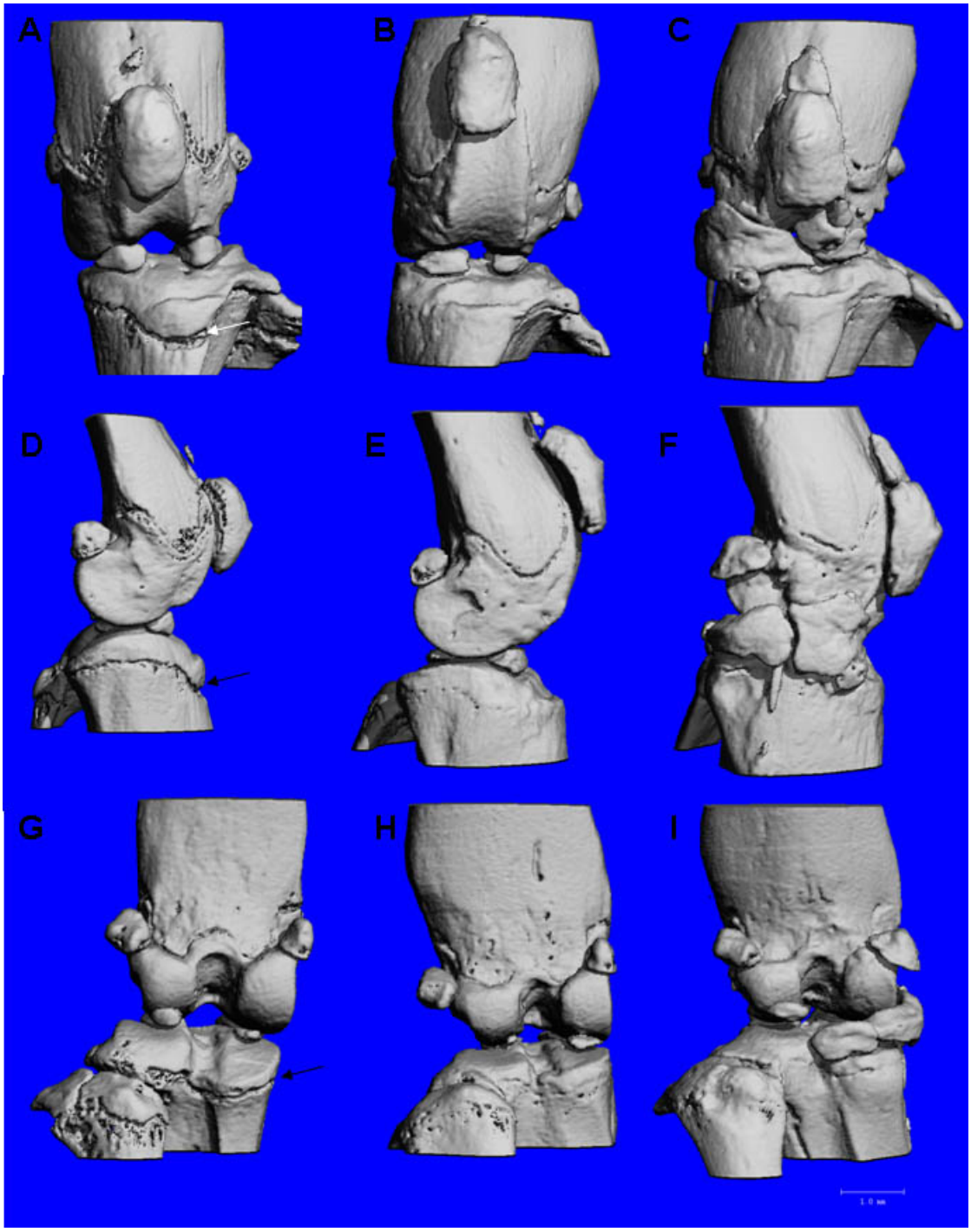


**Figure 3-45. Representative micro-ct reconstructions of 6 month old male knees (21 μm). [A to C] anterior view, [D to F] medial view, [G to I] posterior view. [A, D, G] control, [B, C, E, F, H, I] *Pten*$^{flox/flox}$*:Col2a1Cre* mice. Two *Pten*$^{flox/flox}$*:Col2a1Cre* mice were selected to represent the variation in extent of pathology seen with the phenotype. Note the osteophyte formation in [F], and enlarged patella seen in [E,F]. Arrows indicate the open growth plates only still present in the control mice.**

These changes can also be seen in the histology (Figure 3-46).

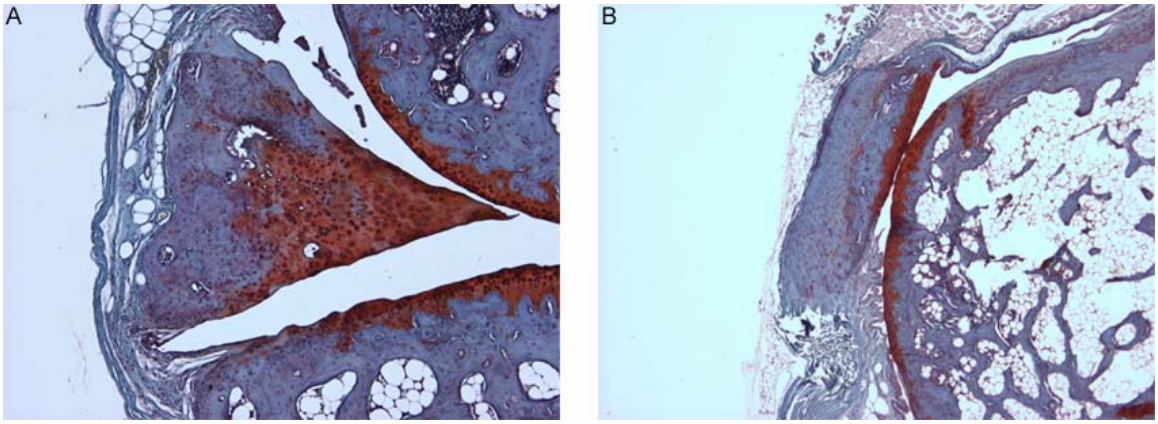


**Figure 3-46. Example of an enlarged meniscus [A] and patella [B] present in 6 month old *Pten*$^{flox/flox}$*:Col2a1Cre* mice. Note how the patella appears to have excess calcified matrix that has formed over the patellar surface.**

### *3.4.2 General changes in 8 and 10 month old mice*

With increased age *Pten*$^{flox/flox}$*:Col2a1Cre* developed a distinct pattern of adipose tissue deposition (Figure 3-47 and Figure 3-48), where more fat is present on the upper half of the body while the lower half remains lean.


**Figure 3-47. Picture depicting control [A] and *Pten*$^{flox/flox}$*:Col2a1Cre* [B] mice at 8.5 months of age. Note the larger upper body size of the *Ptenflox/flox:Col2a1Cre* mice, due to increased in adipose tissue deposition. Right side: anterior view; Left side: medial-lateral view.**


**Figure 3-48. Picture depicting *Pten*$^{flox/flox}$*:Col2a1Cre* [A] and control [B] mice at 10 months of age. Note the larger upper body size of the *Pten*$^{flox/flox}$*:Col2a1Cre* mice, due to increased in adipose tissue deposition.**

Similar to 15 weeks, micro-ct analysis of knees and hind paws revealed that the older *Pten*$^{flox/flox}$*:Col2a1Cre* mice had a higher bone density on x-rays (Figure 3-49A),

increased trabecular bone on the x-rays (Figure 3-49B), and more robust looking long bones of the knee (Figure 3-50) and hind paw (Figure 3-51) compared to control mice.

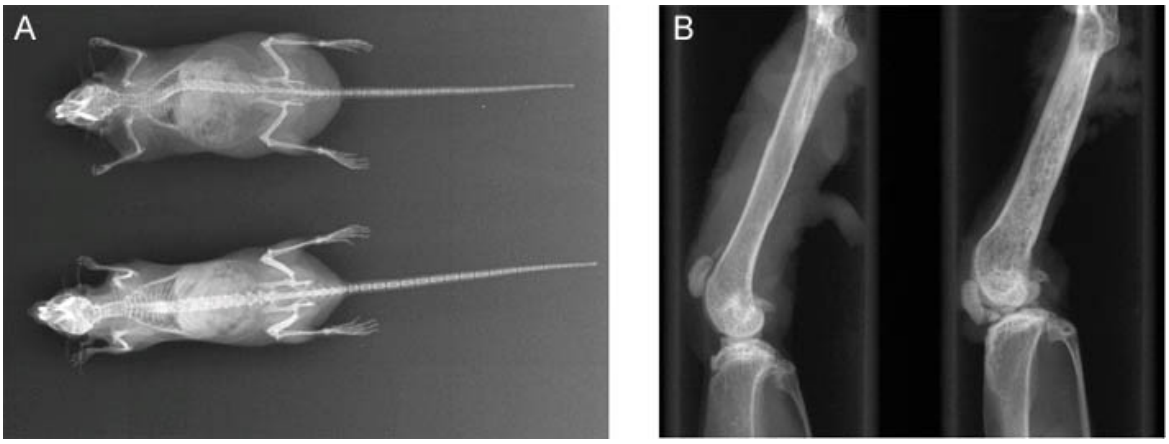


**Figure 3-49. [A] Representative posterior-anterior x-rays of 6 month old control (top) and *Pten*$^{flox/flox}$*:Col2a1Cre* mice (bottom). Notice the increase in bone density in the long bones, vertebrae, and skull of the *Pten*$^{flox/flox}$*:Col2a1Cre* mice. [B] Representative x-ray of 8.5 month old control (left) and *Pten*$^{flox/flox}$*:Col2a1Cre* mice (right) femur. Note the coarsening of trabecular bone in the *Pten*$^{flox/flox}$*:Col2a1Cre* mice.**

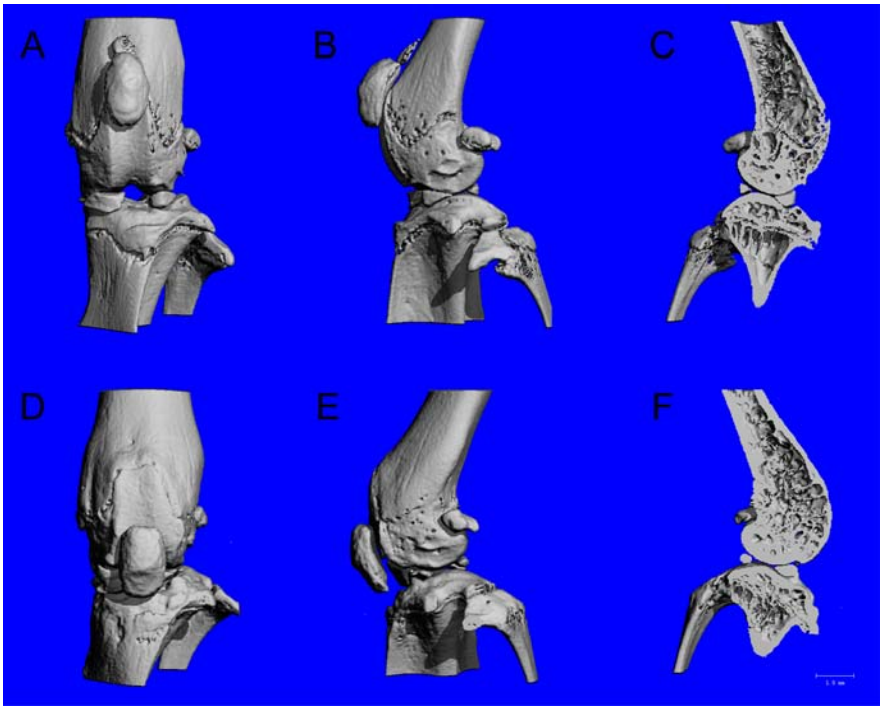


**Figure 3-50. Micro-ct reconstructions (21 μM resolution) of 8.5 month old male knees from control [A, B, C] and *Pten*$^{flox/flox}$*:Col2a1Cre* [D, E, F] mice: [A,D] anterior view; [B, E] lateral view; [C, F] cross-section of medial view. *Pten*$^{flox/flox}$*:Col2a1Cre* have more robust looking bones, and the cross-section reveals thicker cortical bone with what appears to be an increase in amount of trabecular bone.**

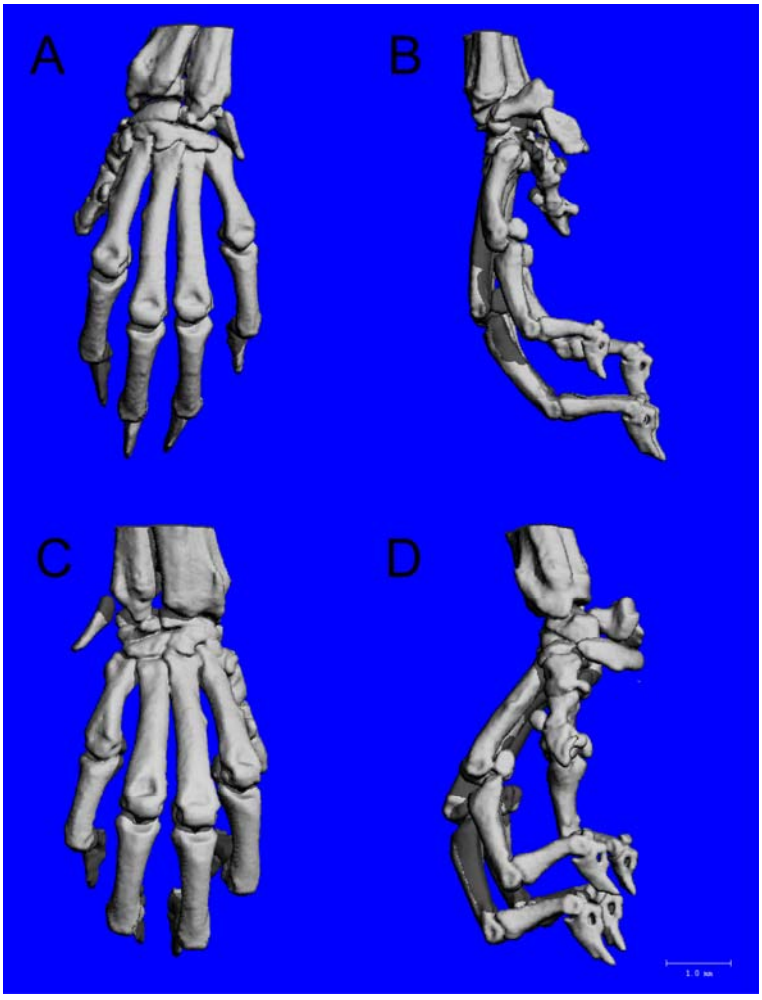


**Figure 3-51. Micro-ct reconstructions (21 μM resolution) of male hind paws from 8.5 month old control [A, B] and *Pten*$^{flox/flox}$*:Col2a1Cre* [C, D] mice: [A,D] anterior view; [B, E] lateral view. *Pten*$^{flox/flox}$*:Col2a1Cre* have larger bones.**

Furthermore, over 6 months of age the *Pten*$^{flox/flox}$*:Col2a1Cre* mice had difficulty moving and a stiffened tail, which may indicate the presence of articular cartilage and joint damage: this will need to be confirmed by histology in future studies.

### 3.5 Osteosarcomas

Within a cohort of 14 *Pten*$^{flox/flox}$*:Col2a1Cre* mice set aside for an aging study, we have seen two examples of sarcomas in mice between 9 and 10 months of age. Large primary

tumours were detected in each mouse, one in the tibia and fibula region, and the second surrounding the humerus, extending over the elbow joint (while sparing the joint cavity) to connect with the radius and ulna, as evidenced by micro-ct (Figure 3-52).

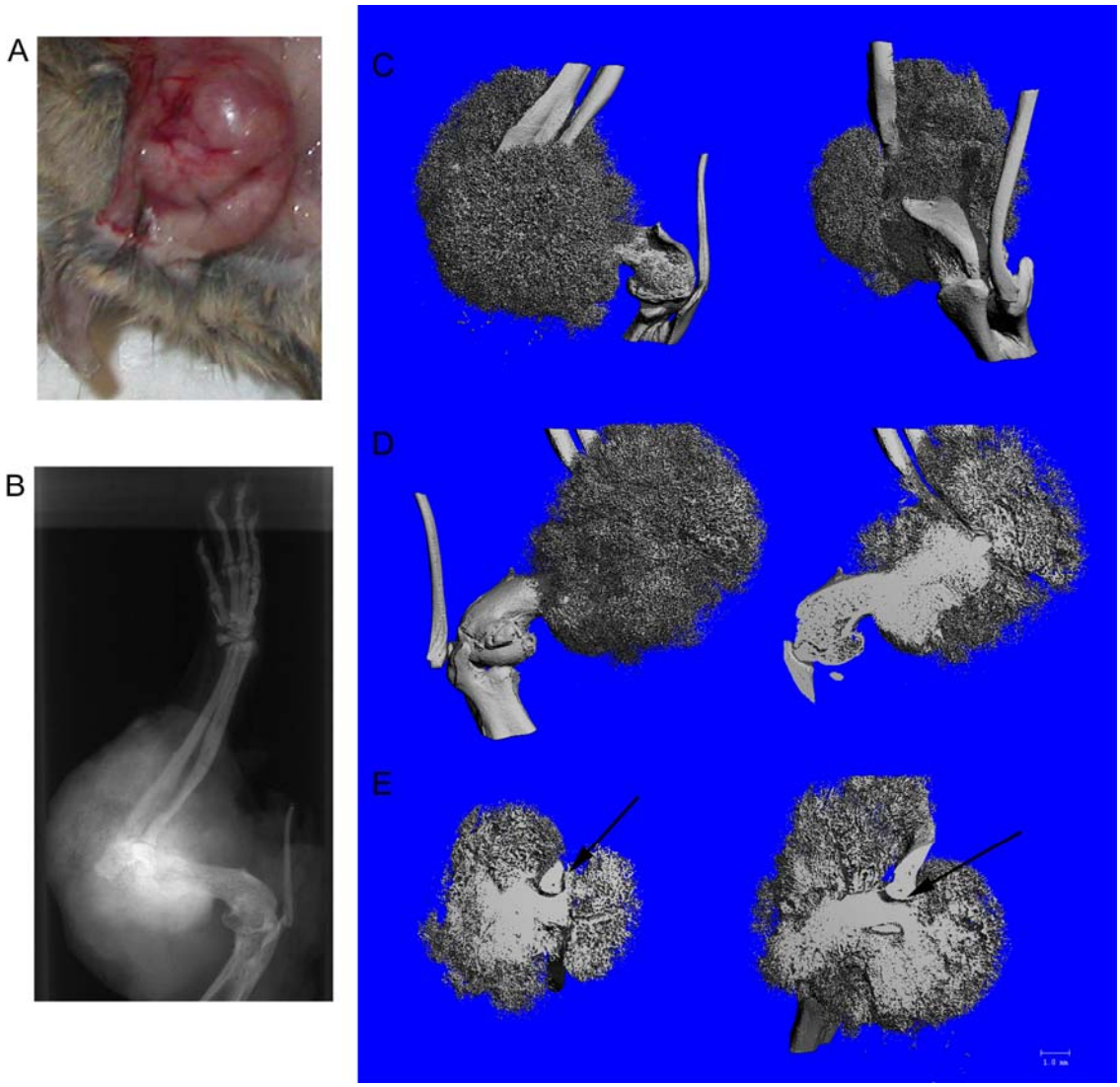


**Figure 3-52. [A] Picture of the primary osteosarcoma affecting the elbow area. [B] X-ray of the primary osteosarcoma. [C, D, E] Micro-ct images of the primary osteosarcoma (10.5 μM resolution). [C,D]; a cross-section reveals the dense bone produced by the tumour which appears to fuse the tumour to the long bones [D]; cross-sections showing the joint space and lack of obliteration by the tumour[E] (see arrows).**

The primary osteosarcoma metastasized and spread, likely via the blood stream, to the lung (Figure 3-53, Figure 3-54, Figure 3-55) with aeroinvasion (tumour growth into bronchi) (Figure 3-56), liver (Figure 3-57), and within the pleura of the thoracic cavity leading the production of malignant osteoid (Figure 3-58).

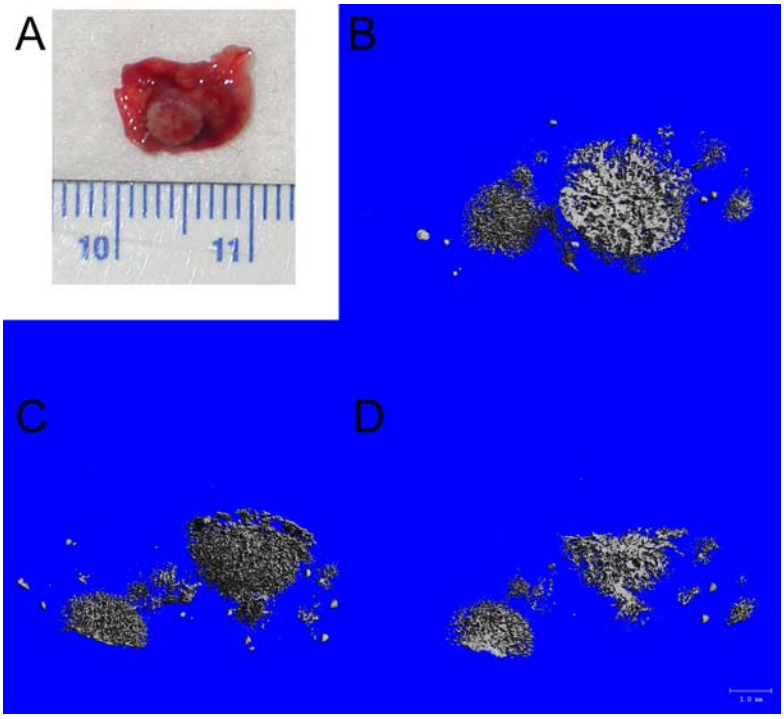


**Figure 3-53. [A] Picture of *Pten*$^{flox/flox}$*:Col2a1Cre* dissected lung, note presence of calcified osteoid extending out of the lung tissue. [B, C] Micro-ct images (10.5µM resolution) of various angles of the calcified osteoid present in the lung. [D] Cross–section through the large neoplastic metastatic nodule.**

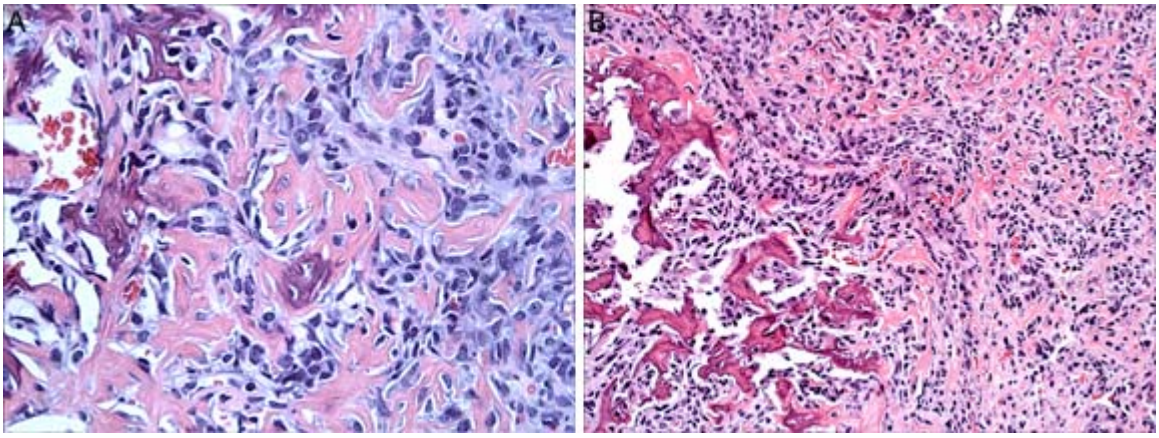


**Figure 3-54. [A] High (400x) and [B] low (100x) magnification views of metastatic osteosarcomas in the lung. The swirls of pink-staining material with the embedded cells is the malignant osteoid, and the darker purple regions are where the osteoid has become calcified.**

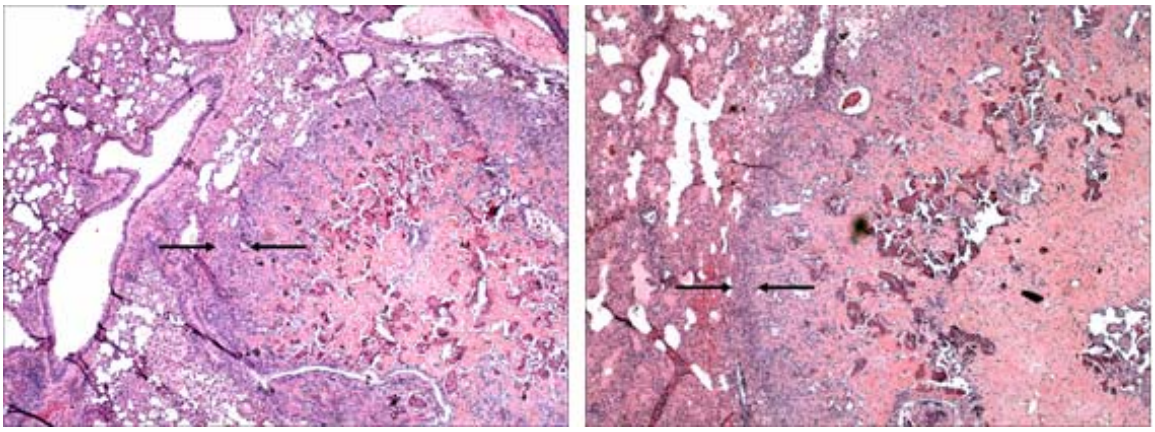

**Figure 3-55. Two examples of osteosarcoma pulmonary metastases. In both cases an expanding outer hyper-cellular rim of poorly differentiated cells (arrows) is invading and compressing the surrounding lung parenchyma, while trailing cells towards the center of the 'ball' differentiate and become actively engaged in producing osteoid (orange-pink). The latter becomes calcified (darker, purple areas); as seen by micro-ct.**

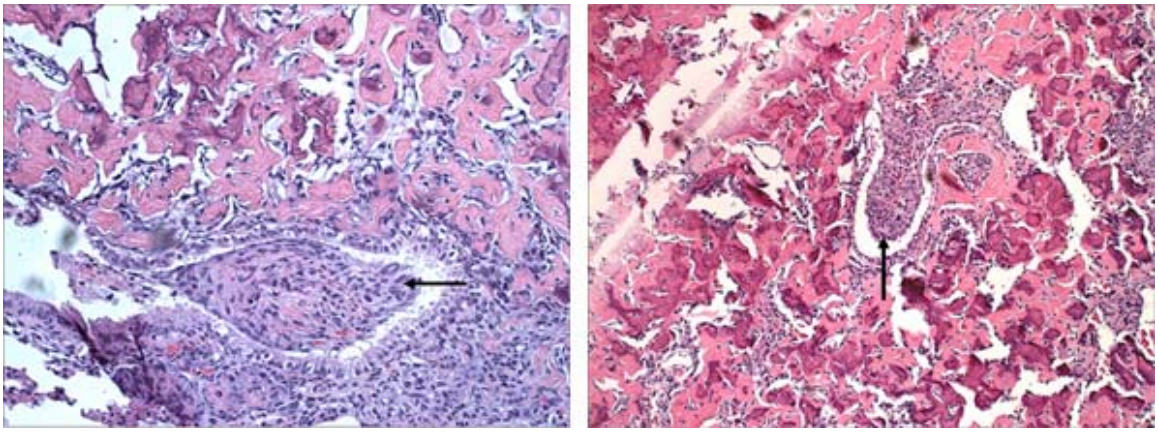

**Figure 3-56. Two examples of osteosarcoma metastases showing aeroinvasion. In both images, a 'tongue' composed exclusively of osteosarcoma cells (arrows) can be seen invading into the lumen of the airway. This is a feature of highly aggressive metastases.**

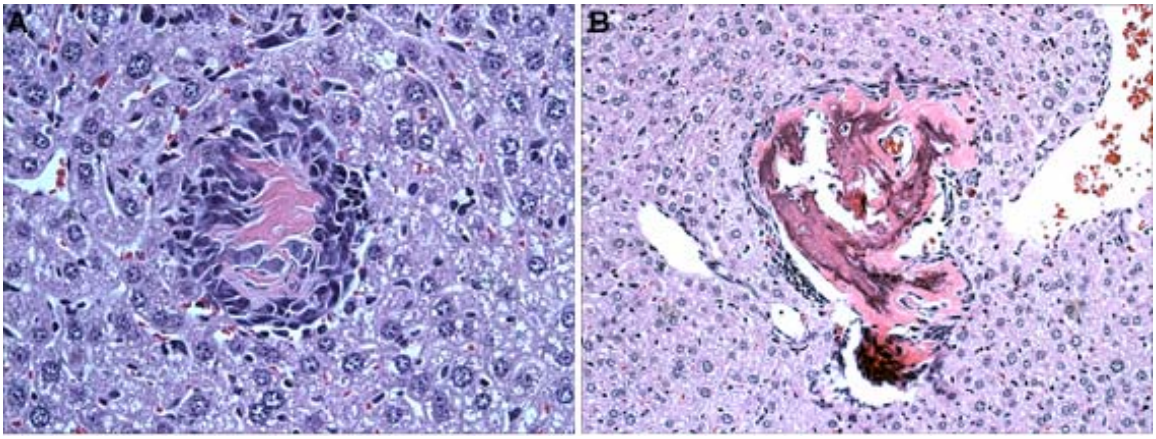


**Figure 3-57. [A, B] Two examples of liver metastases. The immature lesion [A] has a prominent growing rim of undifferentiated cells, and a core of cells laying down osteoid (pink). An outer rim of invading cells is also evident in the lesion below that is more mature, showing calcification of the malignant osteoid (dark purple areas).**

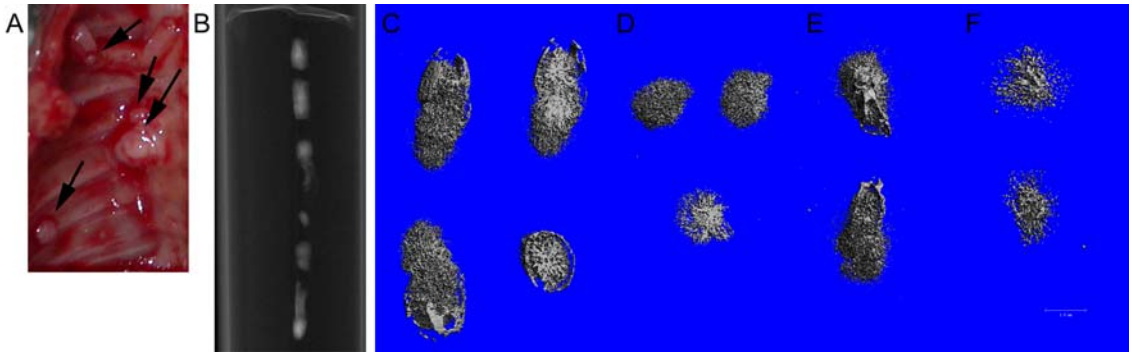


**Figure 3-58. [A] Image of *Pten*$^{flox/flox}$*:Col2a1Cre* thoracic cavity, note presence of osteoid matrix attached to spine and the rib cage. [B] X-rays of dissected tumour nodules removed from the thoracic cavity. [C, D, E, F] Micro-ct images (10.5μM resolution) of various angles of the tumour nodules present in the thoracic cavity. Lower left image in [C] and bottom image in [D] are cross-sectional views through the nodules.**

Tumour cells were spindle-shaped and obviously malignant. They were large and pleomorphic, with a high nuclear:cytoplasmic ratio. The nucleoli were large and sometimes multiple, and the mitotic rate was high. Tumour cells invaded and destroyed native tissue. The presence of neoplastic osteoid confirmed the diagnosis of an osteosarcoma. In the lung and liver, tumour cells with an identical morphology invaded and replaced the native air spaces in the lung, and liver tissues, consistent with a metastatic sarcoma. Additional histological and molecular characterization of the metastatic deposts will be the subject of future studies.

# Chapter Four: Discussion

## 4.1 Progressive ankylosis; a model for micro-ct

Micro-ct is a technology that can yield qualitative and quantitative information about gross morphology, as well as microstructural architecture of the skeletal system. An advantage to this technology is its ability to rapidly generate geometrically accurate representations of skeletal morphology [223]. While previously limited by resolution to the study of larger animals [224, 225], current scan resolutions as small as 5 μm have made possible the study of smaller animals such as rats and mice [223, 226, 227]. High resolution imaging allows tracking of minute changes in bone [226, 228], and permits the use of smaller sample sizes to reach significance [228].

Consistent with previously described histopathological findings [107, 108, 110] the changes identified in the ank mouse by micro-ct imaging are likely due to a combination of soft tissue calcification as well as bony overgrowth of joint structures, including sesamoid bones, joint capsules, and ligaments. A prominent example of the latter is the calcified annular ligament around the head of the radius (Figure 3-3). Our findings correlate well with those previously described using histology, alizarin staining, and radiography [108, 110, 229]. The gradual process of ankylosis was also manisfested by what appeared to be changes secondary to joint fusion and corresponding muscle disuse. Such secondary skeletal changes were most clearly observed in the elbow, where sites of tendinous attachment to bone were atrophic (data not shown). Other sites of what was likely secondary change were found in non-joint structures such as the transverse processes of the caudal vertebrae, and notably, the lateral supracondylar ridge of the humerus (Figure 3-3). The reduction in size of these muscle insertion points was likely the result of decreased

mechanical induction of bone growth as a result of joint ankylosis. Sweet and Green [108] found that *ank/ank* mice tended to weigh less than normal littermates, and that these weight differences were detected prior to overt joint fusion. This finding was interpreted to be indicative of reduced muscle mass resulting from decreased activity, initially due to joint pain, and subsequently, to limitation of joint movement. Micro-ct is ideally suited for the detection of subtle alteration in skeletal architecture, as illustrated by the ability to readily visualize secondary changes in bone structure at the points of muscle insertion in the *ank/ank* mice. Revealing such changes would not be so easily achieved by conventional radiological or histological methods.

The ability to isolate and visualize skeletal elements in three dimensions offers a new means of assessing phenotypic alterations in mutant mice. This technology represents an intermediate level of evaluation lying between gross inspection and histological analysis that is not achievable with other techniques. Histology, for example, permits the visualization of microscopic detail, including cellular changes, but is restricted to 2D sampling of 3D structures. Micro-ct provides a means of evaluating internal and external anatomical features in 3D without the need for physical disruption of the sample. Thus, in this study, joint integrity remained unaltered, allowing for a better understanding the phenotypic changes associated with the *ank/ank* mutation.

Despite its many positive features, micro-ct has some limitations; these include the current inability to visualize changes in non-mineralized tissue, and also the inability to resolve cellular detail. For this reason, micro-ct should be considered complementary to existing approaches. A notable advantage of micro-ct in this regard is that additional forms of analysis can be carried out on the same specimen, as the samples are not altered during

the scanning process. While the results of the qualitative study described herein demonstrate the utility of micro-ct for descriptive types of analyses, quantitative aspects of the technology are also powerful tools. This includes the examination of the external morphology of joints by 3D landmarking (for example, to be able discern volumetric changes in specific joint structures), and also internal morphology through the use of 3D architectural analysis of trabecular bone. These measurements allow for more quantitative characterizations of pathological states and disease progression.

## 4.2 Brachymorph mice; employing micro-ct and histological analysis methods

### *4.2.1 The advantages of using micro-ct and histology to studying bm/bm mice*

As described in section 4.1, micro-ct is a powerful tool that can be utilized for examining changes in skeletal morphology. In this section, we describe the use of micro-ct complemented by histology. This approach allowed the examination of changes in bone structure, in addition to changes at the cellular level in *bm/bm* mice. In this model, micro-ct was used qualitatively to evaluate structural changes, and quantitatively to determine changes in subchondral plate thickness (a sign frequently seen in OA patients). We used histology as a means to investigate the role of PAPSS2 in cartilage over time, and found that loss of PAPSS2 activity lead to a degenerative phenotype that would not have been detected by micro-ct. By using the combination of micro-ct and histology, we were able to speculate on the mechanism of pathogenesis based both on skeletal changes and soft tissue changes.

### *4.2.2 Cartilaginous changes in the bm/bm mice: a role for PAPSS2 in the ECM*

Although the cartilage of brachymorph mice is reported to be undersulfated, normal amounts of GAGs and matrix collagens are apparently present [134, 230]. Vanky *et al.*,

(2000) [136], have shown that this undersulfation leads to changes in the epiphyseal growth plate cartilage, leading to impaired longitudinal growth. Interestingly, changes in the sulfation of proteoglycans has also been observed within osteoarthritic cartilage, although this phenomenon is primarily due to enzymatic degradation and depletion of matrix GAGs, rather than hyposulfation [231, 232]. In addition to an alteration in the physical properties of hyposulfated ECM molecules that may result in instability, a decreased ability of proteoglycans (such as syndecans which are involved in ligand binding [233], decorin, and biglycan [234]) to present growth factors and alter the growth, maintenance, and repair of articular cartilage.

The abnormalities of the ECM in all likelihood contribute to the degenerative changes seen in the articular cartilage of 12 month-old *bm/bm* mice. ECM is supported through a network of collagen fibrils that are highly organized and stabilized via both inter- and intra-molecular cross links [235]. These resist the swelling pressure due to the negatively charged aggregates of aggrecan [236]. These negative charges, mainly due to chondroitin sulfate, are important in maintaining the structure of proteoglycan aggregates [237]. Loss of these charges, as seen in Papss2 deficiency, may cause structural instability due to insufficient water attraction and movement within the ECM, both leading to weakness and or instability of load-bearing joints. This would be predicted to render the articular cartilage more susceptible to damage and thence to premature degenerative joint disease.

Taken together, such factors as abnormal growth factor ligand binding and proteoglycan structure could readily account for the cartilage degeneration observed in *bm/bm* mouse knees. Other mouse models of degenerative joint disease attributed to

instabilities in the ECM, include mice expressing truncated collagen type II transgene [238] and the collagen type IX knockout [76] where an alteration in the structural integrity of cartilage results from loss of a major cross-linking collagen.

Spontaneous degenerative knee joint disease has been observed in the C57BL/6 strain. Thus, with age (after 15.5 months) enlargement of menisci as well as narrowing of the joint space have been observed [239, 240]. Histological evidence of cartilage destruction as early as 6-8 months of age has been reported, albeit with slow progression, whereby 80% of mice examined showed signs at 16-18 months, and almost all mice showed signs at two years [241]. However, the reported changes were confined primarily to the lateral side of the tibio-femoral compartment [242] (Figure 3-11). The *bm/bm* mice, on the other hand, consistently exhibited high-grade cartilage damage at an earlier age (12 months) in both the patello-femoral and medial compartments of the knee. In addition, *bm/bm* animals developed cartilage damage much earlier and to a much greater severity than was observed in the C57BL/6 mice (Table 1). The C57BL/6 mice in our control group most likely exhibited the types of changes that tend to occur spontaneously in the C57BL/6 mouse strain. Therefore, we conclude that the characteristic changes seen in all the 12 month-old *bm/bm* mice we examined were due to the loss of *Papss2* and were not a feature of the C57BL/6 genetic background.

### *4.2.3 Changes in the skeletal structure: altered mechanics from PAPSS2 loss?*

Abnormal biomechanical function of the knee joint, as a consequence of altered morphology of the skeletal elements, may have also played a role in degeneration of the articular cartilage in *bm/bm* knees. Metaphyseal flaring and abnormal epiphyseal morphology observed in the brachymorph mouse are also characteristic of many

dysplasias resulting in dwarfism in humans [243, 244] . The flaring in the metaphyseal region can be attributed to the capacity for normal appositional growth in the diaphysis to occur while endochondral ossificiation in the physis is inhibited. The epiphyseal growth plate of the *bm/bm* mice lacks the organization seen in the control mice at all ages. This finding is in agreement with other reports [136, 245]. Vanky *et al*. [136] found that the chondrocytes in the proliferating zone are in the $G_o$ phase of the cell cycle which would result in a decrease in the number of hypertrophic cells. This paucity of hypertrophic cells was confirmed by our observations in the epiphyseal growth plate of *bm/bm* mice [136]. Although we made no attempt to identify abnormal joint kinematics and gait disturbance in the mutant mice, the skeletal abnormalities that we observed very likely resulted in abnormal contact forces in the patello-femoral and medial compartments.

Precocious development of degenerative joint disease has been associated with human chondrodystrophies [246]. With respect to the *bm/bm* mice, the various morphological alterations observed, including the bowing of the tibia and fibula, and the enlargement of muscle attachments such as the tibial and deltoid tuberosities, plausibly reflect adaptive attempts to compensate for the abnormal and disproportionate bone growth. These features might to some extent also reflect a "muscle packing" problem in that the *bm/bm* mice must accommodate muscles with similar cross-sectional areas to support the nearly normal sized trunk within a context of dramatically shortened limbs. The increased bowing of long bones, altered sites of muscle attachment relative to lever components, and the altered ratio of joint surface area to long bone length could conspire to produce dramatically altered joint mechanics. Such changes, in turn, might contribute to cartilage degeneration due to an abnormal strain patterns.

### *4.2.4 A role for PAPSS2 in human OA*

Might polymorphisms of the human *PAPSS2* gene have a role in predisposition to human OA? Xu *et al*. (2002) [247] examined a sample population and found different polymorphisms both within and outside of conserved regions of the *PAPSS2* gene, some of which could alter enzymatic activity. Thus, a mutation causing hyposulfation of proteoglycans could potentially be used as an indicator of disease predisposition. However, a study of *PAPSS2* genes in a Japanese population revealed no correlation between those affected with knee OA [248]. It remains possible that *PAPPS2* polymorphism(s) in different ethnic populations will be associated with susceptibility to OA. In keeping with this, a form of human SEMD has been attributed to a mutation in the *PAPSS2* gene that results in a truncated protein due to a premature nonsense codon. This results in a protein that is predicted to be reduced from 614 to 437 amino acids in length [139]. It is still unknown as to whether this causes the transcript to be destabilized or whether the truncated protein retains partial activity [139]. Similarities between the human disease and the *bm/bm* model have been noted by ul Haque et *al* [139]. Of most interest to our study is that humans lacking normal *PAPSS2* activity exhibit long bone shortening and bowing, and also show degenerative joint disease, including evidence of knee joint arthrosis. In the human SEMD families, radiographic abnormalities of the hands and spine were also observed [138]. It would be of interest to examine the spines of older *bm/bm* mice to search for evidence of degeneration. Given the premature development of degenerative knee joint disease in the mutant mice and other similarities with the human SEMD kindred, we propose that this mutant represents a model of human *PAPSS2* deficiency-associated arthrosis.

## 4.3 Micro-ct as a powerful quantitative tool

The *ank/ank* and *bm/bm* mouse models illustrated some of the many uses for micro-ct. The *ank* mouse was an ideal model to examine morphological changes. Viewing skeletal morphology in 3D enabled us to clearly visualize the pattern of calcification within the joint space of the vertebrae. By micro-ct we characterized phenotypic gross skeletal changes and performed quantitative analysis of subchondral plate thickness in *bm/bm* mice. By combining this technique with histology, we determined changes in the cartilage, enabling us to describe a degenerative joint disease. We performed trabecular and cortical bone analysis on the $Pten^{fl/fl}$*:Col2a1Cre* mice, and the results of this study are described in section 4.4.3.

A limitation to micro-ct is the inability to see cellular detail. Histology still needs to be performed to view changes in soft tissue. Additional techniques, such as stereological analysis to quantitate changes in the growth plate, and immunohistochemistry to better understand the cell signalling mechanisms must be performed to get a full picture of a musculoskeletal phenotype. Furthermore, static and dynamic histomorphometry is still required to understand changes in bone remodelling, and changes in the osteoblast and osteocyte activity. Being non-destructive, micro-ct allows for these techniques to be performed after samples have been analysed.

## 4.4 Inactivation of *Pten* in osteo-chondroprogenitor cells leads to epiphyseal growth plate abnormalities and skeletal overgrowth

### *4.4.1 Sites of Col2a1Cre–mediated floxed gene excisions*

One of the key issues raised by this study concerns the nature of the skeletal progenitor cells undergoing *Col2a1Cre*-mediated gene excisions. The well-characterized promoter

of the *Col2a1* gene [249-251] has been successfully used to express a wide variety of transgenes in chondrocytes. However, employing the *Col2a1* promoter to express a protein of interest in chondrocytes is different from using the *Col2a1* promoter to drive expression of Cre recombinase, as even transient recombinase expression has the potential to trigger a permanent genetic alteration within a cell. Thus, if the *Col2a1Cre* transgene were even transiently activated in the osteo-chondroprogenitors, then both osteoblasts and chondroblasts would potentially exhibit Cre-mediated genetic changes as was recently reported [210]. In the present study, several lines of evidence suggested that floxed *Pten* excision was not only occurring in chondrocytes, but also in osteoprogenitors of $Pten^{flox/flox}$*:Col2a1Cre* mice: (a) using the R26R system we observed *lacZ*-positive osteoblasts in the perichondrial bone collar and primary spongiosa; (b) *lacZ* expression was present in osteocytes of both the chondro- and dermato-cranium, and scattered throughout the long bones. Taken together, these findings supported the notion that the *Col2a1Cre* transgene was active at the osteo-chondroprogenitor stage. Consequently, the skeletal enlargement phenotype of $Pten^{flox/flox}$*:Col2a1Cre* mice was likely due to a combination of at least three factors: (a) loss of *Pten* expression in chondrocytes was associated with an augmentation of endochondral bone formation, resulting in increased levels of trabecular bone formation and a larger bone collar template as directed by the perichondrium; (b) loss of *Pten* expression in osteoblasts and their differentiated progeny, perhaps leading to augmented responses to factors produced by hypertrophic chondrocytes, mesenchymal cells, and the endocrine system (e.g. IGF-1, GH), with the resulting augmentation in trabecular, intra-membranous, and cortical bone formation; and

(c) *Pten* loss in osteoblasts altering the process of bone remodelling, with bone deposition exceeding bone resorption.

We were unable to show any difference in expression of Pten or P-Akt in isolated chondrocytes from control or *Pten$^{flox/flox}$:Col2a1Cre* mice. In addition, neither of these factors was expressed at a high level, potentially explained by a lack of stimulation of the chondrocytes. If the cells were first stimulated by IGF-1 or FGF to activate the PI3K pathway, one would expect to see an increase in P-Akt followed by an increase in Pten in the control chondrocytes and increasing levels of expression of P-Akt in the *Pten$^{flox/flox}$:Col2a1Cre* chondrocytes.

### *4.4.2 Proximal tibial epiphyseal growth plate abnormalities in Pten$^{flox/flox}$:Col2a1Cre mice*

Loss of *Pten* is predicted to augment the responses of chondrocytes and osteoblasts to extracellular signals capable of activating PI3K, including: insulin, growth hormone, IGFs, FGFs, ECM:integrin interactions [252-256]. Also of potential relevance is an interesting synergism between Runx2 (expressed in hypertrophic chondrocytes as well as osteoblasts) and the PI3K→Akt, regulated by Pten [183]. The increased responsiveness of cells might be reflected in increased cell proliferation, resistance to apoptosis, increased cell soma size and protein production levels, as well as altered patterns of differentiation. We hypothesized that some or all of these parameters might be disturbed in *Pten$^{flox/flox}$:Col2a1Cre* chondrocytes.

Although the growth plates of the *Pten$^{flox/flox}$:Col2a1Cre* animals were predicted to be enlarged and hypercellular due to increased proliferation and decreased apoptosis, they were in fact not wider or hypercellular, and no significant differences in either

chondrocyte proliferation or apoptosis were observed. The growth plates, however, did show evidence of disorganization, and a loss of growth plate 'polarity' in the mid-epiphyseal region that possibly accounted for the trans-epiphyseal 'bridging' observed in *Pten$^{flox/flox}$:Col2a1Cre* mice (Figure 3-31A). To our knowledge, this 'bridging' phenomenon was only once previously reported in the disorganized growth plates of a sulfate transporter-deficient mouse [257]. With respect to increased protein synthesis, matrix over-production was observed in the *Pten$^{flox/flox}$:Col2a1Cre* distal femoral heads (Figure 3-31B). This may have been due to increased activity of the IGF1 receptor→PI3K→mTOR axis, and possibly participation of HIF-1α [177], both resulting in increased chondrocyte anabolic activity, and consequently, the increased GAG deposition. HIF-1α protein stability and transcriptional activity are both stimulated by PI3K→Akt pathway activation [258, 259]; this factor is also required for chondrocyte growth arrest and survival [175]. Similarly, the increased CD31 (PECAM) staining in the primary spongiosa (Figure 3-36 B) is probably due to increased VEGF generation and may have resulted from both increased mTOR activity [168, 169], and HIF-1α levels [171, 177]. VEGF not only regulates blood vessel invasion of the primary spongiosa [21, 173-176], but also plays an important role in chondrocyte differentiation and survival [174, 176, 177, 260].

The proliferating zone chondrocyte lacunae of *Pten$^{flox/flox}$:Col2a1Cre* mice tended to be more rounded in appearance (Figure 3-27D), and together with the expression of type X collagen in this layer (Figure 3-35B) suggests that chondrocyte hypertrophy might be accelerated in these animals. This notion was reinforced by the finding of a greatly

expanded ALP activity pattern in *Pten*$^{flox/flox}$*:Col2a1Cre* tibial growth plates (Figure 3-35D). Together, these results might explain why these growth plates are closed by 6 months of age. If growth plate chondrocytes were reaching terminal differentiation at an accelerated rate in *Pten*$^{flox/flox}$*:Col2a1Cre* mice, over time, a 'burning out' in the germinal zone of the growth plates might occur. Weise et al. (2001), for example, found that rabbit growth plate fusion was triggered when the proliferative potential of the chondrocytes had become exhausted. Loss of *Pten* in the chondrocyte 'stem cell' pool could potentially interfere with the process of self-renewal, leading to inadequate stem cell function as was shown in the case of *Pten*-deficient haematopoietic stem cells [261]. This is further reinforced by our area fraction results of the proliferative zone. We had hypothesized that due to increased ECM seen in the sections we would have a higher ratio of ECM to cells, which was opposite to what we found. We believe a greater number of proliferative cells grouped together as the result of an increased self-renewal, lead to the perception of fewer cells and more matrix.

The increase in self-renewal could also explain the increased fat deposition in the bone marrow of the *Pten*$^{flox/flox}$*:Col2a1Cre* mice. If osteoblasts are also differentiating at an accelerated rate, they might also be depleting their 'stem cell' pool more rapidly. Runx2, the early osteoblastic marker, can down regulate PPARγ expression, causing inhibition of adipocyte formation [262, 263]. If the osteoblasts deplete their 'stem cell' pool, Runx2 expression would be expected to decrease, leading to the loss of PPARγ inhibition and the formation of adipocytes in the marrow.

### *4.4.3 Skeletal Changes in Pten$^{flox/flox}$:Col2a1Cre mice*

The most salient feature of *Pten$^{flox/flox}$:Col2a1Cre* mice was the 13% increase in body length caused by the enlarged vertebrae and intervertebral disk spaces (Figure 3-13B and Figure 3-20A). Interestingly, long bones of *Pten$^{flox/flox}$:Col2a1Cre* mice had only a 4.6% increase in length. Growth of vertebrae is different than in long bones: vertebrae require more remodeling of bone to increase their size, while long bones require more activity at the growth plate to produce an increase in length [2, 264]. Since there is more remodeling than longitudinal growth in vertebral development, growth plates play a less important role in determining their final size. This increase in bone remodeling could account for the larger vertebrae of *Pten$^{flox/flox}$:Col2a1Cre* mice. Appendicular and axial skeletons also respond differently to factors that influence bone formation. For instance, PTH increases cancellous bone more in vertebrae than in the proximal tibia [265]. It has also been suggested that estrogen has a greater effect on fusion of the growth plates in the appendicular skeleton than the axial skeleton [266, 267]. If such stimuli were dependent on PI3K activity for their effects, it might provide an explanation for proportionately larger vertebrae to long bones in the *Pten$^{flox/flox}$:Col2a1Cre* mice.

Hormones, such as GH, IGF-1, glucocorticoids, and sex hormones are known to regulate longitudinal growth and affect the growth plate [268]. Estrogen receptor-α (ERα) and estrogen receptor-β (ERβ) are both widely distributed in the growth plate, and play a role in decreasing longitudinal growth and promoting growth plate fusion [268, 269]. While there is conflicting data, it has been shown that ERβ, and not ERα, is important for longitudinal growth and growth plate fusion in female mice [266, 268]. Androgen, via androgen receptor (AR), also have a direct effect on the growth plate,

which can work independently from estrogens [268, 270, 271]. In male spermatozoa, ERα and ERβ were both shown to be able to up regulate the PI3K pathway [272], furthermore, *in vitro* it has been shown that PI3K can up regulate the transcriptional activity of ERα in neuronal cells [273]. PI3K has also been shown to activate the androgen pathway in vitro [274]. Loss of pten in *pten$^{fl/fl}$:Col2a1Cre* mice could therefore up-regulate the effects of estrogens and androgen in both the growth plates and bone, leading to fusion of the growth plate in the *Pten$^{fl/fl}$:Col2a1Cre* mice. The roles of estrogens is different in males and females [266, 268, 275], and may explain why the long bones were slightly longer in *Pten$^{fl/fl}$:Col2a1Cre* female mice versus controls and not so in males. Estrogen receptor-β (ERβ) has been associated with growth in female, but not male mice, and is a potential candidate to the male/female differences seen in the *Pten$^{flox/flox}$:Col2a1Cre* mice [5, 276].

At five days of age, limb bones enter a rapid growth phase, and much of the body's cartilage framework is converting into bone. If increased bone remodeling is important for the *Pten$^{flox/flox}$:Col2a1Cre* phenotype, then one would not expect to see any invariant size until the mice enter a period of rapid growth. Indeed, there was no increase in bone size in the *Pten$^{flox/flox}$:Col2a1Cre* 18.5 dpc embryos.

The long bones of *Pten$^{flox/flox}$:Col2a1Cre* mice revealed a dramatic increase in the amount of trabecular bone; indeed, to our knowledge, there are no reports of trabecular bone invasion to the femoral mid-shaft similar to that of *Pten$^{flox/flox}$:Col2a1Cre* mice. Various factors could potentially deregulate development of trabeculae. For example, either IGF-1 over-expression in mature osteoblasts, or PPR over-expression, can increase metaphyseal trabecular bone in mice [277-279]. In contrast, increased PPR expression

decreased cortical bone [277]. It is likely that increased endochondral bone-stimulating signals (e.g. VEGF, MMP-13) emanating from *Pten*$^{flox/flox}$*:Col2a1Cre* hypertrophic chondrocytes, in combination with the predicted increased sensitivity of *Pten*-deficient osteoblasts to growth signals, were responsible for the excess trabeculation of *Pten*$^{flox/flox}$*:Col2a1Cre* bones. The finding of increased osteoblast cellularity (Figure 3-27D, F) and intensity of ALP staining (Figure 3-35D) in the sub-hypertrophic region were consistent with increased osteoblastic influx and the more exuberant bone forming activity of *Pten*$^{flox/flox}$*:Col2a1Cre* growth plates. With the increased bone deposition we had expected to see an increase in osteoblast markers. Surprisingly, we found no increase intensity in type I collagen or osteopontin staining. This could indicate that the over-activation at the hypertrophic chondrocyte-bone interface, as evidenced by an increase in type X collagen and ALP, is leading to the increase in bone deposition and not the overactivation of osteoblasts present in the bone matrix. Another explanation could be that the expanded ALP and type X collagen staining represents abnormal mineralized cartilage resorption and replacement by bone rather than increased bone deposition. Alternatively, we may not be seeing an increase in expression because of the semi-quantitative nature of immunohistochemistry. A quantitative technique, such as real-time PCR may show an increase in these two factors.

The increase in osteoclast number under the growth plate could be the direct result of an increase in osteoblast and hypertrophic chondrocyte activity at the cartilage-bone interface. These osteoclasts would be primarily occupied by calcified cartilage matrix removal in *Pten*$^{fl/fl}$*:Col2a1Cre* mice, and thus do not necessarily reflect an increase

in bone remodeling. Static and dynamic histomorphometry is required to determine if there is a change in the rate of bone remodelling.

The heavier cortical bone in the femurs of adult *Pten$^{flox/flox}$:Col2a1Cre* mice (Figure 3-22A) may have stemmed from the presence of thicker bone collars (Figure 3-27F). This in turn, may result in larger templates directing appositional bone growth. Up-regulation of factors such as PTH and colony stimulating factor-1 (CSF-1) have been shown to increase the cortical bone [280-282]. Thus, the effects of even physiological amounts of these stimuli might well be up-regulated due to *Pten* deficiency in *Pten$^{flox/flox}$:Col2a1Cre* osteoblasts and osteocytes.

### *4.4.4 Upper body swelling in males and leanness in female Pten$^{flox/flox}$:Col2a1Cre mice*

One of the most striking features of the *Pten$^{flox/flox}$:Col2a1Cre* mice was the upper body swelling. The thoracic outlets of *Pten$^{flox/flox}$:Col2a1Cre* mice were more square than those of controls, perhaps leading to a thoracic outlet syndrome. The principal structures passing through this space include esophagus, trachea, vagus nerves, brachiocephalic trunk, left common carotid and subclavian arteries, inominate veins, and also numerous lymphatic vessels that join the thoracic duct. The structures that are most vulnerable to external compression would be predicted to be the low-pressure systems: veins and lymphatics. That the edema (or lymphedema) was only seen in males may have been due to increased bone overgrowth, and hence greater thoracic outlet obstruction.

Female *Pten$^{flox/flox}$:Col2a1Cre* mice tended to be lean and long (Figure 3-22), perhaps owing to dysphagia as a result partial esophageal obstruction at the thoracic outlet. Since bone overgrowth in osteopetrosis can lead to cranial nerve compression [283] we also considered the possibility that an abnormality of basicranial growth might

compromise the foramina for cranial nerves involved in food ingestion (e.g. the motor root V, IX, or XII). However, a study performed by Dr. Hallgrìmsson (personal communication) examining selected basicranial foramina by micro-ct showed no significant abnormalities. Additional investigation will be required to gain insight into the cause(s) of the leanness observed in female *Pten$^{flox/flox}$:Col2a1Cre* mice.

### *4.4.5 Articular joint damage with age*

The knee joints *Pten$^{flox/flox}$:Col2a1Cre* mice were analyzed at six months of age to determine whether loss of Pten protein expression might lead to joint pathology. This was based on the hypothesis that loss of Pten would tend to increase the sensitivity of chondrocytes to the range of PI3K-activating factors that they might be exposed to (e.g. FGFs, integrins, chemokines, IGFs, etc.) [252-255], leading to sustained PI(3,4,5)P3 levels, and hence increased PI3K downstream pathway activation. Over time, this might promote increased matrix turnover and even a tendency for chondrocytes to assume a hypertrophic phenotype, leading to degenerative joint disease.

We speculate that the *Pten$^{flox/flox}$:Col2a1Cre* joints become progressively unstable over time due to ligament laxity (because of changes in the fibrocartilage attachment sites); with signs of damage being expressed in the form of synovial reaction, meniscal damage, and osteophytes. This ligamentous problem may be secondary to an abnormality of chondrocyte function that causes a defect in the integrity of the ligaments (e.g. altered tensile property, due, for example, to a decreased ratio of fibrous and elastic tissue to proteoglycan). The hypothesis that joint laxity being present is supported by the capsular thickening in the *Pten$^{flox/flox}$:Col2a1Cre* samples. Two other potential predisposing factors: (*i*) the abnormality of bone shape leading to a biomechanical abnormality that

stresses the knee joint; and (*ii*) subchondral bone rigidity might, in time, lead to articular cartilage and ligament damage.

Bone has been thought to play a role in the pathogenesis of OA for many years. Radin and colleagues proposed that increased density of the subchondral plate was important in initiating articular cartilage fibrillation in early phases of the disease [284-286]. They hypothesized that the stiffer subchondral structure lost its shock-absorbing capabilities, creating increased stress in overlying articular cartilage. However, experimental data failed to show that cartilage lesions can result from subchondral bone stiffening [287, 288]. Yet, it could be responsible for cartilage lesions in individuals whose cartilage is already compromised [288]. Alternatively, subchondral stiffness could be due to generalized bone changes that lead to apparent increases in bone mineral density/volume [288]. Also, primary OA and osteoporosis seldom coexist [289-291]. An association has also been observed between osteophyte development and increased bone mineral density/volume in the femora, which further suggests that a primary attribute of bone formation may play a role in the pathogenesis of OA [288, 292]. Increased osteoblast activity due to PI3K activation could lead to the thickening of subchondral bone, which in turn is associated with degenerative joint diseases. Abnormal osteoblast activity has been observed in OA patients and some believe that is has a role in the breakdown of cartilage [293-295]. Further investigations specifically looking at subchondral bone thickness could be performed in the aged *Pten*$^{flox/flox}$*:Col2a1Cre* mice so see if there is a significant difference when compared to control mice.

Animal models of OA have shown that bony changes can precede changes in articular cartilage [296-298], which supports the hypothesis that cartilage lesions do not

progress in the absence of significant subchondral bone activity [288]. Researchers now believe that a key role for subchondral bone in the progression of OA is the result of the production of cytokines and growth factors [293-295]. Channels and clefts that would allow passage of these molecules from the subchondral bone into the cartilage have been identified early in the progression of OA [299-301]. Bone derived products could have a role in driving cartilage metabolism, such as IFG-1, and -2 [293, 302, 303], and these effects could be further enhanced by the activation of PI3K.

We hypothesize that *Pten*$^{flox/flox}$*:Col2a1Cre* mice aged to nine and twelve months will have knee joint pathology that becomes progressively severe in mice with *Pten* deletions, and will possibly involve all three compartments. This is supported by the difficulties in movement and stiffened tail of the nine and ten month *Pten*$^{flox/flox}$*:Col2a1Cre* mice examined.

As a general hypothesis, the earliest events in spontaneous degenerative joint disease (as in primary OA) may stem from gene polymorphisms leading to abnormal matrix and/or cell signalling, and hence to abnormal remodelling over years. For example, with augmentation of signalling pathways (such as in *Pten* deficiency) chondrocytes and osteoblasts may ‘over-react’ (hyper-activate) to minor daily trauma, leading over time to matrix damage. On the flip-side, hypo function of a key adaptive signalling pathway could also lead to joint damage with time. Such gradual losses of cartilage integrity would set the stage for ‘secondary’ degenerative mechanisms as seen in the widely-studied in acute injury models (ACL transection, intra-articular protease administration, or surgical trauma of cartilage).

### *4.4.6 Tumourigenesis associated with loss of Pten expression in osteo-chondrocytic progenitors*

4.4.6.1 Osteosarcomas

Despite the well-recognized tumour suppressor function of *Pten*, and the *Pten* deletions in proliferating osteo-chondroprogenitor cell populations, none of the young *Pten$^{flox/flox}$:Col2a1Cre* mice described in this study developed either hamartomas, or sarcomas. However, within a cohort of fourteen mice set aside for an aging study, we have seen two examples of sarcomas in mice between nine and ten months of age. It is therefore possible that a high frequency of such tumours will be observed within *Pten$^{flox/flox}$:Col2a1Cre* mouse populations as they age, consistent with the need for additional genetic 'hits' being required for tumourigenesis.

One possible mechanism for tumour progression in the *Pten$^{flox/flox}$:Col2a1Cre* mice is through the IGFR-mTOR pathway. This pathway is known to be important in the differentiation of stem cells into various mesenchymal lineages. IGF has also been shown to be overexpressed in Ewing sarcoma, which is the second most common type of malignant bone tumour in children and young adults [36].

Cytoskeletal proteins have been linked to osteosarcoma progression and metastasis. One such factor is ezrin, a membrane-cytoskeleton organizer, has been suggested to promote tumour metastasis [52, 54]. Ezrin expression is linked to MAPK and Akt expression levels. Ezrin has been shown to directly bind to PI3K [304], and its metastatic behaviour linked to S6K1 and 4E-BP1, both downstream effectors of mTOR. Inhibition of ezrin *in vitro* leads to a decrease in the expression and phosphorylation of both S6K1 and 4EBP1. The link between ezrin and mTOR was further supported *in vivo*,

when administration of rapamycin, an inhibitor of mTOR, was shown to significantly decrease metastasis [305]. The metastasis seen in the *Pten$^{flox/flox}$:Col2a1Cre* mice could very possibly be due increased mTOR/S6K1/4E-BP1 signalling, activated via direct binding of ezrin to PI3K.

All human osteosarcomas have augmentated hepatocyte growth factor (HGF) signalling and overexpression of MET; furthermore studies have linked HGF and its receptor, the proto-oncogene c-MET, with the ability to metastasize. HGF is multifunctional, and has a role in cell scattering, survival, growth, motility, tubular morphogenesis, angiogenesis, and invasiveness. Ezrin is a known regulator of HGF, and this interaction might account for the ability of ezrin to promote tumour metastasis [reviewed in [306]]. MET signalling is mediated via the phosphorylation of two carboxy-terminal tyrosine docking sites, which can be bound by a number of intracellular mediators, including p85, the catalytic subunit of PI3K, leading to the activation of the PI3K pathway [307-311]. Of further interest, it has been shown that coupling to PI3K leads to a decrease in cell proliferation and stimulates differentiation in myoblasts [312]. Whether it has this role in osteoblasts or chondroblasts is unknown. Via activation of HSF/MET, PI3K is shown to be an effector for both morphogenesis and antiapoptosis *in vitro*. If HSF/MET→PI3K pathway is able to promote morphogenesis and differentiation during the mesenchymal to osteoblast differentiation process, it could implicate this pathway not only in metastasis but also in tumourigenesis. Ezrin's potential role in tumour metastasis in the *Pten$^{flox/flox}$:Col2a1Cre* mice may be direct via activation of PI3K, or indirect, through its upregulation of HGF/c-MET and resulting upregulation of

the PI3K signalling pathway. One of these mechanisms may explain how PI3K/AKT signalling has enabled lung metastasis from osteosarcomas *in vitro* [42].

### *4.4.7 Pten and the Regulation of Skeletal Growth*

The osteo-chondrogenic lineage-specific deletion of Pten offers a window on an important component involved in the determination of skeletal size in vertebrates. Our study demonstrates that Pten, and hence the PI3K pathway that this phosphatase regulates, is an important 'rheostat' responsible for determining the extent of normal cartilage and bone development, and hence, the set-point of skeletal size. This is plausible, given that the PI3K→Akt pathway regulated by the Pten phosphatase actually serves as a sort of signal transduction 'funnel', integrating the effects of a wide range of extracellular PI3K-activating stimuli that may be continually impacting cell surface receptors.

## 4.5 Overall summary and primary limitation

Skeletogenesis is a complex process that depends on a variety of extracellular stimuli that activate diverse intracellular signaling pathways. Although many such stimuli activate phosphatidylinositol 3'-kinase (PI3K), the precise role of this pathway in cartilage development and bone formation remains nebulous. The 3' phosphoinositide phosphatase and tumor suppressor, Pten, is a pivotal downstream negative regulator of the PI3K signaling. To gain insight into the role of the PI3K pathway in skeletogenesis, mice with biallelic *lox*P-flanked *Pten* exons were crossed with a type II collagen gene promoter Cre recombinase-expressing line to yield $Pten^{flox/flox}$*:Col2a1Cre* mice. *Col2a1Cre*-mediated gene alterations were observed in mature chondrocytes, as well as in osteo-chondroprogenitors. As revealed by microcomputed tomography, $Pten^{flox/flox}$*:Col2a1Cre*

mice exhibited not only increased skeletal growth post-natally, particularly of vertebrae, but also massive trabeculation and increased cortical thickness of long bones. Consistent with this, primary spongiosa development and perichondrial bone collar formation were augmented in *Pten$^{flox/flox}$:Col2a1Cre* mice. Growth plates of *Pten$^{flox/flox}$:Col2a1Cre* mice were disorganized, with evidence of accelerated hypertrophic differentiation as suggested by altered expression of type X collagen and alkaline phosphatase. Surprisingly, we did not find any change in rate of proliferation or apoptosis in the growth plates. Perhaps consistent with cartilage germinal zone exhaustion, tibial growth plate fusion was observed at 6 months of age. Our results show that Pten, likely via its ability to regulate PI3K pathway activity, is an important determinant of skeletal size and bone architecture.

One of the limitations of this work is that it remains unknown as to which arm of the complex PI3K pathway is involved. Upstream there are numerous factors that could contribute to the phenotype such as IGF, GH, ERs, Adrogen receptor, EGF. Conversely downstream of the PI3K cascade there is a number of components that could conceivably be involved in the Pten-deficient phenotype, including GSK-3, FOXO3, and BAD that are negatively regulated by PKB/Akt. PKB/Akt activation increases resistance to apoptosis, although we have no evidence that an abnormality of apoptosis is important to the Pten phenotype. One could therefore think of this problem as an hourglass, whereby many factors could contribute to the overaction of PI3K, and, numerous factors downstream could be playing a role. We have clearly demonstrated a role for the PI3K pathway in normal skeletal and cartilaginous growth. Owing to its importance in many different tissues and diseases, this area of research is very dynamic and fertile.

## 4.6 Future Studies

Indirectly, via the loss of Pten, we have found evidence that PI3K is an important regulator of chondrocyte and osteoblast function, and in particular, cartilage-directed bone formation. The phenotype of mice lacking Pten is obviously complex, and much future work can be performed to understand this better.

### *4.6.1 Further investigation of osteoblast activity*

Future work characterizing osteoblast activity would better illuminate the role this cell type plays in the *Pten$^{flox/flox}$:Col2a1Cre* mouse phenotype. It would be interesting to see if these cells show a change in apoptosis, proliferation, or cell size. Osteoblast numbers in the sub-hypertrophic zone could also be quantified. Immunohistochemistry could be also performed on isolated osteoblasts to see if there is evidence of P-Akt, S6K, mTOR, 4eBP1, or GSK3 expression. As suggested with the chondrocytes, osteoblasts might not show any change in either of these factors without stimulation, such as addition of IGF-1. This would provide more information as to the role that osteoblasts are playing in the *Pten$^{flox/flox}$:Col2a1Cre* mice.

### *4.6.2 Altered differentiation in mesenchymal cells?*

Since PI3K is suggested to be involved in the differentiation of both chondrocytes and osteoblasts [179, 183], it would be interesting to see how this process is modified in *Pten$^{flox/flox}$:Col2a1Cre* mice. To examine this both control and *Pten$^{flox/flox}$:Col2a1Cre* mesenchymal cells could be isolated [313-315]. IGF-1 can be added to the media to induce chondrogenic differentiation and this process could be measured by alcian blue staining, proteoglycan synthesis, and analyzed for the expression of Col2a1 and Sox-9 by quantitative real time PCR [316, 317]. Endothelial growth factor (EGF) could be used to

stimulate osteoblast differentiation which could be observed by alizarin red staining, ALP activity, and analyzed for the expression of Runx-2 and collagen type 1 by real time PCR. [318].

It would also be of interest to try to dissect out which arm of the PI3K signalling pathway is important in chondrocyte/osteoblast differentiation in the *Pten$^{flox/flox}$:Col2a1Cre* mice. Activation, and therefore phosphorylation, of downstream effectors such as Akt, GSK-3, 4eBP1, S6K, FOXO3, p27, and upregulation of mTOR could be examined. One would expect to see hyper-activation of some, if not all, of these factors in the *Pten$^{flox/flox}$:Col2a1Cre* mesenchymal cells. These factors can be examined by either *in situ* hybridization or immunohistochemistry. Finding out which of these players are affected during differentiation will help discern the role of PI3K signalling in this process.

### *4.6.3 Dissecting out the role of hypertrophic chondrocytes and osteoblasts*

Given the data that indicated that *Col2a1Cre* is activated in both chondro- and osteoprogenitor cells, it would be useful to discern which cell type is important for the bone overgrowth. One of the most compelling phenotypic features of the *Pten$^{flox/flox}$:Col2a1Cre* mice is the bone overgrowth syndrome, characterized by enlarged vertebrae and long bones, and increased cortical thickness and more and thicker trabeculae. It is unknown as to whether the effect of Pten loss is due to increased activation of hypertrophic chondrocytes and/or osteoblasts at the cartilage-interface. To help discern the role of the two cell types we would require a detailed study of the factors produced by both hypertrophic chondrocytes and osteoblasts, especially as the factors they elaborate that are capable of stimulating bone (trabeculae and bone collar)

formation. We hypothesize that the hypertrophic chondrocyte population directs the genesis of the enlarged sclerotic bones by the PI3K-induced excess generation (eg. by transcriptional up-regulation) of one or more of the following factors [16] Ihh, BMP-2, -6, MMP-13, autocrine IGF. We would further examine osteoblast specific markers such as: osteonectin, osteopontin, Runx2, bone sialoprotein, and IGF, to see how they are affected by PI3K upregulation. Perichondrial BMP production would also be examined. These molecules can be assayed by either *in situ* hybridization or immunohistochemistry, and are a logical starting point for the analysis. It is also conceivable that loss of Pten leads to the decreased production of factors, such as the BMP antagonist Noggin that normally decreases osteogenesis. Identifying the PI3K-stimulating ligand(s)-receptor(s) that lead to the bone enlargement phenotype, however would be challenging.

Given that there is significant cross talk between hypertrophic chondrocytes and osteoblasts, it may be difficult to discern which cell type may be expressing the different factors involved in the phenotype, as there is considerable overlap in their expression. This difficulty would be surmountable by laser capture microdissection (LCM). This would allow for the manual selection of either hypertrophic chondrocytes or osteoblasts. Having the two distinct cell populations, one could then perform real-time PCR to examine changes in RNA levels between control and $Pten^{flox/flox}$*:Col2a1Cre* mice of the above listed markers. We believe that the enlargement in bones would be due to loss of *Pten* in chondrocytes, while cortical and trabecular bone overgrowth would stem from the inactivation of *Pten* in osteoblasts.

Alternatively, distinguishing between the two cell types could be performed through the generation of tissue specific knockouts. To examine if the

*Pten*$^{flox/flox}$*:Col2a1Cre* mouse phenotype is a reflection of abnormal hypertrophic chondrocyte function a transgenic line expressing Cre recombinase under the control of the Type X collagen gene promoter could be used. Type X collagen is expressed in hypertrophic cells, and is widely used as a marker for this chondrocyte population. If hypertrophic chondrocytes are involved in the *Pten*$^{flox/flox}$*:Col2a1Cre* phenotype, this may recapitulate the phenotype of mice lacking Pten in all chondrocyte stages. A more likely scenario would be that we would see a partial re-creation of the phenotype.

The Type X collagen gene promoter (mammalian and avian) has been evaluated in transgenic mice by several investigators [319-322]. Depending on integration site, length or upstream sequences used it has been shown to lead to reporter gene expression in hypertrophic chondrocytes. The optimal upstream region appears to be a 4.7Kb segment that includes an enhancer element. Recently, a group reported a transgenic line in which a very short upstream segment (<1.5kb) of the Type X collagen gene promoter was used to drive Cre expression in hypertrophic chondrocytes [321]. Using the R26R reporter mice, it was further shown that hypertrophic chondrocytes stained positive *LacZ* expression, indicating that Cre-recombinase was active [321].

To generate osteoblast specific knockouts, we can use a Cre recombinase expressed under the control of the type 1α collagen promoter. This Cre recombinase is driven by the 2.3-kb proximal fragment of the α1(I)-collagen promoter [323]. Col1α1-Cre recombinase was shown to be expressed at high levels throughout osteoblast differentiation. Using the R26R reporter mice, it was further shown that almost all osteoblasts stained positive for *LacZ* expression, and that expression was not seen in any other cell type [323]. Again it would be interesting to see if deletions in osteoblasts would

be able to replicate the phenotype seen with the Type II collagen gene promoter-Cre-mediated *Pten* excisions.

Once generated, both these knockouts could be further examined by the same techniques previously used to see how their phenotypes differ from the *Pten$^{flox/flox}$:Col2a1Cre* mice.

### *4.6.4 Aging Pten$^{flox/flox}$:Col2a1Cre mice*

Currently, *Pten$^{flox/flox}$:Col2a1Cre* mice are being aged to nine and twelve months. We have shown that some of the six month *Pten$^{flox/flox}$:Col2a1Cre* mice are starting to display degenerative joint changes, including synovial hyperplasia, GAG depletion, articular fibrillations, capsular thickening, and osteophyte production. These effects may worsen with age, especially considering the stiffening of joints we observed in the 9 and 10 month old mice. Histology would reveal any cartilage changes such as articular damage, GAG depletion, and changes in the joint capsule. Micro-ct analysis would allow for the determination of whether the cortical bone thickening and trabecular bone formation increased further with age. In addition to this, subchondral plate thickness could be measured. One might expect to find that the *Pten$^{flox/flox}$:Col2a1Cre* mice have a thicker subchondral growth plate as it is a marker of degenerative joint disease. These techniques will allow for the phenotypic characterization of the changes occurring in the *Pten$^{flox/flox}$:Col2a1Cre* mice.

If joint degeneration were observed, LCM could be utilized to selectively isolate RNA from articular chondrocytes and osteoblast to elucidate which factors are altered due to PI3K overactivation. Factors of interest would include: Col2a1, MMP-9, -13, ADAMT-4, -5, TGF-β, iNOS, IL-1. In addition, it would be of interest to examine PI3K

specific factors, such as Akt, mTOR, Gsk-3, 4eBP1, FOXO3, S6K, and Bad. Variations in how these factors respond between control and *Pten$^{flox/flox}$:Col2a1Cre* mice would aid in the understanding of how PI3K is directly or indirectly causing joint degeneration, and provide us with further insight into factors involved in articular cartilage degeneration.

### *4.6.5 PI3K and osteosarcomas*

One of the more interesting observations thus far were the few osteosarcomas seen in our *Pten$^{flox/flox}$:Col2a1Cre* mice. The low incidence makes this difficult to study and larger numbers are required to ensure that this is a real phenomenon. However, it would be of interest to examine osteoblastic markers present in an osteosarcoma such as: ALP, type I collagen, osteopontin, matrix Gla protein, and osteocalcin, as these are all known markers for osteosarcomas.

As Met/HGF interaction leads to upstream of PI3K activation, it would be of interest to see how isolated osteoblasts responded to MET stimulation. In osteoblasts, overexpression of MET, through lentiviral vector-mediated gene transfer, has led to the single-step conversion of primary human osteoblasts into osteosarcoma cells. These cells displayed a typical *in vitro* osteosarcoma phenotype including: atypical nuclei, aberrant mitoses, production of ALP, secretion of osteoid ECM, and striking neovascularization [324]. If PI3K signalling is indeed one of the primary pathways for osteosarcomas, then osteoblasts from *Pten$^{flox/flox}$:Col2a1Cre* mice should have a stronger response than control osteoblasts, such as increased ALP expression, and neoplastic osteoid production. As PI3K may be implicated in tumour invasion, it would be of interest to see if elevated levels of MMPs and ezrin were produced by osteosarcomas. Furthermore, it would be of interest to dissect out which part of the PI3K pathway is affected. As ezrin has been

implicated in the activation of mTOR, and subsequent increase in metatastic potential [304], it would be of most interest to investigate if there is an activation of S6K1 and 4eBPI. Discovering a key player in the development of the primary osteosarcoma, or even in determining its metastatic potential, could potentially identify a therapeutic target for osteosarcomas.

## References


1. Karaplis, A.C., *Embryonic Development of Bone and the Molecular Regulation of Intramembranous and Endochondral Bone Formation*, in *Principles of Bone Biology*, J.P. Bilezikian, L.G. Raisz, and G.A. Rodan, Editors. 2002, Academic Press: San Diego, California. p. 33-58.
2. Hall, B.K., *Bones and Cartilage: Developmental and Evolutionary Skeletal Biology*. 2005, New York: Elsevier Academic Press.
3. Roelen, B.A. and P. Dijke, *Controlling mesenchymal stem cell differentiation by TGFBeta family members.* J Orthop Sci, 2003. **8**(5): p. 740-8.
4. Hall, B.K. and T. Miyake, *All for one and one for all: condensations and the initiation of skeletal development.* Bioessays, 2000. **22**(2): p. 138-47.
5. Lindberg, M.K., et al., *Estrogen receptor specificity in the regulation of the skeleton in female mice.* J Endocrinol, 2001. **171**(2): p. 229-36.
6. Loeser, R.F., *Chondrocyte integrin expression and function.* Biorheology, 2000. **37**(1-2): p. 109-16.
7. Huang, W., et al., *Phosphorylation of SOX9 by cyclic AMP-dependent protein kinase A enhances SOX9's ability to transactivate a Col2a1 chondrocyte-specific enhancer.* Mol Cell Biol, 2000. **20**(11): p. 4149-58.
8. Ikeda, T., et al., *The combination of SOX5, SOX6, and SOX9 (the SOX trio) provides signals sufficient for induction of permanent cartilage.* Arthritis Rheum, 2004. **50**(11): p. 3561-73.
9. Komori, T., et al., *Targeted disruption of Cbfa1 results in a complete lack of bone formation owing to maturational arrest of osteoblasts.* Cell, 1997. **89**(5): p. 755-64.
10. Mundlos, S., et al., *Mutations involving the transcription factor CBFA1 cause cleidocranial dysplasia.* Cell, 1997. **89**(5): p. 773-9.
11. Otto, F., et al., *Cbfa1, a candidate gene for cleidocranial dysplasia syndrome, is essential for osteoblast differentiation and bone development.* Cell, 1997. **89**(5): p. 765-71.
12. Rice, D.P., et al., *Integration of FGF and TWIST in calvarial bone and suture development.* Development, 2000. **127**(9): p. 1845-55.
13. Opperman, L.A., *Cranial sutures as intramembranous bone growth sites.* Dev Dyn, 2000. **219**(4): p. 472-85.
14. Provot, S. and E. Schipani, *Molecular mechanisms of endochondral bone development.* Biochem Biophys Res Commun, 2005. **328**(3): p. 658-65.
15. Colnot, C., *Cellular and molecular interactions regulating skeletogenesis.* J Cell Biochem, 2005. **95**(4): p. 688-97.
16. Kronenberg, H.M., *Developmental regulation of the growth plate.* Nature, 2003. **423**(6937): p. 332-6.
17. Karsenty, G., *Minireview: transcriptional control of osteoblast differentiation.* Endocrinology, 2001. **142**(7): p. 2731-3.
18. Ornitz, D.M. and P.J. Marie, *FGF signaling pathways in endochondral and intramembranous bone development and human genetic disease.* Genes Dev, 2002. **16**(12): p. 1446-65.

19. Minina, E., et al., *Interaction of FGF, Ihh/Pthlh, and BMP signaling integrates chondrocyte proliferation and hypertrophic differentiation.* Dev Cell, 2002. **3**(3): p. 439-49.
20. Stickens, D., et al., *Altered endochondral bone development in matrix metalloproteinase 13-deficient mice.* Development, 2004. **131**(23): p. 5883-95.
21. Zelzer, E. and B.R. Olsen, *Multiple roles of vascular endothelial growth factor (VEGF) in skeletal development, growth, and repair.* Curr Top Dev Biol, 2005. **65**: p. 169-87.
22. Eames, B.F., L. de la Fuente, and J.A. Helms, *Molecular ontogeny of the skeleton.* Birth Defects Res C Embryo Today, 2003. **69**(2): p. 93-101.
23. Colnot, C., et al., *Indian hedgehog synchronizes skeletal angiogenesis and perichondrial maturation with cartilage development.* Development, 2005. **132**(5): p. 1057-67.
24. Colnot, C., et al., *Distinguishing the contributions of the perichondrium, cartilage, and vascular endothelium to skeletal development.* Dev Biol, 2004. **269**(1): p. 55-69.
25. Inada, M., et al., *Critical roles for collagenase-3 (Mmp13) in development of growth plate cartilage and in endochondral ossification.* Proc Natl Acad Sci U S A, 2004. **101**(49): p. 17192-7.
26. St-Jacques, B., M. Hammerschmidt, and A.P. McMahon, *Indian hedgehog signaling regulates proliferation and differentiation of chondrocytes and is essential for bone formation.* Genes Dev, 1999. **13**(16): p. 2072-86.
27. Vortkamp, A., et al., *Regulation of rate of cartilage differentiation by Indian hedgehog and PTH-related protein.* Science, 1996. **273**(5275): p. 613-22.
28. Chung, U.I., et al., *Indian hedgehog couples chondrogenesis to osteogenesis in endochondral bone development.* J Clin Invest, 2001. **107**(3): p. 295-304.
29. Mankin, H.J., V.C. Mow, and J.A. Buckwalter, *Articular cartilage repair and osteoarthritis*, in *Orthapaedic Basic Science Biology and Biomechanics of the Musculoskeletal System.*, J.A. Buckwalter, T. Einhorn, and S. Simon, Editors. 2000, American Academy of Orthopaedic Surgeons.
30. Poole, A.R., *Cartilage in Health and Disease*, in *Arthritis and Allied Conditions*, W. Koopman and L.W. Moreland, Editors. 2001, Lippincott Willians and Wilkins: Philadelphia, PA.
31. Serra, R., et al., *Expression of a truncated, kinase-defective TGF-beta type II receptor in mouse skeletal tissue promotes terminal chondrocyte differentiation and osteoarthritis.* J Cell Biol, 1997. **139**(2): p. 541-52.
32. Wang, L.L., *Biology of osteogenic sarcoma.* Cancer J, 2005. **11**(4): p. 294-305.
33. Hayden, J.B. and B.H. Hoang, *Osteosarcoma: basic science and clinical implications.* Orthop Clin North Am, 2006. **37**(1): p. 1-7.
34. Papachristou, D.J., et al., *The MAPK-AP-1/-Runx2 signalling axes are implicated in chondrosarcoma pathobiology either independently or via up-regulation of VEGF.* Histopathology, 2005. **47**(6): p. 565-74.
35. Bovee, J.V.M.G., *Bone:Chondrosarcoma. Atlas Genet Cytogenet Oncol Haematol.* March 2002.

36. Matushansky, I. and R.G. Maki, *Mechanisms of sarcomagenesis.* Hematol Oncol Clin North Am, 2005. **19**(3): p. 427-49, v.
37. Bovee, J.V., et al., *Emerging pathways in the development of chondrosarcoma of bone and implications for targeted treatment.* Lancet Oncol, 2005. **6**(8): p. 599-607.
38. Beier, F., *Cell-cycle control and the cartilage growth plate.* J Cell Physiol, 2005. **202**(1): p. 1-8.
39. Lin, C., P.A. Meitner, and R.M. Terek, *PTEN mutation is rare in chondrosarcoma.* Diagn Mol Pathol, 2002. **11**(1): p. 22-6.
40. Unni, K.K., *Osteosarcoma of bone.* J Orthop Sci, 1998. **3**(5): p. 287-94.
41. Ek, E.T., C.R. Dass, and P.F. Choong, *Commonly used mouse models of osteosarcoma.* Crit Rev Oncol Hematol, 2006.
42. Fukaya, Y., et al., *A role for PI3K-Akt signaling in pulmonary metastatic nodule formation of the osteosarcoma cell line, LM8.* Oncol Rep, 2005. **14**(4): p. 847-52.
43. Nielsen-Preiss, S.M., S.R. Silva, and J.M. Gillette, *Role of PTEN and Akt in the regulation of growth and apoptosis in human osteoblastic cells.* J Cell Biochem, 2003. **90**(5): p. 964-75.
44. Levine, R.A., T. Forest, and C. Smith, *Tumor suppressor PTEN is mutated in canine osteosarcoma cell lines and tumors.* Vet Pathol, 2002. **39**(3): p. 372-8.
45. Overholtzer, M., et al., *The presence of p53 mutations in human osteosarcomas correlates with high levels of genomic instability.* Proc Natl Acad Sci U S A, 2003. **100**(20): p. 11547-52.
46. Kirpensteijn, J., et al., *Growth hormone gene expression in canine normal growth plates and spontaneous osteosarcoma.* Mol Cell Endocrinol, 2002. **197**(1-2): p. 179-85.
47. Schmidt, J., et al., *Establishment and characterization of osteogenic cell lines from a spontaneous murine osteosarcoma.* Differentiation, 1988. **39**(3): p. 151-60.
48. Grigoriadis, A.E., et al., *Osteoblasts are target cells for transformation in c-fos transgenic mice.* J Cell Biol, 1993. **122**(3): p. 685-701.
49. Tinkey, P.T., et al., *Postirradiation sarcomas in Sprague-Dawley rats.* Radiat Res, 1998. **149**(4): p. 401-4.
50. Asai, T., et al., *Establishment and characterization of a murine osteosarcoma cell line (LM8) with high metastatic potential to the lung.* Int J Cancer, 1998. **76**(3): p. 418-22.
51. Berlin, O., et al., *Development of a novel spontaneous metastasis model of human osteosarcoma transplanted orthotopically into bone of athymic mice.* Cancer Res, 1993. **53**(20): p. 4890-5.
52. Khanna, C., et al., *Metastasis-associated differences in gene expression in a murine model of osteosarcoma.* Cancer Res, 2001. **61**(9): p. 3750-9.
53. Khanna, C., et al., *The membrane-cytoskeleton linker ezrin is necessary for osteosarcoma metastasis.* Nat Med, 2004. **10**(2): p. 182-6.
54. Yu, Y., et al., *Expression profiling identifies the cytoskeletal organizer ezrin and the developmental homeoprotein Six-1 as key metastatic regulators.* Nat Med, 2004. **10**(2): p. 175-81.

55. *Primer on the rheumatic diseases.* 12 ed, ed. J.e.a. Kilipel. 2001, Atlanta, Gergia: Arthritis Foundation.
56. Buckwalter, J.A., J. Martin, and H.J. Mankin, *Synovial joint degeneration and the syndrome of osteoarthritis.* Instr Course Lect, 2000. **49**: p. 481-9.
57. Felson, D.T., *Epidemiology of osteoarthritis*, in *Osteoarthrits*, K.D. Brandt, M. Doherty, and L. Lohmander, Editors. 1998, Oxford University Press: NY. p. 13--22.
58. Brandt, K.D., L. Lohmander, and M. Doherty, *Introduction: the concepts of osteoarthritis as failure of the diarthrodial joint.*, in *Osteoarthritis*, K.D. Brandt, M. Doherty, and L. Lohmander, Editors. 1998, Oxford University Press: NY. p. 70-73.
59. Flores, R. and M. Hochberg, *Definition and classification of osteoarthritis*, in *Osteoarthritis*, K.D. Brandt, M. Doherty, and L. Lohmander, Editors. 1998, Oxford University Press: NY. p. 1-12.
60. Spector, T.D. and A.J. MacGregor, *Risk factors for osteoarthritis: genetics.* Osteoarthritis Cartilage, 2004. **12 Suppl A**: p. S39-44.
61. Demissie, S., et al., *Genome scan for quantity of hand osteoarthritis: the Framingham Study.* Arthritis Rheum, 2002. **46**(4): p. 946-52.
62. Ingvarsson, T., et al., *A large Icelandic family with early osteoarthritis of the hip associated with a susceptibility locus on chromosome 16p.* Arthritis Rheum, 2001. **44**(11): p. 2548-55.
63. Leppavuori, J., et al., *Genome scan for predisposing loci for distal interphalangeal joint osteoarthritis: evidence for a locus on 2q.* Am J Hum Genet, 1999. **65**(4): p. 1060-7.
64. Loughlin, J., et al., *Linkage analysis of chromosome 2q in osteoarthritis.* Rheumatology (Oxford), 2000. **39**(4): p. 377-81.
65. Wright, G.D., et al., *Association of two loci on chromosome 2q with nodal osteoarthritis.* Ann Rheum Dis, 1996. **55**(5): p. 317-9.
66. Valdes, A.M., et al., *Association study of candidate genes for the prevalence and progression of knee osteoarthritis.* Arthritis Rheum, 2004. **50**(8): p. 2497-507.
67. Kizawa, H., et al., *An aspartic acid repeat polymorphism in asporin inhibits chondrogenesis and increases susceptibility to osteoarthritis.* Nat Genet, 2005. **37**(2): p. 138-44.
68. Pelletier, J.P. and J. Martel-Pelletier, *The Novartis-ILAR Rheumatology Prize 2001 Osteoarthritis: from molecule to man.* Arthritis Res, 2002. **4**(1): p. 13-9.
69. Pelletier, J.P., J. Martel-Pelletier, and S.B. Abramson, *Osteoarthritis, an inflammatory disease: potential implication for the selection of new therapeutic targets.* Arthritis Rheum, 2001. **44**(6): p. 1237-47.
70. Cheung, H.S., et al., *Phosphocitrate blocks calcification-induced articular joint degeneration in a guinea pig model.* Arthritis Rheum, 2006. **54**(8): p. 2452-61.
71. Neidel, J., B. Schroers, and F. Sintermann, *The effects of high-dose methotrexate on the development of cartilage lesions in a lapine model of osteoarthrosis.* Arch Orthop Trauma Surg, 1998. **117**(4-5): p. 265-9.
72. Wilson, W., et al., *Causes of mechanically induced collagen damage in articular cartilage.* J Orthop Res, 2006. **24**(2): p. 220-8.

73. Silberg, M. and R. Silber, *Age changes of bones and joints in various strains of mice.* Amer. J. Anat., 1941. **68**: p. 69.
74. van der Kraan, P.M., et al., *Development of osteoarthritic lesions in mice by "metabolic" and "mechanical" alterations in the knee joints.* Am J Pathol, 1989. **135**(6): p. 1001-14.
75. Ameye, L., et al., *Abnormal collagen fibrils in tendons of biglycan/fibromodulin-deficient mice lead to gait impairment, ectopic ossification, and osteoarthritis.* Faseb J, 2002. **16**(7): p. 673-80.
76. Fassler, R., et al., *Mice lacking alpha 1 (IX) collagen develop noninflammatory degenerative joint disease.* Proc Natl Acad Sci U S A, 1994. **91**(11): p. 5070-4.
77. Glasson, S.S., et al., *Deletion of active ADAMTS5 prevents cartilage degradation in a murine model of osteoarthritis.* Nature, 2005. **434**(7033): p. 644-8.
78. Holmbeck, K., et al., *MT1-MMP-deficient mice develop dwarfism, osteopenia, arthritis, and connective tissue disease due to inadequate collagen turnover.* Cell, 1999. **99**(1): p. 81-92.
79. Mishina, Y., et al., *Generation of Bmpr/Alk3 conditional knockout mice.* Genesis, 2002. **32**(2): p. 69-72.
80. Wadhwa, S., et al., *Mice deficient in biglycan and fibromodulin as a model for temporomandibular joint osteoarthritis.* Cells Tissues Organs, 2005. **181**(3-4): p. 136-43.
81. Wadhwa, S., et al., *Accelerated osteoarthritis in the temporomandibular joint of biglycan/fibromodulin double-deficient mice.* Osteoarthritis Cartilage, 2005. **13**(9): p. 817-27.
82. Xu, L., et al., *Osteoarthritis-like changes and decreased mechanical function of articular cartilage in the joints of mice with the chondrodysplasia gene (cho).* Arthritis Rheum, 2003. **48**(9): p. 2509-18.
83. Yang, X., et al., *TGF-beta/Smad3 signals repress chondrocyte hypertrophic differentiation and are required for maintaining articular cartilage.* J Cell Biol, 2001. **153**(1): p. 35-46.
84. Zemmyo, M., et al., *Accelerated, aging-dependent development of osteoarthritis in alpha1 integrin-deficient mice.* Arthritis Rheum, 2003. **48**(10): p. 2873-80.
85. Young, M.F., *Mouse models of osteoarthritis provide new research tools.* Trends Pharmacol Sci, 2005. **26**(7): p. 333-5.
86. Feldkamp, L.A., et al., *The direct examination of three-dimensional bone architecture in vitro by computed tomography.* J Bone Miner Res, 1989. **4**(1): p. 3-11.
87. Borah, B., et al., *Three-dimensional microimaging (MRmicroI and microCT), finite element modeling, and rapid prototyping provide unique insights into bone architecture in osteoporosis.* Anat Rec, 2001. **265**(2): p. 101-10.
88. Cooper, D.M., et al., *Quantitative 3D analysis of the canal network in cortical bone by micro-computed tomography.* Anat Rec B New Anat, 2003. **274**(1): p. 169-79.
89. Peyrin, F., et al., *Micro-CT examinations of trabecular bone samples at different resolutions: 14, 7 and 2 micron level.* Technol Health Care, 1998. **6**(5-6): p. 391-401.

90. Takeuchi, A., et al., *Submicrometer-resolution three-dimensional imaging with hard x-ray imaging microtomography.* Review of Scientific Instruments, 2002. **73**: p. 4269-4249.
91. Genant, H.K. and Y. Jiang, *Advanced imaging assessment of bone quality.* Ann N Y Acad Sci, 2006. **1068**: p. 410-28.
92. Cartmell, S., et al., *Quantitative microcomputed tomography analysis of mineralization within three-dimensional scaffolds in vitro.* J Biomed Mater Res A, 2004. **69**(1): p. 97-104.
93. Waarsing, J.H., et al., *Detecting and tracking local changes in the tibiae of individual rats: a novel method to analyse longitudinal in vivo micro-CT data.* Bone, 2004. **34**(1): p. 163-9.
94. Klinck, R.J. and S.K. Boyd. *The effect of radiation on bone architecture for in vivo micro-computed tomography*. in *In Orthopaedic Research Society Transaction*. 2006. Chicago, IL.
95. Waarsing, J.H., J.S. Day, and H. Weinans, *Longitudinal micro-CT scans to evaluate bone architecture.* J Musculoskelet Neuronal Interact, 2005. **5**(4): p. 310-2.
96. Duvall, C.L., et al., *Quantitative microcomputed tomography analysis of collateral vessel development after ischemic injury.* Am J Physiol Heart Circ Physiol, 2004. **287**(1): p. H302-10.
97. Badea, C., L.W. Hedlund, and G.A. Johnson, *Micro-CT with respiratory and cardiac gating.* Med Phys, 2004. **31**(12): p. 3324-9.
98. Den Buijs, J.O., Z. Bajzer, and E.L. Ritman, *Branching Morphology of the Rat Hepatic Portal Vein Tree: A Micro-CT Study.* Ann Biomed Eng, 2006.
99. Ritman, E.L., *Micro-computed tomography of the lungs and pulmonary-vascular system.* Proc Am Thorac Soc, 2005. **2**(6): p. 477-80, 501.
100. Ford-Hutchinson, A.F., et al., *Degenerative knee joint disease in mice lacking 3'-phosphoadenosine 5'-phosphosulfate synthetase 2 (Papss2) activity: a putative model of human PAPSS2 deficiency-associated arthrosis.* Osteoarthritis Cartilage, 2005. **13**(5): p. 418-25.
101. Ford-Hutchinson, A.F., et al., *Imaging skeletal pathology in mutant mice by microcomputed tomography.* J Rheumatol, 2003. **30**(12): p. 2659-65.
102. Schwartz, N.B., et al., *Defective PAPS-synthesis in epiphyseal cartilage from brachymorphic mice.* Biochem Biophys Res Commun, 1978. **82**(1): p. 173-8.
103. Sugahara, K. and N.B. Schwartz, *Defect in 3'-phosphoadenosine 5'-phosphosulfate formation in brachymorphic mice.* Proc Natl Acad Sci U S A, 1979. **76**(12): p. 6615-8.
104. Sugahara, K. and N.B. Schwartz, *Defect in 3'-phosphoadenosine 5'-phosphosulfate synthesis in brachymorphic mice. II. Tissue distribution of the defect.* Arch Biochem Biophys, 1982. **214**(2): p. 602-9.
105. Sugahara, K. and N.B. Schwartz, *Defect in 3'-phosphoadenosine 5'-phosphosulfate synthesis in brachymorphic mice. I. Characterization of the defect.* Arch Biochem Biophys, 1982. **214**(2): p. 589-601.
106. Kurima, K., et al., *A member of a family of sulfate-activating enzymes causes murine brachymorphism.* Proc Natl Acad Sci U S A, 1998. **95**(15): p. 8681-5.

107. Ho, A.M., M.D. Johnson, and D.M. Kingsley, *Role of the mouse ank gene in control of tissue calcification and arthritis.* Science, 2000. **289**(5477): p. 265-70.
108. Sweet, H.O. and M.C. Green, *Progressive ankylosis, a new skeletal mutation in the mouse.* J Hered, 1981. **72**(2): p. 87-93.
109. Hakim, F.T., et al., *Hereditary joint disorder in progressive ankylosis (ank/ank) mice. I. Association of calcium hydroxyapatite deposition with inflammatory arthropathy.* Arthritis Rheum, 1984. **27**(12): p. 1411-20.
110. Mahowald, M.L., H. Krug, and P. Halverson, *Progressive ankylosis (ank/ank) in mice: an animal model of spondyloarthropathy. II. Light and electron microscopic findings.* J Rheumatol, 1989. **16**(1): p. 60-6.
111. Johnson, K., et al., *Up-regulated expression of the phosphodiesterase nucleotide pyrophosphatase family member PC-1 is a marker and pathogenic factor for knee meniscal cartilage matrix calcification.* Arthritis Rheum, 2001. **44**(5): p. 1071-81.
112. Johnson, K. and R. Terkeltaub, *Upregulated ank expression in osteoarthritis can promote both chondrocyte MMP-13 expression and calcification via chondrocyte extracellular PPi excess.* Osteoarthritis Cartilage, 2004. **12**(4): p. 321-35.
113. Terkeltaub, R.A., *Inorganic pyrophosphate generation and disposition in pathophysiology.* Am J Physiol Cell Physiol, 2001. **281**(1): p. C1-C11.
114. Hessle, L., et al., *Tissue-nonspecific alkaline phosphatase and plasma cell membrane glycoprotein-1 are central antagonistic regulators of bone mineralization.* Proc Natl Acad Sci U S A, 2002. **99**(14): p. 9445-9.
115. Rutsch, F., et al., *PC-1 nucleoside triphosphate pyrophosphohydrolase deficiency in idiopathic infantile arterial calcification.* Am J Pathol, 2001. **158**(2): p. 543-54.
116. Nurnberg, P., et al., *Heterozygous mutations in ANKH, the human ortholog of the mouse progressive ankylosis gene, result in craniometaphyseal dysplasia.* Nat Genet, 2001. **28**(1): p. 37-41.
117. Pendleton, A., et al., *Mutations in ANKH cause chondrocalcinosis.* Am J Hum Genet, 2002. **71**(4): p. 933-40.
118. Wang, W., et al., *Role of the progressive ankylosis gene (ank) in cartilage mineralization.* Mol Cell Biol, 2005. **25**(1): p. 312-23.
119. Zaka, R. and C.J. Williams, *Role of the progressive ankylosis gene in cartilage mineralization.* Curr Opin Rheumatol, 2006. **18**(2): p. 181-6.
120. Harmey, D., et al., *Concerted regulation of inorganic pyrophosphate and osteopontin by akp2, enpp1, and ank: an integrated model of the pathogenesis of mineralization disorders.* Am J Pathol, 2004. **164**(4): p. 1199-209.
121. Ryan, L.M., *The ank gene story.* Arthritis Res, 2001. **3**(2): p. 77-9.
122. Boskey, A.L., et al., *Osteopontin-hydroxyapatite interactions in vitro: inhibition of hydroxyapatite formation and growth in a gelatin-gel.* Bone Miner, 1993. **22**(2): p. 147-59.
123. Boskey, A.L., et al., *Osteopontin deficiency increases mineral content and mineral crystallinity in mouse bone.* Calcif Tissue Int, 2002. **71**(2): p. 145-54.
124. Johnson, K., et al., *The nucleoside triphosphate pyrophosphohydrolase isozyme PC-1 directly promotes cartilage calcification through chondrocyte apoptosis and increased calcium precipitation by mineralizing vesicles.* J Rheumatol, 2001. **28**(12): p. 2681-91.

125. Sohn, P., et al., *Developmental and TGF-beta-mediated regulation of Ank mRNA expression in cartilage and bone.* Osteoarthritis Cartilage, 2002. **10**(6): p. 482-90.
126. Johnson, K., et al., *Differential mechanisms of inorganic pyrophosphate production by plasma cell membrane glycoprotein-1 and B10 in chondrocytes.* Arthritis Rheum, 1999. **42**(9): p. 1986-97.
127. Lotz, M., et al., *Interleukin 1 beta suppresses transforming growth factor-induced inorganic pyrophosphate (PPi) production and expression of the PPi-generating enzyme PC-1 in human chondrocytes.* Proc Natl Acad Sci U S A, 1995. **92**(22): p. 10364-8.
128. Okawa, A., et al., *Mutation in Npps in a mouse model of ossification of the posterior longitudinal ligament of the spine.* Nat Genet, 1998. **19**(3): p. 271-3.
129. Cadoret, A., et al., *c-myc-induced hepatocarcinogenesis in the absence of IGF-I receptor.* Int J Cancer, 2005. **114**(4): p. 668-72.
130. Reichenberger, E., et al., *Autosomal dominant craniometaphyseal dysplasia is caused by mutations in the transmembrane protein ANK.* Am J Hum Genet, 2001. **68**(6): p. 1321-6.
131. Gibilisco, P.A., et al., *Synovial fluid crystals in osteoarthritis.* Arthritis Rheum, 1985. **28**(5): p. 511-5.
132. Swan, A., et al., *Submicroscopic crystals in osteoarthritic synovial fluids.* Ann Rheum Dis, 1994. **53**(7): p. 467-70.
133. Klaassen, C.D. and J.W. Boles, *Sulfation and sulfotransferases 5: the importance of 3'-phosphoadenosine 5'-phosphosulfate (PAPS) in the regulation of sulfation.* Faseb J, 1997. **11**(6): p. 404-18.
134. Orkin, R.W., R.M. Pratt, and G.R. Martin, *Undersulfated chondroitin sulfate in the cartilage matrix of brachymorphic mice.* Dev Biol, 1976. **50**(1): p. 82-94.
135. Boskey, A.L., et al., *Hydroxyapatite formation in the presence of proteoglycans of reduced sulfate content: studies in the brachymorphic mouse.* Calcif Tissue Int, 1991. **49**(6): p. 389-93.
136. Vanky, P., et al., *Growth parameters in the epiphyseal cartilage of brachymorphic (bm/bm) mice.* Calcif Tissue Int, 2000. **66**(5): p. 355-62.
137. Orkin, R.W., et al., *Defects in the cartilaginous growth plates of brachymorphic mice.* J Cell Biol, 1977. **73**(2): p. 287-99.
138. Ahmad, M., et al., *Distinct, autosomal recessive form of spondyloepimetaphyseal dysplasia segregating in an inbred Pakistani kindred.* Am J Med Genet, 1998. **78**(5): p. 468-73.
139. ul Haque, M.F., et al., *Mutations in orthologous genes in human spondyloepimetaphyseal dysplasia and the brachymorphic mouse.* Nat Genet, 1998. **20**(2): p. 157-62.
140. Franke, T.F., et al., *PI3K/Akt and apoptosis: size matters.* Oncogene, 2003. **22**(56): p. 8983-98.
141. Holland, E.C., et al., *Signaling control of mRNA translation in cancer pathogenesis.* Oncogene, 2004. **23**(18): p. 3138-44.
142. Vanhaesebroeck, B. and D.R. Alessi, *The PI3K-PDK1 connection: more than just a road to PKB.* Biochem J, 2000. **346 Pt 3**: p. 561-76.

143. Cully, M., et al., *Beyond PTEN mutations: the PI3K pathway as an integrator of multiple inputs during tumorigenesis.* Nat Rev Cancer, 2006. **6**(3): p. 184-92.
144. Cantley, L.C. and B.G. Neel, *New insights into tumor suppression: PTEN suppresses tumor formation by restraining the phosphoinositide 3-kinase/AKT pathway.* Proc Natl Acad Sci U S A, 1999. **96**(8): p. 4240-5.
145. Simpson, L. and R. Parsons, *PTEN: life as a tumor suppressor.* Exp Cell Res, 2001. **264**(1): p. 29-41.
146. Stiles, B., et al., *PTENless means more.* Dev Biol, 2004. **273**(2): p. 175-84.
147. Sarbassov, D.D., et al., *Phosphorylation and regulation of Akt/PKB by the rictor-mTOR complex.* Science, 2005. **307**(5712): p. 1098-101.
148. Mora, A., et al., *PDK1, the master regulator of AGC kinase signal transduction.* Semin Cell Dev Biol, 2004. **15**(2): p. 161-70.
149. Mora, A., et al., *Deficiency of PDK1 in cardiac muscle results in heart failure and increased sensitivity to hypoxia.* Embo J, 2003. **22**(18): p. 4666-76.
150. Mora, A., et al., *Deficiency of PDK1 in liver results in glucose intolerance, impairment of insulin-regulated gene expression and liver failure.* Biochem J, 2005. **385**(Pt 3): p. 639-48.
151. Mora, A., et al., *Role of the PDK1-PKB-GSK3 pathway in regulating glycogen synthase and glucose uptake in the heart.* FEBS Lett, 2005. **579**(17): p. 3632-8.
152. Lawlor, M.A., et al., *Essential role of PDK1 in regulating cell size and development in mice.* Embo J, 2002. **21**(14): p. 3728-38.
153. Jope, R.S. and G.V. Johnson, *The glamour and gloom of glycogen synthase kinase-3.* Trends Biochem Sci, 2004. **29**(2): p. 95-102.
154. Inoki, K., M.N. Corradetti, and K.L. Guan, *Dysregulation of the TSC-mTOR pathway in human disease.* Nat Genet, 2005. **37**(1): p. 19-24.
155. Accili, D. and K.C. Arden, *FoxOs at the crossroads of cellular metabolism, differentiation, and transformation.* Cell, 2004. **117**(4): p. 421-6.
156. Ali, A., K.P. Hoeflich, and J.R. Woodgett, *Glycogen synthase kinase-3: properties, functions, and regulation.* Chem Rev, 2001. **101**(8): p. 2527-40.
157. Yaffe, M.B., et al., *The structural basis for 14-3-3:phosphopeptide binding specificity.* Cell, 1997. **91**(7): p. 961-71.
158. Paez, J. and W.R. Sellers, *PI3K/PTEN/AKT pathway. A critical mediator of oncogenic signaling.* Cancer Treat Res, 2003. **115**: p. 145-67.
159. Long, X., et al., *Rheb binds and regulates the mTOR kinase.* Curr Biol, 2005. **15**(8): p. 702-13.
160. Long, X., et al., *Rheb binding to mammalian target of rapamycin (mTOR) is regulated by amino acid sufficiency.* J Biol Chem, 2005. **280**(25): p. 23433-6.
161. Tee, A.R. and J. Blenis, *mTOR, translational control and human disease.* Semin Cell Dev Biol, 2005. **16**(1): p. 29-37.
162. Fingar, D.C., et al., *mTOR controls cell cycle progression through its cell growth effectors S6K1 and 4E-BP1/eukaryotic translation initiation factor 4E.* Mol Cell Biol, 2004. **24**(1): p. 200-16.
163. Hudson, C.C., et al., *Regulation of hypoxia-inducible factor 1alpha expression and function by the mammalian target of rapamycin.* Mol Cell Biol, 2002. **22**(20): p. 7004-14.

164. Majumder, P.K., et al., *mTOR inhibition reverses Akt-dependent prostate intraepithelial neoplasia through regulation of apoptotic and HIF-1-dependent pathways.* Nat Med, 2004. **10**(6): p. 594-601.
165. Treins, C., et al., *Regulation of hypoxia-inducible factor (HIF)-1 activity and expression of HIF hydroxylases in response to insulin-like growth factor I.* Mol Endocrinol, 2005. **19**(5): p. 1304-17.
166. Jiang, B.H., et al., *Phosphatidylinositol 3-kinase signaling controls levels of hypoxia-inducible factor 1.* Cell Growth Differ, 2001. **12**(7): p. 363-9.
167. Jiang, B.H., et al., *Phosphatidylinositol 3-kinase signaling mediates angiogenesis and expression of vascular endothelial growth factor in endothelial cells.* Proc Natl Acad Sci U S A, 2000. **97**(4): p. 1749-53.
168. Brugarolas, J.B., et al., *TSC2 regulates VEGF through mTOR-dependent and -independent pathways.* Cancer Cell, 2003. **4**(2): p. 147-58.
169. El-Hashemite, N., et al., *Loss of Tsc1 or Tsc2 induces vascular endothelial growth factor production through mammalian target of rapamycin.* Cancer Res, 2003. **63**(17): p. 5173-7.
170. Peng, X.D., et al., *Dwarfism, impaired skin development, skeletal muscle atrophy, delayed bone development, and impeded adipogenesis in mice lacking Akt1 and Akt2.* Genes Dev, 2003. **17**(11): p. 1352-65.
171. Cramer, T., et al., *Expression of VEGF isoforms by epiphyseal chondrocytes during low-oxygen tension is HIF-1 alpha dependent.* Osteoarthritis Cartilage, 2004. **12**(6): p. 433-9.
172. Mayr-Wohlfart, U., et al., *Vascular endothelial growth factor stimulates chemotactic migration of primary human osteoblasts.* Bone, 2002. **30**(3): p. 472-7.
173. Gerber, H.P., et al., *VEGF couples hypertrophic cartilage remodeling, ossification and angiogenesis during endochondral bone formation.* Nat Med, 1999. **5**(6): p. 623-8.
174. Maes, C., et al., *Soluble VEGF isoforms are essential for establishing epiphyseal vascularization and regulating chondrocyte development and survival.* J Clin Invest, 2004. **113**(2): p. 188-99.
175. Schipani, E., et al., *Hypoxia in cartilage: HIF-1alpha is essential for chondrocyte growth arrest and survival.* Genes Dev, 2001. **15**(21): p. 2865-76.
176. Zelzer, E., et al., *VEGFA is necessary for chondrocyte survival during bone development.* Development, 2004. **131**(9): p. 2161-71.
177. Pfander, D., et al., *Deletion of Vhlh in chondrocytes reduces cell proliferation and increases matrix deposition during growth plate development.* Development, 2004. **131**(10): p. 2497-508.
178. Starkman, B.G., et al., *IGF-I stimulation of proteoglycan synthesis by chondrocytes requires activation of the PI 3-kinase pathway but not ERK MAPK.* Biochem J, 2005. **389**(Pt 3): p. 723-9.
179. Oh, C.D. and J.S. Chun, *Signaling mechanisms leading to the regulation of differentiation and apoptosis of articular chondrocytes by insulin-like growth factor-1.* J Biol Chem, 2003. **278**(38): p. 36563-71.

180. Koike, M., et al., *Insulin-like growth factor-1 rescues the mutated FGF receptor 3 (G380R) expressing ATDC5 cells from apoptosis through phosphatidylinositol 3-kinase and MAPK.* J Bone Miner Res, 2003. **18**(11): p. 2043-51.
181. Debiais, F., et al., *Fibroblast growth factor-2 induces osteoblast survival through a phosphatidylinositol 3-kinase-dependent, -beta-catenin-independent signaling pathway.* Exp Cell Res, 2004. **297**(1): p. 235-46.
182. Sugimori, K., et al., *BMP-2 prevents apoptosis of the N1511 chondrocytic cell line through PI3K/Akt-mediated NF-kappaB activation.* J Bone Miner Metab, 2005. **23**(6): p. 411-9.
183. Fujita, T., et al., *Runx2 induces osteoblast and chondrocyte differentiation and enhances their migration by coupling with PI3K-Akt signaling.* J Cell Biol, 2004. **166**(1): p. 85-95.
184. Bain, G., et al., *Activated beta-catenin induces osteoblast differentiation of C3H10T1/2 cells and participates in BMP2 mediated signal transduction.* Biochem Biophys Res Commun, 2003. **301**(1): p. 84-91.
185. Kahler, R.A. and J.J. Westendorf, *Lymphoid enhancer factor-1 and beta-catenin inhibit Runx2-dependent transcriptional activation of the osteocalcin promoter.* J Biol Chem, 2003. **278**(14): p. 11937-44.
186. Li, D.M. and H. Sun, *TEP1, encoded by a candidate tumor suppressor locus, is a novel protein tyrosine phosphatase regulated by transforming growth factor beta.* Cancer Res, 1997. **57**(11): p. 2124-9.
187. Li, J., et al., *PTEN, a putative protein tyrosine phosphatase gene mutated in human brain, breast, and prostate cancer.* Science, 1997. **275**(5308): p. 1943-7.
188. Steck, P.A., et al., *Identification of a candidate tumour suppressor gene, MMAC1, at chromosome 10q23.3 that is mutated in multiple advanced cancers.* Nat Genet, 1997. **15**(4): p. 356-62.
189. Myers, M.P., et al., *P-TEN, the tumor suppressor from human chromosome 10q23, is a dual-specificity phosphatase.* Proc Natl Acad Sci U S A, 1997. **94**(17): p. 9052-7.
190. Lee, J.O., et al., *Crystal structure of the PTEN tumor suppressor: implications for its phosphoinositide phosphatase activity and membrane association.* Cell, 1999. **99**(3): p. 323-34.
191. Adey, N.B., et al., *Threonine phosphorylation of the MMAC1/PTEN PDZ binding domain both inhibits and stimulates PDZ binding.* Cancer Res, 2000. **60**(1): p. 35-7.
192. Georgescu, M.M., et al., *Stabilization and productive positioning roles of the C2 domain of PTEN tumor suppressor.* Cancer Res, 2000. **60**(24): p. 7033-8.
193. Tolkacheva, T., et al., *Regulation of PTEN binding to MAGI-2 by two putative phosphorylation sites at threonine 382 and 383.* Cancer Res, 2001. **61**(13): p. 4985-9.
194. Vazquez, F., et al., *Phosphorylation of the PTEN tail regulates protein stability and function.* Mol Cell Biol, 2000. **20**(14): p. 5010-8.
195. Okumura, K., et al., *PCAF Modulates PTEN Activity.* J Biol Chem, 2006. **281**(36): p. 26562-8.

196. Kishimoto, H., et al., *Physiological functions of Pten in mouse tissues.* Cell Struct Funct, 2003. **28**(1): p. 11-21.
197. Backman, S.A., et al., *Deletion of Pten in mouse brain causes seizures, ataxia and defects in soma size resembling Lhermitte-Duclos disease.* Nat Genet, 2001. **29**(4): p. 396-403.
198. Suzuki, A., et al., *T cell-specific loss of Pten leads to defects in central and peripheral tolerance.* Immunity, 2001. **14**(5): p. 523-34.
199. Wang, S., et al., *Prostate-specific deletion of the murine Pten tumor suppressor gene leads to metastatic prostate cancer.* Cancer Cell, 2003. **4**(3): p. 209-21.
200. Hamada, K., et al., *The PTEN/PI3K pathway governs normal vascular development and tumor angiogenesis.* Genes Dev, 2005. **19**(17): p. 2054-65.
201. Li, G., et al., *Conditional loss of PTEN leads to precocious development and neoplasia in the mammary gland.* Development, 2002. **129**(17): p. 4159-70.
202. Suzuki, A., et al., *Keratinocyte-specific Pten deficiency results in epidermal hyperplasia, accelerated hair follicle morphogenesis and tumor formation.* Cancer Res, 2003. **63**(3): p. 674-81.
203. Lakso, M., et al., *Targeted oncogene activation by site-specific recombination in transgenic mice.* Proc Natl Acad Sci U S A, 1992. **89**(14): p. 6232-6.
204. Gu, H., et al., *Deletion of a DNA polymerase beta gene segment in T cells using cell type-specific gene targeting.* Science, 1994. **265**(5168): p. 103-6.
205. Ramirez-Solis, R., P. Liu, and A. Bradley, *Chromosome engineering in mice.* Nature, 1995. **378**(6558): p. 720-4.
206. Nagy, A., *Manipulating the Mouse Embryo A Laboratory Manual*. 3rd ed. 2003, Cold Spring Habor, NY: Cold Spring Habor Laboratory Press.
207. Buchholz, F., et al., *Different thermostabilities of FLP and Cre recombinases: implications for applied site-specific recombination.* Nucleic Acids Res, 1996. **24**(21): p. 4256-62.
208. Hofker, M. and J.V. Deursen, *Transgenic Mouse Methods and Protocols*. Vol. 209. 2003, Totowa, NJ: Humana Press.
209. Sakai, K., et al., *Stage-and tissue-specific expression of a Col2a1-Cre fusion gene in transgenic mice.* Matrix Biol, 2001. **19**(8): p. 761-7.
210. Jacob, A.L., et al., *Fibroblast growth factor receptor 1 signaling in the osteo-chondrogenic cell lineage regulates sequential steps of osteoblast maturation.* Dev Biol, 2006.
211. Ford-Hutchinson, A.F., et al., *Inactivation of Pten in osteo-chondroprogenitor cells leads to epiphyseal growth plate abnormalities and skeletal overgrowth*, in *Development*. 2006. p. under review.
212. Glass, D.A., 2nd, et al., *Canonical Wnt signaling in differentiated osteoblasts controls osteoclast differentiation.* Dev Cell, 2005. **8**(5): p. 751-64.
213. Hosaka, T., et al., *Disruption of forkhead transcription factor (FOXO) family members in mice reveals their functional diversification.* Proc Natl Acad Sci U S A, 2004. **101**(9): p. 2975-80.
214. Hildebrand, T. and P. Ruegsegger, *A new method for the model independent assessment of thickness in three dimensional images.* Journal of Microscopy, 1997. **185**: p. 67-75.

215. Maier, I. and G. Wilhelmi, *Osteoarthritis-like disease in mice: effects of anti-arthrotic and rheumatic agents.*, in *Studies of osteoarthrosis:pathogenesis, intervention, and assessment.*, D.J. Lott, M.K. Jasani, and G.F.B. Birdwood, Editors. 1987, John Wiley and Sons: New York, NY. p. 75-83.
216. Maier, R. and G. Wilhelmi, *Osteoarthrosis-like Disease in Mice: Anti-arthrotic and antirheumatic agents in mice*, in *Studies in osteoarthritis: pathogenesis, intervention and assesement*, L.D.J.e. al., Editor. 1987, John Wiley and Sons: New York. p. 75-83.
217. Salo, P.T., et al., *Evidence for a neuropathic contribution to the development of spontaneous knee osteoarthrosis in a mouse model.* Acta Orthop Scand, 2002. **73**(1): p. 77-84.
218. Ovchinnikov, D.A., et al., *Col2a1-directed expression of Cre recombinase in differentiating chondrocytes in transgenic mice.* Genesis, 2000. **26**(2): p. 145-6.
219. Lefebvre, V., et al., *Characterization of primary cultures of chondrocytes from type II collagen/beta-galactosidase transgenic mice.* Matrix Biol, 1994. **14**(4): p. 329-35.
220. Beier, F., A.C. Taylor, and P. LuValle, *The Raf-1/MEK/ERK pathway regulates the expression of the p21(Cip1/Waf1) gene in chondrocytes.* J Biol Chem, 1999. **274**(42): p. 30273-9.
221. Flores, M.E., et al., *RGD-directed attachment of isolated rat osteoclasts to osteopontin, bone sialoprotein, and fibronectin.* Exp Cell Res, 1992. **201**(2): p. 526-30.
222. Soriano, P., *Generalized lacZ expression with the ROSA26 Cre reporter strain.* Nat Genet, 1999. **21**(1): p. 70-1.
223. Graichen, H., et al., *A non-destructive technique for 3-D microstructural phenotypic characterisation of bones in genetically altered mice: preliminary data in growth hormone transgenic animals and normal controls.* Anat Embryol (Berl), 1999. **199**(3): p. 239-48.
224. Ito, M., et al., *Analysis of trabecular microarchitecture of human iliac bone using microcomputed tomography in patients with hip arthrosis with or without vertebral fracture.* Bone, 1998. **23**(2): p. 163-9.
225. Kapadia, R.D., et al., *Applications of micro-CT and MR microscopy to study pre-clinical models of osteoporosis and osteoarthritis.* Technol Health Care, 1998. **6**(5-6): p. 361-72.
226. Abe, S., et al., *Morphological study of the femur in osteopetrotic (op/op) mice using microcomputed tomography.* Br J Radiol, 2000. **73**(874): p. 1078-82.
227. Yamashita, T., Y. Nabeshima, and M. Noda, *High-resolution micro-computed tomography analyses of the abnormal trabecular bone structures in klotho gene mutant mice.* J Endocrinol, 2000. **164**(2): p. 239-45.
228. McLaughlin, F., et al., *Glucocorticoid-induced osteopenia in the mouse as assessed by histomorphometry, microcomputed tomography, and biochemical markers.* Bone, 2002. **30**(6): p. 924-30.
229. Sampson, H.W., *Spondyloarthropathy in progressive ankylosis (ank/ank) mice: morphological features.* Spine, 1988. **13**(6): p. 645-9.

230. Pennypacker, J.P., K. Kimata, and K.S. Brown, *Brachymorphic mice (bm/bm): a generalized biochemical defect expressed primarily cartilage.* Dev Biol, 1981. **81**(2): p. 280-7.
231. Plaas, A.H., et al., *Glycosaminoglycan sulfation in human osteoarthritis. Disease-related alterations at the non-reducing termini of chondroitin and dermatan sulfate.* J Biol Chem, 1998. **273**(20): p. 12642-9.
232. Bayliss, M.T., et al., *The organization of aggrecan in human articular cartilage. Evidence for age-related changes in the rate of aggregation of newly synthesized molecules.* J Biol Chem, 2000. **275**(9): p. 6321-7.
233. Carey, D.J., *Syndecans: multifunctional cell-surface co-receptors.* Biochem J, 1997. **327 (Pt 1)**: p. 1-16.
234. Hildebrand, A., et al., *Interaction of the small interstitial proteoglycans biglycan, decorin and fibromodulin with transforming growth factor beta.* Biochem J, 1994. **302 (Pt 2)**: p. 527-34.
235. Poole, A.R., in *Arthritis and Allied Conditions*, W.J. Koopman, Editor. 1996, Williams and Wilkins: Baltimore.
236. Sandy, J.D., A.H.K. Plaas, and L.C. Rosenberg, in *Arthritis and Allied Conditiona*, W.J. Koopman, Editor. 1996, Williams and Wilkins: Baltimore. p. 252-275.
237. Mankin, H.J., et al., *Articular Cartilage Structure, Composition, and Function*, in *Orthopaedic Basic Science, Biology and Biomechanics of the Musculoskeletal System*, J.A. Buckwalter, T.A. Einhorn, and S.R. Simon, Editors. 2000, Amercian Academy of Orthopaedic Surgeons: Illinois. p. 444-470.
238. Saamanen, A.K., et al., *Osteoarthritis-like lesions in transgenic mice harboring a small deletion mutation in type II collagen gene.* Osteoarthritis Cartilage, 2000. **8**(4): p. 248-57.
239. Pataki, A., H.P. Graf, and E. Witzemann, *Spontaneous osteo-arthritis of the knee-joint in C57BL mice receiving chronic oral treatment with NSAID's or prednisone.* Agents Actions, 1990. **29**(3-4): p. 210-7.
240. Lapvetelainen, T., et al., *Lifelong moderate running training increases the incidence and severity of osteoarthritis in the knee joint of C57BL mice.* Anat Rec, 1995. **242**(2): p. 159-65.
241. Stanescu, R., et al., *Early lesions of the articular surface in a strain of mice with very high incidence of spontaneous osteoarthritic-like lesions.* J Rheumatol, 1993. **20**(1): p. 102-10.
242. Stoop, R., et al., *Type II collagen degradation in spontaneous osteoarthritis in C57Bl/6 and BALB/c mice.* Arthritis Rheum, 1999. **42**(11): p. 2381-9.
243. Edeiken, J., *Roentgen Diagnosis of Diseases of Bone.* 3rd ed, ed. W. Wilkins. 1981, Baltimore.
244. Greenfield, G.B., *Radiology of Bone Diseases*. 5th ed. 1990, Philadelphia: J.B. Lippincott Company.
245. Wikstrom, B., et al., *Morphological studies of the epiphyseal growth zone in the brachymorphic (bm/bm) mouse.* Virchows Arch B Cell Pathol Incl Mol Pathol, 1984. **47**(2): p. 167-76.

246. *Osteoarthritis*, ed. B. KD, D. M, and L. LS. 1998, Oxford: Oxford University Press.
247. Xu, Z.H., et al., *Human 3'-phosphoadenosine 5'-phosphosulfate synthetase 2 (PAPSS2) pharmacogenetics: gene resequencing, genetic polymorphisms and functional characterization of variant allozymes.* Pharmacogenetics, 2002. **12**(1): p. 11-21.
248. Ikeda, T., et al., *Identification of sequence polymorphisms in two sulfation-related genes, PAPSS2 and SLC26A2, and an association analysis with knee osteoarthritis.* J Hum Genet, 2001. **46**(9): p. 538-43.
249. Krebsbach, P.H., et al., *Identification of a minimum enhancer sequence for the type II collagen gene reveals several core sequence motifs in common with the link protein gene.* J Biol Chem, 1996. **271**(8): p. 4298-303.
250. Leung, K.K., et al., *Different cis-regulatory DNA elements mediate developmental stage- and tissue-specific expression of the human COL2A1 gene in transgenic mice.* J Cell Biol, 1998. **141**(6): p. 1291-300.
251. Zhou, G., et al., *A 182 bp fragment of the mouse pro alpha 1(II) collagen gene is sufficient to direct chondrocyte expression in transgenic mice.* J Cell Sci, 1995. **108 (Pt 12)**: p. 3677-84.
252. Borzi, R.M., et al., *Chemokines in cartilage degradation.* Clin Orthop Relat Res, 2004(427 Suppl): p. S53-61.
253. Hart, K.C., S.C. Robertson, and D.J. Donoghue, *Identification of tyrosine residues in constitutively activated fibroblast growth factor receptor 3 involved in mitogenesis, Stat activation, and phosphatidylinositol 3-kinase activation.* Mol Biol Cell, 2001. **12**(4): p. 931-42.
254. Ong, S.H., et al., *Stimulation of phosphatidylinositol 3-kinase by fibroblast growth factor receptors is mediated by coordinated recruitment of multiple docking proteins.* Proc Natl Acad Sci U S A, 2001. **98**(11): p. 6074-9.
255. Wang, J., et al., *Evidence supporting dual, IGF-I-independent and IGF-I-dependent, roles for GH in promoting longitudinal bone growth.* J Endocrinol, 2004. **180**(2): p. 247-55.
256. Zhu, T., et al., *Signal transduction via the growth hormone receptor.* Cell Signal, 2001. **13**(9): p. 599-616.
257. Forlino, A., et al., *A diastrophic dysplasia sulfate transporter (SLC26A2) mutant mouse: morphological and biochemical characterization of the resulting chondrodysplasia phenotype.* Hum Mol Genet, 2005. **14**(6): p. 859-71.
258. Zhong, H., et al., *Modulation of hypoxia-inducible factor 1alpha expression by the epidermal growth factor/phosphatidylinositol 3-kinase/PTEN/AKT/FRAP pathway in human prostate cancer cells: implications for tumor angiogenesis and therapeutics.* Cancer Res, 2000. **60**(6): p. 1541-5.
259. Zundel, W., et al., *Loss of PTEN facilitates HIF-1-mediated gene expression.* Genes Dev, 2000. **14**(4): p. 391-6.
260. Zelzer, E., et al., *Skeletal defects in VEGF(120/120) mice reveal multiple roles for VEGF in skeletogenesis.* Development, 2002. **129**(8): p. 1893-904.
261. Zhang, J., et al., *PTEN maintains haematopoietic stem cells and acts in lineage choice and leukaemia prevention.* Nature, 2006. **441**(7092): p. 518-22.

262. Aubin, J.E. and J.T. Triffitt, *Mesenchymal stem cells and osteoblast differentiation*, in *Principles of Bone Biology*, J.P. Bilezikian, L.G. Raisz, and G.A. Rodan, Editors. 2002, Academic Press: San Diego, California. p. 59-81.
263. Zhang, X., et al., *Runx2 overexpression enhances osteoblastic differentiation and mineralization in adipose--derived stem cells in vitro and in vivo.* Calcif Tissue Int, 2006. **79**(3): p. 169-78.
264. Shipman, P. and A. Walker, *The Human Skeleton*. 1985, Cambridge, MA: Harvard University Press.
265. Zhou, H., et al., *Anabolic action of parathyroid hormone on cortical and cancellous bone differs between axial and appendicular skeletal sites in mice.* Bone, 2003. **32**(5): p. 513-20.
266. Chagin, A.S., et al., *Estrogen receptor-beta inhibits skeletal growth and has the capacity to mediate growth plate fusion in female mice.* J Bone Miner Res, 2004. **19**(1): p. 72-7.
267. Brinkers, J.M., et al., *The effect of oestrogen treatment on body proportions in constitutionally tall girls.* Eur J Pediatr, 1994. **153**(4): p. 237-40.
268. Savendahl, L., *Hormonal regulation of growth plate cartilage.* Horm Res, 2005. **64 Suppl 2**: p. 94-7.
269. Weise, M., et al., *Effects of estrogen on growth plate senescence and epiphyseal fusion.* Proc Natl Acad Sci U S A, 2001. **98**(12): p. 6871-6.
270. Gunther, D.F., L.E. Underwood, and A.S. Calikoglu, *Androgen-accelerated bone maturation in mice is not attenuated by Faslodex, an estrogen receptor blocker.* Bone, 2001. **28**(4): p. 410-3.
271. Tivesten, A., et al., *Additive protective effects of estrogen and androgen treatment on trabecular bone in ovariectomized rats.* J Bone Miner Res, 2004. **19**(11): p. 1833-9.
272. Aquila, S., et al., *Estrogen receptor (ER)alpha and ER beta are both expressed in human ejaculated spermatozoa: evidence of their direct interaction with phosphatidylinositol-3-OH kinase/Akt pathway.* J Clin Endocrinol Metab, 2004. **89**(3): p. 1443-51.
273. Mendez, P. and L.M. Garcia-Segura, *Phosphatidylinositol 3-kinase and glycogen synthase kinase 3 regulate estrogen receptor-mediated transcription in neuronal cells.* Endocrinology, 2006. **147**(6): p. 3027-39.
274. Sharma, M., W.W. Chuang, and Z. Sun, *Phosphatidylinositol 3-kinase/Akt stimulates androgen pathway through GSK3beta inhibition and nuclear beta-catenin accumulation.* J Biol Chem, 2002. **277**(34): p. 30935-41.
275. Sims, N.A., et al., *Deletion of estrogen receptors reveals a regulatory role for estrogen receptors-beta in bone remodeling in females but not in males.* Bone, 2002. **30**(1): p. 18-25.
276. Windahl, S.H., et al., *Increased cortical bone mineral content but unchanged trabecular bone mineral density in female ERbeta(-/-) mice.* J Clin Invest, 1999. **104**(7): p. 895-901.
277. Calvi, L.M., et al., *Activated parathyroid hormone/parathyroid hormone-related protein receptor in osteoblastic cells differentially affects cortical and trabecular bone.* J Clin Invest, 2001. **107**(3): p. 277-86.

278. Jiang, J., et al., *Transgenic mice with osteoblast-targeted insulin-like growth factor-I show increased bone remodeling.* Bone, 2006.
279. Zhao, G., et al., *Targeted overexpression of insulin-like growth factor I to osteoblasts of transgenic mice: increased trabecular bone volume without increased osteoblast proliferation.* Endocrinology, 2000. **141**(7): p. 2674-82.
280. von Stechow, D., et al., *Differential transcriptional effects of PTH and estrogen during anabolic bone formation.* J Cell Biochem, 2004. **93**(3): p. 476-90.
281. Iida-Klein, A., et al., *Anabolic action of parathyroid hormone is skeletal site specific at the tissue and cellular levels in mice.* J Bone Miner Res, 2002. **17**(5): p. 808-16.
282. Abboud, S.L., et al., *Osteoblast-specific targeting of soluble colony-stimulating factor-1 increases cortical bone thickness in mice.* J Bone Miner Res, 2003. **18**(8): p. 1386-94.
283. Steward, C.G., *Neurological aspects of osteopetrosis.* Neuropathol Appl Neurobiol, 2003. **29**(2): p. 87-97.
284. Radin, E.L., et al., *Response of joints to impact loading. 3. Relationship between trabecular microfractures and cartilage degeneration.* J Biomech, 1973. **6**(1): p. 51-7.
285. Radin, E.L., I.L. Paul, and R.M. Rose, *Role of mechanical factors in pathogenesis of primary osteoarthritis.* Lancet, 1972. **1**(7749): p. 519-22.
286. Radin, E.L., I.L. Paul, and R.M. Rose, *Mechanical facotrs in the aertiology of osteoarthritis.* Lancet, 1975. **34(Suppl)**: p. 132-133.
287. Burr, D.B. and E.L. Radin, *Microfractures and microcracks in subchondral bone: are they relevant to osteoarthrosis?* Rheum Dis Clin North Am, 2003. **29**(4): p. 675-85.
288. Lajeunesse, D. and P. Reboul, *Subchondral bone in osteoarthritis: a biologic link with articular cartilage leading to abnormal remodeling.* Curr Opin Rheumatol, 2003. **15**(5): p. 628-33.
289. Dequeker, J., P. Goris, and R. Uytterhoeven, *Osteoporosis and osteoarthritis (osteoarthrosis). Anthropometric distinctions.* Jama, 1983. **249**(11): p. 1448-51.
290. Raymaekers, G., et al., *Alterations of the mineralization profile and osteocalcin concentrations in osteoarthritic cortical iliac crest bone.* Calcif Tissue Int, 1992. **51**(4): p. 269-75.
291. Verstraeten, A., et al., *Osteoarthrosis retards the development of osteoporosis. Observation of the coexistence of osteoarthrosis and osteoporosis.* Clin Orthop Relat Res, 1991(264): p. 169-77.
292. Hannan, M.T., et al., *Bone mineral density and knee osteoarthritis in elderly men and women. The Framingham Study.* Arthritis Rheum, 1993. **36**(12): p. 1671-80.
293. Massicotte, F., et al., *Can altered production of interleukin-1beta, interleukin-6, transforming growth factor-beta and prostaglandin E(2) by isolated human subchondral osteoblasts identify two subgroups of osteoarthritic patients.* Osteoarthritis Cartilage, 2002. **10**(6): p. 491-500.
294. Paredes, Y., et al., *Study of the role of leukotriene B4 in abnormal function of human subchondral osteoarthritis osteoblasts: effects of cyclooxygenase and/or 5-lipoxygenase inhibition.* Arthritis Rheum, 2002. **46**(7): p. 1804-12.

295. Westacott, C.I., et al., *Alteration of cartilage metabolism by cells from osteoarthritic bone.* Arthritis Rheum, 1997. **40**(7): p. 1282-91.
296. Bailey, A.J. and J.P. Mansell, *Do subchondral bone changes exacerbate or precede articular cartilage destruction in osteoarthritis of the elderly?* Gerontology, 1997. **43**(5): p. 296-304.
297. Carlson, C.S., et al., *Osteoarthritis in cynomolgus macaques: a primate model of naturally occurring disease.* J Orthop Res, 1994. **12**(3): p. 331-9.
298. Carlson, C.S., et al., *Osteoarthritis in cynomolgus macaques. III: Effects of age, gender, and subchondral bone thickness on the severity of disease.* J Bone Miner Res, 1996. **11**(9): p. 1209-17.
299. Imhof, H., et al., *Importance of subchondral bone to articular cartilage in health and disease.* Top Magn Reson Imaging, 1999. **10**(3): p. 180-92.
300. Mital, M.A. and P.F. Millington, *Osseous pathway of nutrition to articular cartilage of the human femoral head.* Lancet, 1970. **1**(7651): p. 842.
301. Sokoloff, L., *Microcracks in the calcified layer of articular cartilage.* Arch Pathol Lab Med, 1993. **117**(2): p. 191-5.
302. Dequeker, J., et al., *Generalized osteoarthritis associated with increased insulin-like growth factor types I and II and transforming growth factor beta in cortical bone from the iliac crest. Possible mechanism of increased bone density and protection against osteoporosis.* Arthritis Rheum, 1993. **36**(12): p. 1702-8.
303. Hamerman, D. and E.R. Stanley, *Implications of increased bone density in osteoarthritis.* J Bone Miner Res, 1996. **11**(9): p. 1205-8.
304. Gautreau, A., et al., *Ezrin, a plasma membrane-microfilament linker, signals cell survival through the phosphatidylinositol 3-kinase/Akt pathway.* Proc Natl Acad Sci U S A, 1999. **96**(13): p. 7300-5.
305. Wan, X., et al., *Rapamycin inhibits ezrin-mediated metastatic behavior in a murine model of osteosarcoma.* Cancer Res, 2005. **65**(6): p. 2406-11.
306. Curto, M. and A.I. McClatchey, *Ezrin.a metastatic detERMinant?* Cancer Cell, 2004. **5**(2): p. 113-4.
307. Fixman, E.D., et al., *Efficient cell transformation by the Tpr-Met oncoprotein is dependent upon tyrosine 489 in the carboxy-terminus.* Oncogene, 1995. **10**(2): p. 237-49.
308. Graziani, A., et al., *Hepatocyte growth factor/scatter factor stimulates the Ras-guanine nucleotide exchanger.* J Biol Chem, 1993. **268**(13): p. 9165-8.
309. Ponzetto, C., et al., *A multifunctional docking site mediates signaling and transformation by the hepatocyte growth factor/scatter factor receptor family.* Cell, 1994. **77**(2): p. 261-71.
310. Zhu, H., et al., *Tyrosine 1356 in the carboxyl-terminal tail of the HGF/SF receptor is essential for the transduction of signals for cell motility and morphogenesis.* J Biol Chem, 1994. **269**(47): p. 29943-8.
311. Royal, I. and M. Park, *Hepatocyte growth factor-induced scatter of Madin-Darby canine kidney cells requires phosphatidylinositol 3-kinase.* J Biol Chem, 1995. **270**(46): p. 27780-7.

312. Leshem, Y., et al., *Preferential binding of Grb2 or phosphatidylinositol 3-kinase to the met receptor has opposite effects on HGF-induced myoblast proliferation.* Exp Cell Res, 2002. **274**(2): p. 288-98.
313. Alhadlaq, A., et al., *Adult stem cell driven genesis of human-shaped articular condyle.* Ann Biomed Eng, 2004. **32**(7): p. 911-23.
314. Alhadlaq, A. and J.J. Mao, *Tissue-engineered neogenesis of human-shaped mandibular condyle from rat mesenchymal stem cells.* J Dent Res, 2003. **82**(12): p. 951-6.
315. Meirelles Lda, S. and N.B. Nardi, *Murine marrow-derived mesenchymal stem cell: isolation, in vitro expansion, and characterization.* Br J Haematol, 2003. **123**(4): p. 702-11.
316. Phornphutkul, C., et al., *Insulin-like growth factor-I signaling is modified during chondrocyte differentiation.* J Endocrinol, 2004. **183**(3): p. 477-86.
317. Longobardi, L., et al., *Effect of IGF-I in the chondrogenesis of bone marrow mesenchymal stem cells in the presence or absence of TGF-beta signaling.* J Bone Miner Res, 2006. **21**(4): p. 626-36.
318. Kratchmarova, I., et al., *Mechanism of divergent growth factor effects in mesenchymal stem cell differentiation.* Science, 2005. **308**(5727): p. 1472-7.
319. Campbell, M.R., et al., *Chicken collagen X regulatory sequences restrict transgene expression to hypertrophic cartilage in mice.* Am J Pathol, 2004. **164**(2): p. 487-99.
320. Gebhard, S., et al., *A highly conserved enhancer in mammalian type X collagen genes drives high levels of tissue-specific expression in hypertrophic cartilage in vitro and in vivo.* Matrix Biol, 2004. **23**(5): p. 309-22.
321. Yang, G., et al., *Transgenic mice that express Cre recombinase in hypertrophic chondrocytes.* Genesis, 2005. **42**(1): p. 33-6.
322. Zheng, Q., et al., *Type X collagen gene regulation by Runx2 contributes directly to its hypertrophic chondrocyte-specific expression in vivo.* J Cell Biol, 2003. **162**(5): p. 833-42.
323. Dacquin, R., et al., *Mouse alpha1(I)-collagen promoter is the best known promoter to drive efficient Cre recombinase expression in osteoblast.* Dev Dyn, 2002. **224**(2): p. 245-51.
324. Patane, S., et al., *MET overexpression turns human primary osteoblasts into osteosarcomas.* Cancer Res, 2006. **66**(9): p. 4750-7.